Geotechnical measurements to characterise slope sediments and to identify landslide mechanisms and their impact on ecosystems

Doctoral Thesis

submitted for the doctoral degree in natural sciences
at the Faculty of Geosciences of Bremen University

zur Erlangung des Doktorgrades der Naturwissenschaften
im Fachbereich Geowissenschaften der Universität Bremen

by
vorgelegt von
Annika Förster

Bremen, Juni 2011

Tag des Kolloquiums:

31. Oktober 2011

Gutachter:

Prof. Dr. Achim J. Kopf

Prof. Dr. Tobias Mörz

Prüfer:

Prof. Dr. Katrin Huhn

Prof. Dr. Rüdiger Henrich

Abstract

Submarine mass wasting processes are not uniformly distributed over the world's ocean. Glaciated margins are also affected as non-glaciated margins including fjords, submarine canyons and river deltas. Observation, monitoring and analysis of the mass wasting processes are of large scientific as well as socio-economic interest due to the hazardous impact of, e.g. landslides on offshore industry installations. Likewise, Tsunamis that are triggered by mass wasting processes, endanger coastal cities and surrounding areas. The distribution of submarine landslides may be controlled by the interaction of morphology, sediment composition, sediment mechanical behaviour (e.g. lowered sediment strength) and external triggers (e.g. earthquakes, sea-level change).

In summary, the presented study investigates the mechanics, mechanisms and factors governing slope instabilities of three different submarine landslides sites evolved from active and passive continental margins. Results of geotechnical measurements from both the stable and the failed part of the different landslides were compared to previously published geophysical and sedimentological data. The three different research sites are i) the passive continental margin of Mauritania, NW-Africa, ii) the low seimic and tectonically active Ligurian margin (Southern France) and iii) the high tectonically active margin of the Cretan Sea (Greece). A combination of several trigger mechanisms in interaction with preconditioning factors are requiered for destabilizing the investigated slope sediments.

At the Mauritania Landslide Complex (NW-Africa), one of the largest landslide events known on the eastern Atlantic margin, the most likely main trigger mechanisms were rapid sedimentation during glacial-interglacial dynamic changes in combination with the presence of weak layers. Geotechnical measurements and strain analyses on both the undisturbed hemipelagic background sediments and the slid sediments infer at least two different source areas with a sequential failure mechanism. While the hemipelagites are characterized by normal consolidation, the slid sediments comprising three different matrix types show normal consolidation at the base, strong overconsolidation in the middle and normal consolidation to slight overconsolidation at the top. Furthermore, the hemipelagic sediments underlying the debris flow units show strong to slight underconsolidation with low friction coefficients of μ=0.18 indicating a weak layer. To constrain the mechanics of the sliding sediments, finite strain analysis techniques are used to quantitatively estimate the amount of deformation. In the undisturbed sediments low deformation grades with R-values (ratio $\varepsilon_1/\varepsilon_3$) of 1-2 were observed resulting from burial or compaction, while several of the remobilized sediments show strong deformation intensities (R= 3->4) related to directional extension or compression.

At the tectonically active continental margins of the Ligurian Sea (Southern France) and the Cretan Sea (North of Crete, Greece), the most important trigger mechanism for slope failure is probably seismic loading. On the steep continental slope (~20°) of the Ligurian margin two distinct landslide complexes were investigated. The first landslide complex is located near to the Var Canyon and show several elongated head scarps. Both undisturbed and failed recovered sediments are characterized by tilted layering and a downward increase in bulk density and shear strength (up to 60 kPa in 4 mbsf). Furthermore, the failed portion show overconsolidation but low friction values with a coefficient of friction μ= 0.27. A one-dimensional stability model for this landslide complex shows that already earthquakes with relatively small magnitudes of M 0.77-~5 with peak ground acceleration (PGA) of 2-22 %g are required for sediment destabilization with estimated recurrence time of 1 to 12 years. Otherwise, the Eastern Landslide

Complex show smooth headwall features containing debrites and hemipelagic silty clays with pebbles. The failed material is characterized by constant bulk density and by underconsolidation with lowered shear strength values. Amalgamation and incorporation of seawater during the sliding process may have retained the underconsolidation state of the sediments.

At the high tectonically active margin of the Cretan Sea submarine landslides with high recurrence times were expected. Instead landslide deposits were found at recurrence interval of approximately 250 ka ± 70 ka, which is relatively low for a strong tectonically active area. Geotechnical investigations on both undisturbed and slid material show high shear strength values (up to 90 kPa in 4 mbsf), which might result due to repeated earthquake loading with low magnitudes. Ring shear experiments show a velocity-weakening behaviour of the slid material with low intrinsic friction (μ= ~0.3), which may lead to catastrophic mass wasting. The most likely trigger mechanisms for mass wasting at the Cretan Sea are neotectonic activities and regional seismicity. A one-dimensional infinite slope stability model shows that PGA-values of 37 %g up to ≥ 64 %g are required for sediment destabilization. In comparison with the Ligurian margin, the recurrence time of the mass wasting events is thousandfold lower that implicates higher required earthquake magnitudes to destabilize shear-resistant sediments.

Zusammenfassung

Weltweit können submarine Massenumlagerungen beobachtet werden, u.a. entlang von aktiven und passiven Kontinentalrändern, in Fjorden, an Flussdeltas oder auch in submarinen Tiefsee-Canyons. Aufgrund des hohen Gefährungspotentials von Offshore-Industrieanlagen, Daten- und Kommunikationskabel oder auch Pipelines sind Analysen und Beobachtungen dieser Massenbewegungen von großem wissenschaftlichen und wirtschaftlichen Interesse. Tsunamis, die von den Hangrutschungen ausgelöst werden können, gefährden an der Küste gelegene Städte und die küstennahe Infrastruktur. Ausgelöst werden die submarinen Hangrutschungen durch verschiedene Faktoren, dazu gehören u.a. die Morphologie des Meeresbodens, die Sedimentzusammensetzung und das dazugehörige mechanische Verhalten der Sedimente, aber auch äußere Einflüsse wie Erdbeben oder Meeresspiegelschwankungen.

Für diese Studie wurden geotechnischer Untersuchungen an gerutschen und ungestörtem Sediment und geophysikalischen Beobachteungen herangezogen um interne Abläufe und Mechanismen während der Rutschungsvorgänge zu charakaterisieren. Aus den Ergebnissen sollenRückschlüsse auf die erforderlichen Auslösemechanismen gezogen werden. Dafür wurden drei submarine Hangrutschungen im Detail untersucht: 1) der Mauritania Rutschungskomplex am passiven Kontinentalrand von Nordwest Afrika, 2) das Ligurische Becken am leicht seimisch aktiven Kontinentalrand von Südost Frankreich und 3) die Kretische See als Forearc-Becken der stark tektonisch aktiven Hellenischen Subduktionszone.

Beim Mauritania Rutschungskomplex (Nordwest Afrika) lässt sich durch geotechnische Messungen ableiten, dass die beprobte Hangrutschung durch mindestens 2 einzelne Rutschungsereignisse entstanden ist. Dabei sind die unteren Sedimente des ersten Ereignisses normal konsolidiert, während der obere Teil stark überkonsolidiert ist. Das auflagerende Rutschungsmaterial des zweiten Ereignisses ist hingegen erneut normal bis nur leicht überkonsolidiert. Um die interne Mechanik der Rutschungsereignisse besser zu verstehen, wurden finite Deformationsanalysen durch-geführt. Die ungestörten hemipelagischen Sedimente zeigen nur geringe Deformations-werte ($R=\varepsilon_1/\varepsilon_3$) von 1-2, die die Verhältnisse während der Ablagerung widerspiegeln. Hingegen zeigt das umgelagerte Material hohe Deformationswerte (R=3->4), die durch Kompression oder Scherung der Sedimente während der Rutschung zustande kommen können. Als Auslösemechansismen für die Hangrutschungsereignisse sind Meeresspiegelschwankungen während glazial/ intergalzial Zyklen in Betracht zu ziehen. Außerdem zeigen die geotechnische Messungen, dass die hemipelagischen Sedimente unterhalb der erbohrten Hangrutschungssedimente durch niedrige Reibungswerte gekennzeichnet sind ($\mu=0.18$) und damit als mechanisch schwache Lagen angesehen werden können.

Aus dieser Studie lässt sich für die aktiven Kontinentalränder der Ligurischen Küste (SE-Frankreich) und der Kretischen See (Griechenland) entnehmen, dass zu den wahrscheinlichsten Auslösemechanismen für Hangrutschungen Erdbeben zu zählen sind. Dazu wurden am Ligurischen Kontinentalhang (SE-Frankreich) im steileren Hangbereich (~20°) zwei verschiedene Hangrutschungskomplexe untersucht. Der erste Komplex befindet sich in einger Entfernung zum Var Canyon und zeigt nur eine abgeflachte Abrisskante. Die Sedimente bestehen aus Debriten und hemipelagischen siltigen Ton. Das umgelagerte Material ist durch ein konstantes Dichteprofil in den Kernen gekennzeichnet. Durch Einbindung von Meerwasser währund der Umlagerung sind diese Sedimente zum Teil unterkonsolidiert. Der zweite untersuchte Rutschungskomplex liegt weiter westlich in der Nähe des Var Canyon und weist mehere einzelne Abrisskanten auf. In den ungestörten wie auch die umgelagerten Sedimenten

lassen sich Verkippungen einzelner Schichten beobachten. Dennoch zeigen alle untersuchten Sedimente eine Zunahme der Scherfestigkeiten mit der Tiefe (bis zu 60 kPa in 4 m Tiefe). Zudem ist das umgelagerte Material überkonsolidiert, obwohl aus geotechnischen Messungen niedrige Reibungskoeffizienten von μ=0.27 hervorgehen. Ein eindimensionales Stabilitätsmodel für diesen Bereich der Hangrutschung hat ergeben, dass die häufig aufteretenden kleineren Rutschungsereignisse durch relativ schwache Erdbeben mit Magnituden von M~1-5,27 (2-22,5 % der Erdbeschleunigung) ausgelöst werden können. Diese Erdbeben haben im Ligurischen Becken eine Wiederkehrrate von 2-9 mal pro Jahr. Hingegen wäre der untersuchte Hang ohne eine seimische Belastung stabil.

Im Fore-arc Becken (Kretische See im Norden Kreta, Griechenland) des stark tektonisch aktiven Kontinentalrand der Hellenischen Subdutionszone werden häufig auftretende submarine Hangrutschungenerwartet. Hingegen wurden in dieser Studie Ablagerungen von Hangrutschungen gefunden, die nur eine Wiederkehrrate von 250 ± 70 Tausend Jahre haben. Geotechnische Untersuchungen an ungestörten wie auch an umgelagertem Material zeigen sehr hohe Scherfestigkeiten mit Werten bis zu 90 kPa in 4 m Tiefe. Dies kann ein Resultat aus zyklisch seismischer Belastung durch Erdbeben sein, die nicht stark genug waren um die Sedimente vollständig zu destabilisieren. Ringscher-Experimente zeigen für das gerutschte Material normale Reibunsgwerte (μ=0.3) aber eine geschwindigkeitsabhängige Abschwächung der Scherfestigkeiten. Als wahrscheinlichster Auslösemechanismus für submarine Hangrutschungen gelten in der Kretischen See Erdbeben im Zusammenhang mit Neotektonik. Ein eindimensionales Hangstabilitätsmodel für die untersuchte Hangrutschung zeigt das Bodenbeschlunigungen von 37-64% der Erdbeschleunigung nötig sind um die abgelagerten Sedimente zu destabilisieren. Im Vergleich mit dem Ligurischen Kontinentalrand sind die Wiederkehrraten der Massenumlagerungen um ein tausendfach niedriger, was darauf hindeutet das Erdbeben mit größeren Magnituden nötig sind um in der Kretischen See Hangrutschungen auszulösen.

1. Introduction

1.1 Motivation

Submarine mass wasting processes are a threat for infrastructures build in coastal areas. Just for the hydrocarbon industry the cost of damage was estimated by the Society for Underwater Technology (SUT) of ~400 million US dollars per year (Mosher et al., 2010). In addition, tsunamis generated by some of the mass wasting processes may endanger coastal areas (including harbours and cities), which could end up with serious consequences because ~41% of the world's population live within 100 km of the coast (e.g. Costanza and Farley, 2007; Martinez et al., 2007). For example, in 1998 a Tsunami hits the northern coast of Papua New Guinea. Therefore a large number of villages were destroyed and ~2200 people lost their lives (Tappin et al., 2001, 2008). It is necessary to understand the mechanisms (evolution and triggering) of mass wasting processes to utilize the results for hazard assessments. Submarine landslides occur in all geological settings and generated in water depths from shoreline to open slope. The current knowledge about mechanics and evolution of submarine mass wasting processes and their related trigger mechanisms is a result of several case studies, international campaigns and drilling programs. In the COSTA program (Continental Slope Stability) an association of researchers analyzed the slope stabilities along the European, NW-African and Canadian margins via investigations of seafloor and sub-seafloor shallow geophysical data (Canals et al., 2004; Lee et al., 2007). Well known study sites are e.g. the Storegga Slide at the NW-Atlantic in front off the Norwegian coast (e.g. Haflidason et al., 2004; Bryn et al., 2005) or the 1929 Grand Banks event in the NE-Atlantic at the Newfoundland coastline, where several communication cables were destroyed (Piper et al., 1999). For these two examples, different types and combinations of pre-conditioning factors and trigger mechanisms may be responsible for the sediment instabilities. However, often the broad spectrum of pre-conditioning factors (e.g. weak layers) and environmental processes (e.g. tectonic movements, human impact) lead to speculations about the role of the type of the triggers and their impact on the mass movement processes (e.g. Masson et al., 2006; Lee et al., 2007; Masson et al., 2010).

The main task of the thesis is to make a contribution to predict temporal and spatial variability of submarine mass wasting processes. To answer that, sediments of different types of mass wasting processes were analyzed with laboratory geotechnical measurements to constrain the mechanics and to reconstruct the temporal evolution of mass movements. Laboratory testing includes the determination of sediment physical properties (bulk density, grain density, water content, porosity), undrained shear strength (C_u, S_u), peak shear strength at failure (τ_f), friction angle (φ) and consolidation (pre-consolidation pressure σ_{pc}). The results were reconciled with, e.g. a fabric analysis study and with sedimentological data. The multimethodological approach proved to be a valuable tool to reconstruct mass wasting processes evolved at two different tectonic areas (active and passive continental margins):

- The Mediterranean Sea is vulnerable for submarine mass movement processes because of the geographical position in a tectonically unstable area at the collision zone of Africa and Eurasia.
- The NW-African continental margin is a passive continental margin with partly high sedimentation rates. Furthermore, this margin is affected by several lapsed and still active channel systems and mass wasting processes.

1.2 Outline of the thesis

When I started to work on my PhD thesis in December 2006, the initial plan was to carry out geotechnical measurements on slope-prone landslide sediments occurred and deposited along active and passive margins. The goal was to identify possible trigger mechanisms and to relate the results from different locations to each other (***Section 2 and 3).*** My PhD thesis was part of the MARUM (Center for Environmental Sciences) research project SD 5 "Trigger and failure mechanisms of gravitational mass movements: Neotectonics – sediment physics – fluid activity" in the research area Sediment Dynamics.

The first aspect of my study should have dealt with the evidences of mass movements in a high seismic and tectonically active area: the Cretan Sea. Sediment cores were already taken in April 2006 during the RCOM cruise P366 with RV Poseidon from mass wasting structures along the north-eastern part of the Cretan Sea. Preliminary investigations of the sediments were done by some of my colleagues, which made it possible for me to start directly to work with a huge data set. Unfortunately, the results of the laboratory measurements just reflect information of hemipelagic drape overlying landslide sediments. It was not possible to figure out conclusions about the development of the mass wasting structures. Nonetheless, the wealth of data found their way into publications to underpin interpretation of seismic profiles to investigate mass wasting structures along the Cretan Sea (***Section 7***).

In order to fill the aspect of mass wasting processes at active margins, I decided to take the Ligurian margin (SE-France) as a new study area. I participated in RV Meteor cruise M73/1 (July-August 2007) that was aimed to recover deposits from several mass wasting events, e.g. Nice Airport Slide, landslides complexes at the deeper slope, turbidity activity. I got the opportunity to learn how operations and deployment of different scientific tools work on a scientific research cruise, and to discuss scientific questions with international colleagues. On the deeper slope of the Ligurian margin, geophysical and bathymetric data are used to identify the geometry of two distinct landslide complexes. In this context, I focused my work on the sedimentary record of the failed as well as the hemipelagic sediments, the physical properties and the geotechnical character of the sediments (***Section 5***).

For ongoing investigations on active continental margins, I attended in October 2007 the RV Meteor cruise M74/2, a leg within the DFG (German Research Foundation) and BMBF (Federal Ministry of Education and Research) funded project "Nitrogen Cycle, Cold Seeps, Carbonate Platform Development in the Northwestern Indian Ocean" at the Makran Accretionary prism in front off the Pakistan coast. I had the opportunity to learn more about other marine research deployments (e.g. Towed Ocean Bottom Instrument) and data processing (e.g. seismic, bathymetry), and to work together with international scientific colleagues. The collected data are summarized in data report in Appendix A of the thesis.

During the same time, colleagues predominately interested in sedimentological research, requested participation in the interpretation of the development of the Mauritania Slide Complex (MSC) offshore the NW-African coast. Sediment samples already recovered in 2006 during the RV Meteor cruise M58/1 offered me to work on mass wasting deposits from a passive continental margin. I decided to focus my research work at first on the MSC because the thesis had to include both aspects, active and passive continental margins. Investigations on the MSC included sophisticated geotechnical measurements and I employed a method for finite strain analysis in "soft" near-surface marine sediments. Strain analyses are more common in hard

rocks, which is why this study was a successful attempt to shed light on deformation processes before, during and after landslide deposition (***Section 4***).

After the work on the Mauritania Slide Complex was completed, I participated on the RV Poseidon cruise P386, where I helped to recover and describe sediment samples taken at the upper slope of the Ligurian margin (in front of Nice, SW France) and to determine first geotechnical sediment properties. I got during the cruise the opportunity to recover some sediment samples from the deeper slope of the area of my research interests. I was also able to connect these newly gained sediment samples and the results from geotechnical tests with the results of my prior research to develop a 1-D infinite slope stability model to unravel seismic loading as the main factor in slope instability in Ligurian margin region (***Section 6***).

2. Mass wasting processes

2.1 Types and definition of mass wasting processes

At continental margins the shelf and slope areas represent important depocentres comprising huge sedimentary sequences with thicknesses of up to several kilometers. Figure 1 shows the range of processes and interactions that influence the transport and the deposition of material from the coast to deeper water regions. Fluvial and coastal input plays an important role for the sediment supply. For example, the 25th world's largest rivers account for ~40 % of the fluvial sediments entering the ocean (Milliman and Meade, 1983; Corbett et al., 2006), in which inherently the Mississippi river accounts for an annual sediment input of ~210 million tons to the Gulf of Mexico (e.g. Corbett et al., 2006; Dail et al., 2007, and references therein). The sediments undergo several cycles of transport and re-deposition, such as floods, currents or torrents, before reaching burial sites. Surface and bottom currents transport sediment particles across the shelf to open waters.

An important factor of transportation and deposition of sediments in deeper water environments are mass wasting processes occurring mainly on continental margins or on island flanks. While continental margins are typically characterised by a low slope gradient with a gentle topography, ocean islands such as the Canary Islands have a great relief with steep slopes up to 15° (Masson et al., 2006). Various classifications of the different mass wasting processes have been conducted and several end-members were identified as slides, slumps, debris flows and turbidity currents (Figs. 1 and 2).

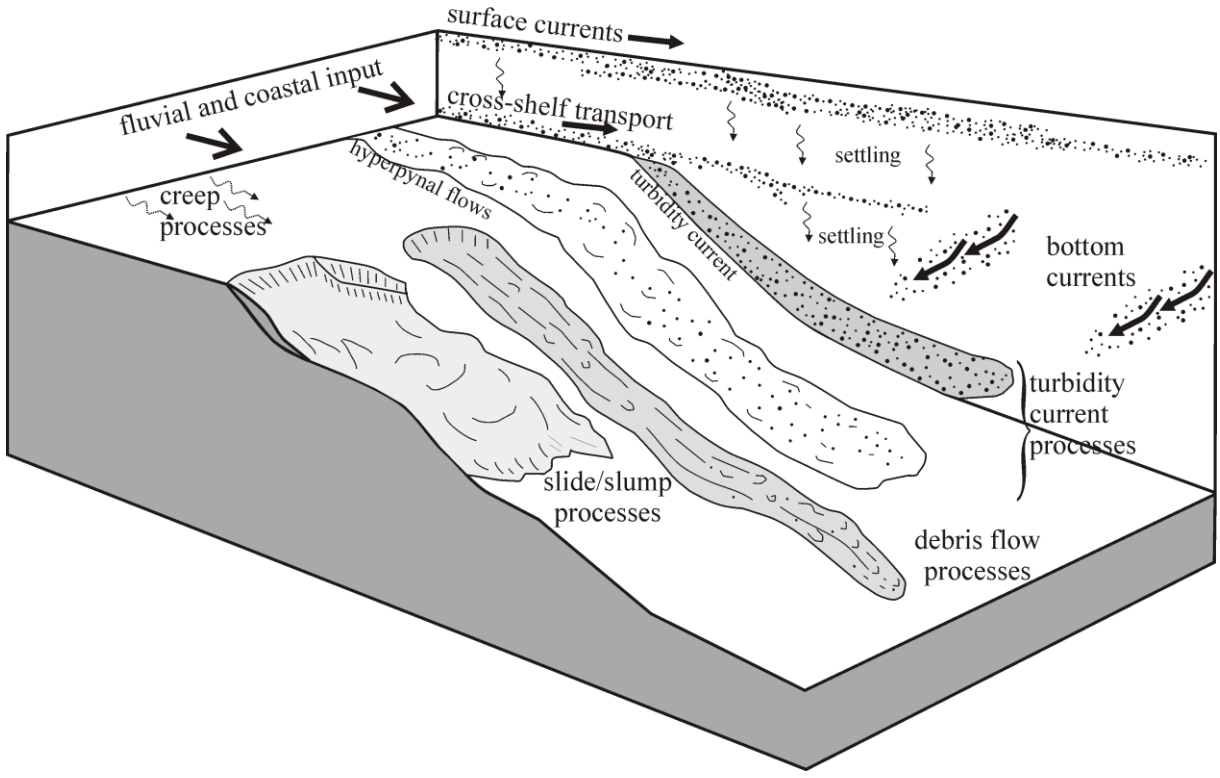

Fig. 1 Schematic diagram of the transportation and deposition processes of sediments in deep-water environments (modified after Stow and Mayall, 2000; Mulder and Alexander, 2001).

An overview about the terminology of the different mass wasting processes used in this study is given as follows (Hampton et al., 1996; Shanmugam, 2000; Mulder and Alexander, 2001; McHugh et al., 2002):

- **Slides** are masses or blocks that moves downslope on a planar shear surface and represents translational movement. The sediment shows minor to no internal deformation structures, but the bedding can be slightly rotated into the hangingwall (e.g. Maltman, 1994). The blocks can be disintegrated in smaller blocks during moving downslope through brittle deformation and can become a **debris slide.**
- Through plastic deformation, blocks and masses move downslope as a **slump**. The sediment failure along a concave glide plane may cause significant internal deformation of the bedding, e.g. folds, boudins, microfaults or shear surfaces (Maltman, 1994).
- Mass flow processes are dominated by plastic flows like **debris flows** and grain flows. Debris flows are laminar, cohesive flows of unsorted clasts in a fine-grained matrix and may results from further disintegration of slumps and mixing the sediment with water. Within this terminology it can be distinguished between sandy debris flows and muddy debris flows, depending on the sediment concentration (Fig. 2). Most debris flow facies tend to show following textures: units with sharp contacts, floating clasts, moderate to high matrix content with inverse grading of the clasts and development of a basal shear zone (McHugh et al., 2002, and references therein). Compared to debris flows, where cohesive and frictional strength of the sediment play an important role, *grain flows* are cohesionless and with sediment concentration of 50-100 vol% (Fig. 2). The grain flows can occur in a viscous regime, where dispersive pressure is derived from interaction of grains and the ambient fluid, while they can also occur in an inertial regime, where the dispersive pressure is caused by elastic grain-to-grain collisions (Middleton and Hampton, 1973, and references therein).

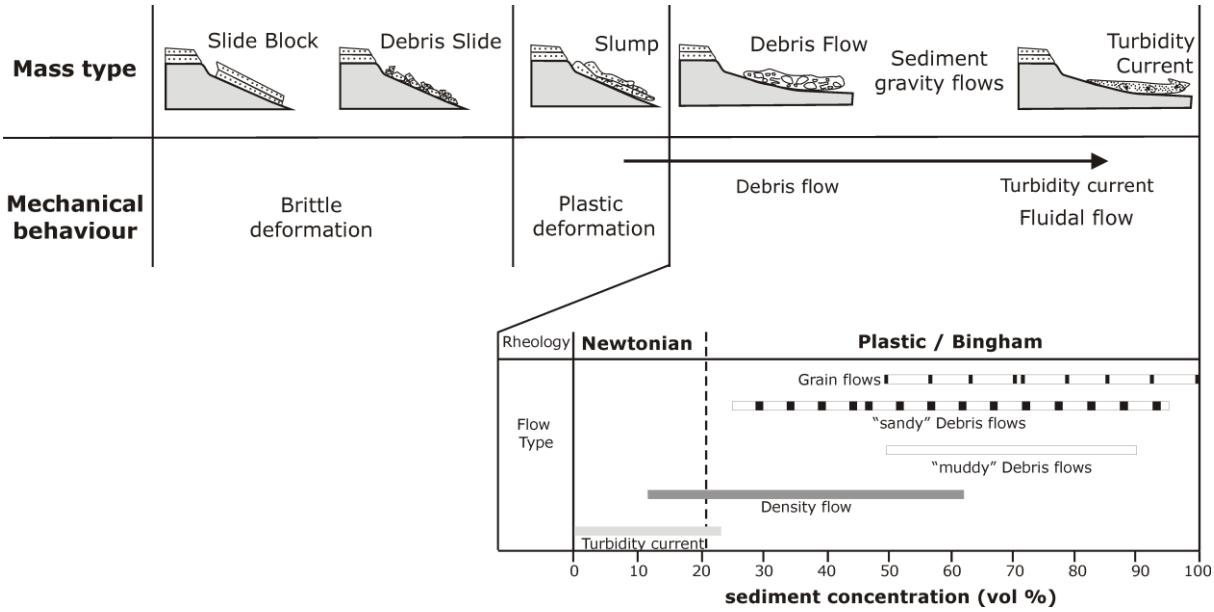

Fig. 2 End-member types of mass wasting processes transporting sediments to the deep-sea, their mechanical behaviour and the different flow types of sediment gravity flows (modified after Middleton and Hampton, 1973; Nardin et al., 1979; Shanmugam, 2000; Mulder and Alexander, 2001; McHugh et al., 2002).

- **Turbidity currents** are gravity flows in which sediments are maintained in suspension by fluid and behave like a Newtonian flow (fluids with no inherent strength). They could result from an increase of the water content (decrease of sediment concentration; Fig. 2) in debris flows and moves further downslope as a turbulent flow. The classical deposit of a turbidity current is a Bouma Sequence (Bouma, 1962) that occurs through unhindered settling of the particles. Hence, normal graded bedded sediments are the results. The ideal Bouma Sequence is characterized by sharp basal contact of massive graded beds, fining-upward grain size with parallel and convolute laminae interpreted as the lower flow regime part and at the top muddy pelagic sediments (Bouma, 1962).
- Figure 1 shows hyperpycnal flows as a part of the turbidity current processes, but strictly speaking they can be counted amongst the *density flows* (high-density turbidity currents), which are characterized by sediment concentrations of 10-60 vol% (Fig. 2). According to the density difference of the flow and the ambient fluid the definition of the hyperpycnal flow is given after Mulder and Alexander (2001), if the density of the flow is larger than the density of the ambient water.
- Besides mass wasting processes it is noticeable that **creeping** is also a mechanism to transport sediments (Fig. 1). It concerns to a steady-state elastic deformation where intergranular cohesionless sliding of particles explains the motion of the sediment. Creeping of the sediments could increase the slope angle preceding initial failures of slides or debris flows (Nemec, 1990).

2.2 Relevance of mass wasting processes

Damages from natural hazards in coastal areas have increased over the last decades beause of the growing population and infrastructure in this realm (e.g. Costanza and Farley, 2007). One part of the natural disasters is submarine mass wasting, which have been studied for decades worldwide, but not fully grasped. Theses processes affect all types of continental margins including glaciated, e.g. the Norwegian continental margin (Laberg et al., 2002; Kvalstad et al., 2005), non-glaciated, e.g. northwestern African margin (Wynn et al., 2000), passive, e.g. eastern US continental margin (McAdoo et al., 2000; McHugh et al, 2002), and active margins such as in the northeastern Mediterranean Sea (Lykousis et al., 2002) and at the western US coast (McAdoo et al., 2000). Along the continental margins several huge landslides are known, from which the Agulhas slump, South Africa, is the largest one with a volume of ~20.000 km³ and an affected area of ~ 79.000 km² (Dingle, 1977).

Because ~41% of the world's population lives within 100 km of the coast (Martinez et al., 2007) and wide distribution of offshore industry installations, scientific and economic investigations of these mass wasting processes are of increasing interest. Submarine landslides, including slides, slumps, debris flows, and turbidity currents are a risk for offshore oil and gas exploitation and installations especially in deep water environments (e.g. piles, conductors and caissons). Furthermore, communication cables, pipelines or wind installations can be destroyed (Hampton et al., 1996; Locat and Lee, 2002; Sultan et al., 2004, Masson et al., 2006; Mackenzie et al., 2010; Thomas et al., 2010). Besides the potential risk analysis, it is important for the oil and gas industry to identify and understand submarine mass wasting processes, because the material is capable as repositories for clastic sediments and hence play an important role for hydrocarbon reservoirs (Barley, 1999; Stow and Mayall, 2000). The potential for tsunamis

triggered by submarine landslides has been recognized all over the world. The 1998 Sissano, Papua New Guinea Tsunami killed more than 2000 people and destroyed three villages completely (e.g. Tappin et al., 2001). The source of the tsunami is postulated as a sediment slump that was preceded by a M 7.1 earthquake. Other examples are the 1945 Makran earthquake (northern Arabian Sea) and the 1929 Grand Banks event (Canada), where great earthquakes (M 7.2 – M 8.1) may cause submarine landslides generating tsunamis (Piper et al., 1999; Rajendran et al., 2008). In the case of the Grand Banks event, the slump transferring to a debris flow initiated a turbidity current that broke transoceanic cables (Piper et al., 1985, 1999).

2.3 Trigger mechanisms and preconditioning factors

Initiation of mass movements occurs when the shear stress acting on sediments exceeds the shear strength, which is defined as the shearing resistance of the sediment. Therefore the shear strength (T_f) resistance is a function of the cohesion (c), the internal friction (φ) and the total normal stress to the failure plane (σ_n) given by the Mohr-Coulomb relation (Coulomb, 1773):

$$T_f = c + \sigma_n \tan \varphi \quad (1).$$

For saturated soils Terzaghi (1943) introduced the principle of the effective stress, σ_{eff}, defined as the total normal stress reduced by pore fluid pressure, u, with

$$\sigma_{eff} = \sigma_n - u \quad (2),$$

resulting in a modification of the Mohr-Coulomb failure criterion for saturated sediments:

$$T_f = c + (\sigma_n - u) \tan \varphi = c + \sigma_{eff} \tan \varphi \quad (3).$$

In the case that the shear stress (destabilizing forces, F_M) exceeds the shear strength (resisting forces, F_R) the sediment will fail. This term can be expressed with the Factor of Saftey (FS) as follows:

$$FS = \Sigma F_R / F_M \quad (4),$$

whereas $FS \leq 1$ indicates sediment failure (see also Chapter 6).

In marine domains different factors have been recognized for destabilizing sediments (Tab. 1). Within such parameters governing sediment instability, we can distinguish between trigger mechanisms and pre-conditioning factors. After Masson et al. (2006, 2010), trigger mechanisms are external short-term events such as earthquakes, storm waves, tectonic movements (including salt movement), volcanic flank collapses and sea-level change. Preconditioning factors are related to a decrease of the sediment shear strength (see above), which may be effected by e.g. presence of weak clay-rich layers, gas discharge, gas hydrate dissociation and excess pore pressure during deposition depending on the sedimentation rate. For example, on the Norwegian coast, more precisely at the Storegga Slide area, glacial sediments are overlying weak layers consisting of water-rich clayey sediments deposited by currents along the continental slope (contourite). Due to rapid loading during glacial periods pore pressure

increased within the clayey sediments that is assumed to be one of the main factors for landslides (Bryn et al., 2005; Kvalstad et al., 2005). Excess pore pressures build up, counteract the normal pressure induced by the weights of solids from the overlying sediment column, and cause a reduction of the shear strength. Also lateral migration of pore fluids (Tab. 1) from adjacent areas to areas with higher sediment thickness may cause excess pore pressure, as fluid pressure can approach equal to the overburden stress (Dugan and Germaine, 2008, and references therein). Change in slope angle induced by e.g. oversteepening or undercutting may also play a role for slope failure. Cochonat et al. (1993) showed that the change of the slope angle in a given time period is an important factor and influences in normally consolidated sediments the thickness of the failed sediment package. Instead Hühnerbach et al. (2004) propose that the steepness of a slope does not influence the occurrence of landslides. Small landslides occurring on steeper slopes involve stiffer material, while landslides occurring on low slopes comprise softer material and tend to be more mobile (Klaucke and Cochonat, 1999).

Oftentimes combinations of two or more triggers and preconditions factors are responsible for sediment failure (Tab. 1). Most continental slopes are stable under the most severe earthquakes, but in combination with other factors the sediments will fail. For the Storegga Slide a combination of weak layers (as mentioned above) and an earthquake were required to change the balance between the stable slope and the mass wasting (Kvalstad et al., 2005; Lee, 2009). Studies of the Amazons fan show that sediment failures occurred in underconsolidated sediments induced by rapid sedimentation during glacial sea-level low stands (Lee, 2009), while at the Mississippi delta the high sediment input procures underconsolidated sediments, which are predestinated to fail under gravitational forces, floods or also during hurricane-induced storm waves (Prior and Coleman, 1980; Hampton et al, 1996, and references therein).

Besides the above mentioned natural conditions or triggers for sediment failure, human activities on the continental slope can also contribute to submarine failures (Tab. 1). Two recent examples are the 1996 Finneidfjord landslide (Norway), and the 1979 Nice Airport landslide event (France). A combination of a heavy rainfall with additional loading of material from a rock blasting tunneling project on an embankment was the main trigger mechanisms for the Finneidfjord landslide (Longva et al., 2003; Cassidy et al., 2008). Heavy rainfall might be the main trigger mechanism for landsliding at the Nice airport too, but at the same time two other combination factors can be taken into consideration as well, like the presence of sensitive weak "quick clays" and an additional load on the upper slope during construction work at the Nice airport (Sultan et al., 2004; Dan et al., 2007).

Table 1 Compilation of factors for the destabilazation of sediments characterized by increasing stress or strength reduction (after Hampton et al., 1996; Masson et al., 2006, 2010).

Increasing stress on the sediment	**Reducing strength of the sediment**	
Earthquakes	Weak layers	Excess pore pressure
Storm wave loading	Gas discharge	
Sedimentary loading	Fluid flow (include seepage)	
Erosion (include undercutting)	Sedimentary loading	
Tectonic movement	Gas hydrate dissociation	
Volcanic island collapses		
Human impact (point loading)		

3. Active vs. passive continental margins: Regional setting of the study areas

3.1 Active vs. passive continental margins

Landslides occur in all geological settings (i.e. active and passive continental margins counting fjords, active river deltas or submarine canyons) and in water depths from the shoreline to the open slope. Comparing the number of landslides with the water depths, the greatest occurrence of mass wasting is found on the slopes of active and passive continental margins (Booth et al., 1993; Hampton et al., 1996; McAdoo et al., 2000; Locat and Lee, 2002; Lee et al., 2007), whereas the distribution of the mass wasting types is not uniformly (Tabs. 2 and 3).

Active margins are marked by either subduction zones or transform fault zones, both characterized by tectonic activity including earthquakes, volcanoes and faulting tectonics. Characteristics of active margins are narrow continental shelves and steep continental slopes as a result of quickly dropping to depths of a trench. Primarily slides and slumps with short run-out distances and small affected volumes are generated (Tab. 2). Involved sediments are dominantly cohesive sediments like hemipelagic sediments. Due to the high tectonic activity it can be assumed that slides and slumps are generated more frequently. Instead, recent studies showed that the contrary is the case (Tab. 2). Only fewer landslides were recognized along the active margins. Higher shear strength in form of overconsolidated accreted sediments may be the key factor for limiting the frequency of sediment failure, because consistently enhanced shear stress may be necessary for sediment failure (i.e. FS ≤ 1). Hence, it was shown that seismic or tectonic activity produce frequent sediment failures.

Similarly, low recurrence times of mass wasting can be observed at passive continental margins (Tab. 3). These margins are marked by a smooth relief with wide continental shelves, minor slope angles and minor or just local tectonic activity. The accumulation of thick sediment piles is mostly controlled by terrigeneous sediments (river or subareal input). The non-cohesive

Table 2 Compilation of some mass wasting assemblages along active continental margins in consideration of their location, type, slope angle, age and affected volume.

Location	Name	Type	Slope angle [°]	Age [ka]	Volume [km³]	Reference
W-Coast USA, California	Sur landslide	slides	5	1.5-5	30	Gutmacher and Normark, 1993
W-Coast USA, Oregon	Cascadian slumps	slumps, slides, debris flows	14-20	110, 450 and 1210	0.5-40	Goldfinger et al., 2000; McAdoo et al., 2000; 2004
	Heceta/Coos Basin/ Blanco Slide				75.6	
Puerto Rico	Insular slope	slides	8.5	not known	1500	Schwab et al., 1993
NW Borneo Trough	Brunei Slide	slides	2-4	1-7	1200	Gee et al., 2007
Syrian margin	Latakia slope	slumps, slides	8-12	not known	10	Tahchi et al., 2010

soil properties of these sediments may cause the occurrence of sediment gravity flows (i.e. debris flow, turbidities; Fig. 2; Tab. 3), which are marked by large run-out distances and large transferred volume compared to the affected volume of slides and slumps (Tabs. 2 and 3). Both margin types can be cut by canyons extending cross the shelves. Turbidites are common mass wasting processes that flush sediments through the canyon building depositional areas where lower canyon gradients were reached.

Landslides occurring at volcanic island flanks are mentioned but not fully discussed here, because the majority of those landslides originate above the sea level. A prominent example of mass wasting processes along volcanic island flanks is the Canary Debris Flow (Canary Island, 13-17 ka B.P.) with a relocated volume of ~400 km³ (Masson et al., 1998). The Hawaii volcanic islands (USA) were consistently affected by slumps and debris avalanches with a total volume of ~5000 km³. Among these, a debris avalanche occurred at Kauai Island affected an area of 14,000 km² (Moore et al., 1989).

Examples where both active and passive margins types could be observed are the two North American margins. An accretionary margin extends along the west coast at the US Pacific margin (e.g. Cascadian; Tab. 2) going along with volcanoes and earthquakes (Hampton et al., 1996; Shanmugam, 2009). Instead, the US Atlantic margin developed by rifting during opening of the Atlantic Ocean and evolved subsidence is influenced by terrigeneous sediment input.

Table 3 Compilation of some mass wasting assemblages along passive continental margins in consideration of their location, type, slope angle, age and affected volume.

Location	Name	Type	Slope angle [°]	Age [ka]	Volume [km³]	Reference
NE Atlantic, Norwegian coast	Storegga Slide	debris flow, turbidite	0.5-2	8, 15	2400-3200	Haflidason et al., 2004; Bryn et al., 2005
NE Atlantic, Norwegian coast	Hinlopen/ Yermak Slide	debris slide, debris flow, turbidite	0.8-3.5	18-30	1350	Vanneste et al., 2006; Winkelmann et al., 2008
E-coast Spain, NW-Mediterranean	Big '95	debris flow	<2	11.5	26	Lastras et al., 2002
SW Sicily, W-Mediterranean	Gela slide complex	debris slide, debris flow	1-3	since 18-24: return intervals 3-4	700	Minisini & Trincardi, 2009
NW-African margin	Bed 5	slide, turbidite	<0.1	60	162	Wynn et al., 2010
S-coast USA	Gulf of Mexico	debris flow, slumps	4	> recent	-687	McAdoo et al., 2000
E-coast USA, North Carolina	Cape Fear Slide	debris flow, slide	3	16.8	1700	Popenoe et al., 1993; Lee, 2009
SE Atlantic, Brazil	Amazon fan	debris flow, slumps, turbidite	<1	14-17, 35, 42-45	2000	Piper et al., 1997; Maslin et al., 1998

As already mentioned above this study intends to relate mass wasting processes and their deposits on passive continental margins (i.e. Mauritania) and along active continental margins (i.e. Ligurian Margin and Cretan Sea), which are influenced by different boundary conditions (e.g. seismicity, tectonic activity, slope morphology, sedimentation rate and climatic conditions). The following chapters provide information about the geological, oceanic and regional setting of each study area.

3.2 Mauritania Landslide Complex, NW Africa: passive continental margin

The research focus for the Mauritania continental margin is the Mauritania Slide Complex (Fig. 3) extending from 17° to 18°N and offshore to 20°W at the passive continental margin of Northwest Africa infront off the coastline of Mauritania. The study focused on the investigation of the mechanics of mass movements and the temporal evolution of the Mauritania Slide Complex (Section 4). The formation of the Northwest African continental margin results from rifting of the Central Atlantic Ocean formation during the Late Triassic and Early Jurassic. The exact onset of the ocean spreading is not well defined but it appears to have initiated first in the southern part. Hence several changes in drift direction occurred, which caused by the South Atlantic opening, Tethys closure and rotation and collision of Iberia. Drift of the African plate started during Jurassic and is still ongoing (Davison, 2005). Rift-sedimentation is marked offshore by deposition of red beds (Brown, 1980) further north of the mapped area extending from 16° N to 23° N within the Senegal-Mauritania Basin (SMB), while onshore Triassic sediments have not been found (Fig. 3; Wissmann, 1982). In other parts of NW-Africa rifting was associated with igneous activity composing of doleritic sills and dykes (drilled ~100 km east of Dakar; Wissmann, 1982 and references therein).

The onshore geological framework of the Senegal-Mauritania Basin along the continental margin is illustrated in Figure 3. The northern boundary of the basin is formed by the Reguibat Shield, a part of the Pre-Cambrian basement. Eastwards and southwards of the basin the Mauritanides extend from Southern Morocco to Sierra Leone (Wissmann, 1982), a Devonian to Carboniferous foldbelt that was thrusted onto cratonic crust and Paleozoic sediments. Westward, the basement dips with ~3° under Mesozoic-Tertiary sediments (i.e. Jurassic-Neogene). Already occurring in Oligocene high sedimentation rates produced the Nouakchott Tertiary Delta that is onshore mostly covered by Quaternary sediments (Fig. 3). During widening of the Southern Atlantic Ocean marine carbonate platform sediments transgressed onto subsiding Paleozoic basement. Onshore these Jurassic carbonates were only recovered east of Dakar (Wissmann, 1982). Offshore, trapped between the Paleozoic basement and the Jurassic carbonates, Late Triassic to Early Jurassic evaporates accumulated in shallow-water conditions. During rifting of the Central Atlantic Ocean a rift shoulder developed a west-dipping normal fault, where in the resulting rift graben salt deposition occurred (Tari et al., 2003). Diapiric structures are present in an elongated zone between 16°N and 19°N (Fig. 3), which extends along the Mauritanian coastline ~300 km in N-S direction (Fig. 3).

Figure 4 shows that the salt and the Jurassic carbonates are separated by an unconformity from the underlying basement, where the carbonates reach several kilometers in thickness. Early Cretaceous sandy rocks are followed by Albian to Lower Cenomanian (Middle Cretaceous) shales and claystones. Transgressive Upper Cenomanian sands and gravels are overlain by Turonian sediments, which pass from sand into gray shales. In the coastal region during the Late Cretaceous carbonates accumulated, while in the offshore part of the SMB sands and gravels are

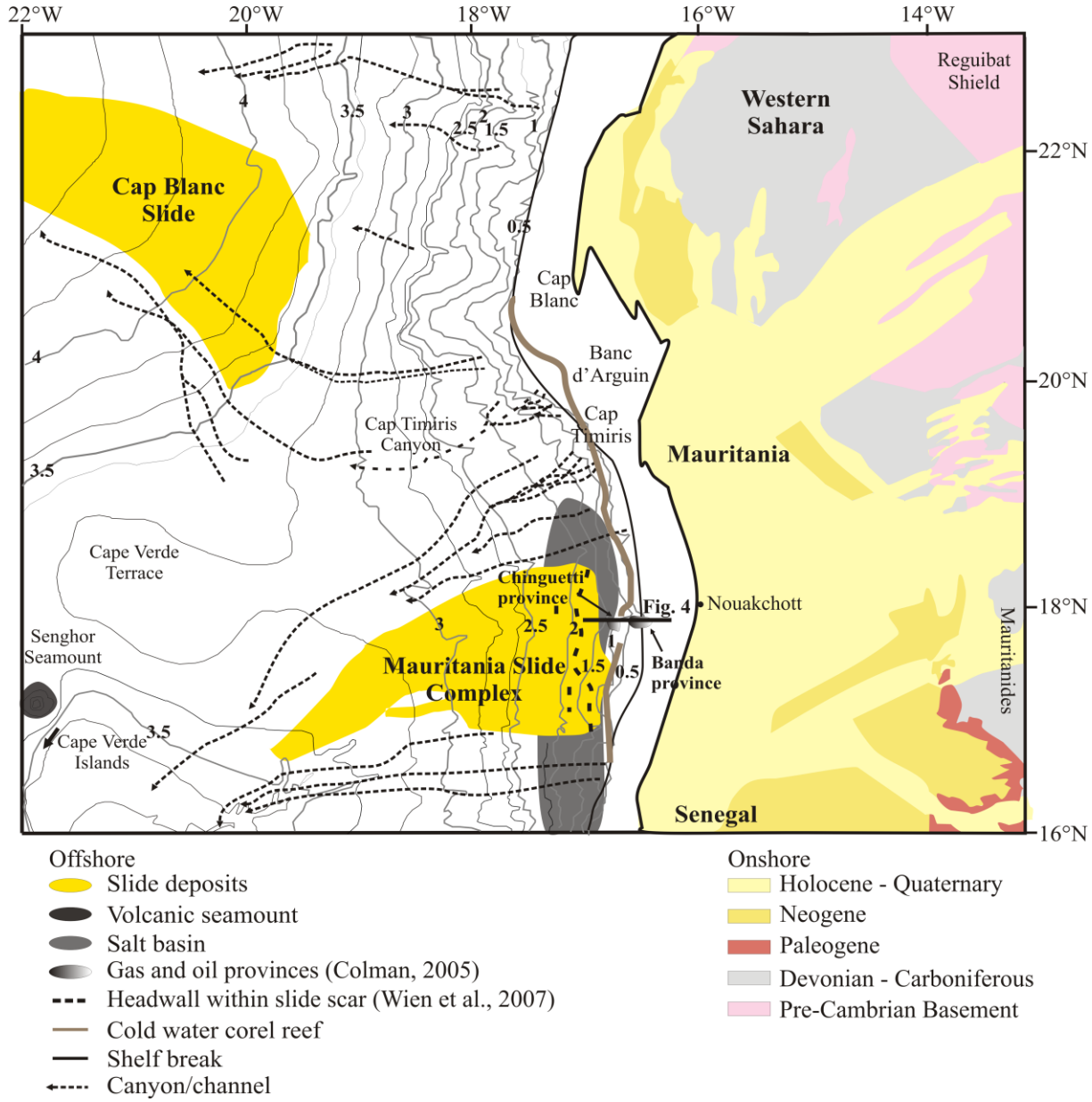

Fig. 3 Onshore geology and offshore bathymetry of the NW African continental margin off the Mauritania coastline. Offshore the extension of two large slides complexes, the Mauritania salt basin and the location of gas and oil provinces are marked after Colman et al., (2005) and Davison (2005).

deposited. A second phase of disintegration of the Paleozoic basement occurred during the Late Cretaceous, established anticlines and accompanied a Jurassic beds climb 3-4 km in synsedimentary fault zones (Fig. 4; Wissmann, 1982). During the Early Tertiary the coastline regressed and carbonates could be deposited. The SMB is flooded as an epicontinental sea (Wissmann, 1982) with developments of canyons, which were filled by sand and turbidites. During the Neogene a reactivation of deep coastal faults occurred. In the Miocene deep water sediments were uplifted and alkaline volcanism took place on the Cape Verde peninsula (Fig. 3). Several slumps and turbidites deposits point towards activity of mass wasting processes starting in the Early Miocene. Canyon and channel systems cut into the sediments since the Pliocene-Pleistocene and outlast several erosional cycles. During the Late Pleistocene sediment supply

was dominated by dust input from the Western Sahara Desert, while fluviatil sediments were restricted to the Senegal region and Banc d'Argiuin (Fig. 3; Zühlsdorff et al., 2007). An increase of fluvial discharge could be related with the onset of the African Humid Period (~15-5 ka BP).

Nowadays, the morphology of the NW-African passive continental margin is affected by several lapsed or still active canyon and channel systems and mass wasting processes (Fig. 3; e.g. Seibold and Hinz, 1974; Jabobi, 1976; Wynn et al., 2000). The continental shelf is 25-50 km wide and breaks at ~ 100 m water depth. The continental slope angle is 1-3° and flattens to <1° in water depths of 2000-2500 m. Located at the shelf edge a cold water coral reef, which consists of a series of large coral mounds, extends ~190 km along the slope from Cap Blanc down to Senegal (Fig. 3). At around 18°N a break of the cold water coral reef can be observed, where two gas and oil provinces are located: the Cinguetti field and the Banda province (Fig. 3). Both hydrocarbon reservoirs show pathways and traps, which were created by salt diapirism and sediment sliding in detachment surfaces of Turonian source rocks (Davison, 2005). High accumulation rates and high local upwelling characterize the whole region of the Mauritania coastline. The recent sedimentation is dominated by upwelling-related biogenic and wind-blown terrigeneous components with sedimentation rates from 0.04 to 0.1 m/ka for midslope and 0.03 to 0.05 m/ka for the lower continental slope (Henrich et al., 2008, 2010). Bottom currents are weak at present, with current velocities ranging between 0.05-0.18 m/s (Lonsdale, 1982; Colman et al., 2005).

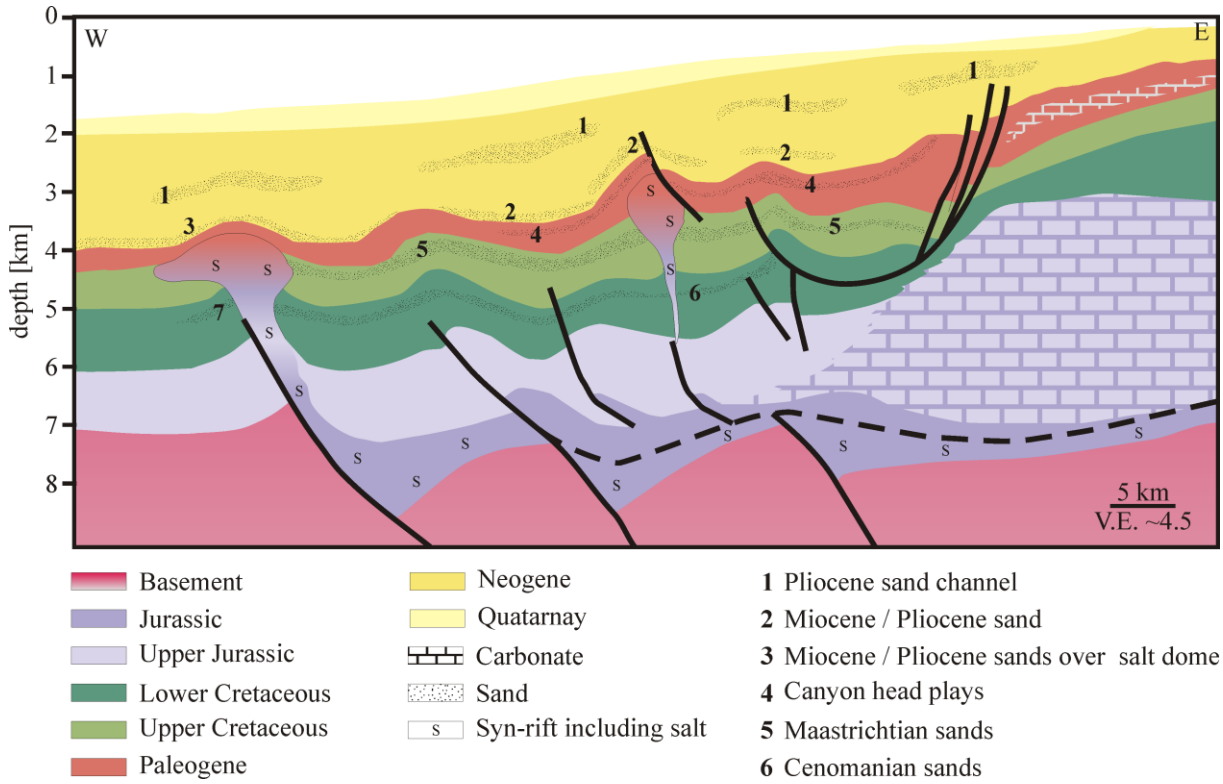

Fig. 4 Offshore geology NW African continental margin off the Mauritania coastline (Davison, 2005 and references therein). Location of the profile is given in Fig. 3.

3.3 Ligurian Basin, SE-France: active margin with low to moderate seismicity

The Ligurian Basin is a tectonically active and complex marginal back-arc basin that was formed by rapid extension during late Oligocene – early Miocene in the Western Mediterranean Sea. The opening and extension of this back-arc basin is known as a consequence of the still ongoing collision between the Africa and Eurasia plates (Fig. 5a) and has led to continental thinning resulting in break up, subsidence and forming oceanic domains (Fig. 5). Rifting of the Ligurian Basin occurred from 30 to 21 Ma (Oligocene – early Miocene), which was locked by the strong continental collision within the Alpine and Apennines belt (Fig. 5a), that led to a ~30° counterclockwise drift of the Corsica-Sardinia block until 16 Ma (e.g. Gueguen et al., 1998; Rollet et al., 2002 and references therein; Béthoux et al., 2008). The present-day active deformation occurs at a small rate of about 1.1 m/ka (Béthoux et al., 1998).

During the Messinian, the sea level drawdown affected the morphology of the Ligurian Basin by strong erosion to depths of about 1500 m below the pre-Messinian sea level (Ryan, 2009). The present morphology of the continental margin and the basin domains result in part from post-Messinian subsidence of about 600 m ± 200 m (Savoye and Piper, 1991; Béthoux et al., 2008 and references therein). The present-day on- and offshore morphology, the geological framework and the major lineaments of the Ligurian Basin are illustrated in Figure 5b. Onshore, three major geological series are present:

- Hercynian basements of the Maures-Estérel Massif and Argentera massif: Variscan metamorphic rocks intruded by Carboniferous granitoids; the Estérel Massif was formed by Permian volcanic eruptions;
- Autochthonous sedimentary cover of the Maures-Estérel Massif;
- Sub-Alpine units comprising e.g. the mesozoic and tertiary nappes of the Castellane and Nice Arcs and the Helminithoides Flysch (Cenomanian-Maastrichtian).

During several seismic studies, the offshore part of the Ligurian Basin was divided into three regions: 1) Ocean domain, 2) transitional zone and 3) continental margins (Fig. 5b). The Ocean domain is characterized by an atypical thinned (<4 km) oceanic crust. Rift-related volcanic activity, which strikes NE-SW, seems to be linked to the subduction processes (Rollet et al., 2002 and references therein). Between the the Ocean domain and the continental margins a transitional zone was identified using multi-channel seismic. This zone is characterized as an oceanic crust consisting of serpentinized periodotites (Contrucci et al., 2001).

The Ligurian continental margin is narrow (~40 km) and formed by two tilted blocks, 20-30 km wide, and a third smaller one only 10-15 km wide (Fig. 5b; Rollet et al., 2002). At the upper continental margin pre-rift sediments containing sedimentary cover of the Maures Massif were discovered. Further downward the continental margin descending to the transitional zone the pre-rift sediments are missing. The acoustic basement, which is interpreted in the transitional zone as volcanic flows (Rollet et al., 2002), is directly overlain by Miocene sediments followed by Pliocene and Quaternary deposits consisting of turbidites and hemipelagic marl. The underlying Miocene sediments can be subdivided into bedded evaporates of the Late Messinian (~5.3 Ma), homogeneous salt layer of the Messinian and into general Miocene slope sediments. The subaereal erosion during the Messinian Salinity Crisis leveled the pre-rift and the synrift sediments of the upper margin and is clearly connected to the base of the Miocene salt layers.

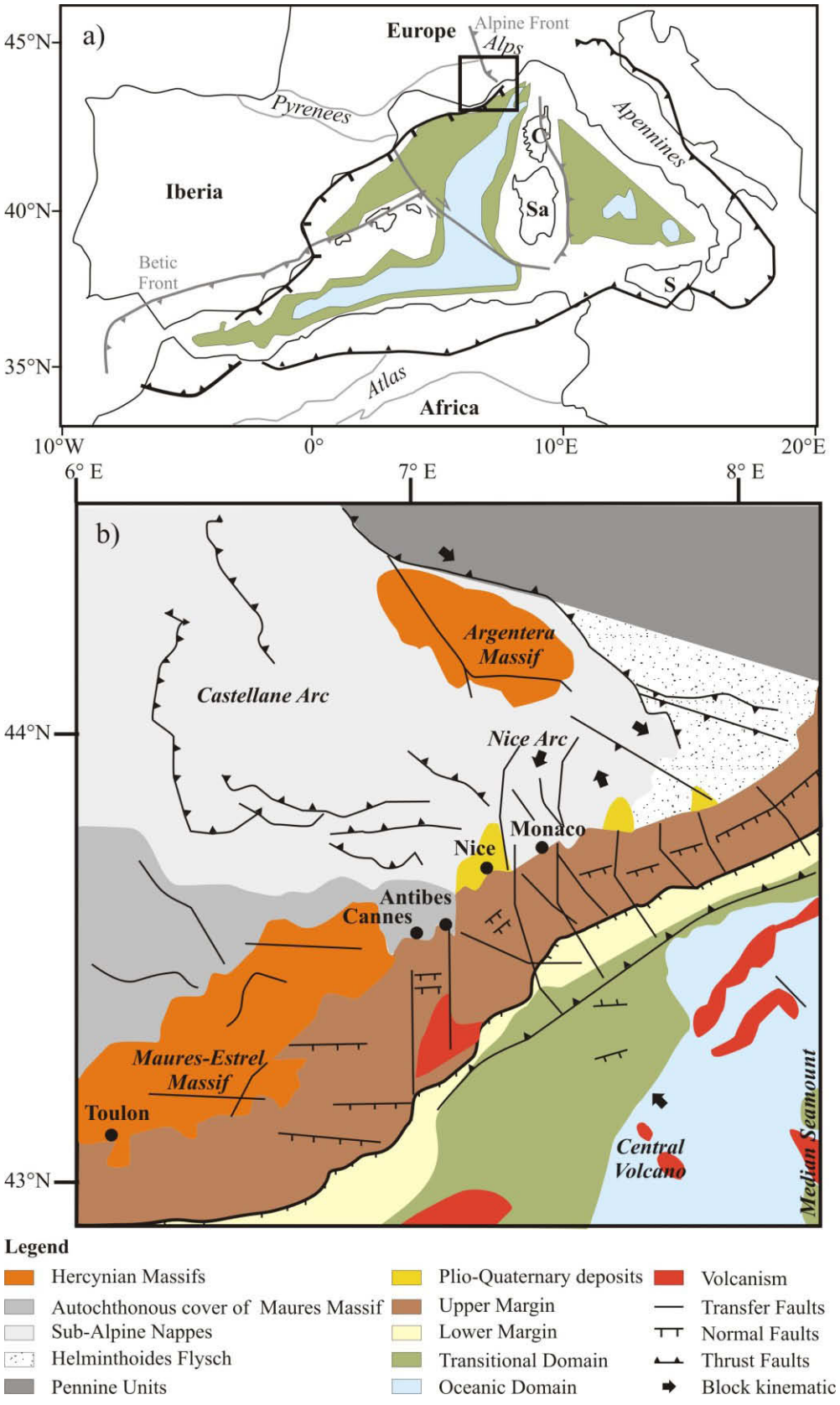

Fig. 5 a) Simplified tectonic sketch of the western Mediterranean with Africa, Iberia, Europe, Silizia (S), Sardinia (Sa) and Corsica (C) modified after Rollet et al. (2002). The black box indicates the position of b) the structural sketch of the Alps-Ligurian (after Larroque et al., 2009).

The permanently installed on- and offshore seismic detection network at the Ligurian margin documents earthquakes with magnitudes of M 2.2 to M 4.5 (Rehault and Béthoux, 1984). Exceptions are destructive earthquakes that are known occurring recently and in historical times, e.g. offshore the 1887 Imperia Earthquake with a magnitude of M 6.5 or the earthquake of July 1963 with M 6.0 and onshore the 1356 Basel earthquake with intensities of the Mercalli Scale IX (Béthoux et al., 1998, 2008) and a smaller one occurred 1999 ~15 km north of Nice and Monaco (M 3.4; Courboulex et al., 2001). It is noticeable that the seismic activity in the Ligurian Basin is concentrated at its northern part, dominantly occurring along the boundary between the continental margin and the transitional or oceanic zone. In contrast the southern and the Corsican margin are aseismic (Béthoux et al., 2008). The occurrence of earthquakes in the hinterland is subjected to the geodynamics of the Alps. In the area between Nice, Monaco and SW of the Argentera massif left-lateral strike-slip faulting along N-NE fractures (Fig. 5b) is the dominant mechanism for occurrence of earthquakes (Courboulex et al., 2007).

The bathymetry of the continental Ligurian margin (Fig. 6) is significantly affected by several canyons, which eroded deeply into Messinian, Pliocene and Quaternary deposits (e.g. Clauzon, 1978; Savoye and Piper, 1991). One good example is the Var River canyon as the offshore extension of the Var River entering the Ligurian Basin west of Nice (Fig. 6). The Var Canyon was excavated during the Messinian Salinity Crisis, filled during the Early Pliocene transgression and became a ria. During the Mid-Pliocene sea level lowstand the canyon was probably activated as a Fan Valley system with a steep delta that leads to the Ligurian abyssal plain (Piper and Savoye, 1993; Migeon et al., 2006). By the time, the direction of the Var Canyon and the Fan Valley shifted a few kilometers to the east and moved to its modern position beneath the northern edge of the high levee of the Var Sedimentary Ridge (Fig. 6). The modern Fan Valley can be subdivided into three sections: 1) The Upper Fan Valley connected at 1600 m water depths to Var Canyon and extending 12 km in SE direction to water depths of ~ 2000 m, 2) the Middle Fan Valley begins where the flow direction bend sharp and extends over 50 km eastwards to ~2500 m water depths with a decrease in slope angle from 2° to 0.3°, and 3) the SE directed Lower Fan Valley reaches in 2700 m water depths the sandy lobe at the base of the slope of Corsica (Piper and Savoye, 1993; Migeon et al., 2001, 2006).

The region of the study area is close to the Nice slope (Fig.6) and is characterised by a very narrow or absent continental shelf (2-3 km) and a steep continental slope with an average slope angle of ~11°. The margin is fed with material from several mountain-supplied rivers. With a river discharge of 180 - 400 m^3/s (Mulder et al., 2001) the Var River is the most relevant one. But during floods sediment concentration can reach tens of kg/m^3 and the river discharge exceeds 1227-2346 m^3/s resulting in hyperpycnal flows (Mulder et al., 2001). Besides the Var Canyon the Paillon Canyon represents an erosive structure but is recently negligible for sediment supply. The three major mass wasting processes at the Var Canyon are 1) earthquake-induced turbidity currents, 2) low-density turbidity currents related to retrogressive failures and 3) hyperpycnal flows during floods (Mulder et al., 2001). During MARUM (Bremen) and IFREMER (Brest) research cruises (e.g. Kopf et al., 2008, 2009) deposits of several mass wasting processes were found (Fig. 6). Due to the fact that mass wasting processes are very common at the Var Canyon area (Fig. 6), sedimentation rates should be treated carefully. A first assumption was done by Sultan et al. (2004) with sedimentation rates of 8 m/ka between 12 ka and 7 ka BP, and 3.5 m/ka from 7 ka BP until now.

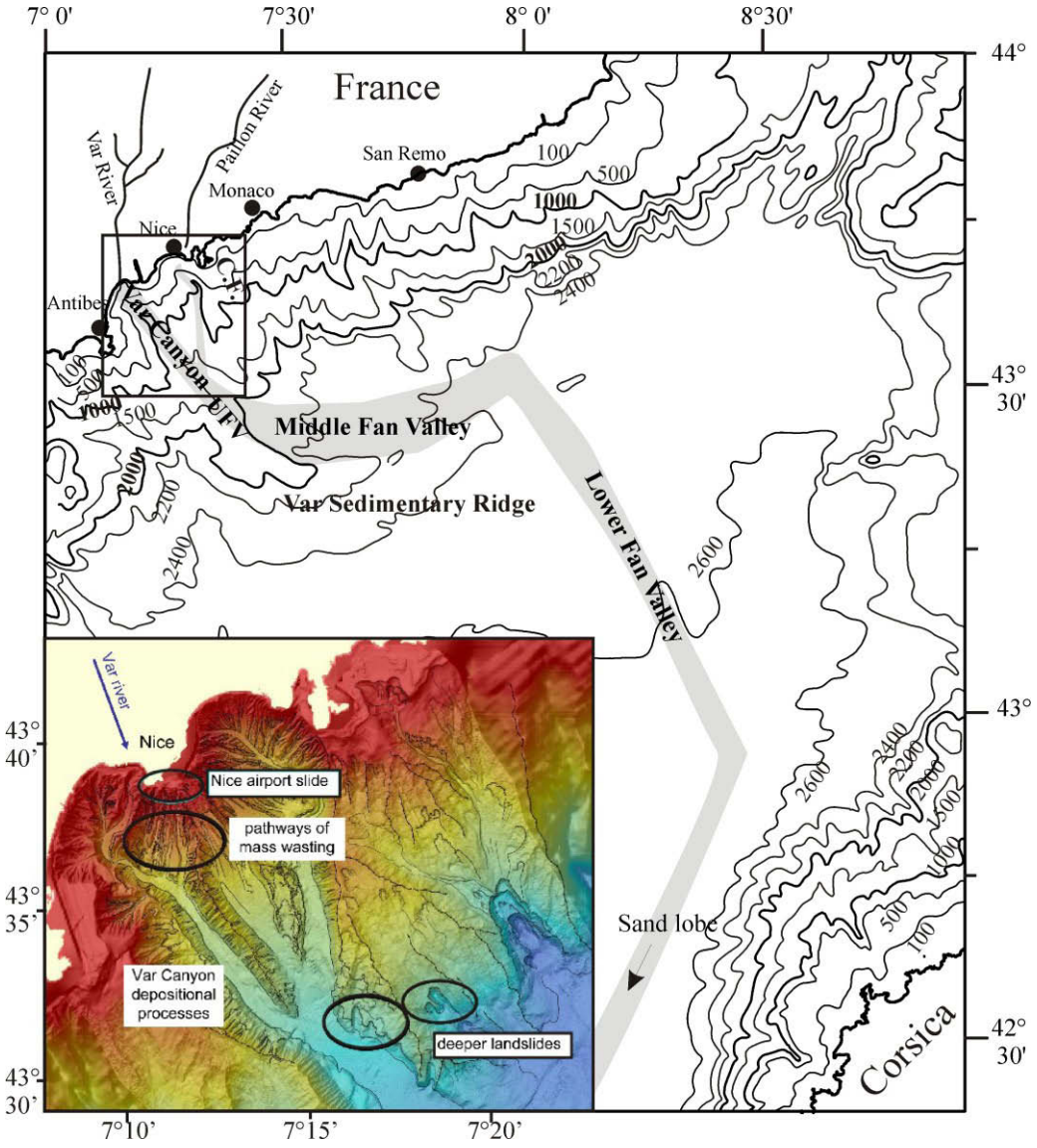

Fig.6 Simplified bathymetric chart of the Alps-Ligurian Basin with depositinal and erosive areas of the Var Canyon (after Piper and Savoye, 1993; Mulder et al., 2001). Small map: detaild high-resolution bathymetric map of the Upper Fan Valley and the Var Canyon with location of several mass wasting processes (Kopf et al., 2008).

3.4 Cretan Sea: active margin with moderate to high seismicity

3.4.1 The Hellenic Subduction Zone

The Cretan Sea is located at the northern margin of Crete (Greece) and represents the fore-arc basin of the Hellenic Subduction Zone at the Eastern Mediterranean Sea (Fig. 7). The geological framework of the Hellenic Subduction Zone is a key feature of the Alpine-Himalayan orogeny and is linked to the collision of the African lithosperic plate with the Aegean micro plate, which collides with the Eurasian plate in ENE-WSW direction (Anderson and Jackson, 1987; Ganas and Parsons, 2009). It is known from metamorphic rocks in the Cyclades (Greece) that during the Mid-Eocene the Aegean area was characterized by a >50 km thick continental crust as a result of a compress ional regime (Sodoudi, 2005). The age of the transition from

compression to extensional regime range from Late Oligocene to Late Miocene, whereas McKenzie (1978) proposes that the plate convergence appears to be active since 35 million years. With a mean speed of ~30 mm/year the plate convergence is still proceeding (Fig. 7), in consequence of the subduction of the African lithosphere (NE-moving direction with a rate of ~10 mm/year) beneath the Aegean micro plate (speed of ~ 40 mm/year in SW-direction). The African slap dips with an average angle of 15-20° increasing eastwards to 30-40° in ~180 km depth beneath the Aegean micro plate (Papazachos et al., 1995; Ganas and Parsons, 2009; Strozyk, 2010). The deformation of these Aegean micro plate, defined as a rigid block (Ganas and Parsons, 2009), is affected by the westward motion of the Anatolian block with a slip velocity of 24 mm/year in the North Anatolian Fault (NAF; Fig. 7.; McClusky et al., 2000), whereas to the boundary to the Anatolian Plate the motion is much slower (Sodoudi, 2005 and references therein). The initiation of the NAF was induced during the Pliocene (~5 My), a time phase where the extension may intensified.

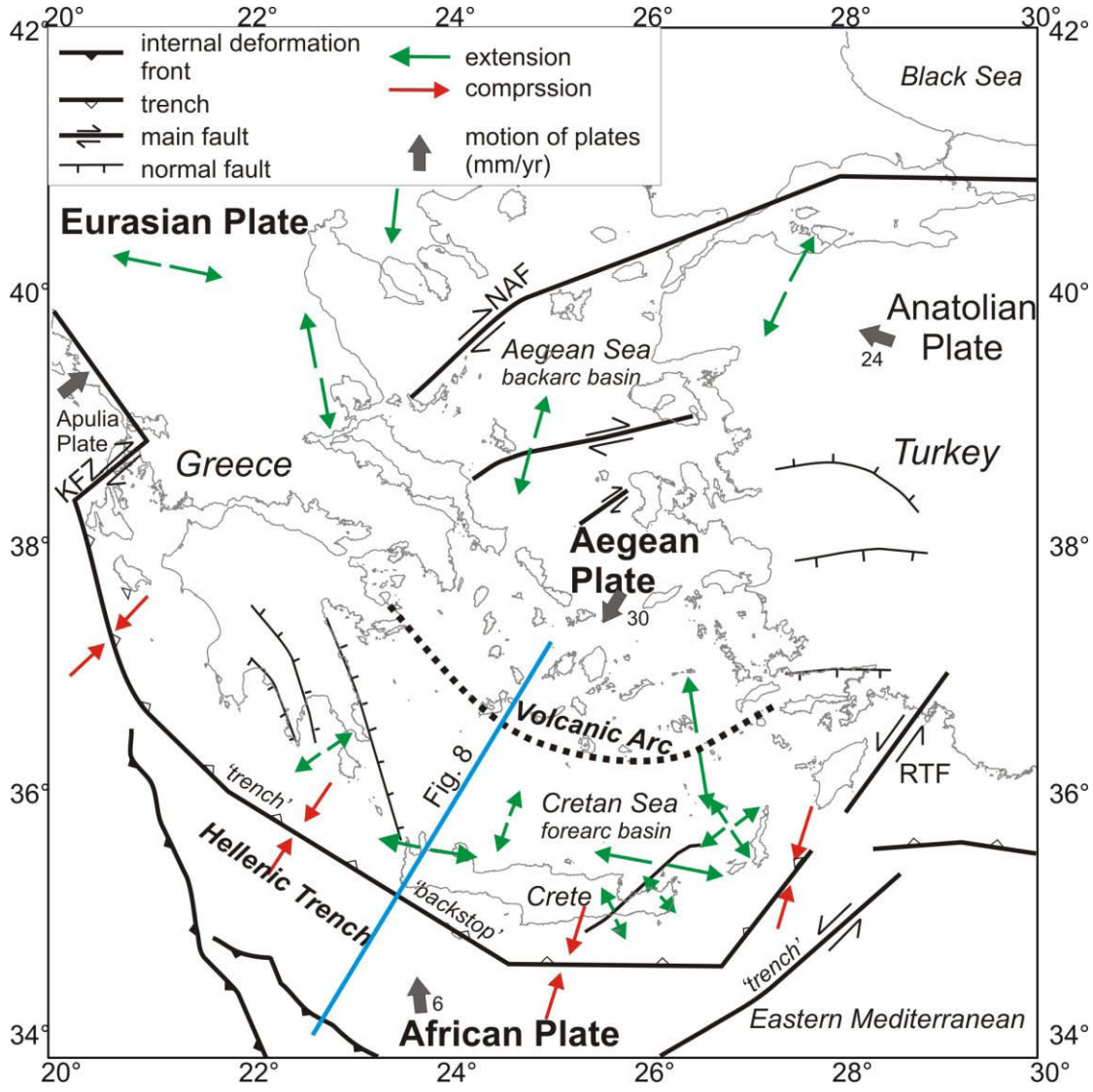

Fig. 7 Sketch of the Eastern Mediterranean plate boundaries and moving directions. Black arrows indicate the direction of the motion relative to the Eurasian Plate. The values (mm/yr) are shown near the arrow (after McClusky et al., 2000). Green and red arrows indicate direction of extension and compression of faults, trenches and internal motion of the plates.

Figure 8 shows a profile crossing the subduction slap and the several accompanying geodynamic processes, e.g. sediment accretion, volcanism and fore- and backarc extension:

- Accretionary complex: the sedimentary cover of the African slap is accreted to the Eastern Mediterranean Ridge south of Crete resulting in an Accretionary complex with E-W total length of 1200 km from 20-29°E and about 250 km N-S-extension from 35-38°N (Fig. 7).
- Backstop domain: known as the inner ridge, is a narrow depression, which is a result of backthrust of the Accretionary wedge (Fig. 8). Thereby it is part of the Hellenic Trench System, comprising several arc-parallel trenches (Meulenkamp et al., 1988; Chaumillon and Mascle, 1996).
- Central fore-arc of the Hellenic Subduction Zone: the island of Crete represents a horst structure of thrust nappes of variable lithologies (more details see e.g. Fassoulas et al., 1994, Ring et al., 2001) governed by the roll back of the Accretionary complex. The backstop provides an uplift of Crete with a continuously rate about 6 mm/a (Ganas and Parsons, 2009). Active tectonic kinematics of the fore-arc shows E-W-extension along the arc as well as N-S-extension in the middle part (Fassoulas, 2001; Ganas and Parsons, 2009).
- Fore-arc basin: a N-S-extension is also retrieval at the Aegean Sea, resulting in E-W elongated depressions. Appendent to the Southern Aegean (Giresse et al., 2003) the Cretan Sea is one of these elongated depression bordered by the volcanic arc /backarc basin in the north and by the fore-arc high (Crete island) in the south. The morphology of the Cretan Sea follows more or less the curvature of the Hellenic trench (Figs. 7 and 8). Extension was accommodated along of N-S-trending normal to strike-slip faults and blocktilting resulting in subsidence. The subsidence rates increase from west to east along the Cretan basin. A more detailed description of the regional setting of the Cretan Sea is given in Section 3.4.2 (see below).
- Back-arc and volcanic arc: the volcanic arc, corresponding to the Cyclades (e.g. Santorini, Milos, Ios), separates the Cretan Sea from the Aegean Sea back-arc basin (Figs. 7 and 8). Just as the Cretan Sea, the volcanic arc follows approximately the curvature of the Hellenic trench and extends from 23-27.5° W to 36.5-38° N (Fig. 7). The back-arc basin is seen as a high plateau (about 350 m water depth) and is dominated by E-W-trending major active crust faults with an N-S extensional regime. Northwards the Aegean Sea is bounded by the North Anatolian Fault, which belongs to the Anatolian plate system (Fig. 7; Sodoudi, 2005).

The region of the Eastern Mediterranean is most prominent for high seismic activity. Major earthquakes generate in the Accretionary complex of the Hellenic Arc south of Crete (Figs. 7 and 8), which is mainly caused by NW-SE convergentl movements of the African and Aegean plates. The largest recent earthquake at the Hellenic Arc had magnitudes of M 7.3 (Ambraseys, 2001). In the fore-arc region earthquakes are caused by the E-W-extension as well as by the backstop, which is related to the uplift of the Island Crete (Meier et al., 2004). Stiros et al. (2001) suggested that earthquakes, which occurred near Crete in 365 A.D. and 1856, had magnitudes of M >8.

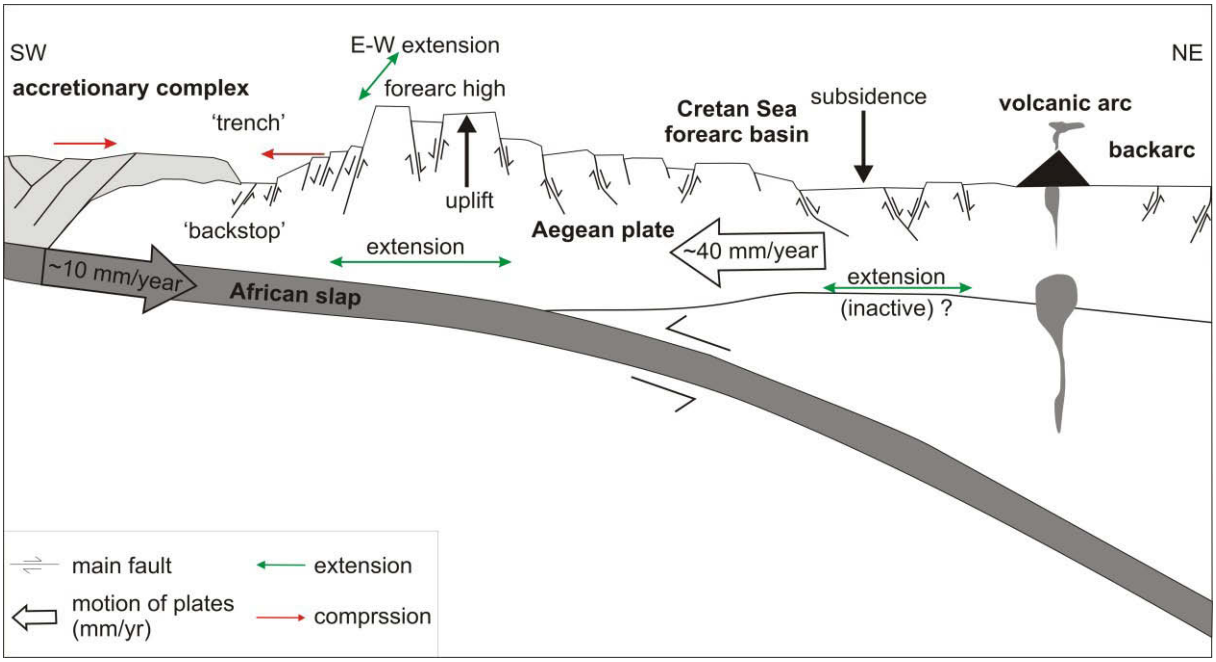

Fig. 8 SW-NE cross-section of the Hellenic Subduction Zone (with vertical and horizontal exaggeration) showing the geodynamic processes: accretion, back-stop, volcanism, forearc- and backarc-extension (modified after Fassoulas, 2001; Kopf et al., 2006). For location of the profile see Fig. 7.

A model for the Hellenic Subduction Zone in the area of Crete based on seismological investigations (Meier et al., 2004; Becker et al,, 2006). The plate boundary and the top 20 km of the continental crust below Crete is characterised by high microseismic activity (Becker et al., 2006, and reference therein). In contrast, the fore-arc basin (Cretan Sea) is an aseismic area because the Aegean plate is decoupled from the subducted African plate. Recent seismic events results from intraplate motions (extension/compression) along seismicity results from northern NE-dipping and southern SW-dipping faults (Meier et al., 2004; Becker et al., 2006). The seismicity of the volcanic arc in the Northeast is generally lower than in the fore-arc region. Volcanic activity may be directly linked to magma/fluids migration towards the surface (Bohnhoff et al., 2006), which is accompanied by seismic events. The two largest recent earthquakes (occurred in 1956) were located between Santorini and Amorgos (eastern part of the Cyclades) and reached magnitudes of M 7.2-7.4 (Bohnhoff et al., 2006). In the northern region of the Aegean plate (Aegean Sea) extensional tectonic with a strike slip component, related to the North Anatolian Fault, may initiate strong shallow earthquakes of M 4-7.3 with epicentre depth of 3-8 km (Lykousis et al., 2002, and references therein).

3.4.2 Regional setting of the Cretan Sea

The Cretan Sea is one of the Southern Aegean subbasins, a large depression border by the volcanic arc of the Cyclades and the Aegan back-arc basin in the north and by the forearc high of the island Crete in the south. The main basin creation phase is suggested to be occurred during the late Miocene and Pliocene (Mascle and Martin, 1990). The extension was accommodated

along of N-S-trending normal to strike-slip faults and blocktilting resulting in subsidence. The subsidence rates increase from west to east along the Cretan Sea. Furthermore, Mascle and Martin (1990) and Ring et al. (2001) suggested that in addition to crustal blocktilting and formation of half-grabens occurred, whether the formation of the graben system could not allocated to compression or extension. However, the N-S and E-W extensional regime still occur today: deformation (extensional) phenomena are minimal while seismicity and volcanic activity is still active in this area. (e.g. McKenzie, 1978; Mascle and Martin, 1990; Ring et al., 2001).

The Cretan Sea comprises several deep sub-basins (>2000 m) separated by ridges of variable heights surrounded by well-developed continental slopes. The water depths are around 1000 m. The Kamilonisi Basin in the eastern part of the Cretan Basin even reaches water depths ~2500 m. At the northern margin of the island Crete the Cretan Sea revealed steep slopes of up to 4° (Kopf et al., 2006 and references therein). Hemipelagic sediments accumulated in the mid-slope region with an estimated sediment accumulation rate off ~7-20 cm/ka for the Northern Cretan Margin as well as for the Cretan Sea sub-basins (e.g. Giresse et al., 2003).

Because of the tectonic movements and the earthquake activity the whole region of the Cretan Sea is prone to landsliding. Also a steep slope angle and the rapid sedimentation rates (see above) may cause potentially unstable slopes. Several former studies investigated the tectonic setting, volcanic activity and the hydrological/sedimentological processes that may lead to landslides (e.g. Lykousis et al., 1995; Chronis et al., 2000; Lykousis et al., 2002; Kopf et al., 2006). In addition a DSDP (Deep Sea Drilling Project) expedition brought up the deep lithostratigraphy of the central Cretan Sea at DSDP Site 378 in the Heraklion Basin (Hsü et al., 1978). The drill site recovered Quaternary marl and ooze with sapropelic layers in the upper 100 m. Several sapropels were also embedded in near-surface sediments, together with ash layers. These ash layers have been used as marker horizons for volcanic eruptions such as the Minoan Z2-Santorini event (3370 BP). Additionally, ash layers from other volcanic events were recovered during several campaigns in the Cretan Sea (Pichler and Friedrich, 1976; Giresse et al., 2003; Kopf et al., 2006).

4. Geotechnical characterization and strain analyses of sediment in the Mauritania Slide Complex, NW-Africa

Förster, A. [1], Ellis, R.G. [2], Henrich, R.. [1], Krastel, S. [3] Kopf, A.J. [1]

Published in *Marine and Petroleum Geology (2010), 27, 1175-1189.*

Abstract

Mass wasting processes are a common phenomenon along the continental margin of NW-Africa. Located on the high-upwelling regime off the Mauritanian coastline, the Mauritania Slide Complex (MSC) is one of the largest events known on the Atlantic margin with an affected area of ~ 30.000 km^2. Understanding previous failure events as well as its current hazard potential are crucial for risk assessment with respect to offshore installations and tsunamis. We present the results of geotechnical measurements and strain analyses on sediment cores taken from both the stable and the failed part of the MSC and compare them to previously published geophysical and sedimentological data. The material originates from water depths of 1500 - 3000 m and consists of detached slide deposits separated by undisturbed hemipelagic sediments. While the hemipelagites are characterized by normal consolidation with a downward increase in bulk density and shear strength (from 1.68-1.8 g/cm³, 2-10 kPa), the slid deposits of the uppermost debris flow event preserve constant bulk density values (1.75 and 1.8 g/cm³) with incisions marking different flow events. These slid sediments comprise three different matrix types, with normal consolidation at the base (OCR=1.04), strong overconsolidation (OCR=3.96) in the middle and normal consolidation to slight overconsolidation at the top (OCR=0.91-1.28). However, the hemipelagic sediments underlying the debris flow units, which have been ^{14}C dated at <24 ka B.P., show strong to slight underconsolidation (OCR=0.65-0.79) with low friction coefficients of μ=0.18. Fabric analyses show deformation intensities R ≥4 (ratio σ_1/σ_3) in several of the remobilized sediments. Such high deformation is also attested by observed disintegrated clasts from the underlying unit in the youngest debrites (^{14}C age of 10.5-10.9 ka B.P.). These clasts show strong consolidation and intense deformation, implying a pre-slide origin and amalgamation into the mass transport deposits. While previous studies propose an emplacement by retrogressive failure for thick slide deposits separated by undisturbed units, our new data on geotechnical properties, strain and age infer at least two different source areas with a sequential failure mechanism as the origin for the different mass wasting events.

Key words: Landslides, Geotechnical characterization, Fabric analyses, Debris flow, NW-Africa continental margin

[1] MARUM - Center for Marine Environmental Sciences, University of Bremen, PO box 330 440, 28334 Bremen, Germany.

[2] Geological Sciences, Brown University, 324 Brook Street, Providence, RI 02912, USA.

[3] Leibniz Institute of Marine Sciences – IFM-GEOMAR, Wischhofstr. 1-3, 24148 Kiel, Germany.

4.1 Introduction

4.1.1 Relevance of the Mauritania Slide Complex

With approximately 41% of the world's population living within 100 km of the coast, (Martinez et al., 2007) investigations of geologic hazards are of increasing importance (e.g. Locat and Lee, 2002; Sultan et al., 2004; Masson et al., 2006). Typical offshore geohazards are earthquakes, landslides, volcanism and tsunamis. This paper focuses on landslides processes whose exact trigger mechanisms are poorly understood. Triggers encompass those driven by external forces such as earthquakes or sea-level change, and those related to the mechanical characteristics of the sediments such as excess pore pressure (rapid sedimentation, oversteepening of the slope gradient), gas discharge and gas hydrate dissociation, seepage or the presence of weak, clay-rich layers (as pre-conditioning factors). Oftentimes, combinations of two or more triggers are responsible for sediment failure. Among the potential geohazards, mass wasting processes are attracting increasing societal interest as they threaten to destroy offshore platforms, communication cables and wind installations, while the resulting tsunamis endanger coastal cities and harbors (Hampton et al., 1996; Masson et al., 2006).

The Mauritania Slide Complex (MSC) is situated on the Chinguetti and Banda Province oil fields (Fig. 1b; Colman et al., 2005) in an area characterized by high accumulation rates and high local upwelling. Hydrocarbon prospecting and production there necessitate a better understanding of submarine sediment stability.

Previous studies focused on the interpretation of the architecture and evolution of the MSC with seismic data (Krastel et al., 2006a; Antobreh and Krastel, 2007) and sedimentological core records (Henrich et al., 2008). These results are the basis for our study using geotechnical laboratory methods (shear and oedometer testing) and quantitative fabric analyses (Fry, 1979) to better constrain the mechanics of the mass movement and to reconstruct the temporal evolution of the debris flow units within the MSC.

4.1.2. Regional setting of the study area

The Mauritania Slide Complex (MSC, Fig. 1) is located at N16°-19° on the passive continental margin off the Mauritanian coastline, NW-Africa. During earlier studies, N-S-trending mass movement deposits and channel systems were found (Seibold and Hinz, 1974; Jacobi, 1976; Jacobi and Hayes, 1982; Wynn et al., 2000). In our study area the shelf is 25-50 km wide and breaks at ~100 m water depth. The continental slope angle is typically 1-3° and flattens at 2000-2500 m water depth to <1° (Fig. 2). However, with an estimated affected area of ~30.000 km^2 and a total volume of 600 ± 100 km^3 the MSC is one of the largest submarine landslides known along the Atlantic margin (Antobreh and Krastel, 2007). The MSC starts some 70 km off the coast of Mauritania and follows a complex channel-levee system more then 300 km westward (Fig. 1a). At the shelf edge (water depths of ~ 500 m) the MSC is limited by a cold-water coral reef which consists of a series of large coral mounds extends 190 km along the slope (Colman et al., 2005; de Mol et al., 2009). Oceanic upwelling is concentrated along the outer shelf and upper slope and undergoes seasonal migration. Wind-born terrigenous and upwelling-related biogenic components dominate recent sedimentation at the MSC. During the late Pleistocene terrigenous sediment supply was dominated by aeolian dust from the Sahara Desert, while fluvial input was restricted to areas north and south of the MSC (Zühlsdorff et al., 2007, and references therein). An increase in fluvial discharge along the Mauritania continental

margin is related to the onset of the African Humid period with interruption by colder and warmer intervals (~15 - 5 ka B.P., deMecocal et al. 2000; Fig. 1a).

At present, river input from the Senegal River (entering the coast southwards) can be excluded as a notable sediment source (Wien et al., 2007). Recent sedimentation rates are given from 0.04 –0.1 m/ka for midslope (Henrich et al., 2008) to 0.03-0.05 m/ka for the lower continental slope (Henrich et al., subm.). Bottom currents along the margin are weak at present, with current velocities ranging between <0.05 m/s (Lonsdale, 1982) and, when using the OCCAM global circulation model, < 0.18 m/s (Colman et al., 2005).

Along the Mauritanian coastline, a flat salt basin extends ~ 300 km in N-S direction (Fig. 1a) and is characterized by Triassic-Early Jurassic age evaporite deposits from a rifting phase of the Central-Atlantic (Tari et al., 2003). Entrapments for gas and oil were found beside the salt domes, which are overlain by Miocene and Upper Cretaceous sediments. The hydrocarbon pathways and traps were created by salt diapirism and sediment sliding on detachment surfaces (Davison, 2005). Gas migration and the resulting decrease in effective stress may add to present-day landslide risk (see discussion below).

4.1.3 Previous studies on the Mauritania Slide Complex

During the RV Meteor cruises M58/1 and M65/2 (Schulz et al., 2003; Krastel et al., 2006b) more than 1200 km of parasound (parametric narrow-beam sediment echosounder) and 900 km of high resolution multi-channel-seismic profiles were collected, covering water depth from 200 m to > 3500 m. In addition, a total of 10 gravity cores were collected during these cruises. Studies by Krastel et al. (2006a), Antobreh and Krastel (2007) and Henrich et al. (2008) took the MCS data as well as results from sedimentological core analyses to show the structural setting of the MSC in detail. Seismic and parasound data show that the headwall area is characterized by detached slide blocks, canyons and gullies and a stepped pattern of slide scars, each ranging 25 m to 100 m in height (Fig. 2; Antobreh and Krastel, 2007). In the shallow slope below 2000 m water depth, the main depositional area of the slide is found to comprise blocky debris (Fig. 2). Stacked debris flow units separated by thin (10-20 m) well-stratified sediment packages were interpreted using seismic data. The youngest of the debris flow units has a length of more than 300 km and displays thicknesses of 25 m to 45 m in its central part (Antobreh and Krastel, 2007; Wien et al., 2007). Similar flow deposits were not found beyond a small channel-levee system (Figs. 1b and 3) on the southern edge of the complex, most likely because it acted as a boundary during the emplacement (Krastel et al., 2006a; Antobreh and Krastel, 2007). Furthermore, small sharp elevations on the seafloor were identified on seismic profiles and later were confirmed to be cold-water coral carbonate mounds based on gravity coring (Fig. 2; Schulz et al., 2003; Krastel et al., 2006a; Antobreh and Krastel, 2007).

The seismic data collected do not show indications of gas hydrates (e.g. bottom simulating reflectors). However, acoustically transparent layers may indicate either the presence of free gas or high porewater contents. Either explanation may be responsible for widespread excess pore pressures in sediments (Krastel et al., 2006a; Antobreh and Krastel, 2007). It is known that gas and oil can be found in turbidites of Miocene to Late Cretaceous age (largely in water depths greater than 500 m; Coleman et al., 2005; Davison, 2005), but a migration into the overlying sediments has not been reported.

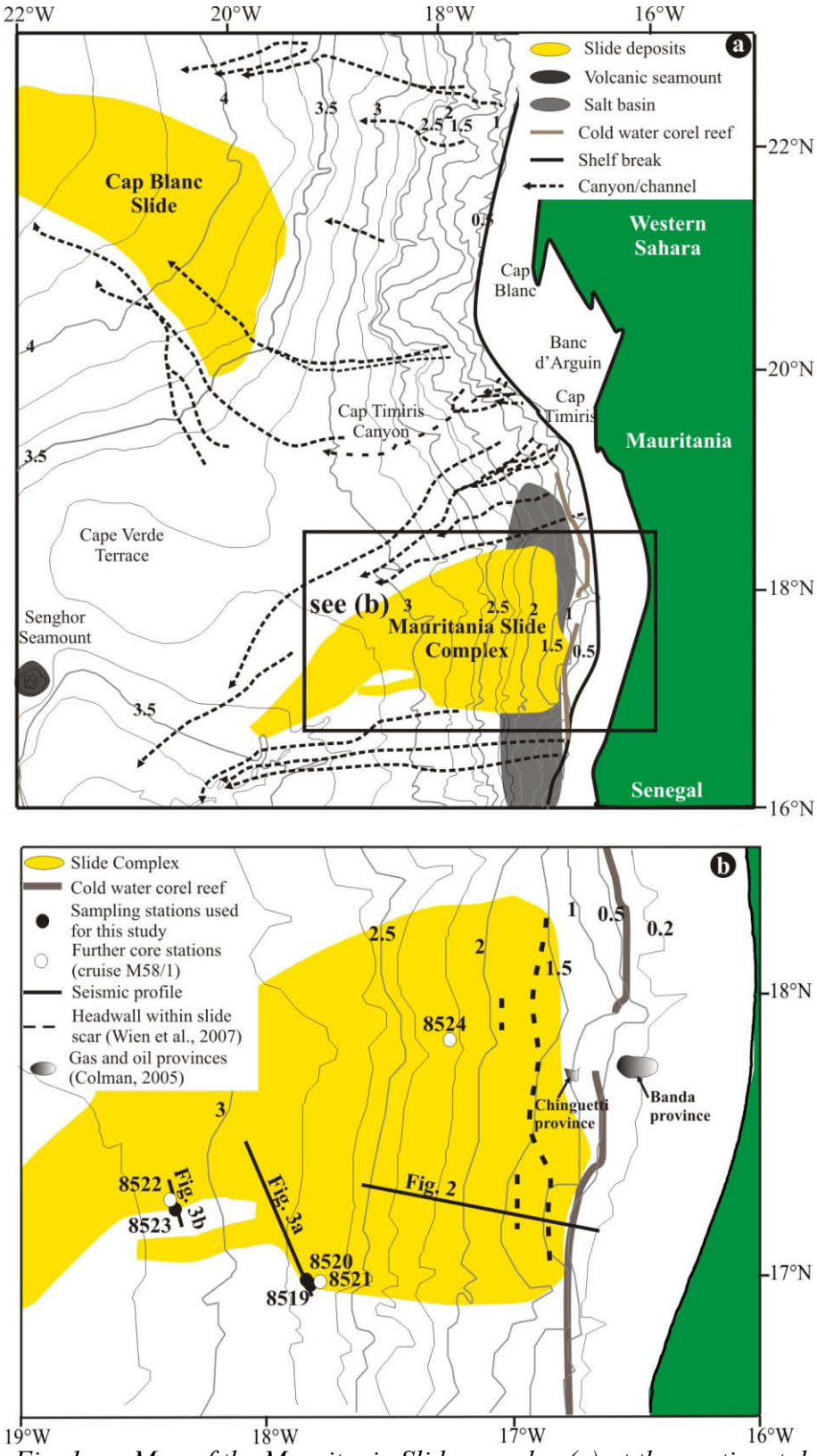

Fig. 1: Map of the Mauritania Slide complex (a) at the continental margin of NW-Africa (Davison, 2005; Krastel et al., 2006a, and references therein) with core locations of cruise M58/1 (b). Cores used in this study are outlined by black dots. The map also shows the Chinguetti and Banda oil and gas provinces (Colman et al., 2005; Davison, 2005). Scales of isobaths are given in km in steps of 200 m. For detailed information see seismic profiles of Figs. 2 and 3.

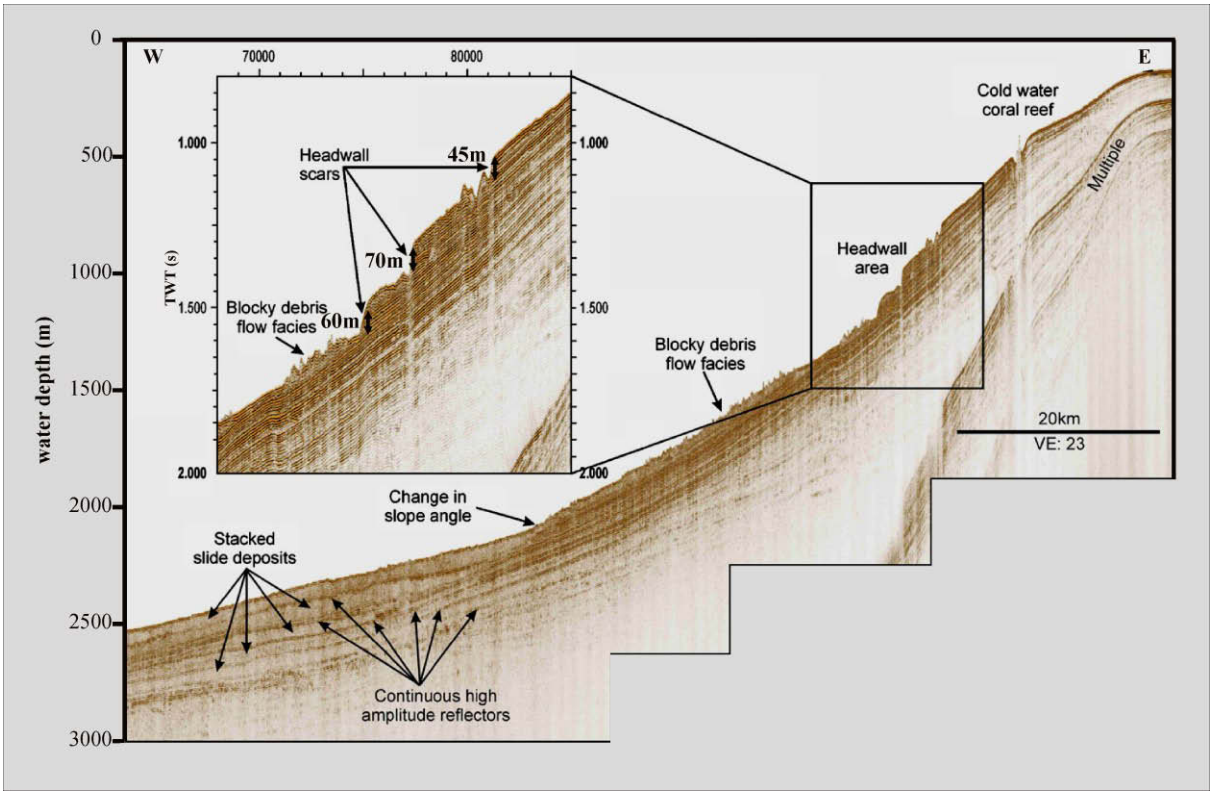

Fig. 2: Seismic profile crossing the headwall and the slid deposits of the Mauritania Slide Complex. The different steps with heights of 45 m, 70 m and 60 m could be identified as different headwall scars (Antobreh and Krastel, 2007). For location see Fig. 1b.

Sediment gravity cores were taken during RV Meteor cruise M58/1 (Schulz et al., 2003) outside of the landslide (GeoB8519; Figs. 1b and 3a), within the slide body at a midslope location (GeoB8520; Figs. 1b and 3a), and further downslope (GeoB852; Figs. 1b and 3b). The mid-slope position is located at the southern edge of the slide body, where the debris flow unit onlaps a small channel-levee structure (see above). The core GeoB8519 (Fig. 3a) is located directly on top of this levee structure (Fig. 3a) and consists only of hemipelagic sediment, interrupted by four thin turbiditic layers, for which this core served as reference (Fig. 4a). The hemipelagites consist of carbonate-rich ooze, silty mud and mud with high organic carbon content (Schulz et al., 2003; Henrich et al., 2008). Core GeoB8520 contains slid deposits of the midslope location (Figs. 3a and 4b). Above and below the slid deposits hemipelagic background sediment was recovered. In the debrite deposits, three different matrix types were identified based on sedimentological description and radiographs (Fig. 4b; Henrich et al., 2008). Debrite matrix types I (DBmI, 1-3.4 mbsf) and II (DBmII, 3.4-6.2 mbsf) consist of a pelagic-dominated particle association with varying amounts of shelf, upper slope and terrigenous components. In detail, DBmI contains 90-99% of foraminifera, 1-3% of shell debris, and <1% of terrigenous components. Terrigenous material is 9-12% in DBmII, whereas foraminifera are 68-74%. In contrast to these two matrix types, debrite matrix type III (DBmIII, 6.2-7.65 mbsf) comprises hemipelagic particles with a high fraction of shelf/upper slope and terrigenous particles (41-50% foraminifera and 19-23% shell fragments, 27-31% terrigenous particles).

Approximately 65 km further downslope, two additional cores (GeoB8522 and -8523) were recovered in an area where the debris flow unit downlaps onto stratified slope sediments (Figs. 1b and 3b). Because core GeoB8522 does not entirely penetrate the debris flow unit, only core GeoB8523 was used for further investigation. Core GeoB8523 recovered the debris flow unit, the underlying hemipelagic sediment sequence as well as an overlying ~0.7 m thick turbidite sequence (Fig. 4c). The hemipelagic sediments show a composition similar to the hemipelagites from the mid-slope location, whereas only debrite flow deposits of type DBmI containing rip-up clasts at the basal plane were observed (Fig. 4c). These rip-up clasts comprise of stiff mud with faint laminae. Due to redeposition, these clasts show deformation structures evoked by thinning, stretching and shearing of the sediments. In addition rotational fold structures were observed (Fig. 4c; Henrich et al., 2008).

In addition to the core descriptions (Fig. 4), the age for the onset of the hemipelagic sediments above the most recent debrite (GeoB8520 and -8523) was determined to be 10.5-10.9 ka BP (^{14}C-age determination of planktonic foraminifera; Henrich et al., 2008). Furthermore, oxygen and carbon isotope records as well as carbonate data (Matthewson et al., 1995; Henrich

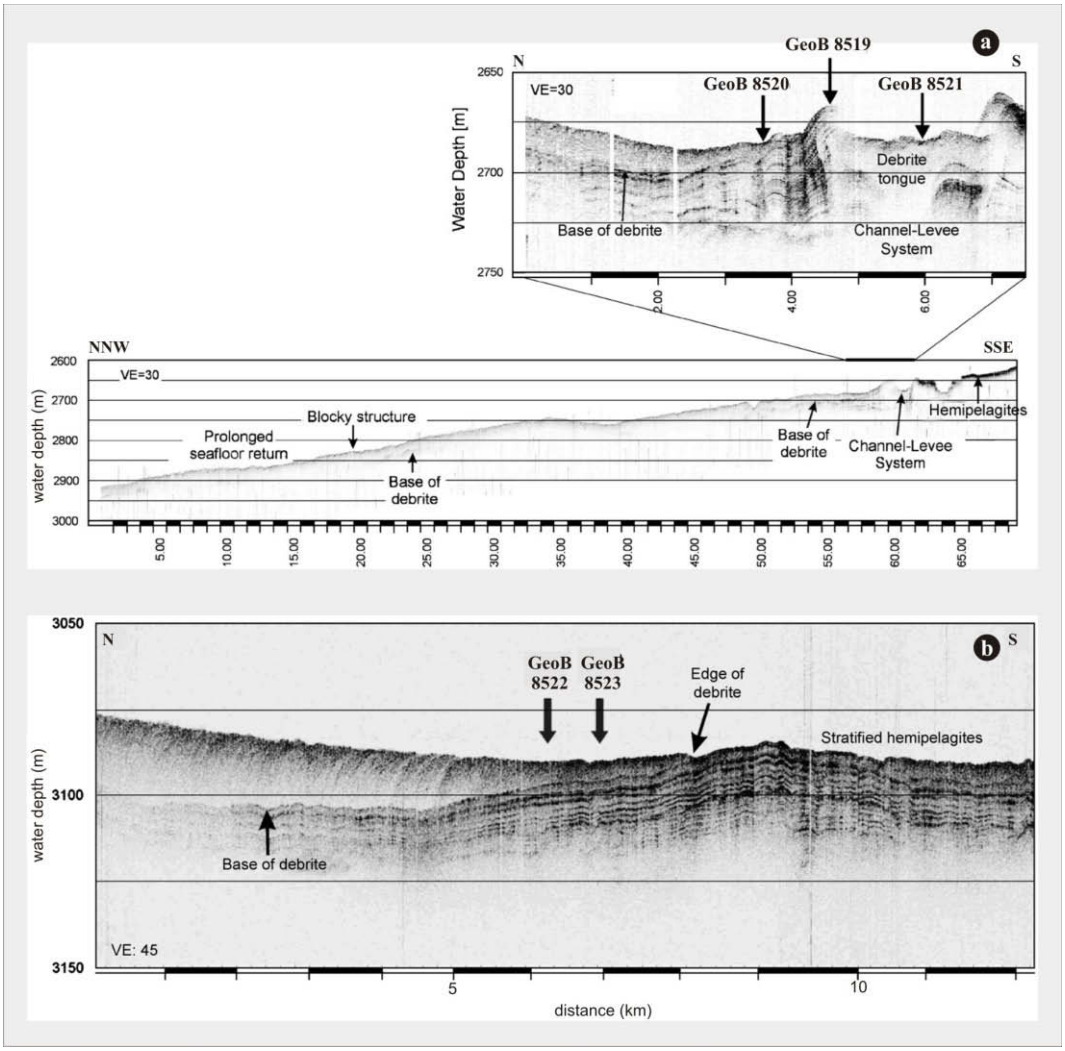

Fig. 3: Parasound profiles with the coring locations (Henrich et al., 2008) with (a) midslope location (including GeoB8519 and -8520) at the southern edge of the debris flow and downslope location (b) of core GeoB8523, which penetrates the debris flow completely.

et al., 2008) indicate that the hemipelagic unit below the debrite (DBmI) in core GeoB8523 can be dated to be Marine Isotope Stage 2 (MIS 2). For the turbidites of core GeoB8519, the age of deposition was estimated to be ~71 ka BP (Turbidite 2) and 129-130 ka BP (Turbidite 3 and 4) from elemental data (Fig. 4a; Wien et al., 2007).

For the discussion of the temporal evolution of the MSC (Ch. 4.4.1) further cores were used (GeoB8521, -8522, and -8524; Fig. 1b). Core GeoB8521 contains very similar sedimentary sequences to GeoB8520 (Fig. 4b); core GeoB8522 also shows the debris flow unit, the underlying hemipelagic sediment sequence and an overlying turbidite sequence similar to GeoB8523 (Fig. 4c). The sediments of core GeoB8524 contain debrite matrix type I, but show no indications of turbidites. For detailed information regarding the lithology of these cores, refer to Henrich et al. (2008).

4.2 Material and Methods

For this study we used cores GeoB8520 and -8523 from the slide and core GeoB8519 (Fig. 1b) as reference for dedicated geotechnical laboratory measurements and for quantitative fabric analysis. Core GeoB8519 was chosen as the reference concerning sediment composition, shear strength and sediment physical properties, because age control already exists (Wien et al., 2007). Sediment physical properties (e.g. P-wave velocity, bulk density, porosity and magnetic susceptibility) were already measured onboard using a Multi-Sensor Core Logger (MSCL). Results are summarized in Schulz et al. (2003) and Henrich et al. (2008).

4.2.1 Laboratory testing

In our shore-based study, we first measured the "index properties" (bulk density, grain density, water content and porosity) as well as grain size distribution. The sediment physical properties were determined in the laboratory on discrete samples using a Quantachrome Pentapycnometer. Grain size was measured using the Aerometer method (for details see DIN18123: 1996-11) where classification followed Wentworth (1922). In addition to ^{14}C-ages of Henrich et al. (2008), age control for the hemipelagic sediments underlying the debrite unit is provided by acceleration mass spectrometry (AMS; *Pozna Radiocarbon Laboratory, Poland*) on planktonic foraminifera. The raw data of the measured ^{14}C-data were calibrated using the software package Calpal-online (Danzeglocke et al., 2009) to convert the ^{14}C age to calender age. The conversion includes a correction for different factors that may affect the ^{14}C record such as the ocean reservoir effect (delay in exchange rates between atmospheric CO_2 and ocean bicarbonate), upwelling effect (dilution effect caused by mixing of surface water with carbon depleted deep water), isotopic fractionation, post-depositional shell recrystallization (bicarbonates of different ages in the same matrix) and changes in the atmospheric ^{14}C content in the atmosphere due to industrialization and atom bomb tests (Stuiver and Polach, 1977; Taylor, 1987; Stuiver and Braziunas, 1993).

Geotechnical measurements include the determination of the undrained shear strength (Cu) using a Fallcone Penetrometer (Hansbo, 1957) to detect "weak layers" in the sediment column. The determined Cu-values should be taken with caution, due to the time between core recovery during the cruise M58/1 and onshore measurements of the undrained shear strength (~3 years). Although stored in the Bremen IODP core repository, dehydration effects of the core material during that period may have led to evaporation, and therefore to an overestimation of

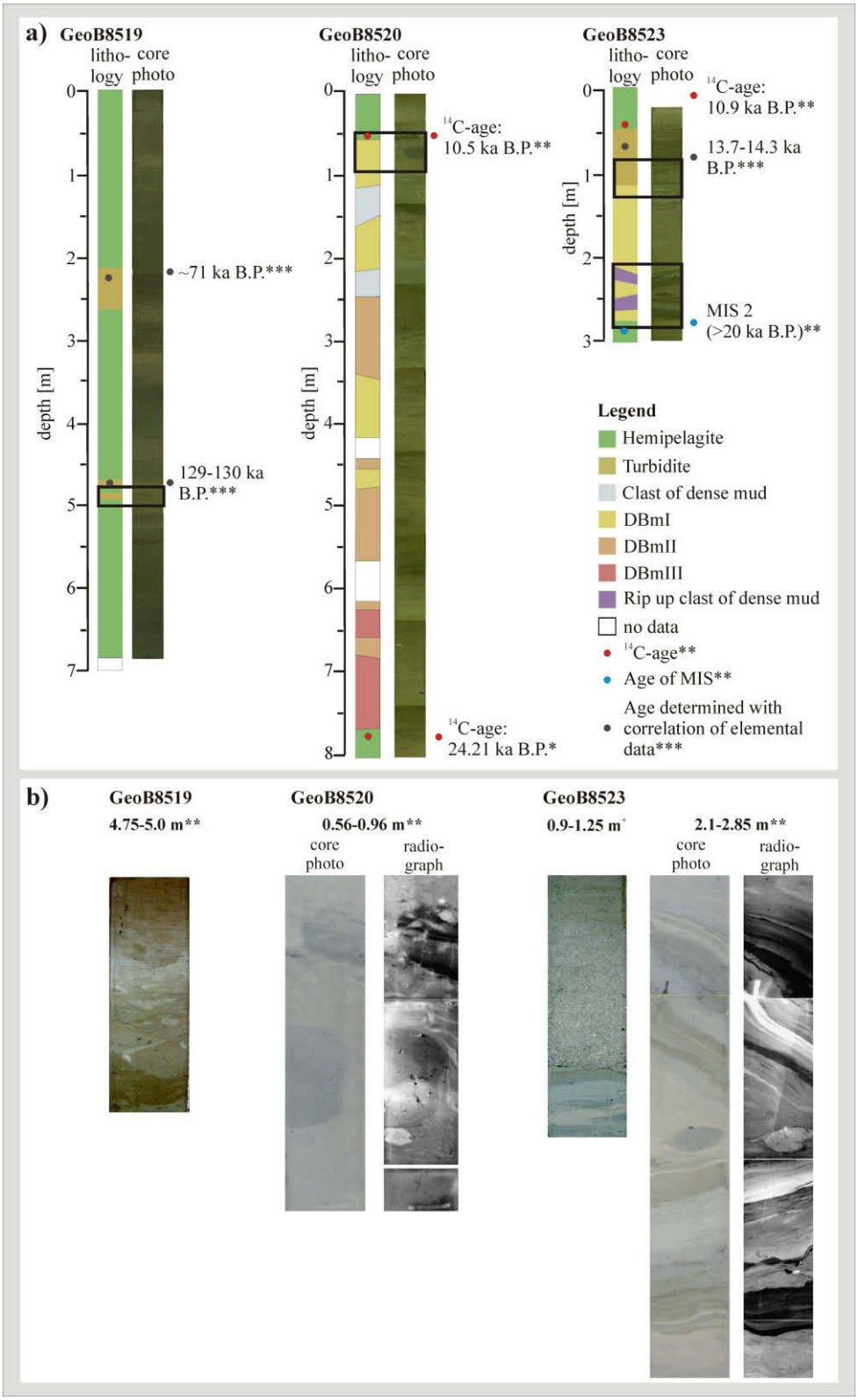

*Fig.4: Schematic core lithology (taken from x-ray pictures), core photos (Schulz et al., 2003) and close-ups from different lithologies (+Schulz et al., 2008; **Henrich et al., 2008) of the three cores a) GeoB 8519, b) GeoB8520 and c) GeoB8523 of the Mauritania Slide Complex. Also the ages for different lithologies are presented from ^{14}C-age determination (* this study; ** Henrich et al., 2008), Marine Isotope Stages (MIS; ** Henrich et al., 2008) and determination with correlation of elemental date (*** Wien et al., 2007). For position of the cores see Fig. 1b.*

the shear strength. A re-calculation of the shear strength values is not easily and safely possible, because numerous other factors could affect the undrained shear strength such as errors in sediment sampling or storage, oxidation effects, degassing or contraction of the sediments (e.g. Ladd and Foott, 1974, and references therein; Lunne et al., 2006).

In addition to the undrained shear strength values, drained shear strength values (□) and information about the frictional stability were collected by means of ring shear and direct shear experiments on remolded samples on six different samples (taken from top down to ~7.6 mbsf) from the three cores. The core sampling strategy (minimum one sample of each lithology) was based on the results from the earlier MSCL runs, from the Fallcone Penetrometer tests as well as from core description. Corresponding to the different possible stress states of the sediments, the normal load in the experimental setup was increased incrementally up to 3.81 MPa (0.04, 0.07, 0.1, 0.17, 0.20, 0.48, 0.96, 1.94 and 3.81 MPa) for the ring shear as well as for the direct shear tests. Apart from measuring the peak strength during failure, the ring shear method allows for quasi-infinite strain on the residual path (Bishop et al., 1971). Variable sliding velocities were used to simulate processes from creep to moderately fast sliding (0.0005 mm/s, 0.001 mm/s, 0.01 mm/s and 0.1 mm/s). From the rate-dependent change in shear strength, it is possible to calculate the [a-b]-value (Scholz, 1998). An [a-b]-value > 0 indicates velocity-strengthening behavior, which suggests stable sliding and frictional stability. In contrast, an [a-b]-value < 0 exhibits velocity weakening and potentially unstable behavior. The direct shear tests were performed with a sliding velocity of 0.01 mm/s to facilitate comparison to the ring shear data at the same rate.

To characterize the consolidation history of the sediments, fixed-ring oedometer tests were performed on the different lithologies (Ch. 4.1.3) at normal stresses up to 250 kPa. The results will be presented in an e-log σ_{eff}-curve (σ_{eff} vertical effective stress), whereas the void ratio, e, is corrected from void-ratio data on discrete samples (see above) to void ratios determined using the onboard MSCL data. The maximum stress the sediments experienced previously (preconsolidation pressure, σ_{pc}) was determined after Casagrande (1936). The consolidation state of the sediments was estimated from the overconsolidation ratio (OCR), which is defined as the ratio of the preconsolidation stress, σ_{pc}, and the vertical effective stress, $\sigma_{eff,}$ (equation 2.1). Following equation 2.2, the stress history of the sediment can be expressed by the overconsolidation difference (OCD) that accounts for the effects of erosion or cohesion (Ladd et al., 1977; Bryant and Bennett, 1988; Sultan et al., 2000):

$$OCR = \sigma_{pc} / \sigma_{eff} \quad [2.1]$$

and

$$OCD = \sigma_{pc} - \sigma_{eff} \quad [2.2].$$

4.2.2 Strain analysis

The concept of strain estimation based on a series of assumptions. In homogeneously strained particles at least two axes do not rotate relative to each other before and after deformation, but the lengths of these two axes change from their initial to their final stage. These vectors represent the axes of the strain ellipse. The method assumes that the marker particles showed an initial random and isotropic distribution in the deposit without any preferred orientation (i.e. the strain ellipse in that case being a sphere). Under such a distribution, the

average distance to neighboring particles would hence be the same in each direction. The change in the distance to the 18 nearest neighbors is used in the strain method (Fry, 1979).

In our study, the strain is estimated by finite strain analysis where final configurations of particle markers in the sediment are determined. The deformation is related to flattening, shearing and rotation of the particles during burial or reworking of sediments. We used active strain markers such as shell fragments and macroscopic marine shells because of their mechanical contrast to the matrix. Following the Fry method (1979), strain analysis was performed on all of the three cores (GeoB8519, -8520 and -8523) using the software package FABRIC 8 (Wallbrecher et al., 1996; Geolsoft 2008). Assuming an initially isotropic particle distribution, the program uses the steric distribution of the marker particles for the strain

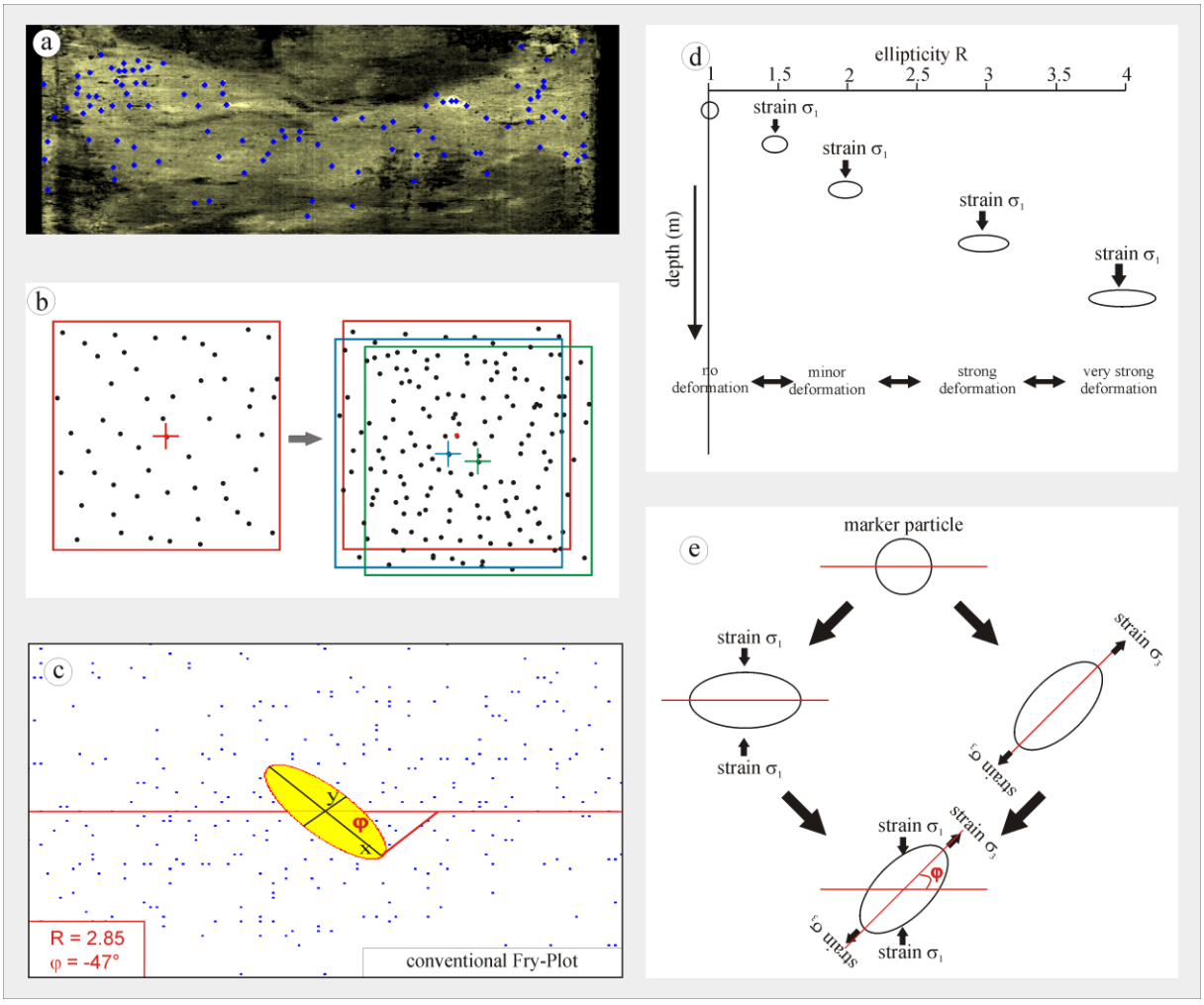

Fig. 5: Marked shell particles on a core photo (a) for strain analysis using software package FABRIC 8 (Wallbrecher et al., 1996; Geolsoft, 2008). The graphical representation of the Fry-Method (1979; used for the strain analysis) using the center points of the shell particles is shown in b). All center points are drawn and a random point is marked (left picture). After that this point is centred at all other points successively, and each time all other points are copied (right picture). The result is a free ellipse whereas the ratio of long to short axis (ellipticity R=x/y) defined the deformation grade and the angle φ resembles the orientation of the strain ellipse (c). The interpretation of alteration of the strain ellipse during burial to depths is shown in d) with stress from one vertical ax (σ_1). Additionally (e), stretching of the strain ellipse (σ_3) may be related to straining or e.g. shearing of the particle. The result is a rotation (-φ or +φ) of the strain ellipse (modified after Behrmann and Kopf, 1993).

determination as follows: Images with identifiable markers (e.g. core photographs or radiographs) were digitized, uploaded to the PC and the center points of each particle were marked within the FABRIC 8 software package (Fig. 5a). The software-immanent analyses use an overlaying technique where a chosen marker is centered. Its 18 closest markers are then projected onto the same central position one-by-one (Fig. 5b). If a consistent strain regime exists, an elliptical area free of points will result (resembling a strain ellipse), once all 18 images have been projected (Fig. 5c). The software package FABRIC 8 displays the ellipticity value R (ratio of long to short axis of the strain ellipse) as an indicator for the grade of deformation of the sediment (Fig. 5d). The angle φ represents the orientation of the long axis of the strain ellipse relative to xy-axes/bedding direction and core axis direction (Figs. 5c and e). During burial or erosion the particles alter in shape and orientation that is reflected in alteration of the corresponding strain ellipse (Figs. 5d and e). More detail regarding the measuring principle is outlined in Ramsey and Huber (1983).

When taken to our study area, the particle size distribution in the turbidite units is very uniform and the packing close (due to gradation). If the initial distribution of the particles was not random and isotropic, the strain analysis results become suspect as several circular or elliptical zones could occur (Ramsey and Huber, 1983).

4.3. Results

4.3.1. Physical properties and grain size analyses

In Figures 6a, b and c we present selected data from the MSCL runs (for more detail refer to Schulz et al., 2003) as well as water content and clay content at discrete samples of cores GeoB8519, -8520 and -8523. In the hemipelagic sediments of the levee system (Ch. 4.1.3, GeoB8519) it can be seen that bulk density values increase slightly from 1.79 g/cm³ to ~ 1.82 g/cm^3 while water content decreases with depth from 0.6 to ~0.45 (Fig. 6a). The sediments of the landslide body at the midslope location (GeoB8520) show a general downhole increase in bulk density and a decrease in water content (Fig. 6b). In agreement with the sedimentological description (Ch. 4.1.3, Fig. 6b) we observed four different intervals: i) in the uppermost centimeters of the hemipelagic sediments, a strong increase in bulk density values was observed; ii) from 0.6 to ~2 mbsf constant density and water content (1.72 g/cm^3, 0.55) correspond to the DBmI-matrix (Ch. 4.1.3), which is underlain by iii) an interval with a constant but slightly higher density and slightly lower water content (DBmII-matrix from 2 to ~4.2 mbsf with 1.75 g/cm^3 and 0.53). Here, DBmII matrix (e.g. GeoB8523) with high bulk densities between 1 and 1.5 mbsf correspond to high-density clasts (1.85 g/cm^3; Henrich et al., 2008). Finally, iv) DBmIII (~4.2 to 7.6 mbsf) shows a subtle linear increase in density up to 1.9 g/cm^3 and a downhole decrease in the water content (0.38). The hemipelagic sediment beneath the debris flow has bulk density values of ~1.83 g/cm^3, which increase with depth. At the downslope position of the landslide (GeoB8523), physical properties of the sediment show significant differences (Fig. 6c). Density values increase from 1.7 to ~1.92 g/cm^3 in the upper 1.1 meters, corresponding to the turbidite layer above the debris flow. Below the turbidite, the bulk density values drop back to 1.75 g/cm^3, representing the DBmI (Fig. 6c). In the embedded layers (~2.1 to 2.65 mbsf), a strong increase in bulk density to 1.9 g/cm^3 was observed, which correlates with rip-up clasts noted by Henrich et al. (2008). In addition to bulk density, water content generally decreased downcore and showed lower values than the midslope core (0.8 to 0.18; Fig. 6c). In

both MSC cores (GeoB8520 and -8523) grain size is fining downwards from 20 wt% clay content in the uppermost centimeters to 75 wt% at 7 mbsf (Figs. 6a-c).

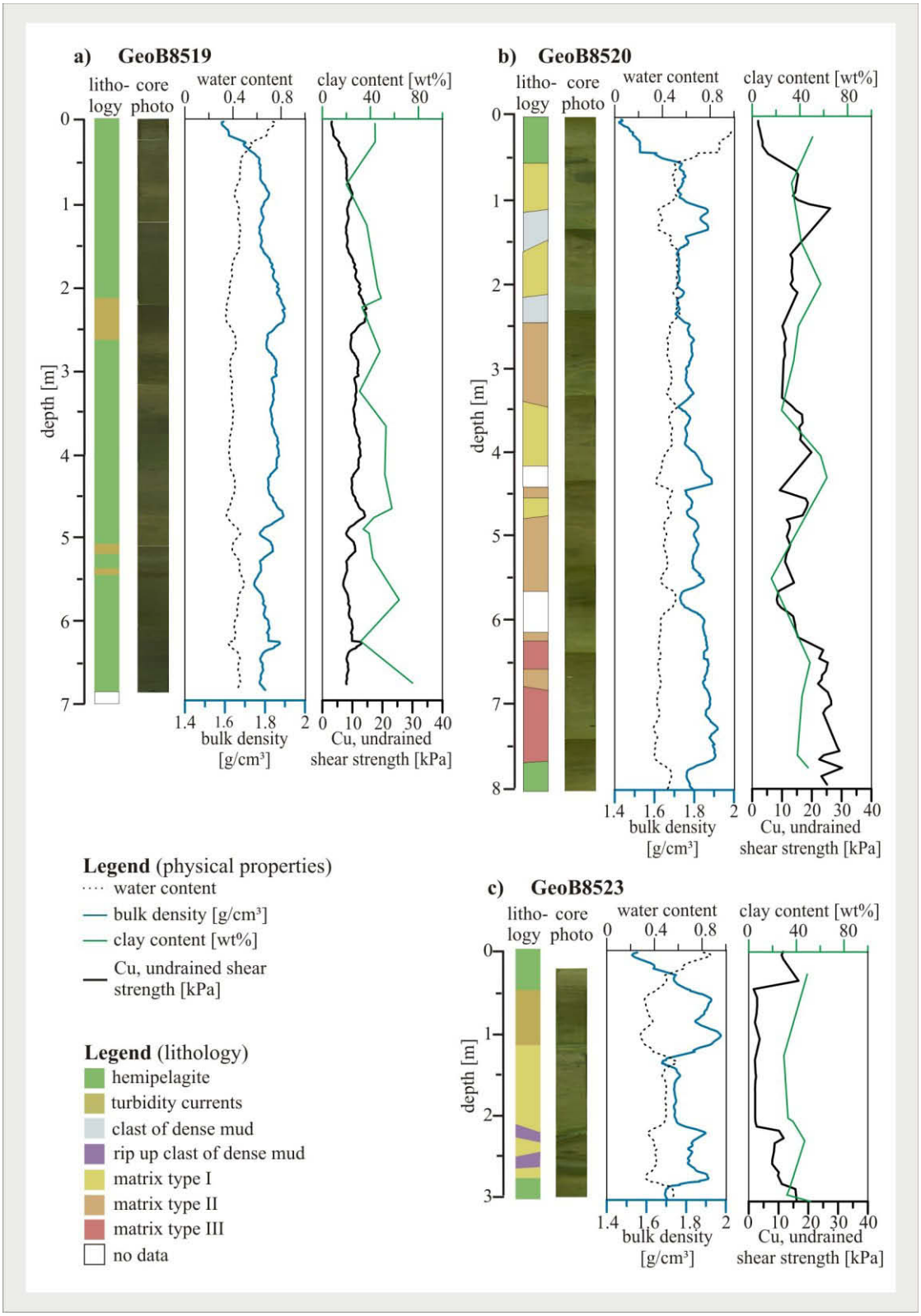

Fig. 6: Schematic core lithology (taken from x-ray pictures) and core photos (Schulz et al., 2003) compared with bulk density (from MSCL), water content, clay content distribution and undrained shear strength values of the three cores a) GeoB 8519, b) GeoB8520 and c) GeoB8523 of the Mauritania Slide Complex (modified after Henrich et al., 2008). For position of the cores see Fig. 1b.

4.3.2 Age determination

To compliment earlier research (e.g. Wien et al., 2007; Henrich et al., 2008), we acquired additional age information. Calibration of the raw data with the software package Calpal-online (Danzeglocke et al., 2009) allowed for direct comparison of our radiocarbon ages to those data of previous studies (Wien et al., 2007; Henrich et al., 2008). Based on Calpal-online values, ^{14}C ages were corrected for factors such as ocean reservoir or upwelling effects, isotopic fractionation and shell recrystallization (see Ch. 4.2.1, and references therein). We calculate a ^{14}C-age of 24.21 ka B.P. for hemipelagic sediments directly underlying the lowest debrite unit (7.6 mbsf) in core GeoB8520 (Fig. 4b). This datum will be discussed in the context of the overall mass wasting deposition in the study area (see below).

4.3.3 Falling cone experiments

Figure 6 shows the undrained shear strength (Cu) in the right columns of each panel, respectively and is compared against the bulk density and water/ clay content values and the sedimentological description. Although the uppermost meter of hemipelagic sediments in reference core GeoB8519 preserve higher than expected Cu-values of 7 kPa, the core generally showed a slight downward increase in Cu-values to ~11 kPa at 7 mbsf (Fig. 6a). The upper meters of both cores from the slide complex (GeoB8520 and -8523) also demonstrated similar high Cu-values (Figs. 6b-c). The reworked debris flow sediments are consistently overconsolidated (Figs. 6b-c) except DBmI in core GeoB8523, which had Cu-values of 2 kPa in 2 mbsf (Fig. 6c). This core also showed a strong increase in Cu-values from 3 to 15 kPa in the deeper portion of the debris unit, which could be correlated with rip-up clasts (Fig. 6c). While the DBmI sediments of core GeoB8523 show normal consolidation, similar deposits further upslope (GeoB8520) are slightly overconsolidated (Cu of 15 kPa in 2.5 mbsf; Fig. 6b). The slid material of DBmII as well as the material of DBmIII shows higher Cu-values than DBmI (Fig. 6b). Furthermore, DBmII shows a decrease from 10 kPa in 3.5 mbsf (slight overconsolidation) to 8 kPa in 5.5 mbsf (normal consolidation), followed by a strong increase in Cu from 12 to 25 kPa (Fig. 6b) to the interface with underlying DBmIII sediments.

4.3.4 Ring shear and direct shear tests

The results of the ring and direct shear tests on discrete samples of the three different matrix types and the background hemipelagites are shown in Figure 7a. Residual shear strength (τ_{res}) was normalized against the normal stress (σ_n). The coefficient of friction, μ_{res}, is defined as the ratio between shear and normal stress. The hemipelagic sediments of the reference core (GeoB8519 in 0.34 m; Fig. 7a) show μ_{res}-values ranging from 0.22 to 0.38. The debrite matrix types (DBm) show an increase in μ_{res}-values with increasing normal stress to a maximum of 0.39 (Fig. 7a), except for DBmIII where a decrease to μ_{res}-values of 0.28 was noted (at σ_n >3.8 MPa). The lowest μ_{res}-value (0.18) was measured in core GeoB8523 (2.92m) and represents the hemipelagic sediment at the base of the debris flow unit (Fig. 7a).

Detailed results for μ_{res} measured at normal stresses of 3.8 MPa and a sliding velocity of 0.01 mm/min are shown in Figure 7b. For a downward profile of the debrite sequence, the hemipelagic sediment sample from the base of the debris flow at site GeoB8523 was projected to the depth of the base from GeoB8520 (Figs. 7b-d). Note that DBmI and DBmII show μ_{res}-values

(0.38) similar to the reference core, while DBmIII and the hemipelagites show lower values (0.28 and 0.18). From velocity stepping tests we calculated [a-b]-values (Fig. 7c). Results range from -0.003 to 0.015, with the highest [a-b]-value calculated for hemipelagites in the reference core, GeoB8519. Low negative [a-b]-values were measured for DBmI (2.75 mbsf) and DBmII (2.91 mbsf) samples of GeoB8520 and for the hemipelagic sediments at the base of the debris flow unit (GeoB8523 projection to 7.6 mbsf of GeoB8520, see above, Fig. 7c), however, data close to zero should not be overinterpreted. In general, we observe the lowest [a-b]-values in sandy intervals of the core (Figs. 7c-d).

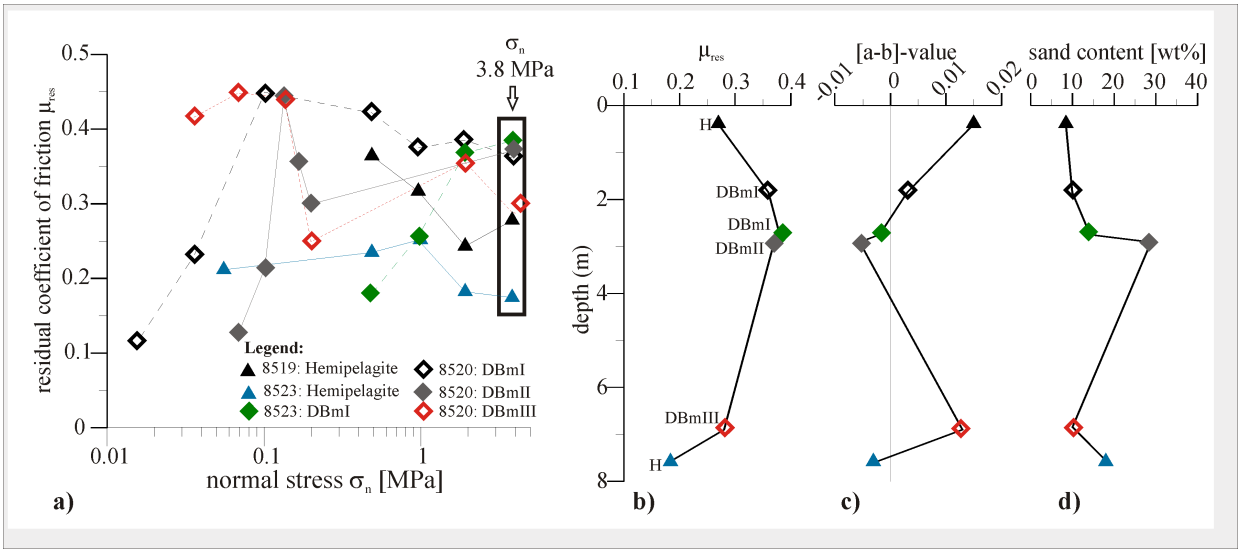

Fig. 7: a) Residual coefficient of friction (μ_{res}) vs. normal stress (σ_n) for discrete samples of the Mauritania Slide Complex from ring shear and direct shear tests (with sliding velocity of 0.01mm/min). For normal stress (σ_n) of 3.8 MPa detailed results of ring shear tests (μ_{res}, [a-b]-value) compared with sand content of the analyses cores GeoB8519, -8520 and –8523 are shown in Figure b) – d). Hemipelagic sediments from GeoB8523 was projected downward the core into depth of the hemipelagites of core GeoB8520. Sliding velocities for the [a-b]-values varied from 0.0005 to 0.1 mm/s. For locations of the cores see Fig.1b.

4.3.5 Oedometer experiments

Void ratio (e) vs. vertical effective stress (σ_{eff}) diagrams for nine samples taken from all different lithologies (hemipelagites, DBmI, DBmII and DBmIII; see Fig. 4) are shown in Figure 8. The preconsolidation stress, σ_{pc} was determined from the oedometer tests (Tab. 1), and used to calculate the Overconsolidation ratio (OCR) and the Overconsolidation difference (OCD), which reveal the consolidation status of the sediment samples. In order to estimate the missing material in comparison to the OCR-values, OCD/γ-values (Tab. 1) were calculated with γ as the submerged unit weight (kg m^{-2} s^{-2}).

While the hemipelagic sediments of the reference core (GeoB8519) show normal consolidation (OCR ~1), similar hemipelagic deposits underlying the debris flow units (GeoB8523 and -8520) are slightly underconsolidated (OCR=0.65-0.79). The slid material of DBmI and DBmIII show slight under- to slight overconsolidation with OCR-values of 0.91-1.28 (Tab.1), while the sediments of DBmII are strongly overconsolidated (OCR=3.96). Based on the OCD/γ-values, we estimate a removal of a 3.5-4 m thick sediment column between recovered DBmI and DBmII. Under-consolidated conditions were measured for the hemipelagic sediments directly at the boundary of the remobilized unit (Tab. 1).

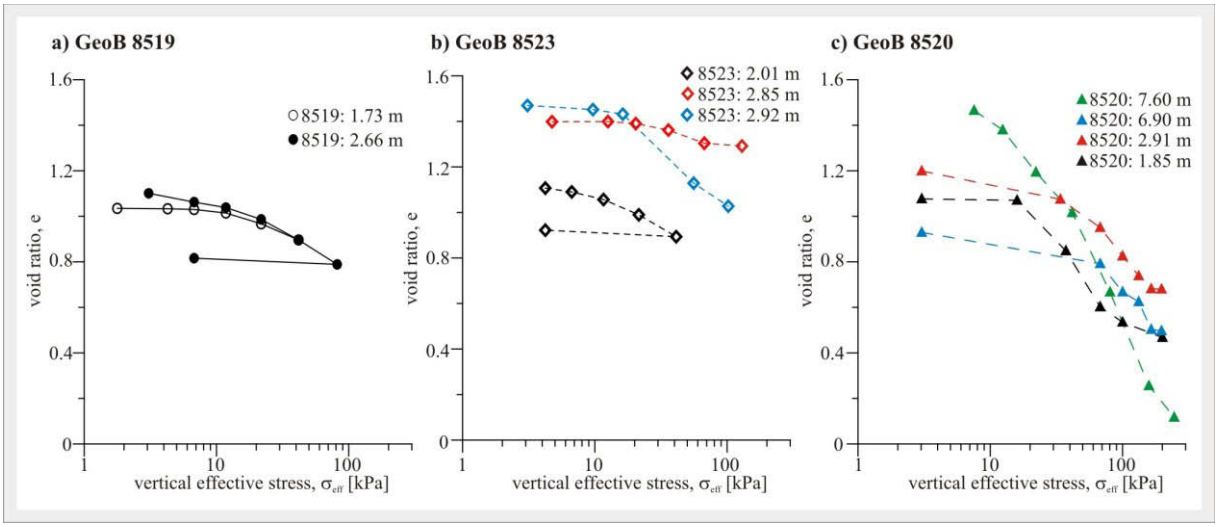

Fig. 8: Results of the oedometer tests in different lithologies. E-log σ_{eff}-curve for the cores GeoB 8519, b) GeoB 8523 and c) GeoB 8520. For locations of the cores see Fig.1b.

Tab. 1: Results of consolidation tests: maximum past stress σ_{pc}, vertical effective stress σ_{eff}, overconsolidation ratio (OCR), overconsolidation difference (OCD) after equation 4.3 and the estimated missing material sequence calculated from OCD and γ' as the sub-merged unit weight (kg m^{-2} s^{-2}). For positions of the cores see Fig.1b.

Sample	depth [m]	σ_{pc} [kPa]	$\sigma_{eff.}$ [kPa]	OCR	OCD	OCD/γ' [m]
8519	1.73 (H)	11.29	13.58	0.83	-2.29	-0.13
	2.66 (H)	20.88	20.53	1.02	0.35	0.02
8523	2.01 (DBmI)	12.3	13.49	0.91	-1.19	-0.07
	2.85 (H)	14.44	18.24	0.79	-3.8	-0.23
	2.92 (H)	15.02	19.21	0.78	-4.19	-0.26
8520	1.85 (DBmI)	16.97	13.27	1.28	3.7	0.22
	2.91 (DBmII)	85	21.44	3.96	63.56	3.65
	6.90 (DBmIII)	43.12	41.33	1.04	1.79	0.11
	7.60 (H)	29.88	46.00	0.65	-16.12	-0.96

4.3.6 Strain Analysis

The results of the quantitative fabric analysis are elliptical areas, which resemble strain ellipses in shape and orientation. Strain is quantified as extension or compression resulting from stress axes ratio (σ_1 and σ_3; Figs. 5d-e) and as rotation of the particles (orientation of long axis of stress ellipse; see Methods above). The ellipticity data, given as R-values, are an indicator of deformation degree and were divided into four groups (Fig. 5d) and compared to the sedimentological observations by Henrich et al. (2008):

- 1 - 2: no to minor deformation
- 2 - 3: moderate deformation
- 3 - 4: intense deformation
- >4: very strong deformation

Results are shown in Figure 9. Strain analysis conducted on the reference core (GeoB8519) shows relatively weak deformation, increasing with depth as a result of burial (Fig. 9a). Between 4.8 and 5.2 mbsf, the hemipelagic sediments show high deformation values >4, indicating that they are not simply undeformed background sediment. In the slid sediments (GeoB8520 and -8523), the majority of R-values are low to moderate (between 1.2 and 3; Figs. 9b-c). Exceptions were noted in the layers between the different debrite matrixes and the erosive bases of the underlying hemipelagites, which have R-values > 4. It is notable that these layers mostly appear in normal to overconsolidated sediments with Cu values of >18 kPa (Figs. 6b-c and 9b-c). The turbidites (R ~4.5) and rip-up clasts of core GeoB8523 (R = 6-7) are heavily strained, although for the first we assume that the boundary conditions of the Fry method are not totally fulfilled (Ch. 4.2.2), so the measured R-values are not used for further interpretation.

If we regard the deviation of the φ-values from horizontal, there seems to be a correlation between the R- and φ-values (Fig. 10). In the hemipelagic sediment we observe that most of the strain ellipse show higher R-values with low rotation (Fig. 10a). In contrast, in the debrite matrix types sediments no correlation between the R- and φ-values is visible, but it is noticeable that the most ration values (~66%) show a positive rotation from 2° to 60° (Fig. 10b). Besides the results from R-value determination, symbols in Figure 9 illuminate the distribution of the φ-values as a function of the lithology. For the hemipelagite of the reference core (GeoB8519) no significant correlation between the angle φ and the lithology was observed. The slid sediments of core GeoB8523 (DBmI) show mainly positive φ-values. While the highest rotation (φ) of +62° was observed in the upper part of the slid sediments, a decrease in the φ-values downcore is visible (Fig. 10c), possibly a result of incipient compaction. In contrast the DBmI sediments of core GeoB8520 show lower φ-values of -40° to +40°. For the slid sediments of DBmII, the rotation of the strain ellipses shows no clear distribution pattern with φ-values of -60° to +60° (Fig. 10b), while the DBmIII sediments show largely positive φ-values (Fig. 10b) between -20° and +50° (69% > +2°). In the Discussion, we will ascertain to wich extent we can relate the elevated strain values to dynamic processes prior, during and after landslide deposition.

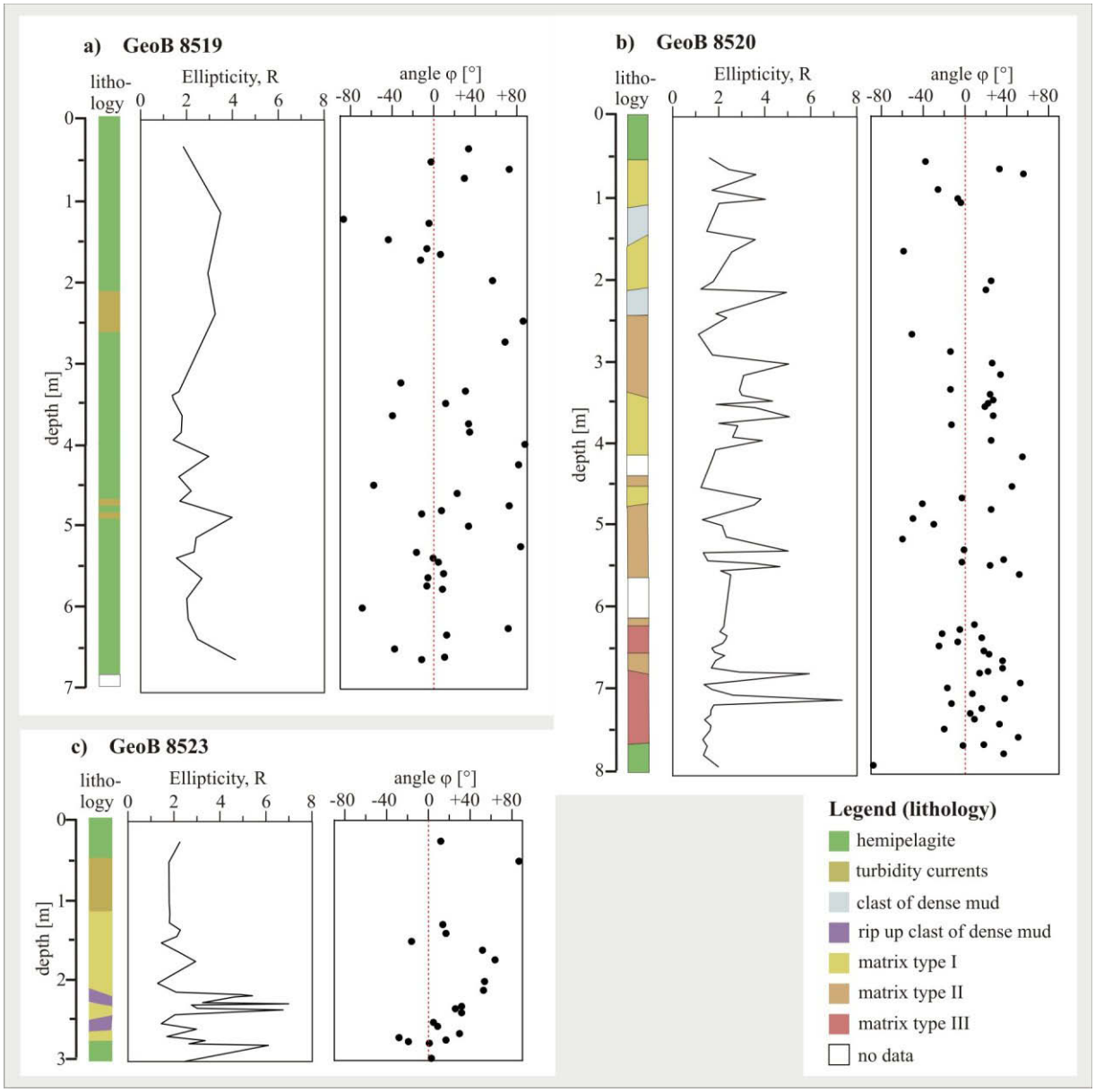

Fig. 9: Core descriptions of x-ray images (modified after Henrich et al., 2008), ellipticity R-values and rotation φ-values (Fry, 1979) of the three cores a) GeoB8519, b) -8520 and c) -8523. For locations of the cores see Fig. 1b.

4.4. Discussion

4.4.1 Evolution of the different debris flow units

Earlier studies hypothesized that the different debris flows within the Mauritania Slide Complex (MSC) was emplaced through retrogressive, multi-phase mass wasting (e.g. several headwalls, numerous transparent units representing mass wasting deposits; Krastel et al., 2006a; Antobreh and Krastel, 2007). A succession of at least five prominent debris flow units separated by stratified undisturbed hemipelagic sediments was observed (Antobreh and Krastel, 2007; Henrich et al., 2008).

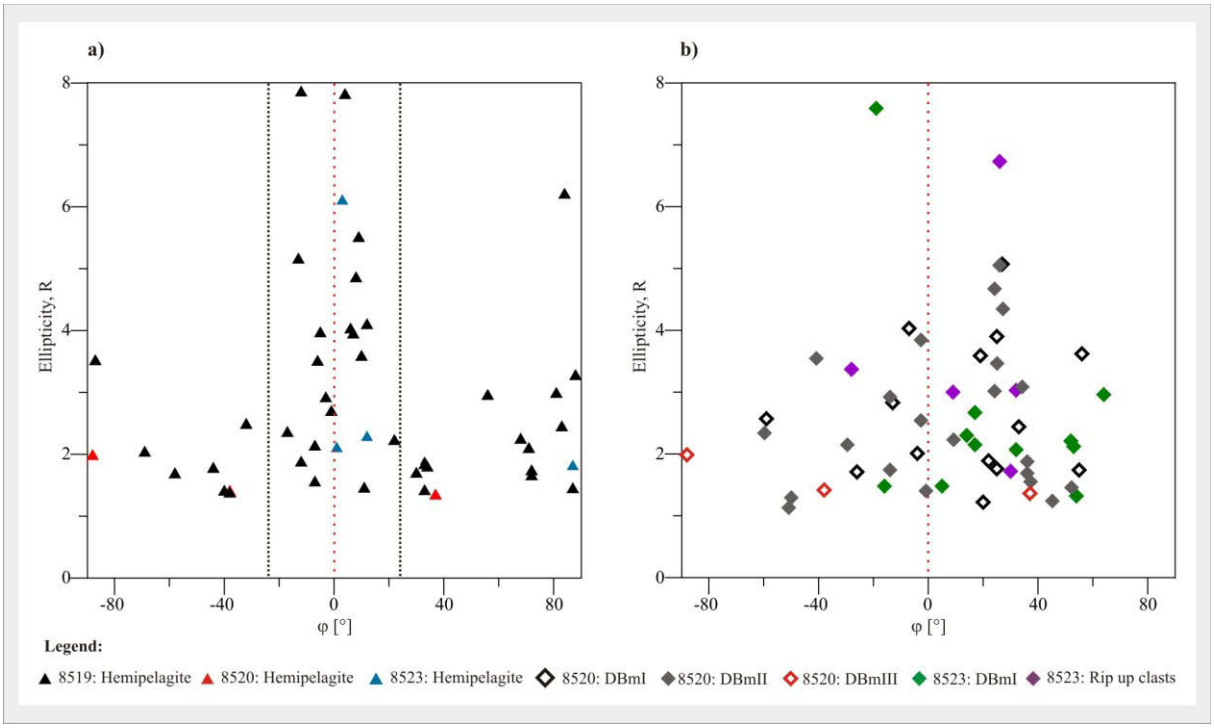

Fig 10: Correlation of the ellipticity values (R) and the rotation values (φ) of the strain ellipse (Fry, 1979) for the hemipelagic sediments (a) and the slid sediments (b). R is defined as the ratio of long to short axis of the strain ellipse and is indicator for the grade of deformation of the sediment. The angle φ represents the orientation of the long axis of the strain ellipse relative to the horizontal line. For detail description of the strain analysis method see Fig. 5.

Unfortunately, our geotechnical investigations are restricted to the recent debris flow unit, which we divide into at least two independent events (multi-phase events). Figure 11 shows a schematic diagram of the temporal evolution of the analyzed debris flow sediments. Combining all our geotechnical results with seismic data and sedimentological results (Antobreh and Krastel, 2007; Henrich et al., 2008), the hypothesis of retrogressive sliding (Antobreh and Krastel, 2007; Henrich et al., 2008), which may be obtained for the thick debris flow evolution, is not supported for the internal evolution of the uppermost unit (Fig. 11). Instead, we propose a sequential evolution of the three debris units (DBmI, DBmII and DBmIII): DBmIII represents the oldest event (Event 1a, Fig. 11a) and is attributed to an upper slope origin based on the high content of upper slope sediments (water depth of 800-1100 m; Ch. 4.1.3) and were recovered at the lowest part of the debris flow deposits directly overlying hemipelagic sediments (Figs. 4b and 11a-b). The recovered sediments are slightly underconsolidated (OCR=0.80) and show evidence of deformation with R-values of 2-6 and inclinations of the long axes to horizontal line (φ-values) of -20° to +40° (Fig. 9b), which may be related to sliding. The hemipelagic sediments directly underlying the debris flow unit show strong to slight underconsolidation (OCR=0.65-0.79) that may be related to sampling disturbance. However, the underconsolidated state may be real and could have been preserved by excess pore pressure, which counteracts the effective vertical pressure of the overburden sediment column. The maximum age of the oldest event (Event 1a) was determined to be 24.21 ka B.P. (^{14}C age determination; Fig. 6b). The DBmII sediments (Event 1b, Fig. 11c) contain more pelagic material than DBmIII and let us suggest a mobilization almost immediately after DBmIII emplacement (OCR=1.04 for DBmIII). The time

lapse between these two flow events is unknown, but is probably short because the observed slight underconsolidation in DBmIII was preserved, with DBmII acting as seal (see above). The DBmII sediments are strongly overconsolidated and show indications of stronger deformation (R>4; φ-values of -60° to +50°; Fig. 10b). Assuming that only uniaxial overburden stress causes compaction during background hemipelagic sedimentation (i.e. a flattening of the strain ellipse; Fig. 5d) this picture may change during sliding or erosion (Fig. 5e). While the lower deformation grades (R=1-2) simply result from burial and compaction, the higher deformation grades (R=3->4) may be related to directional extension or compression during sliding. Additional indications for sliding are given by the φ-values, where high φ-values may indicate strong directional extension or shortening (Fig. 5e). Given these assumptions, our observations (i.e. high deformation grades and high rotation of σ_1 relative to horizontal) let us assume that the DBmII sediments were strongly deformed during sliding.

In contrast to other slid sediments, DBmI reaches the downslope location (GeoB8523; Figs. 1b and 3b), possibly as a result of a bigger failure event that had sufficient energy to reach downslope positions (Fig. 11c). These sediments lie on top of all debris flow deposits and consequently evolved from the youngest slide event (Event 2). This event shows radiocarbon ages of 10.5-10.9 ka B.P. (Henrich et al., 2008). It is notable that the hemipelagic sediments underlying the DBmI sediments are dated to Marine Isotope Stage 2 (MIS 2; Henrich et al., 2008), which fits very well with the calculated age of the hemipelagic sediments underlying the oldest flow event (Event 1a, see above).

Given that rip-up clasts are found in DBmI, this most recent event was probably vigorous enough to rework sediment from the underlying DBmII, consistent with the proposed missing material (see Ch. 4.4.2). The clasts show high deformation values (R>4) but low rotation values (+5° - +8°) and are believed to have been unaffected by sliding (Fig. 9c). The high deformation values may be a result of thinning or lengthening during redeposition or may tentatively be interpreted as approximations of the initial conditions before sliding began.

4.4.2 Origin of Rip-up clasts

As mentioned above (Ch. 4.4.1), the most recent debris flow event (Event 2) reworked sediment from the underlying unit and redeposited it as strongly consolidated indurated rip-up clasts (Fig. 4b) further downslope. The softer material of the reworked portion may have been transported even further downslope and was not found in our study area. The clasts, consisting of stiff mud (Ch. 4.1.3), are characterized by high Cu- and bulk density values (12 kPa in 2.5 mbsf and 1.86-1.92 g/cm³, Fig. 6c) and could be correlated with the upper layer of the DBmII sediments of core GeoB8520 (Fig. 6b). As demonstrated by the fall cone penetration tests, shear strength increased linearly with depth in the reference core GeoB8519 (Fig. 6b). A linear regression was calculated, showing shear strength increasing with a gradient of 2.85 kPa/m. Using this linear relationship, the original depths of the rip-up clasts was estimated to be 4 mbsf based on their peak shear strength of about 12 kPa. Assuming that the Cu-depth gradient of ~2.85 kPa/m can be extrapolated to all cores, the estimated original depth of the clasts correlates with the calculated missing sediment thickness of DBmII (~3.65 m, Tab. 1).

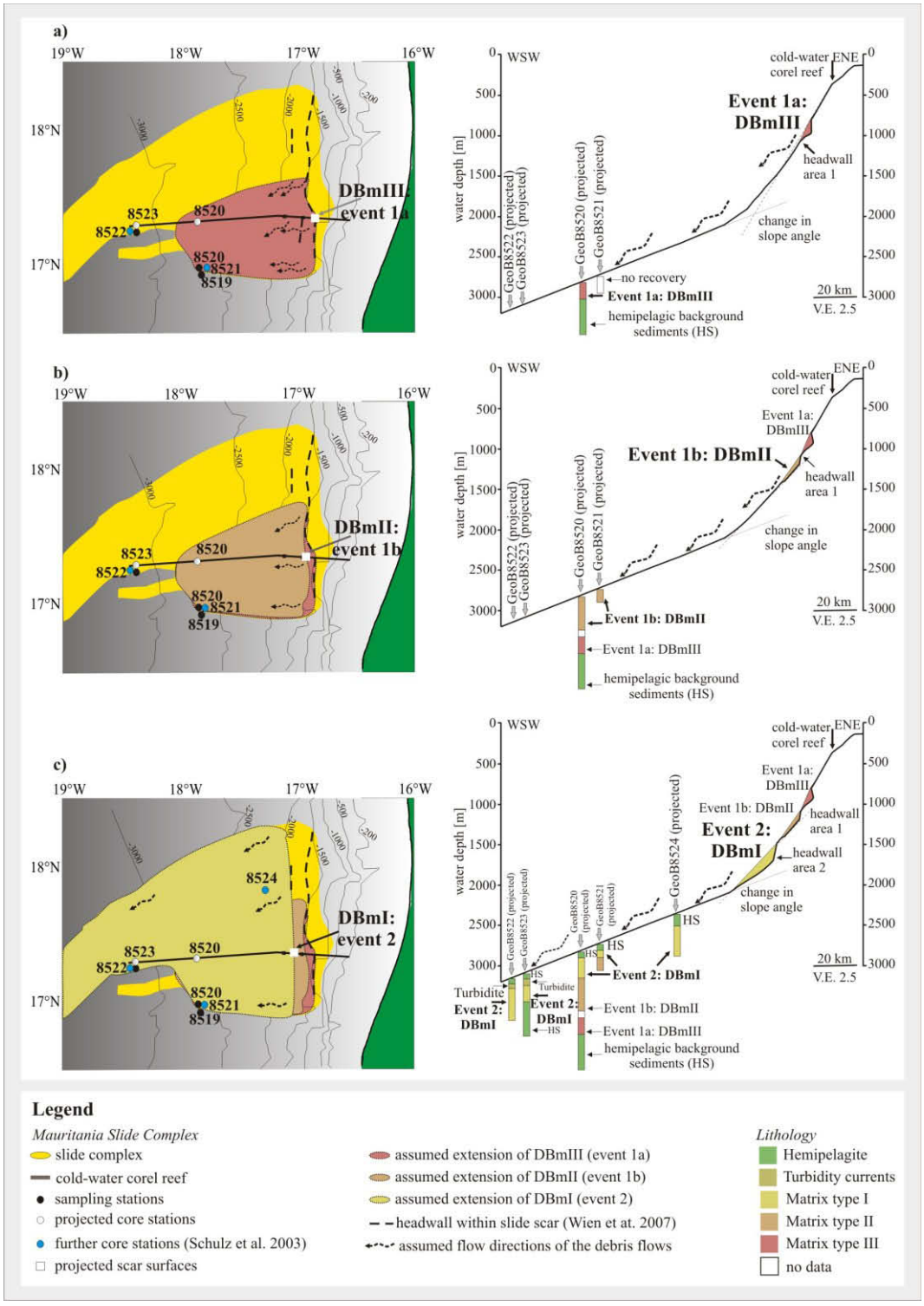

Fig.11: Overview sketches illustrating the temporal evolution of the debris flow units. The oldest events (Events 1a and 1b) are attributed to the upper slope and were generated in the south-eastern part of the slide complex and did not reach the downslope locations GeoB8523 and -8522 (a and b). The temporal and spatial relationship between these events remains uncertain. A younger debris flow of a bigger failure event (Event 2) might have mobilized sediment that now covers the entire slide affected area (c). This event was probably strong enough to rework sediment from the underlying DBmII unit, where we have estimated a missing material unit of 3.65 m thickness. The colors of the legend for DBmI, DBmII and DBmIII are compared to the lithology description of Figs. 4 and 6. For detailed description of the temporal evolution see text (Ch. 4.4..1).

4.4.3 Potential trigger mechanisms

It is known that weak sediment layers may facilitate mass wasting processes including slides and slumps (Haflidason et al., 2003; Masson et al., 2006). For the Storegga Slide on the glacially influenced Norwegian margin, a combination of weak layers and excess pore pressures (enhanced by deglaciation generated earthquakes) were proposed as the main causes. The failure planes were weak layers of marine clays (contourites) deposited during interglacial periods (Kvalstad et al., 2005). Although, the MSC is located at a non-glaciated margin, Antobreh and Krastel (2007) provide evidence for "lithologically weak layers" composed of rapidly deposited, poorly consolidated contourites with organic-rich fine-grained sediments at greater depths. A shallower equivalent of such a debris flow basal plane underwent ring shear and direct shear testing during our study. The majority of the μ_{res}-values measured in this material (μ_{res}=0.29-0.38, Fig. 7a) show typical values for clay-rich silt sediments (Lupini et al., 1981; Kopf and Brown, 2003) while corresponding [a-b]-values favor stable sliding conditions (Fig. 7c). The hemipelagic layer below the debrite unit, a silty greyish mud of glacial origin, shows the lowest strength (μ_{res}=0.18) and may well have lubricated the slope succession and facilitated mass wasting. The lowest [a-b]-values were observed in these layers with a higher sand content (Fig. 7d). Kopf and Brown (2003) showed that a 25-30 wt% of quartz has a profound strengthening effect in ring shear tests on clay samples when solely regarding [a-b] but not in the absolute shear strength. In the hemipelagic sediment underlying the debrite we observed a sand content of only ~18 wt%, suggesting that the low μ_{res} value may reflect the friction characteristics of clay sediments. Further, low [a-b]-values were observed in other sandy layers with sand contents of 15-32 wt% (Figs. 7c and d), but had μ_{res}-values of ~0.38 in contrast to the hemipelagic sandy interval (Fig. 7b). The sand particles tend to velocity weaken mixed clay-rich sediments and may be the reason for unstable deformation.

For our study area, sedimentation rates of 0.03-0.1 m/ka were published (Henrich et al., 2008; subm.), while we calculated sedimentation rates of ~0.05 m/ka for the hemipelagic sediments on top of the uppermost debris flow unit (GeoB8520). This difference in observations may be explained by lower accumulation rates mid- or down-slope caused by strong erosive forces such as younger mass wasting events (< 11 ka), sediment reworking, or redeposition further downslope. Hence, the upper 50 cm of hemipelagic sediment may not reflect the complete record for the calculated period since 10.5 ka B.P. Additionally, during the glacial periods, sediment input increased up to 0.2 m/ka (for 25-20 ka B.P.) and 0.37 m/ka (for 20-15 ka B.P.), which may also lead also to excess pore pressures decreasing sediment stability (Masson et al., 2010). The calculated age of ~10.5 ka B.P. for the uppermost debris flow unit is tied to the beginning of the present interglacial period. In contrast, the oldest debris flow unit was emplaced < 24 ka B.P. (the ^{14}C-age of the underlying hemipelagite), which is known as a period of decreasing sea-level; the maximum sea-level lowstand occurred at about 20 ka B.P. (Siddall et al., 2003). During periods of sea-level fall/lowstand such as the Last Glacial Maximum (LGM), hydrostatic pressure decreased, may have exposed gas seeps on the continental shelf or upper continental slope (Luyendyk et al., 2005; Hill et al., 2006). Migration of the free gas through the sediment column may have led to a decrease in sediment strength, which is favored by excess pore pressures. Indications of overpressured gas or fluids in the sediments were observed by Krastel et al. (2006a) and Antobreh and Krastel (2007).

The interaction between the excess pore pressure, which might be linked to post- and interglacial sea-level fluctuations, and with the presence of lithologically weak layers could be possible causes for the mass wasting. Unfortunately, the discussion of the trigger mechanisms at

this stage of our investigations remains speculative because of the uncertainties regarding triggers such as earthquakes (e.g. far-field events in the Cape Verde region).

4.5 Conclusion

Using data from earlier studies of the Mauritania Slide Complex, we quantified the geomechanical behavior and strain of debrite units interbedded with hemipelagites. From this, we suggest a sequential failure mechanism that controlled the evolution of at least two different slide events:

- The deposits of the oldest slide event (Event 1a and 1b) got emplaced < 24 ka B.P. and are characterized by slightly under- to strongly overconsolidated sediments (DBmIII and DBmII). While the slight underconsolidation results from rapid burial by the second event (Event 1b), the strong overconsolidation results from a reworked and missing sediment column.
- The second slide event (Event 2) evolved further downslope mass wasting (deposits of DBmI) and reworked the sediments from the underlying unit. With a calculated age of ~ 10.5 ka B.P., the deposits (DBmI) are characterized by a normal consolidation state. Besides the debris flow deposits, overconsolidated rip-up clasts were found in the uppermost unit (DBmI), which may be related to the second debrite unit (DBmII).
- Our geotechnical data further identify a "weak layer" of hemipelagic mud beneath the debrites as a potential failure plane. Such layers, in combination with excess in pore pressure from rapid changes in sedimentation rate during glacial-interglacial dynamic changes appear to be the most likely candidates for future landslide failure, in particular since clay-rich, muddy contourite deposits are inferred in seismic profiles at greater depth.

Acknowledgments

We thank the captain and crew of the *RV* Meteor for their support during the cruises M58/1 and M65/2. We also thank the three unknown reviewers for their efforts and suggestions on how to improve the manuscript. This study was financed through the Deutsche Forschungsgemeinschaft (MARUM, Project SD5) and supported by the DFG-Excellence Initiative International Graduate School for Marine Sciences, Bremen.

References

Antobreh, A.A., Krastel, S., 2007. Mauritania Slide Complex: morphology, seismic characterisation and processes of formation. International Journal of Earth Sciences 96, 451-472.

Baraza, J., Ercilla, G., Nelson, C.H., 1999. Potential geologic hazards on the eastern Gulf of Cadiz slope (SW Spain). Marine Geology 155,191-215.

Behrmann, J.H., Kopf, A., 1993. Textures and Microfabrics in fine-grained muds and mudstones from Site 808, Nankai Accretionary Prism. Proceedings of the Ocean Drilling Program, Scientific Results 131, 45-56.

Bishop, A.W., Green, G.E., Garga, V.K., Andresen, A., Browns, J.D., 1971. A new ring shear apparatus and its application to the measurements of residual strengths. Géotechnique 21, 273-328.

Bryant, W.R., Bennett, R.H., 1988. Origin, Physical, and Mineralogical Nature of Red Clays: The Pacific Ocean Basin as a Model. Geo-Marine Letters 8, 189-249.

Casagrande, A., 1936. The Determination of the Pre-consolidation Load and its Practical Significance. Proceedings of the International Conference on Soil Mechanics and Foundation Engeneering 3, 60–64.

Colman, J.G., Gordon, D.M., Lane, A.P., Forde, M.J., Fitzpatrick, J.J., 2005. Carbonate mounds off Mauritania, Northwest Africa: status of deep-water corals and implications for management of fishing and oil exploration activities. In: Freiwald, A., Roberts, J.M. (Eds.). Cold-water Corals and Ecosystems. Springer, Heidelberg, pp 417-441.

Davison, J., 2005. Central Atlantic margin basins of North West Africa: Geology and hydrocarbon potential (Morocco to Guinea). Journal of African Earth Sciences 43, 254-274.

Danzeglocke, U., Jöris, O., Weninger, B., 2009. CalPal-2007^{online}. http://www.calpal-online.de/, accessed 2009-25-03.

deMenocal, P., Ortiz, J., Guilderson, T., Adkins, J., Sarntheim, M., Baker, L., Yarusinsky, M., 2000. Abrupt onset and termination of the African Humid Period: rapid climate responses to gradual insolation forcing. Quaternary Science Reviews 19, 347-361.

De Mol, B., Huvenne, V., Canals, M., 2009. Cold-water coral banks and submarine landslides: a review. International Journal of Earth Sciences 98, 885-899.

DIN 18123:1996-11. Baugrund, Untersuchung von Bodenproben - Bestimmung der Korngrößenverteilung. Beuth-Verlag, Berlin, pp. 396-407.

Fry, N., 1979. Random point distributions and strain measurement in rocks. Tectonophysics 60, 89-105.

Geolsoft, 2008. Avaibalbe from: www.geolsoft.com.

Haflidason, H., Sejrup, H.P., Berstad, I.M., Nygard, A., Richter, T., Bryn, P., Lien, R., Berg, K., 2003. A weak layer feature on the Northern Storegga Slide escarpment. In: Mienert, J., Weaver, P. (Eds.), European Margin Sediment Dynamics, Side-Scan Sonar and Seismic Images. Springer, Berlin, pp. 55-62.

Hampton, M.A., Lee, H.J., Locat J., 1996. Submarine landslides. Reviews of Geophysics 3, 33-59.

Hansbo, S., 1957. A new approach to the determination of the shear strength of clay by the fall-cone tests. Proceedings of the Royal Swedish Geotechnical Institute 14, 7-48.

Henrich, R., Hanebuth, T., Krastel, S., Neubert, N., Wynn, R. B., 2008. Architecture and sediment dynamics of the Mauritania Slide Complex. Marine and Petroleum Geology 25, 17-33.

Henrich, R., Cherubini, Y. and H. Meggers (submitted) Climate induced sediment dynamics in a hyperarid canyon system: the Timiris Canyon off Mauritania (Central Sahara). Marine Geology.

Hill, T.M., Kennett, J.P., Valentine, D.L., Reddy, C.M., Nelson, R.K., Behl, R.J., Robert, C., Beaufort, L., 2006. Climatically driven emissions of hydrocarbons from marine sediments during deglaciation.

Jacobi, R.D. 1976. Sediment slides on the northwestern continental margin of Africa. Marine Geology 22, 157-173.

Krastel, S., Wynn, R.B., Hanebuth, T., Henrich, R., Holz, Ch., Meggers, H., Kuhlmann, H., Georgiopolou, A., Schulz, H.D., 2006a. Mapping of seabed morphology and shallow sediment structure of the Mauritania continental margin, Northwest Africa: some implications for geohazards potential. Norwegian Journal of Geology 86, 163-176.

Krastel, S., Cruise Participants, 2006b. Report and Preliminary Results of Meteor Cruise M 65/2, Dakar- Las Palmas 04.07.-26.07.2005, Berichte, Fachbereich Geowissenschaften, Universität Bremen, 249, 185pp.

Kopf, A., Brown, K.M., 2003. Friction experiments on saturated sediments and their implications for the stress state of the Nankai and Barbados subduction thrusts. Marine Geology 202, 193-210.

Kvalstad, T.J., Andresen, L., Forsberg, C.F., Berg, K., Bryn, P., Wangen, M., 2005. The Storegga Slide: evaluation of triggering sources and slide mechanics. Marine and Petroleum Geology 22, 245-256.

Locat, J., Lee, H.J., 2002. Submarine landslides: advances and challenges. Canadian Geotechnical Journal 39, 193-212.

Ladd, C.C., Foott, R., 1974. New design procedure for stability of soft clays. Journal of the Geotechnical Engineering Division 110, 763-786.

Ladd, C.C., Foott, R., Ishihara, K., Schlosser, F., Poulos, H.G., 1977. Stress-Deformation and Strength Characteristics. Proceedings of the 9th International Conference on Soil Mechanics and Foundation Engineering, 421-495.

Lonsdale, P., 1982. Sediment drifts of the Northeast Atlantic and their relationship to the observed abyssal currents. Bulletin Institute Geologique Bassin Aquitaine, Bordeaux 31, 141-149.

Lunne, T., Berre, T., Andersen K. H., Strandvik, S., Sjursen, M., 1998. Effects of sample disturbance and consolidation procedures on measured shear strength of soft marine Norwegian clays. Canadian Geotechnical Journal 43, 726-750.

Lupini, J.F., Skinner, A., Vaughan, A.E., 1981. The drained residual strength of cohesive soils. Géotechnique 31, 181-213.

Luyendyk, B., Kennett, J., Clark, J.F., 2005. Hypothesis for increased atmospheric methane input from hydrocarbon seeps on exposed continental shelves during glacial low sea level. Marine and Petroleum Geology 22, 591-596

Martinez, M.L., Intralawan, A., Vázquez, G., Pérez-Maqueo, O., Sutton, P., Landgrave, R., 2007. The coasts of our world: Ecological, Economic and Social Importance. Ecological Economics 63, 254-272.

Masson, D.G., Harbitz, C.B., Wynn, R.B., Pedersen, G., Løvholt, F., 2006. Submarine landslides: processes, triggers and hazard prediction. Philosophical Transaction of the Royal Society A 364, 2009-2039.

Masson, D.G., Wynn, R.B., Talling, P.J., 2010. Large Landslides on Passive Continental margins: Processes, Hypotheses and Outstanding Questions. In: Mosher, DC., Shipp, C., Moscardelli, L., Chaytor, J., Baxter, C., Lee, H., and Urgeles, R. (Eds.), Submarine Mass movements and their consequences IV. Advances in Natural and Technological Hazards Series, Springer, pp. 153-165.

Matthewson, A.P., Shimmield, G.B. and D. Kroon, D., 1995. A 300 kyr high-resolution aridity record of the North African continent. Paleoceanography 10 (3), 677-692.

Ramsey, J.G., Huber, M.I., 1983. The techniques of modern structural geology, Vol.1: Strain Analysis. Academic Press, London, pp. 107-125.

Scholz, C.H., 1998. Earthquakes and friction laws. Nature 391, 37-42.

Schulz, H.D., Cruise participants, 2003. Report and Preliminary Results of Meteor Cruise M 58/1, Dakar- Las Palmas 15.04.-12.05.2003, Berichte, Fachbereich Geowissenschaften, Universität Bremen, 215, 186pp.

Seibold, E., Hinz, K., 1974. Continental slope construction and destruction, West Africa. In: Burk, C.A., Drake, C.L. (Eds.). The geology of continental margins, Springer-Verlag, New York, pp. 179-196.

Siddall, M., Rohling, E.J., Almogi-Labin, A., Hemleben, C., Meischner, D., Schmelzer, I., Smeed, D.A., 2003. Sea-level fluctuations during the last glacial cycle. Nature 423, 853-858.

Stuiver, M., Polach, H.A., 1977. Discussion: Reporting of ^{14}C Data. Radiocarbon 19 (3), 355-363.

Stuiver, M., Braziunas, T.F., 1993. Modelling Atmospheric ^{14}C Influences And ^{14}C Ages Of marine Samples To 10,000 BC. Radiocarbon 35 (1), 137-189.

Sultan, N., Cochonat, P., Dennielou, B., Bourillet, J.F., Savoye, B., Colliat, J.L., 2000. Surconsolidation apparente et pression osmotique dans un sédiment marin, Comptes Rendus de l'Académie des Sciences Paris - Earth and Planetary Science 331, 379-386.

Sultan, N., Cochonat, P., Canals, M., Cattaneo, A., Dennielou, B., Haflidason, H., Laberg, J.S., Long, D., Mienert, J., Trincardi, F., Urgeles, R., 2004. Triggering mechanisms of slope instability processes and sediment failures on continental margins: a geotechnical approach. Marine Geology 213, 291-321.

Taylor, RE., 1987. Radiocarbon Dating: An Archaeological Perspective. Academic Press, Orlando, 212 pp.

Tari, G., Molnar, J., Ashton, P., 2003. Examples of salt tectonics from West Africa: a comparative approach. In: Arthur, T., Macgregor, D.S., Cameron, N.R. (Eds.) Petroleum Geology of Africa: New Themes and Developing Technologies. Geological Society, London, Special Publications 207, pp. 85-104.

Wallbrecher, E., Fritz, H., Unzog, W., 1996. Estimation of the shape factor of a paleostress ellipsoid by comparison with theoretical slickenline patterns and application of an eigenvalue Method. Tectonophysics 255, 177-187.

Wentworth, C.K., 1922. A scale of grade and class terms for clastic sediments. Journal of Geology 30, 377-392.

Wien, K., Kölling, M., Schulz, H.D., 2007. Age models for the Cape Blanc Debris Flow and the Mauritania Slide Complex in the Atlantic Ocean off NW Africa. Quaternary Science Reviews 26, 2558-2573.

Wynn, R.B., Masson, D.G., Stow, D.A.V., Weaver, P.P.E., 2000. The Northwest African slope apron: a modern analogue for deep-water systems with complex seafloor topography. Marine and Petroleum Geology 17, 253-265.

Zühlsdorff, C., Wien, K. Stuut, J.B.W., Henrich, R., 2007. Late Quaternary sedimentation within a submarine channel-levee system offshore Cap Timiris, Mauritania. Marine Geology 240, 217-134.

5. Mass wasting dynamics at the deeper slope of the Liguiran Margin (Southern France)

Förster, A. [1], Spieß, V. [1], Kopf, A.J. [1], Dennielou, B. [2]

Published in *Mosher, DC., Shipp, C., Moscardelli, L., Chaytor, J., Baxter, C., Lee, H., and Urgeles, R. (eds.), Submarine Mass movements and their consequences IV. Advances in Natural and Technological Hazards Series 28, Springer, pp. 67-77.*

Abstract

Submarine landslides are very common on the tectonically and seismically active Ligurian margin, NW-Mediterranean Sea. We present geophysical, sedimentological and geotechnical results from two extensive landslide complexes in water depth exceeding 1500 m on the steep continental slope (>11°) near the Var Canyon.

At the Western Landslide Complex, facing the Var Canyon, we observe multiple headwalls and tilted layering. Undisturbed and failed sediments are characterised by a downward increase in bulk density and shear strength, the failed portion of which shows low intrinsic friction coefficients of 0.27. Otherwise, at the Eastern Landslide Complex, which shows smooth headwall features containing debrites and hemipelagic silty clays with pebbles, we observed constant bulk density of the failed sediments; however the shear strength in the remobilized sediment is lower than in the hemipelagites. This indicates that the failed material may have incorporated seawater and has retained its underconsolidated state until the present. The material is hence prone to future landsliding in case of seismic loading and/or the occurrence of other factors destabilizing the sediment.

Key words: Ligurian Basin, Landslide, geotechnical characterisation

5.1 Introduction

Submarine landslides are an important process in transporting sediment to deeper water and are attracting increasing interest due to their tsunamigenic potential or their role as potential hazards for offshore platforms, cables, pipelines, and other installations. The trigger mechanisms of submarine landslides are still incompletely understood (Locat and Lee 2002), so that the study of submarine landslides and mass wasting processes in general at continental margins is a priority in the study of ocean margins (e.g. Hampton et al. 1996, McAdoo et al. 2000, Bryn et al. 2005).

In the Ligurian Basin, a tectonically complex and seismically active area at the NW-Mediterranean Sea, the Var Canyon and its adjacent slopes are particularly susceptible to sediment failure and landslide processes. While previous studies focused largely on the 1979 Nice Airport Slide or Var Canyon processes (e.g. Cochonat et al. 1993, Piper and Savoye 1993, Mulder et al. 1994, Klaucke and Cochonat 1999, Klaucke et al. 2000, Dan et al. 2007), our study uses geophysical data and core material from two landslides located on the deeper (>1500 m

[1] MARUM - Center for Marine Environmental Sciences, University of Bremen, PO box 330 440, 28334 Bremen, Germany.

[2] IFREMER – French Research Institute for Exploitation of the Sea, Département des Géosciences Marines, PO box 70, 29280 Plouzané Cédex France.

water depth), steep Ligurian slope. Data acquisition took place during expedition M73/1 of R/V *Meteor* in July 2007 (Fig. 1). This paper focuses on the geometry of the landslide complexes from bathymetric and seismic data, the sedimentary record of the failed sediments relative to adjacent hemipelagic sediments, the physical properties and the geotechnical character of the sediments. Dating of the events has not been performed yet, but is required to comprehend timing of mass wasting.

5.1.1 Geological background in the study area

The Ligurian Basin is a marginal back-arc basin that formed by rapid continental extension during the Upper Oligocene-Miocene (Burrus et al. 1987, Pasquale et al. 1996). Drift of the Corsica-Sardinian block and formation of the Apennines range until the early Miocene are major consequences. During the Messinian (late Miocene), Mediterranean sea level drawdown subaereal erosion affected the margin to a depth of about 1500 m below the pre-Messinian sea level (e.g. Ryan 2009). In the present-day basin active deformation occurs offshore at a small rate of about 1.1 m/ka (Bethoux et al. 1998). Furthermore, seismic activity is well known in this area with earthquakes of magnitudes up to M 6.3 (July 1963), although more common are smaller magnitude earthquakes of M 2.2 - M 4.5 (Rehault and Bethoux 1984).

The Quaternary uplift of the Alps and associated erosion supply large volumes of sediment to the Ligurian Basin. The system is fed from small mountain-supplied rivers (Var, Paillon and Roya rivers). During floods, suspended sediment concentration can reach tens of kg/m^3, resulting in hyperpycnal flows and, later, underconsolidated deposits (Mulder et al. 1998). The submarine Var Canyon system represents the offshore extension of the Var River, one of the major rivers entering the Ligurian Basin west of Nice (Fig. 1). The area is

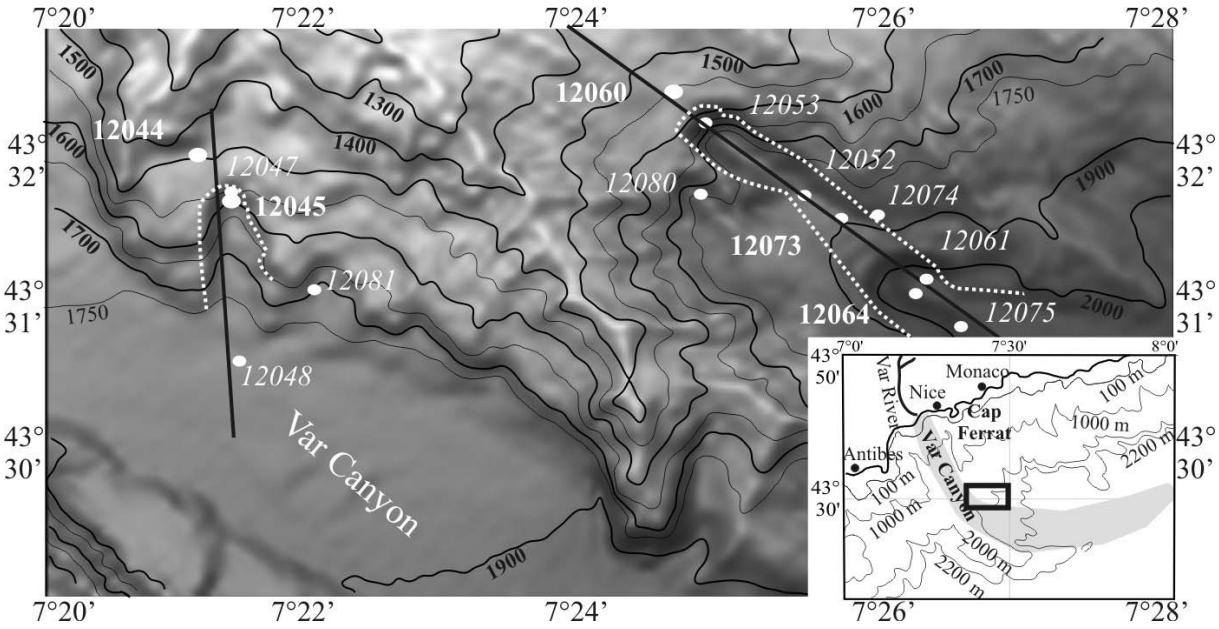

Fig.1: Shaded relief bathymetric display with contour lines of the study area with core locations of cruise M73/1 in water depths ranging from 1170 m to 2100 m. Cores used in this study are outlined by bold numbers. Profile lines see Fig. 2. Small map: Map of the Ligurian continental margin (modified after Piper and Savoye 1993) with the study area indicated by the black box.

characterised by a very narrow continental shelf (2-3 km) and a steep continental slope with an average angle in excess of 11° (Cochonat et al. 1993). While sediment supply in the Var system is high, Sultan et al. (2004) have quantified sedimentation rates as 8 m/ka between ~12 ka and ~7 ka BP, and 3.5 m/ka from 7 ka BP until now.

5.2 Methods

During R/V Meteor cruise M73/1 the entire Var Canyon area and adjacent slopes were mapped using a bathymetry system (SIMRAD EM120 and EM710) and a high-resolution, 16-channel seismic reflection system. For more comprehensive descriptions of the instruments and measurement techniques used, refer to Kopf et al. (2008). Based on the multibeam swathmapping and seismic reflection data, 16 gravity cores (length 2-10 m, 0.1 m diameter; further details in Kopf et al. 2008) were taken in two large-scale landslide complexes (Fig. 1). To illuminate the mass wasting dynamics and timing of the events, coring took place at various locations outside the landslide complexes and within the slide complex in various locations from the headwalls down to the run-out zones. All cores were studied sedimentologically and sediment physical properties were recorded by using a Multi-Sensor Core Logger (MSCL), whose results can be found in Kopf et al. (2008). For this post-cruise study, we selected two cores from each landslide complex for dedicated geotechnical measurements. Reference sites (GeoB12044 and -12060) and cores of the slide body (GeoB12045 and -12064) should give information about the textural change and evolution of the sediments during failure.

In addition to the physical properties, the sediment samples were tested for their stiffness to detect “weak layers”. For this, the undrained shear strength C_u was determined using a Vane shear apparatus (Blum 1997). To compare the strength of small clasts to that of the matrix in the landslide sediment, we used a falling cone penetrometer (Wood 1985) to calculate C_u -values at discrete sampling points that were too small for the use of the Vane shear apparatus.

Furthermore, information about the frictional response of the sediments was collected by means of direct shear tests on remolded samples (drained shear strength values). The core sampling strategy was based on the results from the MSCL runs as well as from core descriptions. The drained shear strength values were normalised against the normal stress, where the coefficient of friction, μ, is the ratio between shear stress and normal stress. The compressibility of the specimens was measured using a fix-ring oedometer apparatus. In direct shear and oedometer tests, the experimental setup corresponds with the current stress state of the sediment; therefore, the load was increased incrementally up to 300 kPa. For the direct shear tests, a sliding velocity of 0.01 mm/min was chosen. The maximum stress the sediment experienced (i.e. the preconsolidation pressure σ_{pc}) was determined after Casagrande (1936). The consolidation status of the sediment was estimated from the overconsolidation ratio (OCR) of preconsolidation stress, σ_{pc} to vertical effective stress, σ_{eff}:

$$OCR = \sigma_{pc} / \sigma_{eff} \quad (2.1).$$

5.3 Results

5.3.1 Geophysical characterization

Bathymetric, seismic reflection and parasound data reveal two different extensive slide complexes between 7°20'E to 7°30'E and 43°30'N to 43°33'N in about 1500-2000 m water depth (Figs. 1 and 2). The Western Landslide Complex lies within the Var Canyon and shows many steep (32°) elongated head scarps with heights of ~ 40 m and talus at their base. Above the headwall area rough seafloor reflectors are visible. Failed sediments could not be unambiguously observed in the seismic profile (Fig. 2a). At the transition to the Var Canyon valley the slope angle decreases to ~11°. A similar, Eastern Landslide Complex is found farther away from the Var Canyon, striking to the Southeast in an area with slope angle of about 20° (Figs. 1 and 2b). It is characterized by a single, rather smooth headwall (Fig. 2b). In contrast to the Western landslide complex, we observe several indications for mass wasting processes, such as the failed deposits along a SSE- trending pathway, including hummocky topography and transparent units in the seismic reflection lines (Fig. 2b).

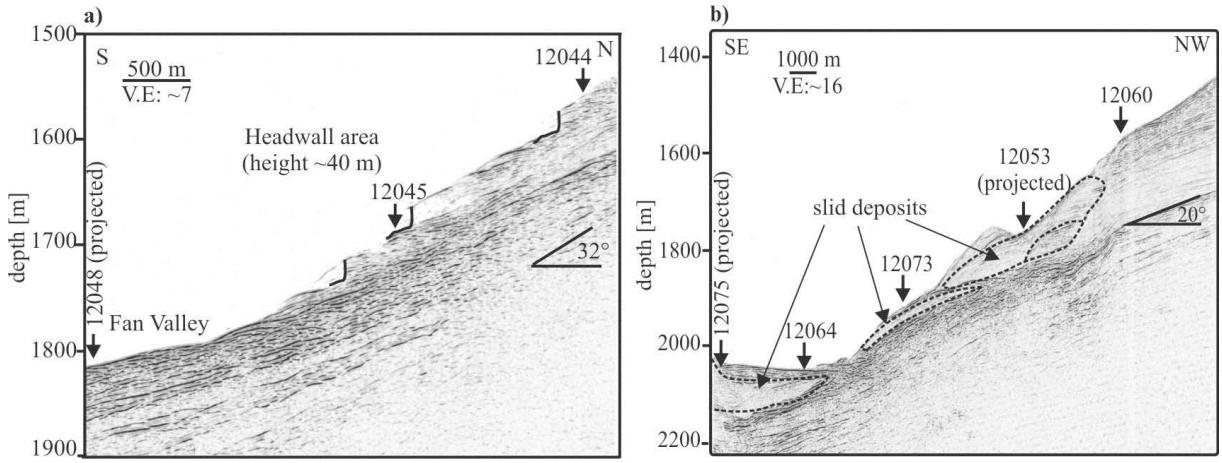

Fig.2: Headwall striking profiles with core locations of the (a) Western (with incisions in the headwall area) and (b) Eastern Slide Complex (with failed deposits). For locations of the profiles see Fig.1.

5.2.2 Western Landslide Complex

On top of the majority of the 5 cores taken at the Western Slide Complex (Ch. 2) a similar lithostratigraphic succession (back-ground sediment) characterized by homogeneous, but in places also bioturbated, fine-grained hemipelagic silty clay with some coarser-grained intervals. Minor lithology is pelagic ooze with shell fragments (mostly pteropods shell debris, Kopf et al. 2008). Sediments interpreted as reworked along the assumed pathway of the landslide consist of dark grey silty-clay with some sandy intervals and inclusions of organic material or pelagic ooze (Figs. 3a and b and; Kopf et al. 2008).

In the reference core GeoB12044 sharp oblique contacts (20-45°) are present both within the hemipelagic sediment drape and into the underlying dark-grey, stiff silty clay. Bulk density increases slightly downward from ~1.75 g/cm^3 in the hemipelagic sediments to 1.90 g/cm^3 while C_u remains more or less constant. Following Cochonat et al. (1993), we calculated the C_u/σ_{pre}-values to eliminate the effect of apparent overconsolidation on normally consolidated sediments

(C_u/σ_{pre}= 0.2-0.4). As can be seen in Figure 4a, the undisturbed sediments are more or less normally consolidated (station GeoB12044). In the reworked silty clays of core GeoB12045 collected near the headwall bulk density and C_u increase downward from 1.95 to ~ 2.08 g/cm^3 and from 25 to ~75 kPa with a sharp gradient at the transition between the hemipelagics above and the silty clays below at 3.2 m core depth (from 1.82 to ~1.95 g/cm^3 and from 3 to ~25 kPa (Figs. 3b and 4a). The residual coefficient of friction (μ_{res}) of the hemipelagic sediments is between 0.36 and 0.42, which is typical for normally consolidated clay-rich silt sediments (Kopf and Brown 2003). However, μ_{res} of silty clays in core GeoB12045 located in the deeper portion of the headwall is 0.27-0.29, significantly lower than in the hemipelagics, and argues for a different sediment compositions (see above). The overconsolidation ratio (OCR) of the hemipelagic sediment slightly exceeds 1, thus indicating a slight overconsolidation, whereas the reworked silty clays results show either normally consolidated (OCR = 1) or slightly underconsolidated (OCR = 0.79 (Fig. 3a).

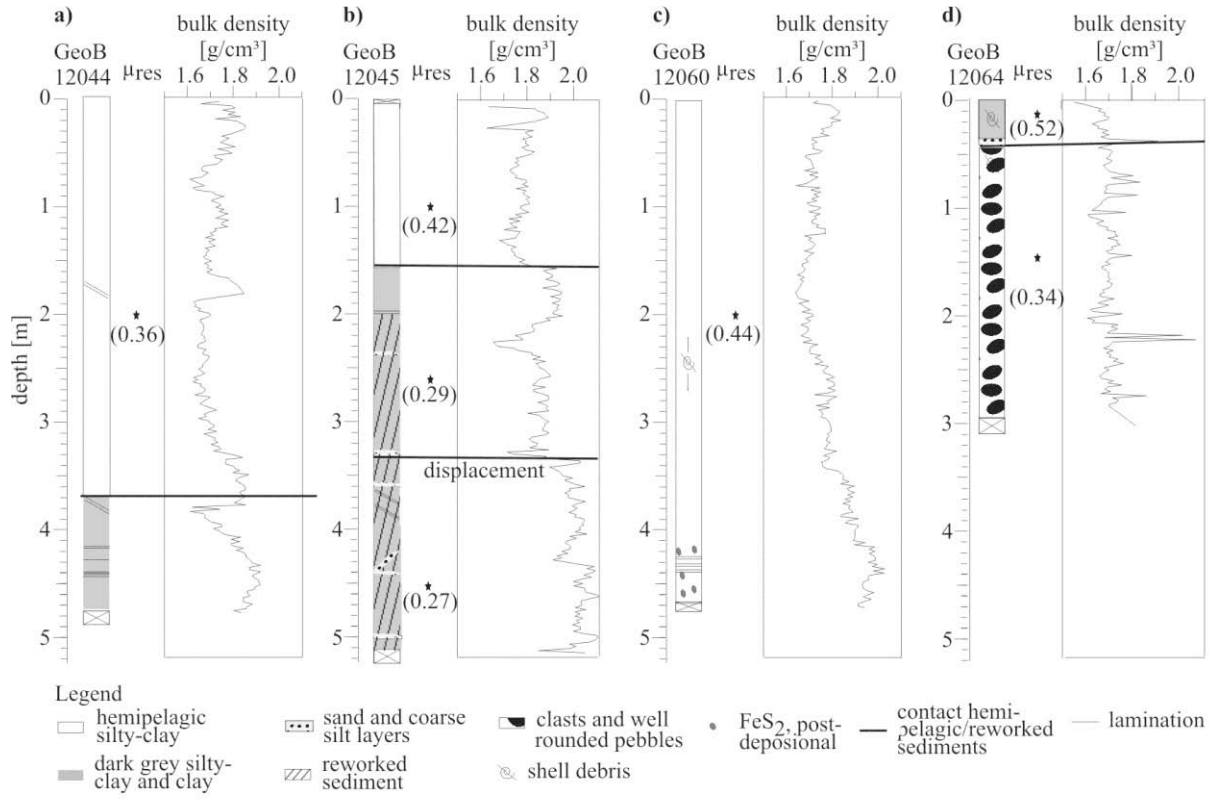

Fig.3: Core description, bulk density (MSCL) and residual coefficient of friction (μ_{res}) from direct shear tests: Western Slide Complex core taken above (a) and below the headwall (b). Eastern Slide Complex cores taken above the headwall (c) and further downslope (d). Positions of the cores: Fig. 1.

5.3.3 Eastern Landslide Complex

On the Eastern Slide Complex, the hemipelagic drape comprises a mixture of bioturbated silty mud and mud with varying contents of sand and clay (Fig. 3c). In these sediments there are diagenetic fronts determined by colour banding and pyritization of shell fragments (Fig. 3c; Kopf et al. 2008). In contrast to the Western Slide Complex, the debrites resulting from mass wasting contain poorly rounded, indurated clasts and pebbles in a dark silty-clay matrix (Fig. 3d; Kopf et

al. 2008). Hemipelagic drape in core GeoB12060 shows a linear increase in bulk density and undrained C_u downward, reaching 1.90 g/cm^3 and ~20 kPa respectively. Peaks between 4.2 and 4.8 m correlate with pyrite layers (Fig. 3c). The reworked sediments are characterized by lower bulk density 1.70 g/cm^3, and variable C_u from 5 to 15 kPa (Figs. 3d and 4b). While hemipelagic sediment above the headwall (core GeoB12060) are normally consolidated, those sampled farther downslope in Core GeoB12064 are slightly overconsolidated (OCR=1.73). Reworked sediments are slightly underconsolidated (OCR = 0.72 [Fig. 4b]). Surprisingly, there is no significant difference in shear resistance between the hemipelagic and the reworked sediments (μ_{res} ranging between 0.34 and 0.52; Figs. 3c and d).

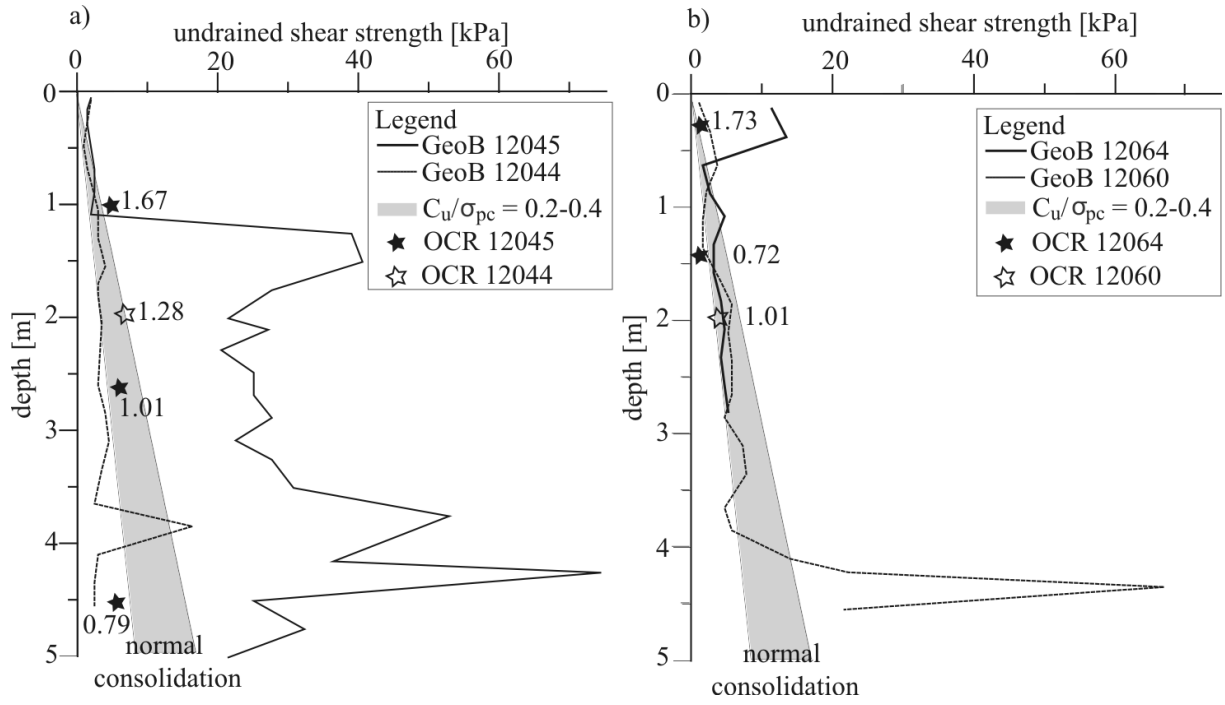

Fig. 4: Undrained shear strength from Vane shear apparatus, OCR, and C_u/σ_{pre} used as an indicator for normal consolidation state (from Cochonat et al. 1993) from Western (a) and the Eastern (b) landslide complexes. For calculation of OCR, see text and equation 2.1.

5.4. Discussion

5.4.1 Mechanical behaviour of the sediment

In both landslide complexes the OCR-values obtained for the hemipelagic sediments indicate slight overconsolidation (Fig. 4). This may result from "apparent" overcon-solidation (e.g. Sultan et al. 2000) that is typical for superficial sediments and is often associated with colour banding (syn- as well as post-depositional), pyritization, burrows and other evidence for physico-chemical and biogeochemical processes (Ch. 3.2 and 3.3; Kopf et al. 2008). To eliminate the effect of the "apparent" overconsolidation on the interpretation of the data, C_u/σ_{pre}-values were consulted. Based on this correction, hemipelagic sediments in both landslide complexes are normally consolidated (Fig. 4).

The recovered failed deposits at the Eastern Slide Complex (downslope location GeoB12064) are slightly underconsolidated (OCR=0.72, C_u = ~3 kPa in 1.5 mbsf), most likely because of incorporation and amalgamation of surface sediments. Such rapid redeposition inhibits fluid expulsion to the overlying sediment column. As a consequence excess pore pressure may be preserved during burial (Dugan et al. 2000, Sultan et al. 2004) and result in underconsolidation of the sediments.

Further upslope of station GeoB12064 (Fig. 1), in the seismic profile across the landslide, some deposits along the slope appear as if they have failed (Fig. 2b), however, in the core no evidence for debrites has been found (e.g. at station GeoB12073 at the middle part of the landslide body). Instead we recovered very stiff silty-clay sediments, covered by hemipelagic sediment, characterised by high C_u-values of 12 kPa at 1mbsf and bulk density values up to 1.85 g/cm^3 (Kopf et al. 2008). This mismatch may be explained by low core penetration (core length: 1.7 m), lack of vertical resolution of the multichannel seismic system (see review Kopf et al. 2008), or the fact that the stiff silty-clay material recovered at GeoB12073 represents older sediment that has been unroofed when the slide complex formed.

In the downslope location GeoB12064, we observe clasts in the normally consolidated debrite deposits with the same composition, color and similar C_u-values of 10-15 kPa when compared to the stiff sediments of core GeoB12073. Also the clasts are poorly rounded and hence suggest a short transport distance downslope. These observations support two hypotheses of the slide development. Our first contention is that the Eastern Slide may originate in at least two stages: One initial phase that caused the upper portion of the landslide scar removed some of the overlying sediment. In order to readjust the slope angle, some of the unroofed material (of GeoB12073-type) may have then been amalgamated in a silty clay mass flow in the deeper portion of the slide (as evidenced by GeoB12064). A second alternative hypothesis is that the slide developed as split debris flow with high density at the base and a lower density at the top. The high density debris flow is characterised by stiff sediments (high C_u-values) and arrives only at the midslope part of the landslide body (GeoB12073). Due to higher flow velocity, the low density flow, characterized by low C_u-values, arrives further downslope (GeoB12064) and would partly rework sediments from the underpassing debris unit so that some clasts of the high density/stiff unit may then be deposited further downslope within the low density unit (Postma et al. 1988). However, in the absence of the exact dating or deeper coring/drilling, no final conclusion of timing of the landslide can be drawn.

At the Western Slide Complex, the mechanical behaviour of the sediments (GeoB 12045) during failure seems to have been different (Figs. 3a, 3b and 4a). Two distinct excursions could be observed in the bulk density values, each accompanied by a strong initial increase. Interestingly, one lies between the hemipelagite and the reworked silty-clay, but the other within itself (Fig. 3b). These steps may be related to different failure events. In addition, several layers containing coarser-grained material interrupt the dark silty-clay sediment column. Furthermore, in the deeper part of core GeoB12045, the failed sediments are characterized by overconsolidation with C_u up to 30 kPa at 2.8 mbsf and ~52 kPa in 3.8 mbsf. These high C_u-values may result from removal of overlying sediments by mass wasting prior to the deposition of the hemipelagic drape (Fig. 4a). We could estimate a removal of a ~ 20 m thick sediment column for the upper part and a missing sediment sequence of ~ 13 m between the lower and the upper part of the failed material. The generally low intrinsic friction values of 0.27-0.29 provide sufficient weakness for repeated failure events, which may be mirrored by tilted layers with angles of 25° to 40° observed in the hemipelagic sediments as well as in the assumed reworked

sediment column (Figs. 3a and b). Also, seismic reflection data show a rough seafloor above and several incisions in the headwall area (see Fig. 2a), which might be a result of older sliding activity or multiple small failure events. However, the glide plane and other sliding induced features are not clearly visible owing to a lack of resolution in the profiles (e.g. Fig. 2; see also Kopf et al. 2008). Given the above-mentioned observations, we suggest that the sedimentological features as well as the different thickness of sediment removal could be explained by different time shifted slide events with contortion of strata along curved slide surfaces at a spacing of meters.

5.4.2 The role of the slope angle to determining failure type and variability of failure events

Slope angle as a governing factor for slope instability in both granular and cohesive materials, has been shown by stability analysis (Cochonat et al. 1993). Assuming that C_u-values increase linearly downward in the sediment column (see review by Bartetzko and Kopf 2007), normally consolidated sediments with a strength of 8 kPa in 2.5 mbsf may fail at a slope angle of 20° (Cochonat et al. 1993). With a lower slope angle of 10° these sediments may fail at a sediment thickness of 6 mbsf with C_u-values of 12 kPa (Cochonat et al. 1993, Mulder et al. 1994). In our study, we observed high slope angles of ~32° at the Western Slide Complex adjacent to the Var Canyon flanks (Figs. 1 and 2a). In the Var Canyon upper Fan valley, in which hyperpycnal flows that transfer sediment from the shelf to the deeper basin have been described, the accumulation rate is high (Migeon et al. 2006). We suggest that these conditions together with the mechanical behaviour of the sediments (Ch. 4.1) and a high slope gradient greatly enhance the frequency of failure events at the Western Slide Complex, because it does not favor the development of thick stable deposits (Klaucke and Cochonat 1999).

To produce voluminous landslides, thick deposits of fine-grained material are necessary. Such units may evolve by low sediment accumulation rates in areas with moderate slope angles if sufficient time is allowed (Klaucke and Cochonat 1999, Migeon et al. 2006). The Eastern Slide Complex, with moderate slope angles of ~ 20° (Fig. 2b), is located further away from the Var Canyon and therewith east of the Cap Ferrat Ridge (Fig. 1). Klaucke and Cochonat (1999) show that this area is not connected to sediment sources from rivers or canyons, but covered by hemipelagic sediments with low sedimentation rates. Given such conditions and the above mentioned geotechnical data (Ch. 4.1), we follow the interpretation of those workers that less frequent but more voluminous landslide activity may be prevalent here in contrast to the Western Complex.

Among the trigger mechanisms of failure events in the area are sedimentary loading or seismic loading (Mulder et. al. 1994, Klaucke and Cochonat 1999), and undercutting (see review by Densmore at al. 1997) of the slope sediments adjacent to Var Canyon. At this stage of the investigations, the discussion of the trigger mechanisms for both the Eastern and Western Slide Complex is very speculative; however, we can rule out undercutting for the Eastern Slide complex. To identify the trigger mechanisms for each slide complex, sedimentological analysis, dating of the events, and measurements of geotechnical parameters across the failure plane seem mandatory.

Acknowledgments

We thank the captain and crew of the *RV* Meteor for their support during the cruise M73/1. IFREMER Brest (France) is acknowledged for having provided the bathymetric map. We also thank the reviewers Angelo Camerlenghi and Brian McAdoo for their efforts and suggestions to improve the manuscript. This study was financed through the Deutsche Forschungsgemeinschaft (RCOM-MARUM, Project C8/D3) and supported by the DFG-Excellence Initiative International Graduate School for Marine Sciences, Bremen.

References

Bartetzko A, Kopf A (2007) The relationship of undrained shear strength and porosity with depth in shallow (< 50 m) marine sediments. Sediment Geol 196: 235-249.

Bethoux N, Ouillon G, Nicolas M (1998) The instrumental seismicity of the western Alps: spatio-temporal patterns analysed with the wavelet transform. Geophys J Int, 135: 177-194.

Blum P. (1997) Physical properties handbook: a guide to the shipboard measurement of physical properties of deep-sea cores. Techn Note 26, ODP, doi:10.2973/odp.tn.26.1997.

Bryn P, Berg K, Forsberg CF, Solheim A, Kvalstad TJ (2005). Explaining the Storegga Slide. Mar Petrol Geol 22:11-19.

Burrus J, Bessis F, Doligez B (1987) Heat flow, subsidence and crustal structure of the Gulf of Lions (NW Mediterranean): a quantitative discussion of the classical passive margin model. In: Beaumont C, Tankard AJ (eds) Sedimentary Basins and Basin-Forming Mechanisms. Mem Can Soc Petrol Geol 12: 1–15.

Casagrande A (1936) The Determination of the Pre-consolidation Load and its Practical Significance. Proc Int Conf SMFE, 3: 60–64.

Cochonat P, Bourillet JF, Savoye B, Dodd L (1993) Geotechnical characteristics and instability of submarine slope sediments, the Nice slope (N-W Mediterranean Sea). Mar Georesourc Geotech, 11: 131-151.

Dan G, Sultan N, Savoye B (2007) The 1979 Nice harbour catastrophe revisited: Trigger mechanism inferred from geotechnical measurements and numerical modelling. Mar Geol 245: 40-64.

Densmore AL, Anderson RS, McAdoo BG, Ellis, MA (1997) Hillslope Evolution by Bedrock Landslides. Sci 275: 369-372.

Dugan B, Flemings PB (2000) Overpressure and Fluid Flow in the New Jersey Continental Slope: Implications of Slope Failure and Cold Seeps. Sci 289:288-291.

Hampton MA, Lee HJ, Locat J (1996) Submarine landslides. Rev. Geophys, 3:33-59.

Klaucke I, Cochonat P (1999) Analysis of past seafloor failures on the continental slope off Nice (SE France). Geo-Mar Lett 19: 245-253.

Klaucke I, Savoye B, Cochonat P (2000) Patterns and processes of sediment dispersal on the continental slope off Nice, SE France. Mar Geol 162: 405-422.

Kopf A, Brown KM (2003) Friction experiments on saturated sediments and their implications for the stress state of the Nankai and Barbados subduction thrusts. Mar Geol 202: 193-210.

Kopf A, Cruise Participants (2008) Report and Preliminary Results of Meteor Cruise M 73/1: LIMA-LAMO (Ligurian Margin Landslide Measurements & Observatory), Cadiz, 22.07.2007 - Genoa, 11.08.2007. Berichte Fachbereich Geowissenschaften, Universität Bremen, 264.

Locat J, Lee HJ (2002) Submarine landslides: advances and challenges. Can Geotech J, 39:193-212.

McAdoo BG, Pratson LF, Orange DL (2000) Submarine landslide geomorphology, US continental slope. Mar Geol 169: 103-136.

Migeon S, Mulder T, Savoye B, Sage F (2006) The Var turbidite system (Ligurian Sea, northwestern Mediterranean) – morphology, sediment supply, construction of turbidite levee and sediment waves: implications for hydrocarbon reservoirs. Geo-Mar Lett 26: 361-371.

Mulder T, Tisot JP, Cochonat P, Bourillet JF (1994) Regional assessment of mass failure events in the baie des Anges, Mediterranean Sea. Mar Geol 122: 29-45.

Mulder T, Savoye B, Syvitski JPM, Piper DJW (1998) The Var Submarine System: understanding Holocene sediment delivery processes and their importance to the geological record. In: Stoker MS, Evans D, Cramp A (Eds.), Geological Processes on Continental Margins: Sedimentation, Mass Wasting and Stability. Spec. Publ. Geol. Soc. Lond, 145-166.

Pasquale V, Verdoya M, Chiozzi P (1996) Heat flux and timing of the drifting stage in the Ligurian-Provencal basin (Northwestern Mediterranean). J Geodyn, 21: 205–222.

Piper DJW, Savoye B (1993) Processes of late Quaternary turbidity current flow and deposition on the Var deep-sea.fan, northwest Mediterranean Sea. Sedimentol 40: 557-582.

Postma G, Nemec W, Kleinspehn KL (1988) Large floating clasts in turbidites: a mechanism for their emplacement. Sed Geol, 58: 47-61.

Rehault JP, Bethoux N (1984) Earthquake relocation in the Ligurian Sea (Western Mediterranean): Geological interpretation. Mar Geol 55: 429-445.

Ryan, WBF (2009) Decoding the Mediterranean Salinity Crisis. Sedimentol, 56: 95-136.

Sultan N, Cochonat P, Dennielou B, Bourillet JF, Savoye B, Colliat JL(2000) Surconsolidation apparente et pression osmotique dans un sédiment marin. C R Acad Sci Paris - Ear Planet Sci, 331: 379-386.

Sultan N, Cochonat P, Canals M, Cattaneo A, Dennielou B, Haflidason H, Laberg, JS, Long D, Mienert J, Trincardi F, Urgeles R (2004) Triggering mechanisms of slope instability processes and sediment failures on continental margins: a geotechnical approach. Mar Geol, 213: 291-321.

Wood DM (1982) Cone penetrometer and liquid limit. Géotechnique, 32: 152-157.

6. Frequent failures at the deeper slope of the Ligurian margin, Southern France

Förster, A. [1], Stegmann, S. [2], Kopf, A.J. [1]

Planned for *submisson to Marine Geology*

Abstract

The Ligurian margin (NW-Mediterranean Sea) is a tectonically and seismically active margin, and several mass wasting processes are known in the deeper slope. We present sedimentological and geotechnical data from sediment cores recovered from a slide complex on the steep continental slope (~20°) near to the Var Canyon as well as results of related slope stability analysis. Seismic reflection and bathymetric data show that the headwall base area is characterized by several scars and talus chutes with a total height of ~ 40 m. The material in the slide originates from water depths of 1500 - 2000 m and consists of failed stiff silty-clay to clay and undisturbed hemipelagic clay sediments. While the hemipelagic sediments reflect normal to slight overconsolidation (OCR=1.03-1.67), the failed sediments preserve strong over-consolidation (OCR=1.53-2.14). The failed sediments from the headwall area also reflect strong overconsolidation (OCR=1.21-3.87), but show low intrinsic friction coefficients of 0.27-0.29. In all sediments recovered, several incisions in the bulk density values and tilted layering were observed, indicating multiple sliding events. Slope stability analyses show that based on the mechanical behavior of the sediments the slope would be stable and that other governing factors are required for slope failure. These included oversteepening or undercutting of the slope and cyclic loading during earthquakes. Based on the sediment physical properties, the slope angle has to increase up to >32° for the sediments to fail. When using infinite one-dimensional models to estimate the earthquake-induced peak ground accelerations (PGA) required to destabilize the slope, we get values of 0.13 to 2.22 m/s², which corresponds to magnitudes of M=0.77-5.27. Such earthquakes are frequently observed in the area. Overall, our data on geotechnical properties and slope stability analysis infer i) an origin of different mass events with sequential failure mechanisms, and ii) that the material is hence prone to future landsliding in case of factors destabilizing the sediments such as presence of weak layers, change in slope angles and seismic loading.

Key words: Ligurian Margin, slope instability, NW-Mediterrenean, submarine landslide

6.1 Introduction

Landslides are a hazard for on- and offshore regions worldwide. Investigations of these processes are attracting increasing interest because such mass wasting events threaten to destroy offshore platforms, pipelines, communication cables and other installations, while the resulting tsunamis may endanger coastal areas (Locat and Lee, 2002; Masson et al., 2006; Lee, 2009). Our understanding of these submarine landslides is currently limited so even the fundamental question of why some slopes are stable while others are not, cannot be answered unequivocally. Trigger mechanisms for slope instabilities encompass external forces, those operating on timescales of seconds to minutes (e.g. earthquakes) and those related to geological processes on

[1] MARUM - Center for Marine Environmental Sciences, University of Bremen,PO box 330 440, 28334 Bremen, Germany.

[2] IFREMER – French Research Institute for Exploitation of the Sea, Département des Géosciences Marines, PO box 70, 29280 Plouzané Cédex France.

timescales of tens to thousands of years (sea-level change, oversteepening of the slope). Oftentimes, combinations of the external forces together with internal governing factors, such as excess pore pressure, gas discharge, weak clay-rich layers which influence the sediment mechanical behaviour, may be responsible for slope failure (Hampton et al., 1996; Masson et al., 2006).

In the Mediterranean Sea and the surrounding areas (Gibraltar and Gulf of Cadiz), two examples of major earthquake-related landslides are the 1755 Lisbon landslide (Portugal) and the 1956 seismic-induced landslide event in the Southern Aegean Sea (E-Mediterranean Sea). Both were followed by tsunamis with catastrophic consequences for coastal and offshore regions (Ambraseys, 1960; Johnston, 1996; Baptista et al., 1998; Perissoratis and Papadopoulos, 1999). In the Eastern Mediterranean Sea, earthquakes with magnitudes >7 and with high peak ground accelerations (PGA) are observed, while in the Western Mediterranean Sea, ground motion is lower and PGA-values range from 1.0 to 1.6 m/s² (Grünthal et al., 1999). Even lower PGAs were recorded at the continental margin of SW-France (Ligurian Margin) with values ranging from 0.2 m/s² to 1.2 m/s² (Grünthal et al., 1999; DASE, 2009). Rehault and Béthoux (1984) and Courboulex et al. (2007) show that the Ligurian Margin is affected by common micro-seismic events with earthquake magnitudes of M1.3 – 4.5, while also strong earthquakes with M6-6.5 are present (Béthoux et al., 2008).

In the Ligurian margin region, previous slope stability analysis focused on the Nice upper slope or the Baie des Anges (Cochonat et al., 1993; Mulder et al., 1994; Sultan et al., 2004). This study presents slope stability analysis of a landslide complex located at the deeper steep slope in water depths of 1500 – 2000 m (Fig. 1). Previous work characterized the architecture and evolution of this landslide complex (Kopf et al., 2008; Förster et al., 2010), while our study uses a geotechnical characterization of the sediments and a 1D infinite slope stability model to unravel and to refine our understanding of earthquake ground shaking as the key-factor in slope instability in this regionally densely populated area.

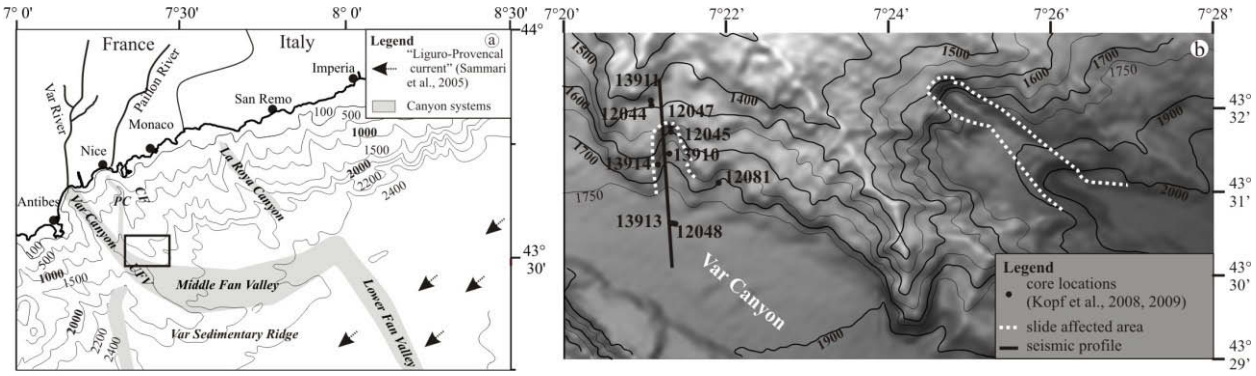

Fig. 1 (a) Map of the Ligurian continental margin (modified after Piper and Savoye, 1993 and Savoye et al., 1993) with the study area indicated by the black box. PC: Paillon Canyon, CF: Cap Ferrat, UFV: Upper Fan Valley. (b) Shaded relief bathymetric display with contour lines of the study area and with core locations of cruise M73/1 and P386 at the Western Slide Complex (modified after Kopf et al., 2009; Förster et al., 2010).

6.2 Regional setting of the study area

The Ligurian Basin is a marginal back-arc basin, formed by rifting and continental extension initiated during the late Oligocene (Burrus et al., 1987; Savoye et al., 1993) within the African-European convergence zone (Pasquale et al., 1996). Further, the related Ligurian Basin subsidence has been relatively stable since the Messinian Salinity Crisis at ~ 5-6 Ma (Béthoux et al., 2008). Also during the Messinian (late Miocene), extensive erosion and evaporite deposition caused by a major sea-level fall in the Mediterranean Sea affected the continental margin topography (Clauzon, 1978; Savoye et al., 1993; Ryan, 2009). The basin axis trends NNE-SSW, although the main transform faults are NW-SE (Rehault and Béthoux, 1984; Rehault et al., 1984). Currently, active basin deformation occurs offshore at a slow rate of about 1.1 m/ka NNW-SSE (Béthoux et al., 1998), which involves moderate seismic activity with common earthquake magnitudes of M 2.2 to M 4.5 (Rehault and Béthoux, 1984). However, earthquake magnitudes up to M 6.5 (Béthoux et al., 2008) are known in this area. Onshore measurements at the Ligurian coastline show peak ground accelerations (PGA) from 0.5 to 1.0 m/s², which is very low compared to the Eastern Mediterranean Sea with PGAs from 2.0 to 4.3 m/s² (Grünthal et al., 1999). The recent structure of the Ligurian Basin is a result of interactions between the Messinian topography and Pliocene-Quaternary processes (Savoye et al., 1993, references therein); through the Pliocene and the Quaternary, river systems formed in the basin and eroded deeply to form the present-day canyons (e.g. Var Canyon, Paillon Canyon) dissecting the recent slope. The submarine Var Canyon system is the main canyon originating from the Var River, which enters the Ligurian Basin west of Nice, SE-France (Fig. 1a). In this area, the continental margin consists of a narrow shelf 2-3 km wide, which breaks at a water depth of 100m (Assier-Rzadkiewiez et al., 2000), and a steep continental slope angle of ~11° (Cochonat et al.. 1993). The slide complex of our study is located on this margin (Ligurian Margin) adjacent to the Var Canyon (Fig. 1b) at N43° 30' and between E7° 20' and E7° 28'. Here, the slope angle is approximately 20° and flattens towards the Var Canyon to 7° in water depths of 1500-2000 m (Fig. 2). In an earlier study, this slide was termed the Western Slide Complex (WSC), mainly to

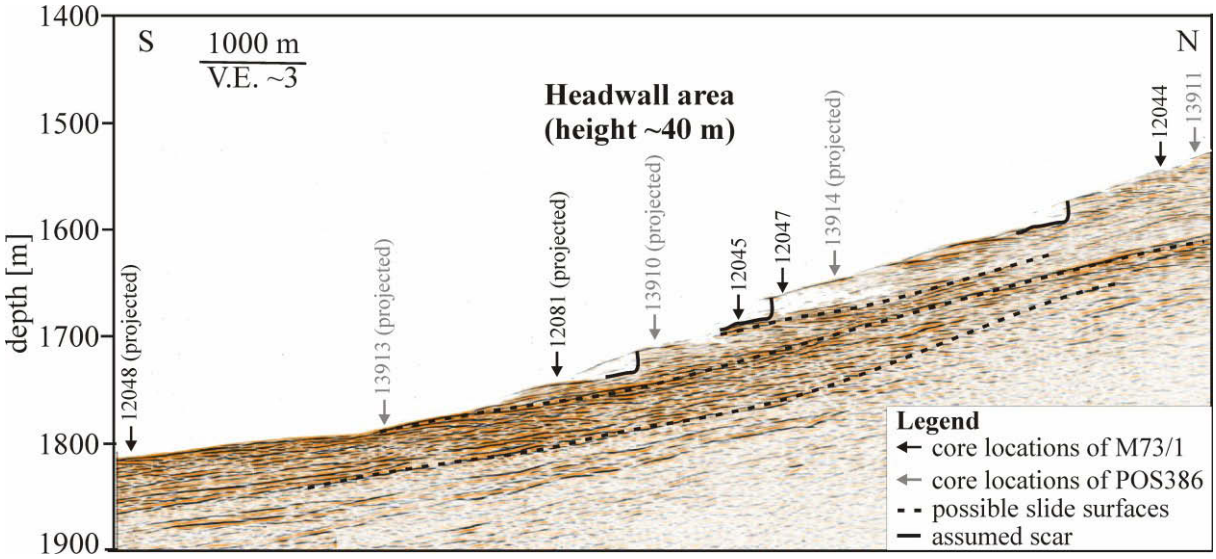

Fig. 2 Headwall striking profile of the Western Slide Complex with core locations of the research cruises M 72/1 and POS 386 (Kopf et al., 2008, 2009; Förster et al., 2010). The Headwall is characterized by several incisions and talus at their base. For locations of the profile see Fig. 1b.

distinguish it from a prominent retrogressive slide somewhat further to the east (the Eastern Slide Complex; for details see Förster et al., 2010). We will stick to the earlier nomenclature and call the mass wasting deposit in the manuscript the WSC.

The sediment supply in the Var canyon area is dominated by river input from small mountain-supplied rivers, which supplies sediment by erosion from the Quaternary uplift of the Alps. At the upper slope, the sediment concentration reaches tens of kg/m³ during floods, heavy rains, rapid.snowmelts and torrents. These conditions can result in hyperpycnal currents, which transport sediments to deeper water regions (Mulder et al., 1997). Current peak velocities of 0.27 m/s to 0.59 m/s were measured using mooring systems, which were set up along the whole canyon down to 2300 m water depths (Khripounoff et al., 2009). The mean currents of the Ligurian Basin (e.g. Liguro-Provencal current) are directed south-west following the bathymetry, and have maximum speeds of ~1m/s at the surface and ~0.05 m/s at 400 m water depth (Sammari et al., 1995). Recent sedimentation rates for the study area were estimated to be 3.5 m/ka, however higher sedimentation rates of 8 m/ka were estimated for the time period from ~12 ka to ~7 ka (Sultan et al., 2004).

6.3 Previous studies on the Western Slide Complex

During RV Meteor Cruise M73/1 and RV Poseidon Cruise P386, the Var Canyon system and its adjacent slopes were mapped using bathymetry systems (SIMRAD EM120 and EM710). Additionally, Parasound (parametric narrow-beam sediment echosounder) and high resolution multi-channel-seismic (MCS) profiles were collected over an area of ~ 2000 km² (Kopf et al., 2008, 2009). Based on these data, 9 gravity cores were collected in water depths ranging between 1400 mbsf and 1850 mbsf on the Western Slide Complex (WSC). Studies by Kopf et al. (2008) and Förster et al. (2010) used these data to illuminate mass wasting dynamics on the deeper slope of the Ligurian Margin. Seismic and parasound data show a headwall area made up of steep scars (32°) with heights of ~40 m. While transparent layers in the sub-seafloor were not observed, a rough seafloor topography is visible above the headwall area. At ~40-70 mbsf, prominent reflectors are visible and may be hypothesized to be possible slide surfaces (Fig. 2; Förster et al., 2010).

The sediment cores were taken at various locations (Fig. 1b; Kopf et al., 2008; 2009) outside of the landslide complex (GeoB12044 and -13911) and within the slid material from the headwalls (GeoB12045, -12047, -13910 and -13914) down to the run-out zones (GeoB12081). Recovery varied at lengths from 0.3 to 5.2 m. The headwall cores can be divided into two groups: i) GeoB13914 and -12047 that were recovered at the upper headwall area and ii) GeoB12045 and -13910 taken in the lower headwall area (Fig. 2). In the upper part of the majority of the cores similar lithostratigraphic successions are present (Fig. 3). The hemipelagic sediments are characterized by homo-genous, bioturbated, fine-grained silty clays with some coarser intervals. In two cores (GeoB12044 and -13911, Fig. 3-b) taken from outside of the landslide complex where the slope angle reach its highest values (Fig. 2), the hemipelagic sediments are underlain by dark-grey silty clay sediments from 1.4 mbsf (GeoB13911) and 3.65 mbsf (GeoB12044) to the bottom. In both lithostratigraphic successions, sharp oblique contacts (20-45°) were observed. These oblique contacts were also observed in the core from the landslide run-out zone (GeoB12081) and the core of the lower headwall area (GeoB12045 and -13911). Additionally, core GeoB12081 contained several sandy layers encased by hemipelagic silty-clay (Fig. 3g). The oblique contacts in the headwall cores (see above) were observed in a

reworked sediment unit composed of silty-clay sediments with some coarser intervals (Fig. 3e and f). In contrast to the lower headwall area, one core recovered from the upper headwall area (GeoB13914) contains sandy to silty intervals overlain by rounded indurated pebbles as evidence of mass wasting (Fig. 3c). The second core from the upper headwall (GeoB12047) contains stiff dark grey silty-clay (Fig. 3d). Due to the low recovery of only 0.3 m, no indications of mass wasting were given.

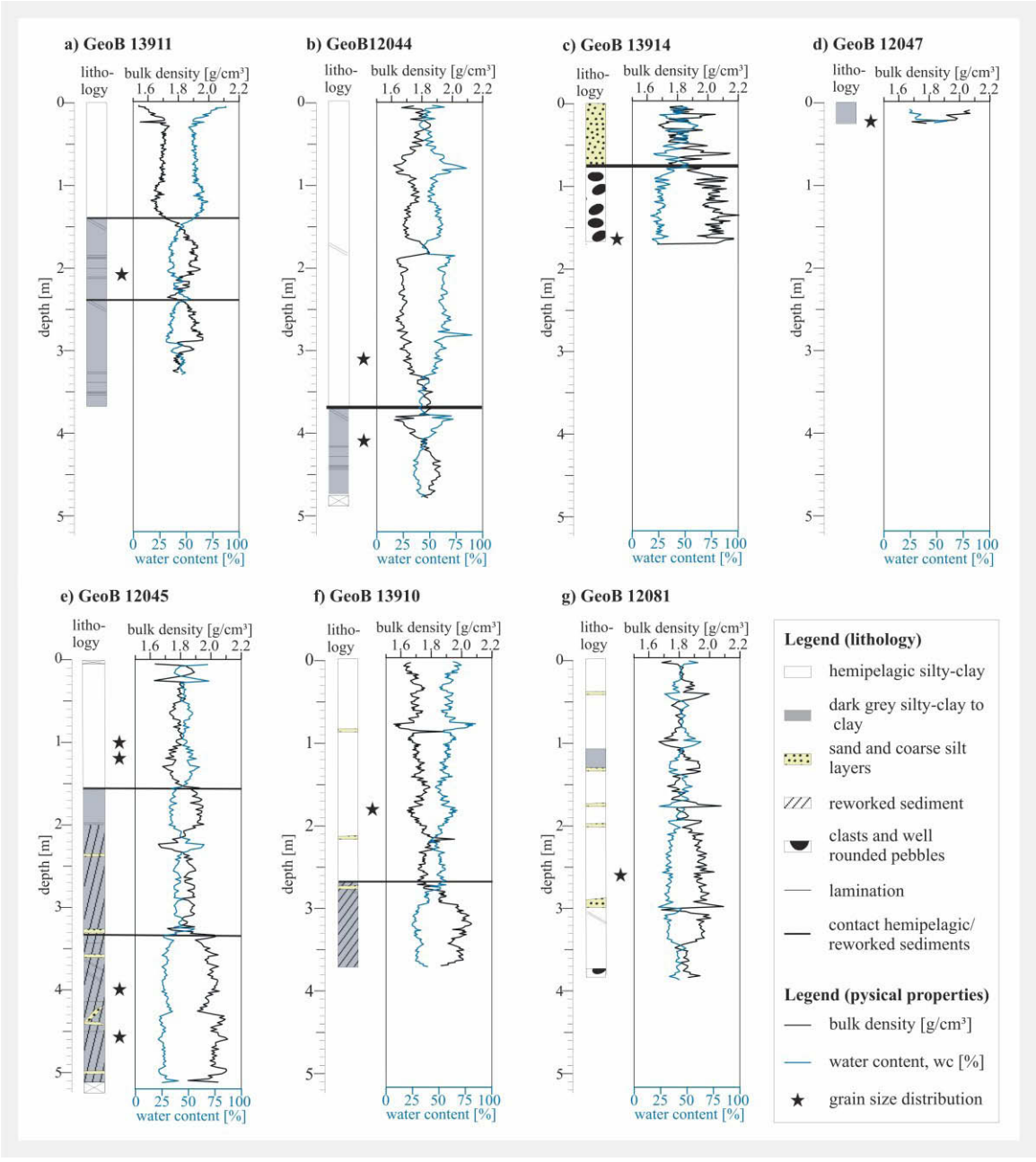

Fig. 3: Core descriptions, bulk density (from MSCL) and water content from cores outside of the Western Landslide Complex (a, b), within the headwall area (c-f) and close to the run-out zone (g). Markers show the depths of the sediment samples for grain size determination (see Fig. 4). For location of the cores see Figs. 1b and 2.

6.4 Material and Methods

For this shore-based study, we used 7 gravity cores (GeoB12044, -12045, -12047, -12081, -13910, -13911 and -13914; Figs. 1b, 2 and 3) for dedicated sedimentological and geotechnical laboratory measurements and resultant slope stability calculations (see Section 5). The hemipelagic units of cores GeoB12044 and -13911 were used as a reference concerning sediment physical properties and shear parameters (e.g. shear strength, cohesion, friction angle). Sediment physical properties (e.g. P-wave velocity, bulk density, porosity and magnetic susceptibility) were measured using a GEOTEK Multi-Sensor Core Logger (MSCL). The results can be found in Kopf et al. (2008, 2009) and Förster et al. (2010). For identification of the lithology of the different sediment cores on selected samples (see Fig. 3) the grain size distribution was determined using the Aerometer method (for details see DIN ISO/TS 17892-4:2004), where the classification followed Wentworth (1922).

6.4.1 Laboratory testing

After recovery of the cores, onboard measurements include the determination of the undrained shear strength (Su) using a Vane Shear apparatus (Blum, 1997) to detect "weak layers" in the sediment column. Following Ladd et al. (1977), we calculated the Su/σ_{eff}-ratio (SHANSEP approach) to obtain 'normalized shear strength' values, where Su/σ_{eff} values between 0.2 and 0.4 are typical for normally consolidated sediments. Here σ_{eff} is defined as the vertical effective stress. Laboratory tests at MARUM (Univ. Bremen) included static triaxial tests to determine the peak shear strength at failure (T_f). Each triaxial test consists of at least three single tests with different cell pressures to the approximated in-situ stress state of each sediment sample at the depth of recovery (e.g. 20 kPa for 1.9 mbsf in GeoB13914). First the sediment samples are allowed to consolidate under the selected pressures until consolidation is completed and no excess pore pressure is revealed. However, the boundary condition of totally drained tests is not fulfilled because the shear displacement is applied to maintain low pore pressures established due to incremental loading of each sample. The shear tests allowed us to identify cohesion (c') and friction angle (φ) at failure resulting in determination of the peak shear strength (T_f) after the Mohr-Coulomb criterion with the normal load (σ_n) of the sediments:

$$T_f = c' + \sigma_n \tan \varphi \quad (1).$$

To characterize the consolidation history of the sediments, fixed-ring oedometer tests were performed at MARUM (Uni. Bremen) and IFREMER (Brest) on selected lithologies, using normal stresses up to 300 kPa. The maximum stress the sediment experienced (i.e. the preconsolidation pressure, σ_{pc}) was determined after Casagrande (1936). The consolidation status of the sediments was estimated from the overconsolidation ratio (OCR), the preconsolidation stress, σ_{pc}, and vertical effective stress, σ_{eff} based on the following equation:

$$OCR = \sigma_{pc} / \sigma_{eff} \quad (2).$$

Fluid escape and entrapment are controlling factors of the effective stress during consolidation. The effective stress represents the stress transmitted through the mineral framework. An approach to estimate the effective stress that affects the sediments is given by Terzaghi und Peck (1948) and describes the relationship between the effective stress and the

pore space, where plastic deformation dominates the reduction of void ratio and pore space during consolidation. This vertical effective stress estimation follows the equation:

$$e = e_0 - C_c * \log(\sigma_{v'} / \sigma_0) \quad (3),$$

where e is the void ratio (calculated from MSCL porosity data), e_0 is the initial void ratio at the initial effective stress, σ_0, and C_c is the compression index, as was determined from oedometer tests. With a back-analysis it is possible to estimate the excess pore pressure, Δu, in the sediments, as defined by Sultan et al. (2004) using equation 4 with σ_t as the total stress of the sediment, σ_h as the hydrostatic pressure and $\sigma_{v'}$ as the vertical effective stress:

$$\Delta u = \sigma_t - \sigma_h - \sigma_{v'} \quad (4).$$

6.4.2 Slope stability analysis

A one-dimensional infinite slope stability analysis was carried out by considering the following aspects. First, we assume that the mass wasting processes applicable in this study are translational slides, a reasonable assumption given that 90% of the offshore landslides show this type of sliding mechanism (Mulder et al., 1994). Second, we implemented geotechnical results from GeoB cores for the following calculations.

The stability analysis is made by detecting the Factor of Safety (FS), which is defined as:

$$FS = \Sigma F_R / \Sigma F_M \quad (5),$$

where F_R are the resisting forces and F_M are the destabilizing forces. A FS ≤ 1 indicates that the destabilizing factors exceed the failure resistance of the sediments and, therefore, that failure may occur.

Based on our triaxial tests we made an assumption about the sediment behavior under partly drained conditions. After the Mohr-Coulomb criterion we identified the c' is the cohesion (kPa) of the sediments at the depth, z (m), and the friction angle (φ). The excess pore pressure, Δu (kPa) was determined using equation 4. The equilibrium equation of the Factor of Safety implies also the slope angle β (°) and γ' as the submerged unit weight (kN/m). For static conditions the FS-calculations are given after Lambe and Whitman (1979) and Dugan and Flemings (2002) as:

$$FS = c' + \frac{\left[\left(\gamma' z \cos^2\beta - \Delta u\right)\tan\varphi\right]}{\gamma' z \left(\sin\beta \cos\beta\right)} \quad 6).$$

Since the study area is located in a seismically active zone, our estimates should include the stability behavior of the sediments during earthquake loading (pseudo-static conditions). The seismic response is controlled by parameters such as ground motion, inclination of the slope angle or presence of weak layers (Biscontin and Pestana, 2006). The seismic response is included in the FS equation as the peak ground acceleration (PGA) factor k:

$$FS = c' + \frac{\left[\left(\gamma' z \cos^2\beta - \Delta u\right)\tan\varphi\right]}{\gamma' z \left((\sin\beta \cos\beta o + k(\gamma'/\gamma)\cos^2\beta\right)} \quad (7),$$

where k is the ratio of the peak horizontal ground acceleration to gravitational acceleration (%g) and γ is the total unit weight (kN/m). The other boundary conditions are the same as in equation 6. The pore pressure that may be generated during earthquakes and which could not be relieved is not taken into account in the FS-analysis. An approximation of the excess pore pressure is given by the Δu-values, which are determined by the static oedometer and triaxial tests after equation 4.

6.5 Results

6.5.1 Sediment physical properties and grain size analyses

In Figure 3 we present the lithology, water content and bulk density data as taken from the MSCL runs; for more detail refer to Kopf et al. (2009) and Förster et al. (2010). Additionally Figure 4 shows the grain size distribution for determination of different soil units. In the hemipelagic sediments of both reference cores (GeoB12044 and -13911), bulk density values increase slightly from ~1.62 to ~1.80 g/cm³, while water content decreases with depth from ~88% to 56% or ~63% to ~40% (Figs. 3a-b). For core GeoB13911 (Fig. 3a), sharp transitions to dark-grey silty clay were observed both in and beneath the core, which correspond to a change in bulk density and water content values at depths of 1.4 mbsf (from 1.70 to 1.76 g/cm³, 56 to 47%) and 2.37 mbsf (from 1.73 to 1.82 g/cm³, ~55 to 43%). In contrast to these observed bulk density and water content trends, the transition between the hemipelagics and the dark-grey silty clay in core GeoB12044 (Fig. 3b) is characterized be a decrease in bulk density (1.82 to 1.69 g/cm³) and an increase in water content (from 41 to 52%). The grain sizes show a different distribution for an assumed equal unit: in the sediment sample of both reference cores the main part of the grain sizes is silt. The sample of GeoB13911 (2.1 mbsf) shows also a high content of fine-sand, whereas the GeoB12044 (4.1 mbsf) sample contains more clay fraction (Fig. 4). The run-out zone sediments (GeoB12081) show a general downcore increase in bulk density (from 1.75 to 1.96 g/cm³) and a decrease in water content (from 60 to 31%; Fig. 3g). The peak density values of 1.99 g/cm³ (0.44 mbsf), 2.07g/cm³ (1.80 mbsf) and 2.09 g/cm³ (3.02 mbsf) are clearly related to sandy intervals (Fig. 3g). In the reworked silty clay from the lower headwall area of both GeoB12045 and -13910, bulk density increases downward from 1.8 to ~2.08 g/cm³ while the water content decreases from 70% to 27%. A sharp transition between the hemipelagic sediments and the underlying dark-grey silty clay was observed in core GeoB12045 at 1.55 mbsf and at 2.67 mbsf core GeoB13910 (Fig. 3e-f), which corresponded to increases in bulk density from 1.82 to 1.95 g/cm³ and 1.79 to 1.90 g/cm³, respectively. Bulk density values in the upper headwall are higher whereas the water contents are lower, likely a result of the different sediment compositions (Fig. 3c-d); an increase in bulk density values from 1.96 to ~2.18 g/cm³ for GeoB13914 but a decrease from 2.08 to 1.71 g/cm³ for GeoB12047 were observed. Water content values in core GeoB13914 decrease downcore from 42% (seafloor) to 33% (0.91 mbsf; Fig. 3c). Below 1 mbsf, the water content scatters between 21 and 31% with no visible trend. Grain size distributions determined from samples taken at the lower (GeoB12045 1 mbsf, 1.2 mbsf, 4 mbsf and 4.5 mbsf; GeoB13910 1.8 mbsf) and from the upper headwall (GeoB13914 1.7mbsf; GeoB12047 0.3 mbsf) are akin with the composition of clayey-silt. Exceptions are GeoB13914 and -13910 containing high contents of sand and gravel (Fig. 4).

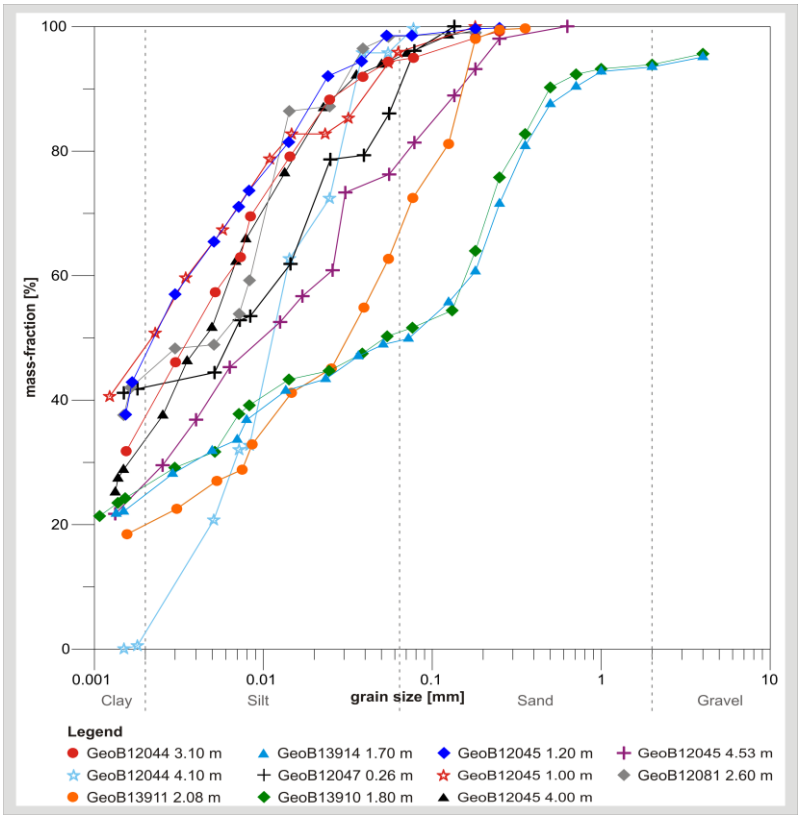

Fig. 4: Grain size distributions from different lithological units (see. Fig. 3), performed after DIN ISO/TS 17892-4:2004.

6.5.2 Geotechnical characterisation

According to the SHANSEP approach (Ladd et al., 1977), Su/σ_{eff} ratios were calculated and the corresponding undrained shear strength values (Su) were plotted in Figure 4. Both reference cores (GeoB12044 and -13911) show a steady downcore increase in Su to ~12 kPa in 3 mbsf, which is mirrored by a Su/σ_{eff} ratio of 0.12 to 0.38 (Fig. 5), a typical value for normally consolidated sediments (Ladd et al., 1977). Results from the Vane shear tests, performed in the sediments from the headwall cores, could be divided into two groups: i) cores GeoB12047 and -13914 show an overconsolidation state based on their Su-values of ~30 kPa in 1.75 mbsf and Su/σ_{eff} ratio > 2 (Fig. 5), while ii) even lower, but also overconsolidated sediments with Su-values of 20 kPa (1.75 mbsf) and ~30 kPa (3.5 mbsf) were observed in cores GeoB12045 and -13910 where Su/σ_{eff} ratios range between 0.6 and 1.2 (Fig. 5).Extremely high undrained shear strength values of ~40 kPa at 1 mbsf were observed in the reworked sediments of GeoB12081 (taken from the run-out zone) and GeoB 13914 (taken from the headwall), which may be related to the presence of pebbles and sandy layers (Fig. 3c-g). However, most of the cores show a downward increase in Su-values. From 13 different samples taken from different cores outside of the landslide, within the slide complex from the headwalls down to the runout zones the overconsolidation ratio (OCR) were determined after equation 2 (see Section 4.1). While the OCR of the hemipelagic back-ground sediments slightly exceeds 1, indicating a slight

overconsolidation, the reworked silty-clay layers show a slight to strong overconsolidation (OCR=1.21-3.81) with the sediment sample from 1.23 m of core GeoB12081 as the sole exception (OCR=0.94; see Tab. 1).

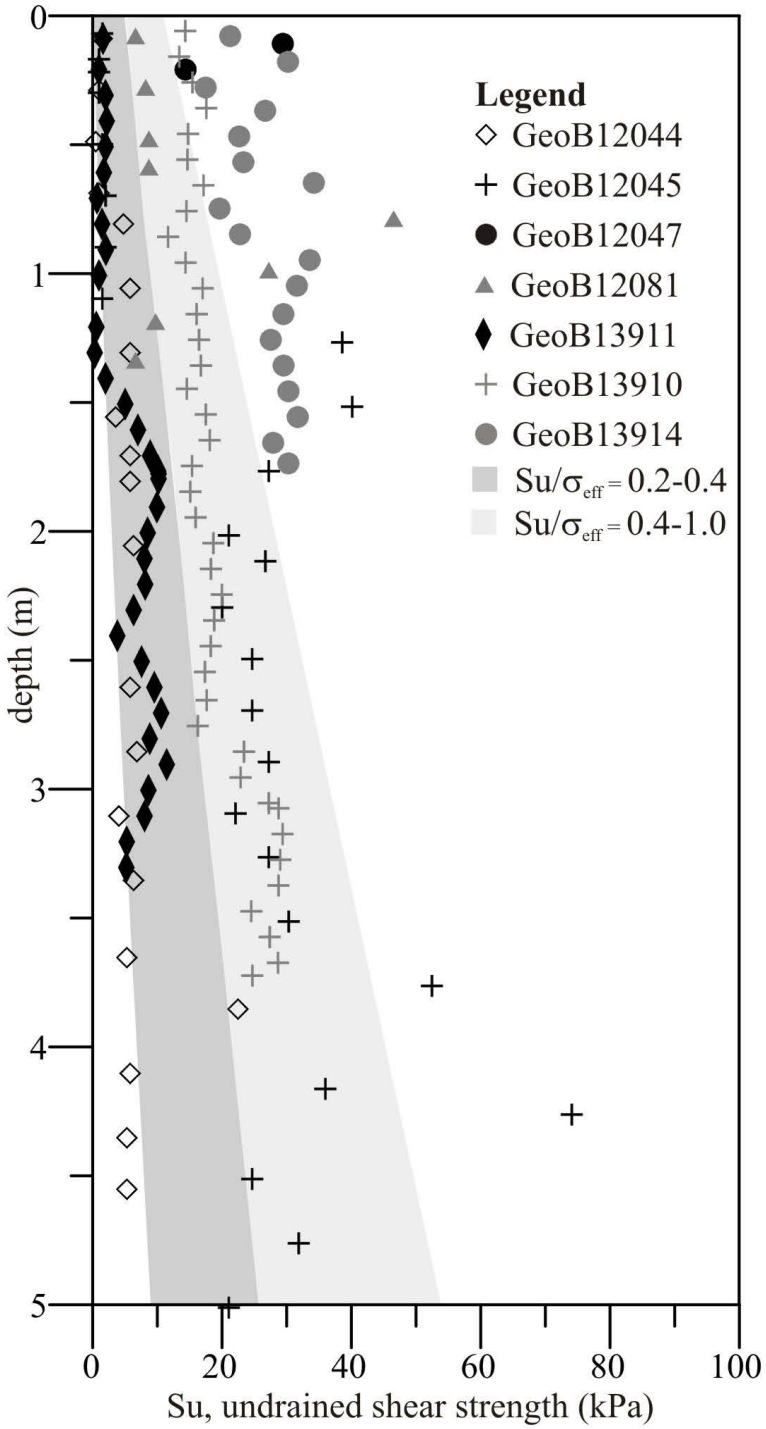

Fig. 5 Results from Vane Shear tests on un-drained shear strengths (Su) along sediment cores GeoB12044, -45, -47, -81 and GeoB13910, -11 and -14. The hemipelagic sediments of GeoB12044 and -13911 reflect normal consolidation with Su/σ_{eff} values of 0.2-0.4, while the most reworked sediments are overconsolidated with Su/σ_{pc} values of 0.4 ->1 (Ladd et al., 1977).

Tab. 1 Results of consolidation tests for the different lithologies (H=Hemipelagite, FM=Failed material). The overconsolidation ratio (OCR) was calculated after equation 2 with maximum past stress σ_{pc}, and effective stress σ_{eff}. The excess of pore pressure Δu was estimated after equation 4. For positions of the cores see Fig. 1b.

sample	depth [m]	lithology	σ_{pc} [kPa]	σ_{eff} [kPa]	OCR	Δu [kPa]
12045	1.03	(H) silty-clay to clay	12.85	9.31	1.38	3.96
	2.63	(FM) silty-clay to clay	33.86	26.72	1.27	14.82
	4.53	(FM) sandy clay-silt	45.16	37.45	1.21	18.81
12044	2.0	(H) silty-clay	17.28	13.50	1.28	11.63
	4.10	(FM) clayey-silt	40.13	26.16	1.53	18.32
12047	0.26	(FM) sandy clayey-silt	7.47	1.93	3.87	1.02
12081	1.23	(FM) silty-clay to clay	9.53	10.16	0.94	9.60
	2.60	(H) clayey-silt	26.90	25.62	1.05	10.81
13910	1.90	(H) silty-clay	13.53	12.33	1.09	13.09
	2.75	(FM) silty-clay to clay	62.94	19.04	3.31	20.92
13911	2.05	(FM) sandy silt	26.69	14.22	1.88	18.41
	3.18	(FM) silty-clay to clay	50.20	23.39	2.14	30.64
13914	1.05	(FM) silty-clay to sand	21.31	8.50	2.51	8.11

6.5.3 Slope Stability Analysis

The results of the one-dimensional infinite slope stability analysis are presented in Figure 6. As slope geometry plays an important role in slope instability, calculations were carried out with different slope angles following equation 6, where the resisting forces were determined from 8 triaxial and 13 oedometer tests: cohesion and friction angles values were determined as 1.5 kPa to ~ 46 kPa and 15° to 35° respectively, the calculated excess pore pressure scatters between 2 kPa and 21 kPa (Tab. 2) and bulk densities ranging of 1.7 g/cm³ (GeoB13910) to 2.0 g/cm³ (GeoB12081) were determined with the MSCL (Fig. 3). In general, we observe the highest

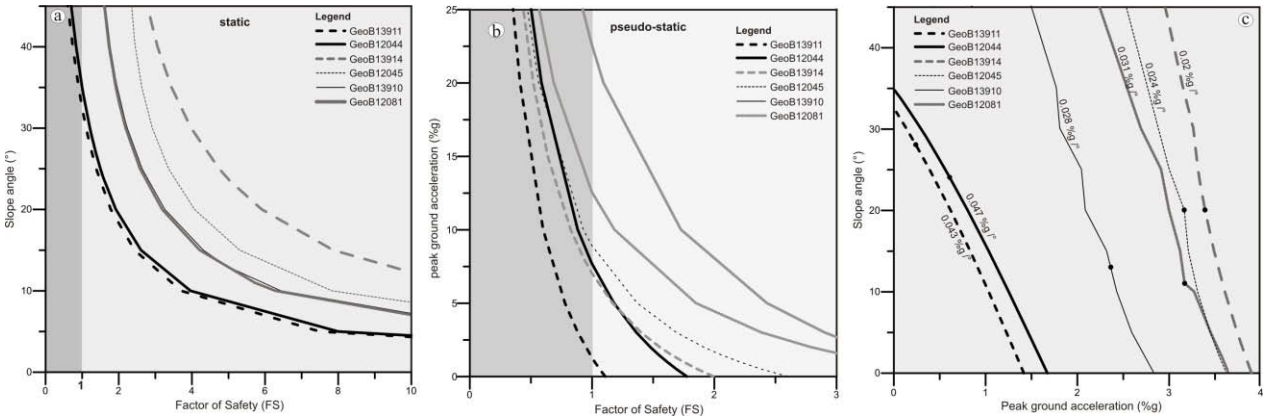

Fig. 6 Results of the slope stability analysis under drained conditions. For the static case a) the Factor of Safety (FS) was determined depending on the slope angle after equation 6. Concerning to the high seismic activity in the study area, the FS calculation b) was done with the results from the triaxial tests (Tab. 2) for assumed peak ground accelerations (PGA, %g). The dark grey shaded area indicates PGAs that are needed for failure (FS <1). The decrease of the supplemented PGAs with an increase in slope angles is shown is c.

friction angles in the sandy/gravel intervals. The clayey-silt sediments are characterized by high friction angles and low cohesion values except the samples of core GeoB12045, where low friction angles and high cohesion values could be observed (Tab. 2).

For slope angles ranging from 2° to 45°, FS values exceed 1 in most cases (Fig. 6a), suggesting that the slope is generally stable under these conditions. Exceptions are cores GeoB12044 and -13911, where for the used sediments the FS values fall below 1 for slope angles ≥ 32° (Fig. 6a). To determine the effect of the earthquakes on slope stability, the ground motion is taken into account after equation 7. The results show that for present-day boundary conditions (see above) added PGAs of 1.3 %g (GeoB13911) to ~22 %g (GeB12081) are required to induce sediment failure (Fig. 6b). These PGAs correspond to ground accelerations of 0.13 m/s² to 2.22 m/s². In order to account for topographic variations, we estimated the PGAs at various given slope angles (Fig. 6c). With a steeper slope angle the required PGA becoming lower with gradients of 0.02 %g (GeoB13914) to 0.047 %g (GeoB12044) per one degree change in slope angle (Fig. 6c). These values will be discussed in the context of the possible trigger mechanisms for mass wasting processes in the study area.

Tab.2 Results of the triaxial tests (friction angle φ, cohesion c') and determined peak shear strength T_f. The excess pore pressure Δu was calculated after equation 3 and 4 from the triaxial tests. The lithology was determined from the grain size analysis (Fig. 4).

Sample	Depth (m)	lithology	T_f (kPa)	φ (°)	c' (kPa)	Δu (kPa)
12044	3.1	clayey-silt	44.09	26.4	7.2	1.76
13911	2.08	sandy silt	21.93	34	1.5	3.89
13914	1.7	clayey sand with gravel	57.53	34.9	1.7	1.77
12045	1.2	clayey silt	42.7	15.9	58.3	6.88
	4.0	clayey silt	71.77	23.3	46.6	21.2
13910	1.80	clayey sand with gravel	22.28	31.9	0	0.43
12081	2.6	clayey silt	32.76	26.4	7.1	3.09

6.6 Magnitudes and recurrence times of earthquakes

The magnitudes required for these PGAs were calculated after Neumann (1956) and Murphy and O'Brien (1977), assuming that the seismic activity emanates from shallow events located in 5 to 20 km depth (Béthoux et al., 1998, Courboulex et al., 2007). The earthquake magnitudes associated with our determined PGAs range between M=0.77 and M=5.27 (Tab. 3). For the lower PGAs of 0.13 m/s² the method of Murphy and O'Brien (1977) yielded questionable results, because this method was based on the use of PGA values >>0.1 m/s². As proposed by Béthoux et al. (1998), we calculated the recurrence times of the assumed earthquakes by the frequency-magnitude distribution log (N) = a - b x M after Gutenberg and Richter (1949). N is the number of earthquakes with magnitudes >M during a given time interval, while a and b are constants. Béthoux et al. (1998) deduced the following values from seismicity data of the Ligurian Basin: a = 4.4 (± 0.1) and b = 0.85 (±0.03). Using these values calculated for the earthquakes magnitudes the recurrence times (Fig. 7). For the shallower earthquake nuclei (5 km) we determined recurrence times of one month ± 20 days (M=0.77) to

15 months ± 6 days (M=3.57). For the deeper earthquakes (20 km) the recurrence times are increasing from 2 months ± 1.5 days (M=2.47) up to 12 years ± 8.5 months (M=5.27). We will assess these data in the discussion below.

Tab. 3 Estimation of earthquake magnitudes corresponding to calculated peak ground accelerations (PGA) from this study and from the GSHM (Global Seismic Hazard Map; Grünthal et al., 1999) computed after Neumann (1956) and Murphy and O'Brien (1977).

PGA (m/s²)	Distance of epicenter (km)	Magnitude
0.13	5	0.77
	20	2.47
0.2 (GSHM)	5	1.19
	20	2.90
0.69	5	2.42
	20	4.12
0.76	5	2.51
	20	4.22
0.88	5	2.66
	20	4.36
1.2 (GSHM)	5	2.90
	20	4.60
1.23	5	2.99
	20	4.70
2.22	5	3.57
	20	5.27

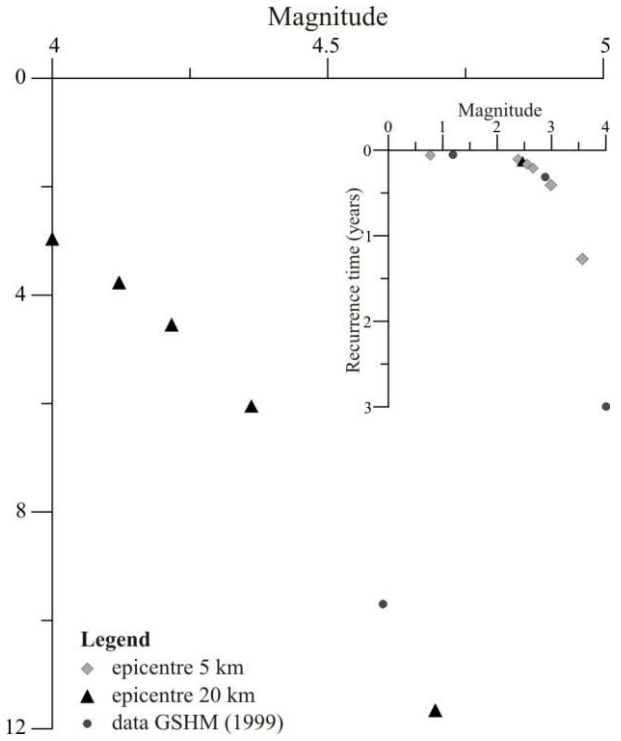

Fig. 7 Recurrence times for the calculated earthquake magnitudes estimated after Béthoux et al. (1998) and Courboulex et al. (2007) with seismic epicentre depths of 5 km and 20 km

6.7 Discussion

6.7.1 Evolution of the Slide Complex: Multi-phase events?

Förster et al. (2010) hypothesized that the evolution of the Western Slide Complex followed an emplacement by sequential multi-phase mass wasting with enhanced failure frequency. Our data confirm and support this hypothesis and show that the slope stability around and in the WSC depends on the composition and mechanical behaviour of the sediments. The slope sediments are inhomogeneous containing of hemipelagic silty-clay and stiff silty-clay or clay units interrupted by sandy and coarser silt layers (Fig. 3). While the hemipelagic sediments are normally to slightly overconsolidated (OCR=1.05-1.28), the dark-grey silty clay unit underlying the hemipelagic sediments (cores GeoB13911 and -12044) show slight to strong overconsolidation (OCR=1.53-2.14). Furthermore, the reworked sediments from the headwall cores show overconsolidation that could be divided into two groups: i) the reworked sediments of cores GeoB12047 and -13914 (upper headwall area) are characterized by a strong overconsolidation with Su/σ_{eff}-ratios >2 (Fig. 5), while ii) in cores GeoB12045 and -13910,

lower Su/σ_{eff}-ratios of 0.6-1.2 were observed but still demonstrate some overconsolidation. The high Su/σ_{eff}-ratios may result from the removal of overlying sediments by different mass wasting events. However, it is also possible that repeated episodes of cyclic loading (e.g. during earthquakes) may have strengthened the sediments (Locat and Lee, 2002, references therein), because pore water is expelled and grain-to-grain contacts are reinforced.

Assuming that the Su-values increase linearly with depth (see review by Bartetzko and Kopf, 2007), a linear regression was calculated in the hemipelagic sediments with a gradient of 2.75 kPa/m. Using this linear relationship and assuming that the Su-depth gradient can be extrapolated to all cores, we estimate the original depths of the reworked sediments from GeoB12045 and -13910 based on the peak shear strength. For the upper part of the reworked sediment column of GeoB12045 (Fig. 3e) a removal of a 7.7 ± 1 m was estimated based on Su-values of 18-24.5 kPa, while a missing sediment unit of 4.7 ± 0.5 m was estimated between the lower and the upper part of the failed material. The original depth of the reworked sediment column of core GeoB13910 (Fig. 3f) is 9.1 ± 1m; therefore the missing ~7.3 m of sediment correlates with the removal of the upper part (7.7 ± 1 m) of GeoB12045.

Seismic reflection and the parasound data show reflectors with a rough topography that is possibly related to several older failure events (Förster et al., 2010). In the headwall area several scars could be observed, which let us assume that several different failure events were involved in the evolution of the WSC. Other evidences for the frequent failures are given by a stepwise of the bulk density values, lying between the hemipelagic sediments and the underlying dark-grey silty clays or reworked sediments as well as within the reworked sediment column (Fig. 3). Additionally, tilted layers with angles of 25° to 40° are visible in the reworked sediment units as well as in the hemipelagic sediments that may be related to different failure events.

Summarizing the above mentioned observations, we suggest that our geotechnical data and the sedimentological results (Kopf et al., 2008, 2009; Förster et al., 2010) could be explained by different failure events, although the time lapse between the events is unknown.

6.7.2 Potential trigger mechanisms

For the slope of the Ligurian margin previous studies has been shown that the change of the slope angle is a governing factor for sediment failure (e.g. Cochonat et al., 1993; Mulder et al., 1994; Förster et al., 2010). In our study area two scenarios may play a role for oversteepening the slope induced i) by sediment loading and ii) by undercutting of strong currents. First, hyperpycnal flows transfer sediment along the Var Canyon system (Fig. 1a) from the shelf to the deeper basin and might be a result of high sedimentation rates. Klaucke and Cochonat (1999) mentioned that high sedimentation rates on steep slopes may cause frequent sediment failures. Indications for several distinct failure events were observed in our study area adjacent to the Var Canyon (Ch. 6.1), which is characterized by a high sedimentation rate (Sultan et al., 2004) and resulting in oversteepened slope gradients. Secondly, an overstepping of the slope may caused by currents undercutting the slope. This process may play a long-term role in destabilizing the slope sediments. Piper and Savoye (1993) and Mulder et al. (1998) estimated flow velocities of 10-40 m/s for the turbidity event induced by the 1979 Nice Airport Slide, while Khripounoff et al. (2009) measured flood-induced current peak velocities of only 0.3-0.59 m/s. Klaucke et al. (2000) suggest that the currents are not strong enough to erode upper slope sediments. After Sundberg (1956, references therein), the critical medium erosion velocity for silty-clay is 0.2-8 m/s depending on state of consolidation. We therefore suggest that the

turbidity and flood controlled current velocities may be high enough to erode sediment from the deeper slope canyon flank, however, this assumption is uncertain and is currently tested by moorings deployed along the Var canyon (Kopf et al., 2009).

Our modelling let us suggest that under the given static conditions, the sediments used for this study are more or less stable, while the sediments of the two reference cores (GeoB12044 and -13911) are only stable to a slope angle of <32° (Fig. 7a). Seismic reflection and bathymetric data show recent slope angles ranging from 24° to 28° at the reference sites (Figs. 1b and 2), so that only a small change in the slope angle might be sufficient to initiate a new slide phase.

We already demonstrated that under aseismic conditions the slope is more or less stable (see above). Hence, additional trigger mechanisms are required for sediment failure. Because it is known that the Ligurian margin is seismically active (Rehault and Béthoux, 1984; Courboulex et al., 2007; Béthoux et al., 2008), we tested the hypothesis that earthquakes are the main trigger mechanism in the study area. Under pseudo-static loading (triaxial tests) the sediments of the reference cores (GeoB12044 and -13911) are characterized by FS equal to 1 with addition PGAs of ~ 1.3 %g up to 7.7 %g (Fig. 7b). For the sediments of the headwall area and the run-out zone (Figs. 1b and 6b) the PGAs required for failure increase up to 22 %g (GeoB13910). Our proposed pseudo-static model approximates the excess pore pressure determined by oedometer tests, while the excess pore pressure generated by earthquakes does not take into account. These pore pressure will lead to a decrease of the sediment stability (Masson et al., 2010). Therefore required PGAs for sediment failure may be lower than our model offers. The effect of the excess pore pressure should be incorporated into further analyses.

To assess how often the calculated PGAs occur in the study area, the recurrence times if the seismic events were calculated (Fig. 9). Our determined PGAs for slope instability (1.3-22 %g) correspond to earthquake magnitudes of M=0.77-5.27. Following Béthoux et al. (1998) and Courboulex et al. (2007) we estimated recurrence times of 20 months (M=0.77) up to 12 years (M=5.27) based on our PGA data (see above). However, without dating each of the events, discussion of the recurrence times remains speculative. While we observed several indications of frequent mass wasting processes (e.g. tilted layers also within the hemipelagic sediments, rough seafloor topography), we suggest that these processes are responsible for the present-day slope morphology and, hence, that beside the big earthquakes with M=6-6.5 (Béthoux et al., 2008) the smaller micro-seismic events (M=1.3-~4, Tabl. 3.) are sufficient for slope instability in our study area.

Besides the two above mentioned potential trigger mechanisms, some pre-condition factors may also play a role for the sediment instabilities. First, it is known that weak sediment layers may facilitate sliding and slumping (e.g. Masson et al., 2006). Förster et al. (2010) provides evidences for weak units by results of ring shear tests. The hemipelagic sediments have residual coefficient of friction values of 0.36 to 0.42 (μ_{res}), whereas the reworked sediments are characterized by lower μ_{res}-values of 0.27-0.29 (corresponding φ-values: 15-16°), which may be sufficiently low and lead to repeated failure events. Our triaxial tests show φ-values ranging from 3° to 53°, whereas the lowest ones correspond to the samples with the highest clay content (Fig.). Kopf and Brown (2003) show that 20-30% clay lower the μ-values of medium sized samples. In the sediments containing higher silt and sand contents (e.g. GeoB12044, -13910 and -13911), we observe higher friction angles, suggesting that the high φ-values reflects the friction characteristics of the silt and sand particles.

Secondly from the upper slope of the Ligurian margin fluid flow is known e.g. at the base of the 1979 Nice Airport Slide or in the lower Var fan valley (e.g. Guglielmi and Prieur, 1997; Kopf et al., 2008, 2009, 2010), so that it could be an assumption that also lateral fluid flow may play a role for the sediment instability at the lower slope. But in our study area evidences of lateral fluid flow are missing, that may converge at the base of the slope and lead to retrogressive failure evolution (Orange et al., 2003).

6.8 Conclusion

While mass wasting processes on the upper continental slope of the Ligurian Margin and at the Baie des Anges are well-defined (e.g. Cochonat et al., 1993; Mulder et al., 1994; Dan et al., 2007), this study focuses on slope stability of the deeper slope. The margin is affected by on- and offshore seismicity. The main purpose was to relate seismic, sedimentological and geotechnical data of the Western Slide Complex with slope instability results.

While laboratory geotechnical measurements showed normal consolidation for the hemipelagic background sediments, the failed material is characterized by overconsolidation associated with the removal of significant overlying sediment units. The reworked sediments are characterized by low coefficient of friction values, which have behaved as structurally weak layers during sliding. Evidences for different failure events were seen in sedimentological and physical properties data at different core depths. Several incisions and tilted layering were observed in the hemipelagic as well as in the failed sediments, which may be related to several different mass wasting events.

At least three factors (trigger mechanisms and pre-conditioning factors) are likely responsible for destabilizing the slope: a) presence of mechanically weak layers, b) oversteepening of the slope and c) cyclic loading during earthquakes. These three factors form the basis of the one-dimensional stability analysis. The calculations show that most of the sediments of the slide complex are characterized by a FS >1 based on sediment loading with variable slope angles. Exceptions are two cores at the steepest slope (24°-28°) which are only stable to an slope angle <32°. The steep slope angle (~20°) and the mechanical behavior enhance the frequency of failure events, so that only a small trigger may be required for sediment failure. The calculations show that for sediment failure peak ground accelerations (PGA) of 0.13 m/s² to 2.22 m/s² are required. The geometry of the slide complex (taken from seismic and bathymetric data) that we considered could led to an under- or overestimated of the FS, which will result in an over- or underestimation of the PGAs that are required for sediment failure. However, determined earthquake magnitudes of M=0.77-5.27 have recurrence times of 20 months increasing up to 12 years. These low recurrence times suggests a high frequency of mass wasting processes, which was supported by several other indications in the sediment cores (see above).

To better predict the stability of the deeper slope, additional measurements such as in-situ piezometer tests are needed to determine the role of excess pore pressure on the observed failure events. Additionally, dating of the different failure events as well as geotechnical measurements on sediments across the failure plane seem mandatory to correlate these data to real seismic events.

Acknowledgements

We thank the captain and the crew of the RV Meteor and RV Poseidon for their support during the cruises M73/1 and P386. Sebastien Garziglia and Nabil Sultan (IFREMER, Brest) are acknowledged for having performed additional oedometer tests. This study was financed through the Deutsche Forschungsgemeinschaft (MARUM, Project SD 5).

References

Ambraseys, N.N., 1960. The Seismic Sea Wave of July 9, 1956, in the Greek Archipelago. J Geophys Res 65: 1257-1265.

Assier-Rzadkiewicz, S., Heinrich, P., Sabatier, P.C., Savoye, B., Bourillet, J.F., 2000. Numerical Modelling of a Landslide-generated Tsunami: The 1979 Nice Event. Pure Appl Geophy 157: 1707-1727.

Baptista, M.A., Miranda, P.M.A., Miranda, J.M., Mendes, V.L., 1998. Constrains on the source of the 1755 Lisbon tsunami inferred from numerical modelling of historical data on the source of the 1755 Lisbon tsunami. J Geodyn 25: 159-174.

Bartetzko, A., Kopf, A., 2007. The relationship of undrained shear strength and porosity with depth in shallow (<50 m) marine sediments. Sediment Geol 196: 235-249.

Béthoux, N., Ouillon, G., Nicolas, M., 1998. The instrumental seismicity of the western Alps: spatio-temporal patterns analysed with the wavelet transform. Geophys J Int 135: 177-194.

Béthoux, N., Tric, E., Chery, J., Beslier, M.O., 2008. Why is the Ligurian Basin (Mediterranean Sea) seismogenic? Thermomechanical modelling of a reactivated passive margin? Tectonics 27: TC5011, doi:10.1029/2007TC002232.

Biscontin, G., Pestana, J.M., 2006. Factors affecting seismic response of submarine slopes, Nat Haz Earth Sys Sci 6: 97-107.

Blum, P., 1997. Physical properties handbook: a guide to the shipboard measurement of physical properties of deep-sea cores. Techn Note 26 ODP doi:10.2973/odp.tn.26.1997.

Burrus, J., Bessis, F., Doligez, B., 1987. Heat flow, subsidence and crustal structure of the Gulf of Lions (NW Mediterranean): a quantitative discussion of the classical passive margin model. In: Beaumont, C., Tankard, A.J., (Eds). Sedimentary Basins and Basin-Forming Mechanisms. Mem Can Soc Petrol Geol 12: 1-15.

Casagrande, A., 1936. The Determination of the Pre-consolidation Load and its Practical Significance. Proc Int Conf SMFE 3: 60-64.

Clauzon, G., 1978. The Messinian Var Canyon (Provence, southern France) – paleo-geographic implications. Mar Geol 27: 231-246.

Cochonat, P., Bourillet, J.F., Savoye, B., Dodd, L., 1993. Geotechnical characteristics and instability of submarine slope sediments, the Nice slope (N-W Mediterranean Sea). Mar Georesourc Geotech 11: 131-151.

Courboulex, F., Larroque, C., Deschamps, A., Kohrs-Sansorny, C., Gélis, C., Got, J.L., Charreau, J., Stéphan, J.F., Béthoux, N., Virieux, J., Brunel, D., Maron, C., Duval, A.M., Perez, J.L., Mondielli, P., 2007. Seismic hazard on the French Riviera: observations, interpretations and simulations. Geophys J Int 170: 387-400.

DASE - Direction des applications militaries - Science de la Terre et de l'Environnement, 2009. http://www-dase.cea.fr/public/dossiers_thematiques/evaluation_de_l_alea_sismique/description_en.html,accessed 2009-27-11.

DIN ISO/TS 17892-4:2004, Stand 2007-03. Geotechnische Erkundung und Untersuchung – Laborversuche an Bodenproben – Teil 4: Bestimmung der Korngrößenverteilung, Beuth-Verlag, Berlin, 28p.

Dugan, B., Flemings, P.B., 2002. Fluid flow and stability of the US continental slope offshore New Jersey from the Pleistocene to the present. Geofluids 2: 137-146.

Förster, A., Spieß, V., Kopf, A., Dennielou, B., 2010. Mass wasting dynamics at the deeper slope of the Ligurian Margin (Southern France). In: Mosher, DC., Shipp, C., Moscardelli, L., Chaytor, J., Baxter, C., Lee, H., and Urgeles, R. (eds.), Submarine Mass movements and their consequences IV. Advances in Natural and Technological Hazards Series 28, Springer, pp. 67-77.

Grünthal, G., Bosse, C., Sellami, S., Mayer-Rosa, D., Giardini, D., 1999. Compilation of the GSHAP regional seismic hazard for Europe, Africa and the Middle East. Annali Geofis 42: 1215-1223.

Guglielmi, Y., Prieur, L., 1997. Locating and estimating submarine freshwater discharge from an interstitial confined coastal aquifer by measuremnts at sea: example from the lower Var valley, France. J Hydrology 190: 111-122.

Gutenberg, B., Richter, C.F., 1949. Seismicity of the Earth and Associated Phenomenon, Princeton University Press, Princeton, 273pp.

Hampton, M.A., Lee, H.J., Locat, J., 1996. Submarine landslides. Rev Geophys 3:33-59.

Johnston, A.C., 1996. Seismic moment assessment of earthquakes in stable continental regions-III. New Madrid 181 1-1812, Charleston 1886 and Lisbon 1755. Geophys J Int 126: 314-344.

Khripounoff, A., Vangriesheim, A., Crassous, P., Etoubleau, J., 2009. High frequency of sediment gravity flow events in the Var submarine canyon (Mediterranean Sea). Mar Geol 263: 1-6.

Klaucke, I., Cochonat, P., 1999. Analysis of past seafloor failures on the continental slope off Nice (SE France). Geo-Mar Lett 19: 245-253.

Klaucke, I., Savoye, B., Cochonat, P., 2000. Patterns and processes of sediment dispersal on the continental slope off Nice, SE France. Mar Geol 162: 405-422.

Kopf, A., Brown, K.M., 2003. Friction experiments on saturated sediments and their implications for the stress state of the Nankai and Barbados subduction thrusts. Mar Geol 202: 193-210.

Kopf, A., Cruise Participants, 2008. Report and Preliminary Results of Meteor Cruise M 73/1: LIMA-LAMO (Ligurian Margin Landslide Measurements & Observatory), Cadiz, 22.07.2007 - Genoa, 11.08.2007. Berichte Fachbereich Geowissenschaften, Universität Bremen, 264, 169pp.

Kopf, A., Cruise Participants, 2009. Report and Preliminary Results of Poseidon Cruise P386: NAIL (Nice Airport Landslide), La Seyne sur Mer, 20.06.2009 – La Seyne sur Mer, 06.07.2009. Berichte Fachbereich Geowissenschaften, Universität Bremen, 271, 161pp.

Kopf, A.J., Kasten, S., Blees, J., 2010. Geochemical Evidence for Groundwater-Charging of Slope Sediments: the Nice Airport 1979 landslide and Tsunami Revisited. In: Mosher, DC., Shipp, C., Moscardelli, L., Chaytor, J., Baxter, C., Lee, H., and Urgeles, R. (eds.), Submarine Mass movements and their consequences IV. Advances in Natural and Technological Hazards Series 28, Springer, pp. 203-214.

Ladd, C.C., Foott, R., Ishihara, K., Schlosser, F., Poulos, H.G., 1977. Stress-deformation and strength characteristics. State of the art report. 9th Intern. Conf on Soil Mech & Found Eng 2: 421-494.

Lambe, T.W., Whitman, R.V., 1979. Soil Mechanics, SI Version. John Wiley & Sons, New York, 281pp.

Lee, H. J., 2009. Timing of occurrence of large submarine landslides on the Atlantic Ocean margin. Mar Geol 264: 53-64.

Locat, J., Lee, H.J., 2002. Submarine landslides: advances and challenges. Can Geotech J 39:193-212.

Masson, D.G., Harbitz, C.B., Wynn, R.B., Pedersen, G., Løvholt. F., 2006. Submarine landslides: processes, triggers and hazard prediction. Phil Trans R Soc A 364: 2009-2039.

Masson, D.G., Wynn, R.B., Talling, P.J., 2010. Large Landslides on Passive Continental margins: Processes, Hypotheses and Outstanding Questions. In: Mosher, DC., Shipp, C., Moscardelli, L., Chaytor, J., Baxter, C., Lee, H., and Urgeles, R. (eds.), Submarine Mass movements and their consequences IV. Advances in Natural and Technological Hazards Series 28, Springer, pp. 153-165.

Morgenstern, N.R., Price, V.E., 1965. Analysis of stability of general slip surfaces, Géotechnique 15: 79-93.

Mulder, T., Tisot, J.P., Cochonat, P., Bourillet, J.F., 1994. Regional assessment of mass failure events in the baie des Anges, Mediterranean Sea. Mar Geol 122: 29-45.

Mulder, T., Savoye, B., Syvitski, J.P.M., 1997. Numerical modelling of a mid-sized gravity flow: the 1979 Nice turbidity current (dynamics, processes, sediment budget and seafloor impact). Sedimentol 44: 305-326.

Mulder, T., Savoye, B., Syvitski, J.P.M., Piper, D.J.W., 1998. The Var Submarine System: understanding Holocene sediment delivery processes and their importance to the geological record. In: Stoker MS, Evans D, Cramp A (Eds.), Geological Processes on Continental Margins: Sedimentation, Mass Wasting and Stability. Spec Publ Geol Soc Lond, pp.145-166.

Murphy, J.R., O'Brien, L.J., 1977. The correlation of peak ground acceleration amplitude with seismic intensity and other physical parameters. Bull Seism Soc Am 67: 877-915.

Neumann, F., 1954. Earthquake intensity and related ground motion. University of Washington Press, Seattle, 77pp.

Orange, D.L., Saffer, D., Jeanjean, P., Al-Khafaji, Z., Humphrey, G., Riley, G., 2003. Measurements and modelling of the shallow pore pressure regime at the Sigsbee Escarpment : Successful prediction of overpressure and ground-truthing with borehole measurements. The Leading Edge 22: 906-913.

Pasquale, V., Verdoya, M., Chiozzi, P., 1996. Heat flux and timing of the drifting stage in the Ligurian-Provencal basin (Northwestern Mediterranean). J Geodyn 21: 205-222.

Perissoratis, C., Papadopoulos, G., 1999. Sediment instability and slumping in the southern Aegean Sea and the case history of the 1956 tsunami. Mar Geol 161: 287-305.

Piper, D.J.W., Savoye, B., 1993. Processes of late Quaternary turbidity current flow and deposition on the Var deep-sea.fan, northwest Mediterranean Sea. Sedimentol 40: 557-582.

Rehault, J.P., Béthoux, N., 1984. Earthquake relocation in the Ligurian Sea (Western Mediterranean): Geological interpretation. Mar Geol 55: 429-445.

Rehault, J.P., Boillot, G., Mauffret, A., 1984. The Western Mediterranean Basin Geological Evolution. Mar Geol 55: 447-477.

Ryan, W.B.F., 2009. Decoding the Mediterranean Salinity Crisis. Sedimentol 56: 95-136.

Sammari, C., Millot, C., Prieur, L., 1995. Aspects of the seasonal and mesoscale variabilities of the Northern Current in the western Mediterranean Sea inferred from the PROLIG-2 and PROS-6 experiments. Deep Sea Res 42: 893-912.

Savoye, B., Piper, D.J.W., Droz, L., 1993. Plio-Pleistocene evolution of the Var deep-sea fan off the French Riviera. Mar Petr Geol 10: 550-571.

Sultan, N., Cochonat, P., Canals, M., Cattaneo, A., Dennielou, B., Haflidason, H., Laberg, J.S., Long, D., Mienert, J., Trincardi, F., Urgeles, R., 2004. Triggering mechanisms of slope instability processes and sediment failures on continental margins: a geotechnical approach. Mar Geol 213: 291-321.

Sundberg, A., 1956. The River Klarälven: a study of fluid processes. Geografiska annaler 38: 127-316.

Terzaghi, K., Peck, R., 1948. Soil Mechanics in Engineering Practice. John Wiley & Sons, New York, 566 pp.

Wentworth, C.K., 1922. A scale of grade and class terms for clastic sediments. Journal of Geology 30, 377-392.

7. Cretan Sea

7.1 Slope failure repetition in active margin environments – constraints from submarine landslides in the Hellenic forearc, eastern Mediterranean

Frank Strozyk[1], Michael Strasser[1], **Annika Förster[1]**, Achim Kopf[1] & Katrin Huhn[1]

Published in *Journal of Geophysical Research (2010)*, 115, B08103, doi:10.1029/2009JB006841

Abstract

It has been shown that submarine landslides can occur less frequently at subduction zone forearcs despite the general expectation of extensive slope failures from high neotectonic activity in active margin settings. The Hellenic subduction zone, Greece, represents an example where modern evidence for slope failure is scarce. Taking the deeper parts of the forearc basin into account, however, a sequence of massive landslide deposits are found at recurrence intervals of approximately 250 ka ± 70 ka. Given high seismicity in the forearc area, this rate of slope failure appears to be low. In order to improve our understanding on the relationship between low landslide recurrence rates and the frequency and settings of the required trigger mechanism, we here assess the mechanical behaviour of the slope sediment cover during instability scenarios. Seismic profiles and geotechnical measurements from cores of midsize landslides found on the northeastern Cretan mid-slope are used to back-analyze slope destabilization in one-dimensional, infinite slope models for static conditions as well as for the case of seismic loading. Results reveal that today only critically steepened parts of the Cretan slope can fail from high loading stresses of peak ground acceleration (PGA) of 37 %g, maybe up to ≥ 64 %g. We further deduce that long-term tectonic processes are important pre-conditioning factors controlling an occasional development of critically inclined slope parts. Therefore the impact of seismic triggers is strongly limited in time and space: For an initially stable slope, the critical seismic intensity to trigger failure is being reduced with increasing tectonically-controlled steepening of the slope through time, until an earthquake is sufficient to trigger a large landslide. Before that, the slope rather gets more resistant, because smaller PGA may rather result in dynamic compaction (seismic strengthening). Our findings imply that low frequencies of landslides in the Hellenic forearc are not in conflict with high seismicity in this region, because seismic loading is only sufficient to trigger major collapses of a generally shear-resistant "cohesive" slope (increasing with time due to seismic strengthening) if long-term tectonic movement provides a critical steepening. This may explain the relatively scarce occurrence of large submarine landslides in this and similar tectonically-active environment.

7.1.1 Introduction

Gravitational mass movements are of significant interest as they are leading agents for submarine landscape development [e.g., *O'Grady*, 2001; *Hutton and Syvitski*, 2003] and the stratigraphic evolution of sedimentary systems in different environmental settings [e.g., *Cochonat et al*., 2002; *Shanmugam,* 2009]. As subaquatic mass movements can involve large volumes of wasted material, both the flow itself and the possible tsunami triggered by it are of high societal concern regarding their geohazardous impact on on- and offshore infrastructure [e.g., *Bardet et al*., 2003]. Numerous mass movements of different types, scales, triggers, and

[1] MARUM - Center for Marine Environmental Sciences, University of Bremen,PO box 330 440, 28334 Bremen, Germany.

consequences were imaged in different active margin settings [e.g., *McAdoo et al., 2004; Canals et al., 2004; Lee et al., 2007*]. Active margin systems are known to commonly produce $M_s > 8$ earthquakes, thus linked to a high probability for frequent, extensive mass wasting because of the earthquake-induced ground acceleration [e.g., GSHAP global seismic hazard map (Giardini, 1999)] and induced shear stresses and pore water pressures [e.g., *Locat and Lee*, 2002; *Canals et al.,* 2004; *Strasser et al.,* 2007, *Lee et al.,* 2007]. Based on that, recurrences rates of mass movements are often used to reconstruct paleo-seismicity and its impact on slope stability in active margin systems [e.g., *Goldfinger et al*., 2003; *McAdoo and Watts*, 2004] as well as other environmental settings [e.g., *Strasser et al*., 2006; *ten Brink et al.,* 2009].

In contrast, active margin case studies have shown that earthquake recurrence-times may differ significantly from those of mass movement in the same region [e.g., *McAdoo et al.,* 2000, 2004; *Camerlenghi et al*., 2009]. Although these settings often show a frequent recurrence of seismic loads, their slopes appear to remain stable for long periods of time. This resistance may be explained by high mechanical sediment strength [e.g., *Sultan et al*., 2004; 2008] or high consolidation state, as it may naturally result from exhumation of older sediment in accretionary complexes [e.g., *McAdoo et al.,* 2004; *McAdoo and Watts*, 2004].

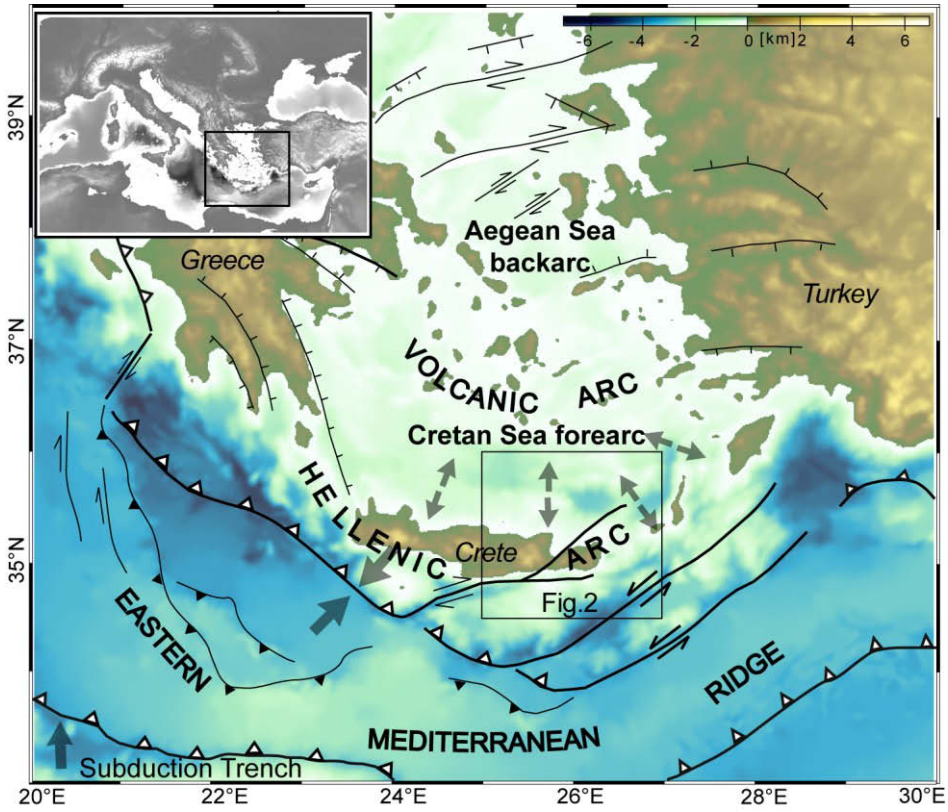

Fig.1 Principal setup of the Hellenic subduction zone, eastern Mediterranean, and main tectono-sedimentary settings, comprising the eastern Mediterranean Ridge accretionary complex, the Hellenic arc, the Cretan Sea forearc basin, the volcanic arc, and the Aegean backarc basin. Arrows indicate direction of plate convergence in the south, backstop of the eastern Mediterranean Ridge south of Crete, and forearc basin extension further north (complied after Angelier et al. [1982], Mascle and Martin [1990], and Ganas and Parsons [2009]).

However, to date a number of questions remain open concerning the importance of pre-conditioning factors, trigger requirements, and the temporal relationship between slope failure and triggering conditions [*Camerlenghi et al.,* 2010]. Pre-conditioning factors such as slope steepening, changes in sediment charging and slope re-charging, the dissociation of gas or meteoric water, gas-hydrate destabilization or deep-seated fluid flow can influence slope stability as well as timing and scale of submarine landslides [*Locat and Lee*, 2002; *Sultan et al*., 2004; *Masson et al*., 2006; *Sultan et al*., 2008].

The Cretan Sea, the forearc basin of the Hellenic subduction zone in the Eastern Mediterranean, is situated in a tectonically highly active setting (Fig. 1), where so far only scattered mass movements of maximum cubic-kilometre-scale were observed [e.g., *Chronis et al.,* 2000; *Kopf et al.,* 2006; 2007; *Strozyk et al.,* 2009; 2010]. Conversely, the irregular, steep relief [*Chronis et al*., 2000], a complex system of faults [e.g., *Angelier et al*., 1982; Fig. 2] and regional seismicity [e.g., *Meier et al.,* 2004; Fig. 2] provide a framework suggesting high frequency mass wasting. To improve our conceptual understanding of relatively low recurrence times of submarine landslides as well as conditions of triggering and pre-conditioning requirements in this setting, we here use multi-channel seismic reflection profiles, bathymetry charts and gravity cores from the northeastern mid-slope of Crete and the adjacent Kamilonisi Basin, representing a forearc basin of the Hellenic subduction zone, and derived results from a detailed study of cubic-kilometre-scale landslides in a mid-slope position [*Strozyk et al., 2010*] as the basis to analyze slope stability under static and seismic loading conditions. We compare our results derived from quantitative slope stability analysis with the seismicity of the Hellenic Arc and other potential triggers. We consequently focus on constraints for a required trigger in terms of mechanical sediment attributes, long-term development of slope geometry and frequencies of possible trigger mechanisms and pre-conditioning factors to infer scenarios that explain the observed low spatial and temporal distribution of mass-transport deposits (MTDs) along the NE Cretan slope. The results then are discussed in a more general context of causes for infrequent submarine landslides in such particularly active margin environments.

7.1.2. Tectonic settings

The island of Crete is located in the centre of the active convergent margin of the African and Eurasian lithospheric plate collision zone in the eastern Mediterranean (Fig. 1). The convergence between these two plates results in subduction of the African plate to the north beneath the Aegean region and forms the Hellenic Arc [e.g., *Meulenkamp et al*., 1988; Fig. 1]. Rooted on a deep-seated detachment fault, Crete was exhumed approximately 19 Ma ago and now presents a topographic high that is still being uplifted [*Bonneau,* 1984]. The island has acted as a backstop to the eastern Mediterranean Ridge (Fig. 1), a large accretionary complex south of Crete [*Polonia et al.,* 2002; *Kopf et al.,* 2003]. North of Crete, the Cretan Sea represents a large, N-S- as well as E-W-extensional forearc basin, bordered to the north by the volcanic arc, which is followed further north by the Aegean Sea backarc (Fig. 1). With respect to the arcuate shape of the entire Hellenic arc and the orthogonal to oblique subduction (Fig. 1), trends of the Cretan Sea extension and subsidence rates strongly vary from the west to the east [*Angelier et al.,* 1982; *Mascle and Martin*, 1990; see arrows in Fig. 1]. This results in the formation of several sub-basins, e.g. the Heraklion Basin and the Kamilonisi Basin, which increase in depth from the west to the east [e.g., *Angelier et al*., 1982; *Chamot-Rooke et al*., 2005; Fig. 2]. Ongoing forearc extension during the incremental curvature of the subduction system (see Fig. 1) caused the

formation of a Cretan Sea half-graben system [*Mascle and Martin*, 1990; Fig. 2] as well as multiple fault-sets [*Angelier et al.,* 1982; Fig. 2], whose dominant pattern is linked to forearc basin extension and follows the general structural trend of the Hellenic arc. Sets of minor faults in various orientations are genetically linked to neotectonic movement at variable subsidence rates [*Angelier et al*., 1982]. It has been shown that the northern Cretan margin hence experienced long-term tectonic steepening, based on Cretan Sea sub-basin subsidence as well as the countering uplift of the island of Crete, from normal faults with increasing slip towards the deeper basin [*Angelier et al.,* 1982; *Bonneau,* 1984]. *Mascle and Martin* [1990] reconstructed the last main basin creation phase in the forearc to have occurred during the Late Miocene and Pliocene, and propose that extension and the magnitude of tectonic movement have decreased afterwards. However, some of the regional major faults are recognized being seismically active also in recent times, for instance the prominent, southwest-northeast-trending Hera-Petra Fault [e.g., *Lykousis et al.,* 1995; Fig. 2], indicating that the system today is still tectonically active.

The largest recent earthquake at the Hellenic Arc plate boundary was recorded with M_s = 7.3 [*Ambraseys*, 2001], whereas historical and archeological studies suggest that earthquakes of $M_s > 8$ may have occurred [e.g., *Guidoboni and Comastri*, 1997; *Stiros*, 2001]. A maximum magnitude calculated from ISC catalogue data (International Seismological Centre, UK)

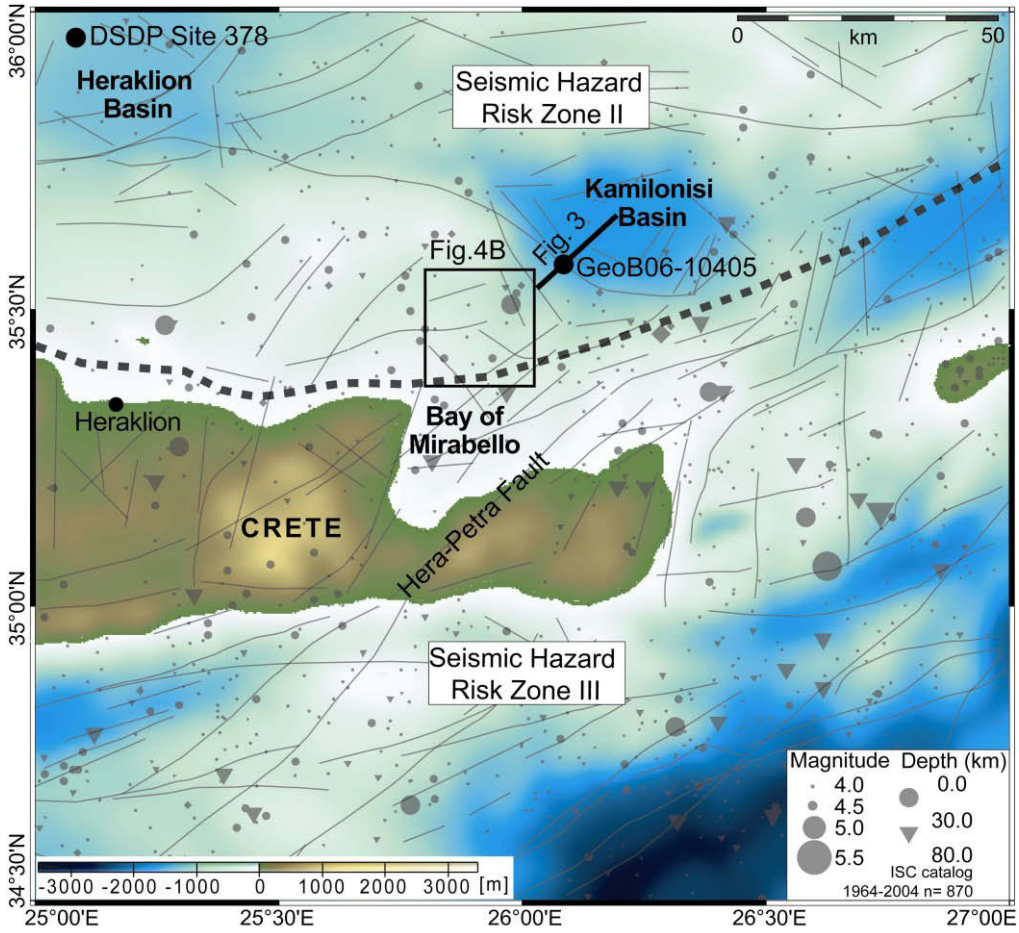

Fig. 2 Bathymetry map of the northeastern Cretan margin and the adjacent region. Faults (thin black lines) are compiled from Mascle & Martin (1990) and Angelier et al. (1982). Earthquakes (grey symbols) are obtained from the ISC catalog 1964 - 2004 (http://wwweic.eri.u-tokyo.ac.jp). The dotted line indicates the boundary between the EPPO (1992) seismic hazard risk zones II to III.

suggests an M_s = 7.8 ± 0.4 value [*Hamouda*, 2006]. Subduction thrusting and large-scale neotectonic movements are responsible for this high seismicity being recorded by a network of seismic recording stations throughout the Hellenic forearc region (ISC catalogue [e.g., *Engdhal and Villaseñor*, 2002]). Earthquake source-mechanisms correspond to deep-seated N-S-directed plate-interface seismicity, the Cretan island block uplift tectonics and E-W- as well as N-S-extension in the forearc [*Meier et al.,* 2004]. These mechanisms lead to a clustered distribution of earthquake epicentres with varying implication for the regional seismic hazard [e.g., *Manakou and Tsapanos,* 2000].

The EPPO (Earthquake Planning and Projection Organization of Greece; e.g., *Moratto et al*., 2007) defined four seismic hazard risk zones from the more than 4000 earthquakes of $M_s \geq 4$ recorded and localized since 1964 (Fig. 2). This risk zone classification provides most probable maximum values of peak ground acceleration (PGA) as a function of the mean repeat time (T_m). The southern Cretan Sea in Zone II is characterized by a 'moderate risk' (Fig. 2), whereas the northern margin of Crete traces the boundary between Zone II and Zone III, thus indicating higher risk (dashed line in Fig. 2). Maximum constraints provided by the EPPO catalogue from the currently available earthquake records indicate that T_m for 22 %g PGA in Zone II and 29 %g for Zone III is expected not to exceed 500 years.

7.1.3. Data and methods

7.1.3.1 Acoustic data

Methodological details of acoustic data acquisition techniques are given in the P-336 cruise report [*Kopf et al.,* 2006]. For further details of data processing and imaging strategy we also refer to *Strozyk et al*. [2010].

7.1.3.2 Sediment physical properties data

Gravity cores of 1.5 to 4.6 m length and 10 cm diameter were recovered during P-336 with a standard gravity corer of approximately 1.5 tons weight (core locations in Figs. 2 and 3 (GeoB-10405) and 4A (GeoB-10452, -53, -54, -55, -58)). Cores were analyzed for their sediment composition and physical properties (additional methodological detail and core data acquisition techniques are given in the P-336 cruise report [*Kopf et al.,* 2006] and in *Kopf et al.* [2007]): Bulk density was derived from a Multi-Sensor Core Logger (MSCL). The geotechnical measurements include the determination of the undrained shear strength (*Su*) with a Wykeham-Farrance cone penetrometer on the intact split gravity core surfaces [*Wood*, 1985]. Additionally, the SHANSEP approach ('Stress History and Normalized Soil Engineering Properties' [*Ladd et al*.,1977]) was used to obtain 'normalized shear strength' values from the *Su*-vs.-overburden pressure-ratio (Su / σ_v'), where σ_v' is the effective vertical stress, derived from σ_v (vertical stress [kPa]) – u (pore pressure under hydrostatic conditions) [kPa]). For comparison, we also use *in situ* shear strength and pore-pressure data from P-336 Cone Penetration Tests (CPT) published in *Stegmann et al.* [2007] and *Kopf et al.* [2007].

Furthermore, the sediment's total carbonate content was determined using the HCl-digestion method after *Heinrichs & Herrmann* [1990]. To identify marker horizons for dating, selected intervals from cores were analyzed for microfossil assemblages (i.e., Globigerinoides

ruber and Globorotalia inflata) due to their distinct stratigraphic distribution in uppermost Cretan slope strata; e.g., *Geraga et al.* [2005]).

7.1.3.3 One-dimensional, undrained, infinite slope stability analysis

Slope failure may be triggered either by an increase of loading forces, a decrease of resisting forces, or a combination of both [*Lee et al.*, 2007]. In the limit equilibrium approach, a slope is classified as stable until one or more effects trigger the resisting-to-loading-force ratio to a critical Factor of Safety (*FS*) below 1. To evaluate the *FS* for distinct stable and destabilized slope portions at the Cretan Margin, we implement results from geotechnical experiments into one-dimensional, undrained, infinite slope stability analysis (SSA; *Morgenstern and Price* [1965]). Observed linear trends of measured undrained shear strength are extrapolated to the depth of the inferred shear plane following the SHANSEP approach [*Ladd et al*., 1977]. Initial resisting forces of the sediment correspond to *Su* values measured on the intact gravity cores. Loading forces under static conditions are calculated from the gravitational shear stress in the sediment column, derived from the effective normal stress (σ_n') acting on an inclined shear plane. Additional shear forces from seismic loading (*Ts*) are implemented using a pseudo-static acceleration based on peak ground acceleration (PGA) generated by an earthquake. Our analysis assumes that the earthquake acceleration is applied over a significantly long period of time so that the induced stress can be considered constant [e.g., *Hampton et al.* [1996]). This may lead to some minor uncertainties in slope stability analysis due to dynamic behaviour of the sediment, e.g. accumulation of plastic strain or shear-induced excess pore water pressures with increasing number of loading cycles [e.g., *Sultan et al.,* 2004; *Biscontin, and Pestana*, 2006]. However, as this simplified approach was successfully applied in other studies [e.g., *Urgeles et al*., 2006; *Strasser et al.,* 2007; *ten Brink et al.,* 2009; *Stigall & Dugan.,* in press], we adopt it here to gain insights on trigger quantity requirements and constraints. Our back-analysis assumes failure may only occur if $FS \leq 1$. *FS* is defined as the ratio between undrained shear strength and the sum of static and pseudo-static shear forces:

$$FS = Su^* / (\gamma' h (\sin(\alpha) \cos(\alpha) + k (\gamma / \gamma') \cos^2(\alpha))) \quad (1),$$

whereof *Su** is the undrained shear strength in failure depth (kPa), γ' the submerged unit weight (kN/m³), γ the bulk saturated unit weight (kN/m³), *k* the ratio of the pseudo-static horizontal acceleration to gravitational acceleration (%g), α the slope inclination to horizontal (°), and *h* the depth of slide surface below seabed (m). The pseudo-static horizontal acceleration used to model the earthquake-induced shear stress driving a slope towards failure cannot be directly compared to PGA, the parameter generally used for seismic hazard assessments. PGA values usually are higher [*Seed and Idriss,* 1971; *Seed*, 1979] and pseudo-static horizontal accelerations as the average equivalent uniform shear stress imposed by seismic shaking may only represent 65 % of the effective seismic PGA as empirically calibrated by *Seed & Idriss* [1971].

7.1.4. Results

7.1.4.1 Geophysicsical data base

The starting point for this study was the discovery of thick, widespread, acoustically incoherent sequences interbedded between layered deposits from background sedimentation of the Kamilonisi Basin. In general, seismic reflection profiles show different sedimentary units defined by seismic reflection pattern attributes such as amplitude, continuity and configuration. High-amplitude, layered units are smooth, undisturbed slope and basin background sediments (Figs. 3 and 4B) whereas less coherent, fuzzy packages are interpreted as MTDs (Figs. 3 and 4B).

In the SW to central portion of the Kamilonisi Basin, a sequence of at least three, up to 50-m thick MTDs is identified within the background sediment-succession (Fig. 3). The MTDs are interbedded by 15-25 m-thick (mean thickness: 20 m) background sediment packages, while the stratigraphically youngest MTD is draped by sediment of almost same thickness (i.e. ~20 m). Reconstructed geometries for these wedge-shaped MTDs to the SW basin flank as well as only little option for mass wasting along the steep northeastern basin flank imply that their source areas may have been located in the southwest (see also data by *Strozyk et al.* [2010]). Since available data do not allow for basin wide mapping of these massive MTD series in the Kamilonisi Basin, we use publicly available bathymetric charts (e.g. Fig. 2) and extrapolate symmetrically over the locally restricted Kamilonisi Basin for rough volume estimations of MTDs. When using an almost basin-wide extent (i.e. ~600 km²) and keeping the sediment thickness of the MTDs at an average of measured 30 - 50 m, a first order volume of 30 - 50 ±10 km³ can be estimated for each event. Despite the large range of uncertainty in MTD volume estimates, however, these events are much larger compared to all prior findings of mass movement deposits on the northern Cretan margin and the closer vicinity [*Chronis et al.,* 2000; *Kopf et al.,* 2006; 2007; *Strozyk et al.,* 2009; 2010].

Within the inferred provenance area of these MTDs, we do not observe prominent large-scale scars along the margin that would explain the large MTD volumes in the basin. However, mid-sized landslides and associated source scars in the order of 0.5 to 2 km³ volumes occur at the mid-slope area (500 - 900 m water depth; see Fig. 4A and B). *Strozyk et al.,* [2010] reconstructed retreating sediment failures during the evolution of these mass-transport complexes that relate to the steepening of the slope over longer time scales as a consequence of the subsiding forearc basin and the uplift of the island of Crete. Hence, the lower, continuously steepening slope now is mostly eroded, masking evidences of older scars that potentially relate to the larger Kamilonisi Basin MTDs. Nevertheless, these mid-sized landslides are suggested to reflect similar lithologies and a comparable evolution regarding sediment mechanics, failure site geometry and trigger requirements. Therefore, we here utilize the well-constraint mid-slope mass-transport complex as representative case study site to constrain a conceptual relationship of sediment mechanics and respective trigger requirements for this northeastern Cretan slope portion.

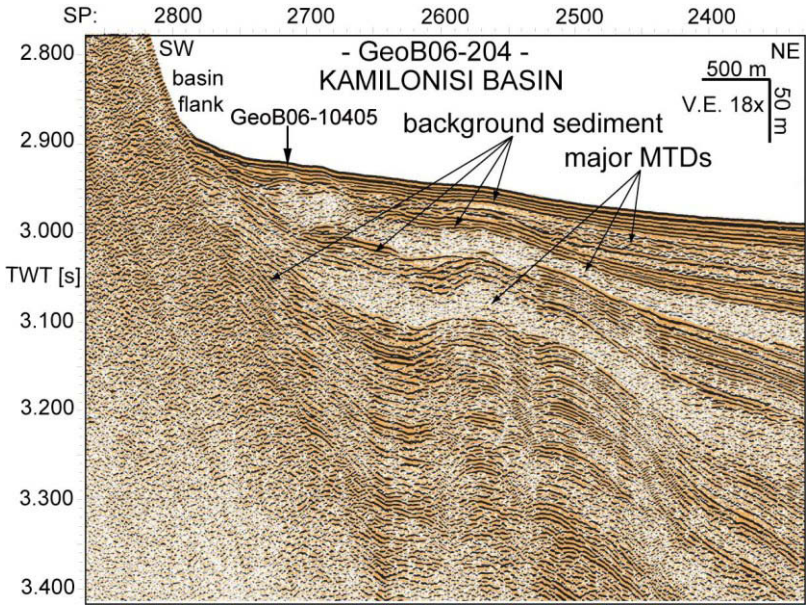

Fig. 3 Southwest-northeast seismic profile GeoB06-204 (for location see Fig. 2) slices the southwestern Kamilonisi Basin and the basin flank and shows three sequenced, large-scaled MTDs in the basin sediment succession, and shows the projected location of P-336 core GeoB-10405.

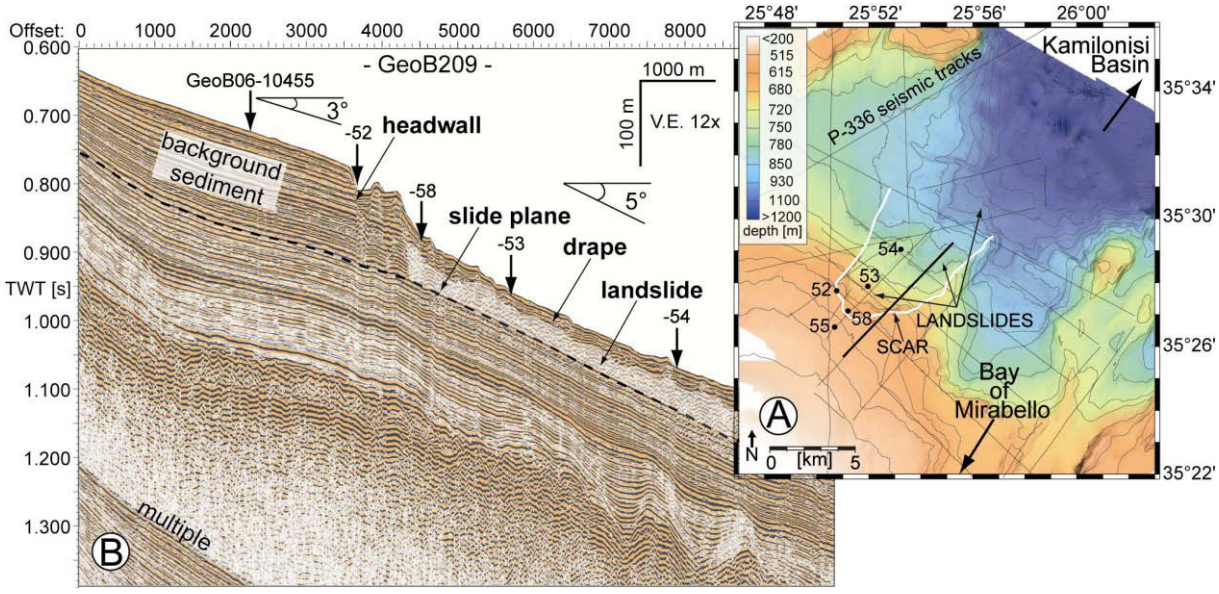

Fig. 4 A: Bathymetric chart of the mid-slope study site north of the Bay of Mirabello (for location see Fig. 6.2). Note the prominent scar and interpreted landslides in the central part. Black dots indicate P-336 coring locations, the thick black line the location of GeoB06-209 (Fig. 4B). B: Southwest-northeast seismic profile GeoB06-207 (see Fig. 4A for location) slices undisturbed background sediments (i.e. lefthandside up to the headwall and below landslide), one of the mid-slope landslides, and the associated headwall in transport direction of the slide. It further shows projected P336 mid-slope core locations (see Fig. 4B for location).

7.1.4.2 Sediment composition, lithostratigraphy and accumulation rates

7.1.4.2.1 Sediment composition and lithostratigraphy

Five cores from the mid-slope study site (Fig. 4A; see projected location on Fig. 4B) and one core from the Kamilonisi Basin were analysed (Fig. 2; see projected location on Fig. 3). Cores were recovered from the undisturbed slope (GeoB-10455), from headwall-drape (-52, -58), from the drape on top of mid-slope MTDs (-53 and -54), and from the drape overlying the stratigraphic youngest MTD in the Kamilonisi basin (-05). For all cores, the main lithofacies is a mud-rich, sandy to silty sediment [*Kopf et al.,* 2006; Fig. 5]. It is interrupted by a sapropel at 0.45 - 0.8 mbsf (meters below seafloor), except core GeoB-10458, where the sapropel occursat 1.5 - 1.85 mbsf (Fig. 5). Based on colour, grain size distribution, sediment composition and organic material content, the dominantly hemipelagic lithologies correlate to the existing stratigraphic framework of the northern Cretan margin mid-slope sediments [*Aksu et al.,* 1995; *Giresse et al*., 2003]. Analysis of planktonic microfossil species below and above the sapropel reveals an assemblage that is characteristic for the sapropel 'S1' [*Geraga et al.,* 2005]. This reinforces the stratigraphic correlation of the sapropel to S1, which is dated to 9.6 - 6.4 ka B.P. [*Giresse et al.,* 2003]. Furthermore a pronounced ash layer recovered in all cores, except the headwall core GeoB-10452, is correlated to the Z2-Santorini event (3370 B.P. [*Pichler and Friederich*, 1976]), providing a second robust time-marker for the age model of drape overlying MTDs.

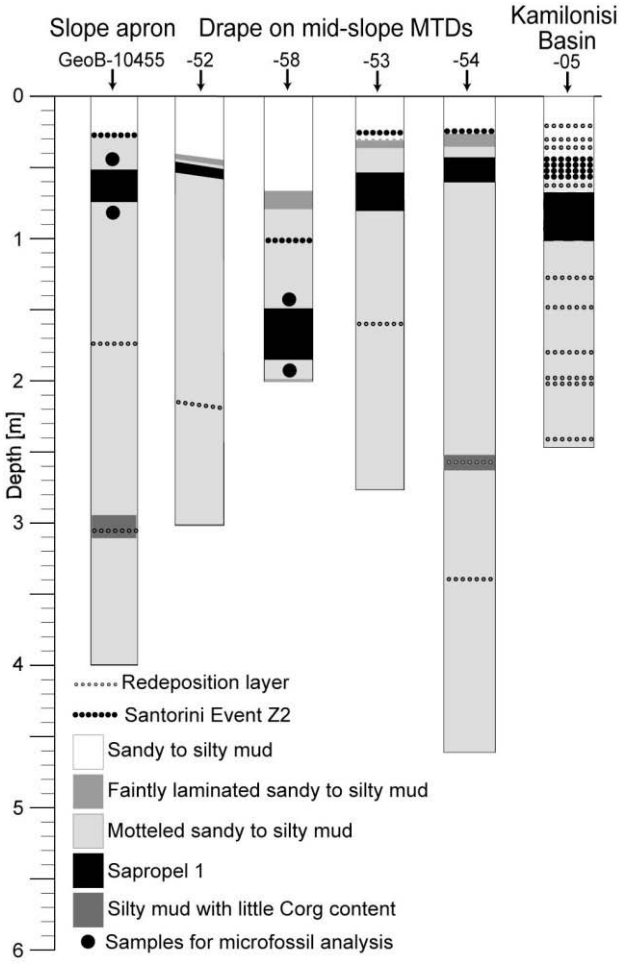

Fig. 5 Gravity core logs from the mid-slope (see Figs. 6.4A and B for locations) and one core from the Kamilonisi Basin (see Figs. 2 and 3 for location) showing the lithostratigraphic framework. Black points above and below Sapropel 1 in cores GeoB-10455 and -58 mark positions of microfossil content sampling.

The single gravity core in the Kamilonisi Basin shows a similar sediment succession including S1 and Z2 (Fig. 5). In contrast to the mid-slope cores, however, it is characterised by a larger number of thin interbedded redepositional events (few mm to cm in thickness) that are interpreted as small scale sediment remobilization events. While the five cores recovered at the mid-slope scar and surroundings have in average ca. 0.5 events m^{-1}, core GeoB-10405 exhibits 4 events m^{-1} core length. This implies that mass-wasting efficiency is enhanced in the exposed lower slope and basin flank areas where gradients are steeper (Figs. 2, 3 and 4A).

In order to get a more solid data base on the regional stratigraphy, we considered a DSDP (Deep Sea Drilling Project) core recovered from Site 378 in the Heraklion Basin [*Hsü et al*., 1978; for location see Fig. 2]. The 343.5-m-deep boring recovered Quaternary to late Miocene lithologies. The upper 64 meters comprise Quaternary nanofossil marl with cm- to dm-scaled interlayers of sapropelic marl and marl conglomerates, with the latter being interpreted as sedimentary slump conglomerates. Core data for 64 - 131.5 mbsf show Quaternary nanofossil marl and ooze with interlayered sapropelic marls [*Hsü et al.,* 1978]. As this Quaternary sediment composition correlates with our findings in the shallow P-336 cores, we assume that this sedimentary succession can be applied also to the deeper strata at the northeastern Cretan mid-slope as well as the SW Kamilonisi Basin.

7.1.4.2.2 Sediment accumulation rate estimates

We use age constraints identified from cores GeoB-10453, -54, and -55 to determine an accumulation rate of 7.8 cm ka^{-1} (range of uncertainty: 7.0 - 8.5 cm ka^{-1}) for the topmost meters of intact drape recovered above the already described mid-slope MTDs and scars. Cores GeoB-10452 and -58 from the headwall region were neglected as higher sediment accumulation rates at the foot of the headwall are biased by talus. This interpretation is reinforced by high concentration of mussel shell fragments in core -58 and evidence for erosion in core -52 from the upper part of the headwall (i.e., missing Z2-marker layer and condensed S1; Fig. 7). For the Kamilonisi Basin, the age model of the uppermost part of core GeoB-10405 consistently reveals sediment accumulation rates of 7.8 cm ka^{-1}.

For the deeper portion of the drape, there are no age-tie points available in core data and no information of ‘pre-S1’ sedimentation rates along the southern Cretan sea mid-slope region and the Kamilonisi Basin is documented in the literature. We therefore can only assume almost constant sedimentation rates, as also proposed for the upper 120 m of the sediment column in the Heraklion Basin from DSDP Leg 42 [*Hsü et al.,* 1978] Site 378 core interpretation. Accordingly, we transpose their dimension of accumulation rate estimates (i.e. 7.7 cm ka^{-1}) for the Heraklion Basin (see Fig. 2), apply it to our interpretation for the Kamilonisi Basin (i.e., 7.8 cm ka^{-1}) and extrapolate to depth.

7.1.4.2.3 Timing and evolution of MTDs

As reasoned above, both cores and seismic profiles independently indicate a continuous background sediment accumulation since the emplacement of mid-slope MTDs. Also the sediment accumulation rates from gravity core data in the mid-slope and those inferred for the Kamilonisi Basin as well as those from the Heraklion Basin (DSDP Site 378 [*Hsü et al.,* 1978]) are almost the same. These data show mean MTD drape thicknesses of 15 m in the mid-slope, which corresponds to a landslide age of about 192 ka B.P. (range of uncertainty when using min.

and max. accumulation rates and a ±2.5 m drape thickness uncertainty according to the resolution of the seismic system: 250 - 147 ka B.P.).

Adopting this concept also for largest identified landslide deposits in the slope toe region, the 15 - 20 m thick drape on top of the youngest MTD in the Kamilonisi Basin implies an age-range of 192 - 250 ka B.P. (range of uncertainty: 320 - 147 ka B.P.). Given an almost equal spacing of the MTD layers in seismic data (Fig. 3) and using thicknesses of only well-stratified background sediment layers in between the individual Kamilonisi Basin MTDs, their recurrence times are back-calculated to approximately 250 ka (range of uncertainty: 200 - 320 ka).

We further can determine recurrence times of minor sediment dislocations identified in core data by thin event layers. Represented by 0.5 to 4 events per meter core length, these smallest identified mass movement events occur in 25 ka to 3 ka frequencies, respectively.

7.1.4.3. Geotechnical tests

Physical and mechanical sediment properties were measured regularly along all six cores of both study sites. MSCL bulk densities range in between 1.7 - 2.0 g cm^{-3}. Undrained shear strength (*Su*) is found to be more variable, with 10 - 15 kPa close to the seafloor and a steady increase with depth to 160 kPa at the maximum terminal depth of 4.5 mbsf (Fig. 6A). According to the SANSHEP approach, *Ladd et al.* [1977] propose a normal consolidation state for *Su*-vs.-overburden pressure-ratios of 0.1 - 0.4. Calculated values of these values for our core data show 0.48 - 1.4 and indicate an apparent sediment over-consolidation [e.g., *Sultan et al.*, 2004]. Elevated calcite concentrations of 40 - 55 Vol.-% were monitored for the upper two core meters, which may indicate cementation processes that increase shear strength. However, a minimum *Su*-vs.-depth-correlation for the sediment succession is given by a gradient about 5 kPa m^{-1} while a maximum trend is assumed to approximately 8.75 kPa m^{-1} (Fig. 6A).

When compared to the review paper on shear strengths-vs.-depths trends in ODP (Ocean Drilling Program) cores, the minimum gradient obtained here is much higher than the average 1

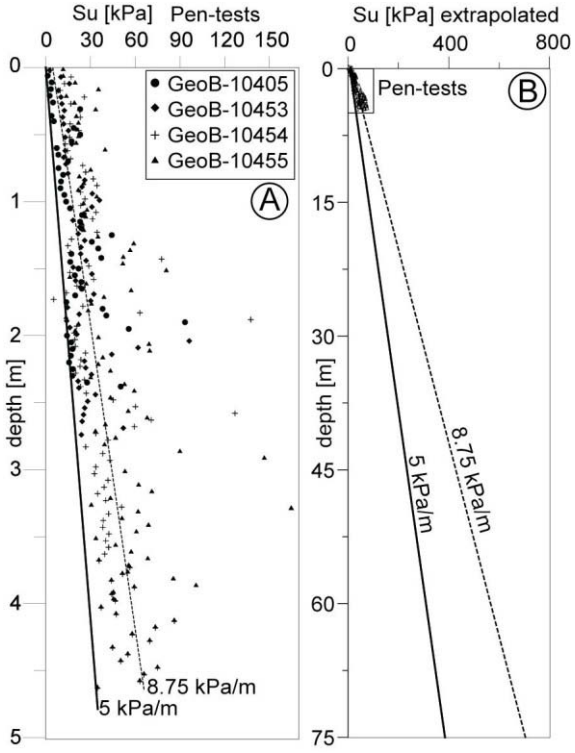

Fig. 6 A: *Results from Wykeham-Farrance cone penetrometer measurements on undrained shear strengths along sediment cores GeoB-10405, -53, -54, and -55 in up to ~ 4.6 mbsf. The minimum Su-vs.-depth-gradient (~5 kPa* m^{-1}*) is marked as solid line, the 'best-fit' gradient (~8.75 kPa* m^{-1}*) as dotted line;* ***B:*** *5 and 8.75 kPa* m^{-1} *Su-vs.-depth-gradients obtain-ed from the PEN (falling cone penetrometer) tests extrapolated to the slide plane depths of 60 and 75 mbsf observed for mid-slope landslides.*

kPa m^{-1} for deeper drillholes, but also suggests a linear increase of *Su* with depth [*Bartetzko and Kopf*, 2007]. Again, the superficial 'apparent' over-consolidation processes (see data in e.g. *Sultan et al.,* 2000) and calcareous cements may serve as an explanation. Accordingly, our *Su*-vs.-depth-model does not account for maximum peaks of measured *Su*-values (i.e., all values above the *Su*-vs.-depth-gradient of > 8.75 kPa m^{-1}), as they may derive from an occasionally occurrence of carbonaceous clasts and nodules in cores influencing the measurements. However, the relatively high trends given by core data are also supported by *Su* derived from *in situ* CPT deployments using a shallow-water probe in a landslide complex in the upper slope [*Kopf et al.,* 2007].

7.1.5. Discussion

Given the observed low frequency of larger landslide events (250 ± 70 ka) in the investigated part of the northern Cretan margin that strongly challenges our expectation regarding landslide distribution in space and time in this tectonically-active setting, we here first discuss conceptually slope instability scenarios which may explain both a low recurrence time of slope failure and the trigger required to drive this slope towards failure. In the second part, we use quantitative slope stability calculations to investigate the impact that large earthquake may have in controlling submarine landslide initiation and how this relates to the seismicity and tectonic evolution of the northeastern margin.

7.1.5.1. Preconditioning factor vs. trigger mechanism

Large failures of the highly shear-resistant Cretan slope sediments either requires a relatively large trigger or unfavourable preconditioning factors that may influence slope stability conditions over geological time-scales. As for the latter, an obvious possible control on the reconstructed 250-ka-frequency of major events identified in the Kamilonisi Basin could be related to cyclic climatic changes in the Pleistocene. Sea level change, variation in the hinterland sediment delivery due to changes in the precipitation pattern or changes in ocean circulation on these timescales can influences the hydrological regime and changes in sedimentation rates charging and/and or re-charging the slope and thus exerting variations in effective stress conditions through time. However, as outlined above and documented in more detail by *Strozyk et al.* [2010], the NE Cretan margin was retrogressively eroded during progressive tectonically-controlled steepening. Due to progressive steepening of the presently eroded lower slope, stability there becomes more critical with time and hence does not allow for significant sediment re-charging due to its overcritical steepness. Consequently, once generated scar areas will not be sufficiently recharged, but slope failure propagates upslope. Additionally, the post-Messinian sediment column in seismic data is generally characterized as smooth, regularly accumulated sedimentary section [*Mascle and Martin*, 1990; *Strozyk et al*., 2010]. No evidence for significant changes in the sedimentation pattern and rates are documented on 100ka – climatically-forced time scales. Furthermore, we deduce that the 250-ka-cyclicity of at least the large Kamilonisi Basin major MTDs does not correlated to first-order Pleistocene sealevel fluctuations, which generally occur in different frequencies [e.g., *Zachos et al.,* 2001; *Ridente et al*., 2009]. Shelf-edge sediment failures and related gravity-driven processes have already been attributed to e.g. fall in sea level (see summary by *Shanmugam* [2009] and *Lee et al.* [2007]). However, failed slope sites at the NE Cretan slope occur in >500 m water depth and the smooth, regularly

accumulated, post-Messinian sediment column is not expected being eminently prone to eustatic sealevel changes. Hence, compared to typically glacial affected passive margin slope failure records [e.g., *Masson et al*., 2006; *Lee et al.,* 2007], NE Cretan mass failure do not force a first-order correlation to the frequency and environmental impacts associated to climate cycles. However, it cannot conclusively be excluded that they may play a role as lower-order slope failure pre-conditioning factors (e.g., *Locat and Lee*, [2002]).

The progressive tectonic steepening, in contrast, appears to impart a more significant control on critical slope condition over longer time scale, but by itself also cannot explain the ~ 250 +/- 70 ka recurrence interval of large MTD in the Kamilonisi basin. We thus hypothesis that large earthquakes are a likely mechanism providing the final 'kick' destabilizing the high shear strength of Cretan slope strata (i.e. > 5 kPa m^{-1}) and initiating large landslides in place. However, we observe that the high frequency of regional seismic shakings, including also large magnitude earthquakes in the vicinity of the study site along the Hellenic Arc, do not reflect the much lower landslide recurrence rate. Therefore it is hypothesized that with progressive steepening of the slope through time, the critical seismic trigger is being reduced, until an earthquake is sufficient to trigger large landslide. Once eroded, the sediment column upslope of the failure scar overlying generally less inclined slopes becomes the source of the next landslide (i.e. retrogressive slope failures). At the beginning of the next cycle, the slope generally is very stable and only may become unstable if first tectonic subsidence of the basin and uplift of Crete further steepens the critical slope segment and then a corresponding large nearby earthquake my produce ground shaking intensities high enough to trigger failure. As earthquakes up to a moderate magnitude cause reactivation as well as small-scaled sediment sliding along the numerous normal faults, these processes may counteract this cyclic steepening of the slope, and hence help to avoid a higher frequency of critical slope steepening and thus large-scale mass wasting. With time this compensation does not work and the critical earthquake intensity for triggering of larger landslides will decrease with the progressively steepening to a critical slope segment.

In order to quantitatively test this hypothesis and to get control on how local seismic loadings may provide the critical shear stresses impacting slope sediment instability in place, we utilize the well-constraint mid-slope mass-transport complex [*Strozyk et al*., 2010] as representative case study site to back-analyze sediment stability and instability under static and pseudo-static seismic loading conditions, on apparently stable, critical and over-critically inclined slopes.

Geometrical proportions of stable, post-Messinian slope sediment cover [*Mascle and Martin*, 1990; *Strozyk et al*., 2010] as well as of the eroded areas of these mid-slope failures (see Fig. 4B) are measured from pre-failure sediment thicknesses reconstructions above interpreted slide planes (dashed line Fig. 4B;). The measured slope gradients and pre-failure sediment thicknesses are used as a bracket for the assessment (see also Table 1). We adopt the measured gradients (i.e. 3° and 5°) and pre-failure thicknesses (i.e. 75 m and 60 m) for both the intact slope apron and failed slope portions, respectively (Figs. 4B; 7A; Table 1). For both scenarios of failure conditions, a uniform sediment column of the hemipelagic, mud-rich sediment is assumed with a mean bulk density of 1.90 g cm^{-3} and *Su*-vs.-depth-correlation in-between 5.0 and 8.75 kPa m^{-1} (see Fig. 6B; see also Table 1).

Table 1) Geometrical slope proportions and according geotechnical sediment characterizations as incorporated to slope stability analysis (α = gradient; σ_n' = effective normal stress; T = static shear stress). Note that all values address the critical depths ('c.d.' [1]) of 60 m and 75 m.

	α	c.d. [1]	σ_n' [kPa]	*T* (kPa)	*Su*-vs.-depth gradient 5 kPa m^{-1}	*Su*-vs.-depth gradient 8.75 kPa m^{-1}
Failed sites	5°	60 m	512.25	44.81	280 kPa in c.d.	510 kPa in c.d.
Stable sites	3°	75 m	643.45	33.72.	347.5 kPa in c.d.	633.75 kPa in c.d.

1 depth in between the interpreted slide plane reflector and the reconstructed pre-failure seafloor

7.1.5.2 Slope stability under static conditions

From slope stability analysis (SSA) under static conditions, which incorporates the *Su* against shear stress from inclination of the sediment load (k = 0, see equation 1), the resulting Factor of Safety (*FS*) exceeds a value of 4 in all cases (Fig. 7B) and suggests a stable slope (given FS ≤ 1 represents slope failure). Additional tests using higher slope gradients up to 10° and sediment thickness-variations of ± 25 m result in FS ≥ 2.5, and thus also favour a stable slope. Consequently, the measured slope gradients and sediment load thicknesses cannot explain the observed slope failures under static conditions, further providing independent evidence that sediment charging is not the first-order control mechanism (see above) but that an additional, large trigger mechanism is required.

7.1.5.3 Slope stability under pseudo-static seismic loading conditions

To get control on how PGAs may impact on slope instability scenarios, pseudo-static accelerations were applied for models of the total range of possible Su-vs.-depth-correlations. Results back-analyzing critical earthquake intensities that may have triggered instabilities along the 5°-inclined slope show that pseudo-static acceleration in the order of 24 %g for the minimum (5 kPa m^{-1}) and 42 %g and the maximum (8.75 kPa m^{-1}) Su-vs.-depth-trends may be sufficient for failure initiation. Consequently, PGAs corrected *sensu Seed and Idriss* [1971] result in between approximately 37 %g and >64 %g providing shear stresses sufficient for driving a 5°-inclined slope portion towards failure (Fig. 7B). Critical PGAs for destabilizing the 3°-inclined slope portion that remained stable are in the order of ~40 % g and >66 % g indicating an upper threshold for maximum PGAs that occurred in the studied area. Although derived critical PGAs that triggered the landslide are very high, and certainly only can occur during sever large earthquakes in the close vicinity of the study area, however, such PGAs from local seismic shakings, as they may be extrapolated from the EPPO catalogue data (see section 7.1.2) are expected to have occurred more frequently than detected landslides in place. This may suggest that our analyzed case study along the mid-slope area today represents a snap shot in time where long-term tectonically-controlled slope steepening already has decreased slope stability conditions through time. Additionally, this can also be explained by additional consolidation and strengthening of the sediment during earthquake shaking with PGAs below the critical threshold for landslide initiation. This may rather strengthen the sediment column through development of

excess pore-water pressures and subsequent drainage as well as densification during the intervening periods (i.e. seismic strengthening [*Locat and Lee*, 2002; *Lee et al.,* 2007]). On 250-ka-timescales slope sediment thus may become more stable through time. Linking mechanical sediment attributes, resulting high trigger requirements and the long-term tectonic development of the NE Cretan margin, we interpret that the frequency of larger landslides compared to the recurrence rate of local seismic shakings can be limited by a combination of (i) the shear-resistant nature (likely increasing with time due to seismic strengthening) of sediment cover which appears to be stable on slopes with low inclination angles (<5°); (ii) the requirement of high PGAs capable of initiating failure along critically inclined slopes (≥5°) that are seen to only occur infrequently from large earthquakes at low epicentral distances (i.e., ~40-60 km epicentral distances from Hellenic Arc earthquake clusters to the failed NE Cretan margin sites); (iii) the variances in tectonic movement and thus further steepening of these explicit slope portions that results in a long-term reduction of the critical PGA values needed to initiate failure, and (iii) the fact that once released landslides can also deposit at the critical slope portion, as the slope angle critical for larger sediment failure appears to also provides conditions for an accumulation of MTDs [*Strozyk et al.,* 2010]. Hence, further steepening of the critical slope portions to > 5° may be required to cause the final transport of sediment masses down the slope into Kamilonisi basin.

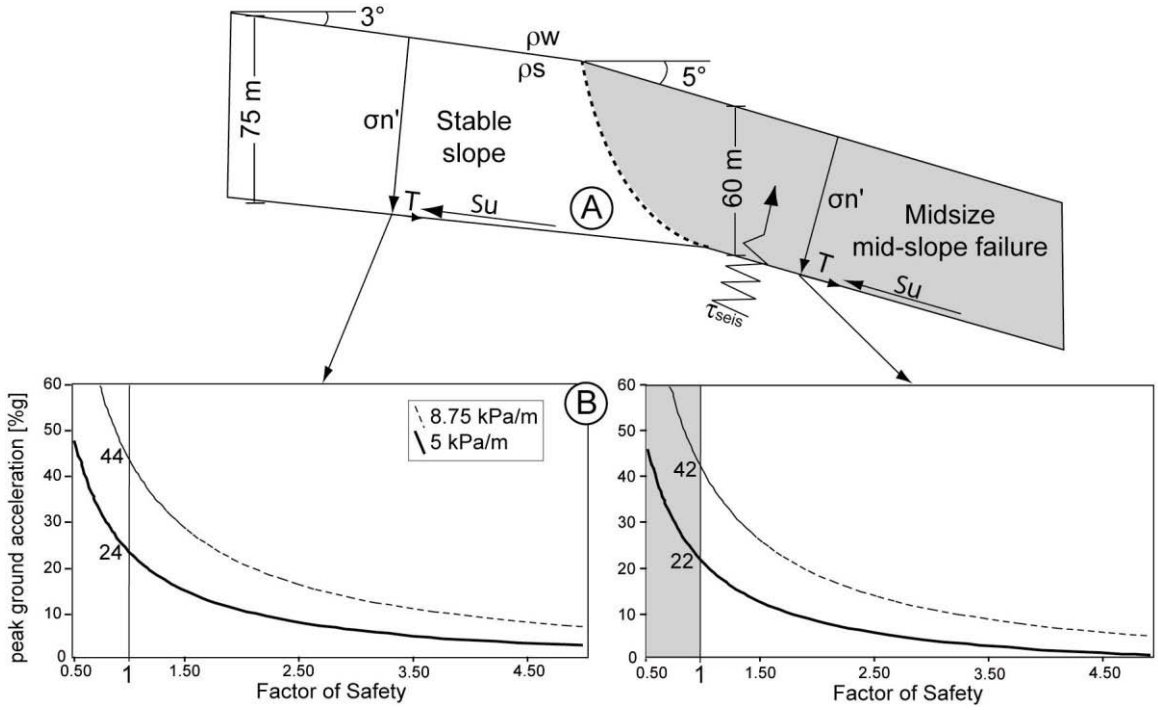

Fig. 7 ***A:*** *Sketch of geometrical setups and acting forces (see Table 1) as pre-defined for failed and already stable sediment portions in the mid-slope, and used for slope stability analyses;* ***B****: results of slope stability analyses for the intact slope apron (left chart) and midsize landslides (right chart), incorporating the Su-vs.-depth-gradients 5.0 and 8.75 kPa* m^{-1} *as a function of the Factor of Safety (FS) against peak ground acceleration. The intersection points of the two resulting trends with FS = 1 = failure (grey shaded area) indicates PGAs that are required for sediment destabilization depending on the shear strength.*

7.1.6. Conclusions and general implications

We have shown that the frequency of landslides at the NE Cretan margin, as implied by age models of sequenced major MTDs in the slope's toe region, is low compared to seismicity in this active margin environment. We deduce that this low frequency is controlled by active armouring of the cohesive slope strata on one hand and long-term variations in tectonic movement controlling sufficiency of impacts from regional seismicity on the other hand. Thereby, high shear strength of the sediment and critical slope steepening are suggested preparing a pre-conditioning setup strongly limiting the impacts of seismicity driving this slope towards larger failure. The long-term dynamics of such an active margin slope may further provide a setting where the sequencing of MTDs in the deep Kamilonisi basin may not be in-line with sediment failure in the upper slope region, because the Cretan margin situation may imply that there can also be a temporal delay due to first MTD accumulation at upper slope portions and their later reactivation and transport down the slope.

When comparing the low recurrence rate of the large PGA-triggered landslides to other areas, similar conclusions were drawn from studies investigating submarine landslides along active continental margins [e.g., McAdoo et al., 2000; Camerlenghi et al., 2009]. At accretionary and erosive subduction margins forearc slopes also show large infrequent landslides because of tectonically exhumed sediments that tend to be over-consolidated, therefore bearing a high shear resistance and requiring large earthquakes as triggers [McAdoo et al., 2004; Camerlenghi et al., 2009]. Additionally, in such forearc settings, tectonic processes and fault activity controlling slope steeping on the frontal side of anticline structures in the hanging wall block of thrust faults also exert key pre-condition setups for slope failure initiation; Hence, they control spatial and temporal distribution of submarine landslide that thus relates to the tectonic cycles of the margin (e.g., Yamada et al., 2010; Strasser et al., 2009). Similarly, the low repetition time of critical conditions for large landslides in the southern Hellenic forearc basin shows analogies to the „cohesive slope failure"-model sensu McAdoo et al. [2000], while the sediment history of this forearc basin flank cover as well as the mechanism of progressive slope steepening (here a consequence of the subsiding forearc basin and the uplift of the island of Crete) impacting on slope geometry differs from the accretionary margin examples. Yet, our study shows that, conceptually, occurrence of landslides may be governed by similar pre-conditioning setups in which the critical seismic intensity to trigger failure is being reduced with increasing tectonically-controlled steepening of the slope through time, until an earthquake is sufficient to trigger large landslide. Then, at the beginning of the next cycle, the slope initially is very stable and only may become unstable if ongoing tectonic movements further steepen the critical slope segment and corresponding large seismic tremor produces ground shaking intensities large enough to trigger failure. With time, the critical earthquake intensity for triggering landslides again will decrease along with progressively steepening of the critical slope segment.

We conclude that the causal relationship of earthquake activity and infrequent large-scale slope collapses in such active margin settings can strongly be governed by (i) an armoured slope sediment cover and (ii) temporal variances in tectonic movements providing only infrequently a critical steepening of some parts of the slope. Overall, our findings imply that low frequencies of landslides in active margin settings are not in conflict with high plate boundary seismicity with short seismic cycles, because additional transient shear stresses from seismic loadings are only sufficient to trigger major collapses of a generally shear-resistant "cohesive" slope, if long-term tectonic movements provide a critical steepening. Further, permanent taper adjustment and

dynamic compaction from background seismicity may favor the sediment's large resistance to seismic loadings or other potential triggers over longer periods of time, and thus explaining the relatively scarce occurrence of large submarine landslides in such tectonically-active environments .

Acknowledgements

We thank the scientific party and the ship crew of P-336 for faithful and detailed recording of data. We thank all involved scientists at the Hellenic Centre for Marine Research, Greece, for their scientific input and discussions as well as support of the P-336 cruise, and the MARUM for scientific support and all involved scientists and members for fruitful discussions and outcomes, especially Dr. Barbara Donner for microfossil species identification. We further would like to thank reviewers Homa J. Lee and Brian G. McAdoo for their fruitful comments that highly improved the quality our paper. This publication is funded through the DFG-Research Centre/ Excellence Cluster „The Ocean in the Earth System".

References

Aksu, A.E., D. Yasar, and P. J. Mudie (1995), Paleoclimatic and paleooceanographic conditions leading to development of sapropel layer S1 in the Aegean Sea, Palaeogeogr. Palaeoclimat. Palaeoecol., 116, 71-101.

Ambraseys, N. N. (2001), Far-field effects of eastern Mediterranean earthquakes in lower Egypt, J. Seismol., 5, 263 – 268, doi:10.1023/A:1011476718680.

Angelier, J., N. Lyberis, X. Le Pichon, E. Barrier, and P. Huchon (1982), The Tectonic development of the Hellenic arc and the sea of Crete: a synthesis, Tectonophysics, 86, 159-196.

Bardet, J.-P., C. E. Synolakis, H. L. Davies, F. Imamura, and E. A. Okal (2003), Landslide Tsunamis: Recent Findings and Research Directions, Pure appl. geophys., 160, 1793–1809.

Bartetzko, A., and A. J. Kopf (2007), The relationship of undrained shear strength and porosity with depth in shallow (<50 m) marine sediments, Sed. Geol., 196, 235-249.

Biscontin, G., and J. M. Pestana (2006), Factors affecting seismic response of submarine slopes, Natural Hazards and Earth System Sciences, 6, 97-107.

Bonneau, M. (1984), Correlation of the Hellenide nappes in the south-east Aegean and their tectonic reconstruction, Geol. Soc., London, Special Publications17, 517-527.

Camerlenghi, A., R. Urgeles, and L. Fantoni (2010), A database on submarine landslides of the Mediterranean Sea. In: Submarine Mass Movements and Their Consequences IV, edited by D.C. Mosher, C. Shipp, L. Moscardelli, J. Chaytor, C. Baxter, H. Lee, and R. Urgeles, Fourth International Symposium on Submarine mass movements and their consequences, November 8-11, 2009, Austin, Texas, Advances in Natural and Technological Hazards Research, in press.

Canals, M., G. Lastras, R. Urgeles, J. L. Casamor, J. Miernert, A. Cattaneo, M. De Batist, H. Haflidason, Y. Imbo, J. S. Laberg, J. Locat, D. Long, O. Longva, D. G. Masson, N. Sultan, F. Trincardi, and P. Bryn (2004), Slope failure dynamics and impacts from seafloor and shallow sub-seafloor geophysical data: case studies from the COSTA project, Mar. Geol., 213, 9-72.

Chamot-Rooke, N., A. Rabaute, and C. Kreemer (2005), Western Mediterranean Ridge mud belt correlates with active shear strain at the prismbackstop geological contact, Geology, 33, 861 – 864, doi:10.1130/G21469.1.

Chronis, G., V. Lykousis, C. Anagnostus, A. Karageorgis, S. Stavrakakis, and S. Poulus (2000), Sedimentological processes in the southern margin of the Crete Sea (NE Mediterranean), Progr. Oceanogr., 46, 143-160.

Cochonat, P., J. P. Cadet, S. J. Lallemant, S. Mazzotti, H. Nouze, C. Fouchet, and J. P. Foucher (2002), Slope instabilities and gravity processes in fluid migration and tectonically active environment in the eastern Nankai accretionary wedge (KAIKO-Tokai'96 cruise), Mar. Geol., 187, 193-202.

Engdahl, E.R., and A. Villaseñor (2002), Global Seismicity: 1900–1999. In: Lee, W.H.K., Kanamori, H., Jennings, P.C., Kisslinger, C. (Eds.), International Handbook of Earthquake and Engineering Seismology, Part A, Ch. 41 Academic Press, San Diego, 665–690.

EPPO (Earthquake Planning and Projection Organization of Greece) (1992), Appendix to the new building code of Greece.

Ganas, A., and T. Parsons (2009), Three-dimensional model of Hellenic Arc deformation and origin of the Cretan uplift, J. Geophys. Res., 114, B06404, doi:10.1029/2008JB005599

Geraga, M., S. Tsaila-Monopolis, C. Ioakim, G. Papatheodorou, and G. Ferentinos (2005), Short-term climate changes in the southern Aegean Sea over the last 48,000 years, Palaeogeol., Palaeoclim., Palaeoeco., 220, 311-332.

Giresse, P., R. Buscail, and B. Charriere (2003), Late Holocene multisource material input into the Aegean Sea: depositional and post-depositional processes, Oceanol. Acta, 26, 657-672.

Goldfinger, C., C. H. Nelson, and J. E. Johnson (2003), Holocene earthquake records from the Cascadia subduction zone and northern San Andreas Fault on precise dating of offshore turbidites, Annu. Rev. Earth Planet. Sci., 31, 555-577.

Guidoboni, E., and A. Comastri (1997), The large earthquake of 8 August 1303 in Crete: Seismic scenario and tsunami in the Mediterranean area, J. Seismol., 1, 55– 72, doi:10.1023/A:1009737632542.

Hamouda, A. Z. (2006), Seismic hazard of the eastern Mediterranean, Acta Geophys., 54, 165–176, doi:10.2478/s11600-006-0013-z.

Hampton, M., H. J. Lee, and J. Locat (1996), Submarine Landslides, Rev. Geophys., 34, 33-59.

Heinrichs, H., and A. G. Hermann (1990), Praktikum der Analytischen Geochemie, 357-361. Springer, Heidelberg.

Hutton, E. W. H., and J. P. M. Syvistski (2003), Advances in the numerical modeling of sediment failure during the development of a continental margin, Mar. Geol., 203, 367-380.

Hsü, K. J., L. Montadert, D. Bernouilli, G. Bizon, M. Cita, A. Erickson, F. Fabricius, R. E. Garrison, R. B. Kido, F. Mellieres, C. Muller, and R. C. Wright (1978), Site 378: Cretan Basin. Init. Rep. Deep-Sea Drill. Proj., 42, 321-257, doi:10.2973/dsdp.proc.42-1.108.1978.

Kopf, A., J. Mascle, and D. Klaeschen (2003), The Mediterranean Ridge: A mass balance across the fastest growing accretionary complex on Earth, J. Geophys. Res., 108, 23-72, doi:10.1029/2001JB000473.2003

Kopf, A., T. Alves, B. Heesamnn, M. Irving, N. E. Kaul, I. Kock, S. Krastel, M. Reichelt, R. Schäfer, S. Stegmann, M. Strasser, and M. Thölen (2006), Report and preliminary results of Poseidon cruise P336: CRESTS – Cretan Sea Tectonics and Sedimentation, Heraklion 28.04.-17.05.2006, Berichte, Fachbereich Geowissenschaften, Universität Bremen, 253.

Kopf, A., S. Stegmann, S. Krastel, A. Förster, M. Strasser, and M. Irving (2007), Marine deep-water Free-fall CPT Measurements for landslide characterisation off Crete, Greece (Eastern Mediterranean Sea) - PART 2: Initial data from the western Cretan Sea. In: Lykousis, V., Sakellariou, D., Locat, J. (eds.), Submarine Mass movements and their consequences, Advances in Natural and Technological Hazards Series, Springer, 199-208.

Ladd, C. C., R. Foott, K. Ishihara, F. Schlosser, and H. G. Poulos (1977), Stress-deformation and strength characteristics, State of the art report, Proceedings, 9th International Conference on Soil Mechanics and Foundation Engineering, 2, 421 -494.

Lee, H. J., J. Locat, P. Desgagnes, J. D. Parsons, B. G. McAdoo, D. L. Orange, P. Puig, F. L. Wong, P. Dartnell, and E. Boulanger (2007), Submarine mass movements on continental margins. In: Nittrouer, C.A., Austin, J.A., Field, M.E., Kravitz, J.H., Syvitki, J.P.M., Wiberg, P.L. (eds.), Continental Margin Sedimentation, Blackwell Publishing, UK, 213-274.

Locat, J., and H. J., Lee (2002), Submarine landslides: advances and challenges. Can. Geotech. J., 39, 193-212.

Locat, J., and J. Mienert (2003), Submarine mass movements and their consequences, Advances in natural and technological hazards research 19, Kluwer, Dordrecht, 540 pp.

Lykousis, V., C. Anagnostou, G. Anastasakis, P. Pavlakis, G. Roussakis, and M. Alexandri (1995), Quaternary sedimentary history and neotectonic evolution of the eastern part of Central Aegean Sea, Mar. Geol., 186, 281-298.

Manakou, M. V., and T. M. Tsapanos (2000), Seismicity and seismic hazard parameters evaluation in the island of Crete and the surrounding area inferred from mixed data files, Tectonophysics, 321, 157–178.

Mascle, J., and L. Martin (1990), Shallow structure and recent evolution of the Aegean Sea: a synthesis based on continuous reflection profiles, Mar. Geol., 94, 271–299.

Masson, D. G., C. B. Harbitz, R. B. Wynn, G. Pedersen, and F. Løvholt (2006), Submarine landslides: processes, triggers and hazard prediction, Phil. Trans. R. Soc. A, 364, 2009–2039.

McAdoo, B. G., L. F. Pratson, and D. L. Orange (2000), Submarine landslide geomorphology, US continental slope, Mar. Geol., 169, 103-136.

McAdoo B. G., M. K. Capone, and J. Minder (2004), Seafloor geomorphology of convergent margins: Implications for Cascadia seismic hazard, Tectonics, 23, TC6008, doi:10.1029/2003TC001570.

McAdoo, B. G., and P. Watts (2004), Tsunami hazard from submarine landslides on the Oregon continental slope, Mar. Geol., 203, 235-245.

Meier, T., M. Rische, B. Endrun, A. Vafidis, and H.-P. Harjes (2004), Seismicity of the Hellenic subduction zone in the area of western and central Crete observed by temporary local seismic networks, Tectonophysics, 383, 149-169.

Meulenkamp, J. E., M. J. R. Wortel, W. A. van Wamel, W. Spakman, and E. Hoogerduyn Strating (1988), On the Hellenic subduction zone and the geodynamic evolution of Crete since the late Middle Miocene, Tectonophysics, 146, 203-215.

Moratto, L., B. Orlecka-Sikora, G. Costa, P. Suhadolc, C. Papaioannou, and C. B. Papazachos (200), A deterministic seismic hazard analysis for shallow earthquakes in Greece, Tectonophysics, 442, 66–82.

Morgenstern, N. R., and V. E. Price (1965), Analysis of stability of general slip surfaces, Geotechnique, 15, 79-93.

O'Grady, D. B. (2001), Sedimentary Geomorphology of siliciclastic continental slopes, Ph.D. thesis Faculty of the Graduate School of the University of Colorado.

Pichler, H., and W. Friedrich (1976), Radiocarbon-dates of Santorini Volcanics, Nature, 262, 373-374.

Polonia, A., A. Camerlenghi, F. Davey, and F. Storti (2002), Accretion, structural style and syn-contractional sedimentation in the Eastern Mediterranean Sea, Mar. Geol., 186, 127-144.

Ridente, D., F. Trincardi, A. Piva, and A. Asioli (2009), The combined effect of sea level and supply during Milankovitch cyclicity: Evidence from shallow-marine Î´18O records and sequence architecture (Adriatic margin), Geology, 37, 1003-1006.

Seed, H. B., and I. M. Idriss (1971), Simplified procedure for evaluating soil liquefaction potential. Journal of the Soil Mechanics and Foundations division, Proc. Am. Soc. Civil Eng. 97 1249-1273.

Seed, H.B. (1979), Considerations in earthquake-resistant design of earth androck-fill dams, Géotechniques, 29, 215-263.

Shanmugam, G. (2009), Slides, Slumps, Debris Flows, and Turbidity Currents, Encyclopedia of Ocean Sciences, 4509-4529, Elsevier.

Stegmann S., M. Strasser, F. Anselmetti, and A. Kopf (2007), Geotechnical in situ characterization of subaquatic slopes: The role of pore pressure transients versus frictional strength in landslide initiation, Geophys. Res. Lett., 34, L07607, doi:10.1029/2006GL029122.

Stigall, J., and B. Dugan (2010), Overpressure and earthquake initiated slope failure in the Ursa region, northern Gulf of Mexico, J. Geophys. Res., doi:10.1029/2009JB006848, in press.

Stiros, S. C. (2001), The AD 365 Crete earthquake and possible seismic clustering during the fourth to sixth centuries AD in the eastern Mediterranean: A review of historical and archaeological data, J. Struct. Geol., 23, 545– 562, doi:10.1016/S0191-8141(00)00118-8.

Strasser, M., G. F. Moore, G. Kimura, Y. Kitamura, A. J. Kopf, S. Lallemant, J.-O. Park, E. L. Screaton, X. Su, M. B. Underwood, and X. Zhao (2009), Origin and Evolution of a spaly fault in the Nankai accretionary prism, Nature Geoscience, 2, 648-652.

Strasser, M., S. Stegmann, F. Bussmann, F. S. Anselmetti, B. Rick, and A. Kopf (2007), Quantifying subaqueous slope stability during seismic shaking: Lake Lucerne, Central Switzerland, as model for ocean margins, Mar. Geol., 240, 77-97.

Strasser, M., F. S. Anselmetti, D. Fäh, D. Giardini, and M. Schnellmann (2006), Magnitudes and source areas of large prehistoric northern Alpine earthquakes revealed by slope failures in lakes, Geology, 34, 1005-1008.

Strozyk, F., M. Strasser, S. Krastel, M. Meyer, and K. Huhn (2010), Reconstruction of retreating mass wasting in response to progressive slope steepening of the northeastern Cretan margin, eastern Mediterranean, Mar. Geol. (in press), doi:10.1016/j.margeo.2010.01.008.

Strozyk, F., K. Huhn, M. Strasser, S. Krastel, I. Kock, and A. Kopf (2009), New evidence for massive gravitational mass-transport deposits in the southern Cretan Sea, eastern Mediterranean, Mar. Geol., 263, 97–107.

Sultan, N., P. Cochonat, M. Canals, A. Cattaneo, B. Dennielou, H. Halifladson, J. S. Laberg, D. Long, J. Mienert, and F. Trincardi (2004), Triggering mechanisms of slope instability processes and sediment failure on continental margins: a geotechnical approach, Mar. Geol., 213, 291-321.

Sultan N., A. Cattaneo, R. Urgeles, H. J. Lee, J. Locat, F. Trincardi, S. Berne, M. Canals, and S. Lafuerza (2008), A geomechanical approach for the genesis of sediment undulations on the Adriatic shelf, Geochem. Geophys. Geosyst., 9, Q04R03, doi:10.1029/2007GC001822.

Sultan, N., P. Cochonat, B. Dennielou, J. F. Bourillet, B. Savoye, and J.L. Colliat (2000), Surconsolidation apparente et pression osmotique dans un sédiment marin, Comptes Rendus de l'Académie des Sciences Paris - Earth and Planetary Science, 331, 379-386.

ten Brink, U., H. J. Lee, E. L. Geist, and D. Twitchell (2009), Assessment of tsunami hazard to the U.S. East Coast using relationships between submarine landslides and earthquakes, Mar. Geol.,264, 65-73, http://dx.doi.org/ 10.1016/j.margeo.2008.05.011.

Urgeles, R., D. Leynaud, G. Lastras, M. Canals, and J. Mienert (2006) Back-analysis and failure mechanisms of a large submarine slide on the ebro slope, NW Mediterranean, Mar. Geol. 226, 185-206.

Wood, D.M. (1985), Some fall-cone tests, Géotechnique, 35, 64-68.

Yamada, Y., Y. Yamashita, and Y. Yamamoto (2010), Submarine landslides at subduction margins: Insights from physical models, Tectonophysics, 484, 156-167, doi:10.1016/j.tecto.2009.09.007 .

Zachos, J. C., M. Pagani, L. Sloan, E. Thomas, and K. Billups (2001), Trends, Rhythms, and Aberrations of Global Climate 65 Ma to Present, Science, 27, 686-693.

7.2 Marine deep-water Free-fall CPT measurements for landslide characterisation off Crete, Greece (Eastern Mediterranean Sea) PART 2: initial data from the western Cretan Sea

A. Kopf[1], S. Stegmann[1], S. Krastel[1], **A. Förster[1]**, M. Strasser[2], M. Irving[3]

Published in *Lykousis, V., Sakellariou, D. and Locat, J. (2007.), Submarine Mass movements and their consequences III. Advances in Natural and Technological Hazards Series 27, Springer, pp. 199-208.*

Abstract

Pore pressure and shear strength are major controlling parameters for slope stability, which can be measured *in situ* using CPT (cone penetration testing) instruments. This paper presents results from initial tests with two free-fall CPT probes deployed in the neotectonically active submarine slope of northern Crete, Greece. Research expedition P336 investigated landslide-prone areas in the Cretan Sea using multibeam swathmapping, seismic reflection profiling, *in situ* CPT measurements, and gravity coring. Several large landslide complexes at the NE Cretan Margin as well as a small, but steep landslide scarp structure further east were identified on the seismic profiles. CPT devices were deployed in undisturbed slope sediments, across the slide scar, and in the main body of the slide, and remained stuck in the sediment for ~10 minutes to monitor pore pressure dissipation upon insertion. Excess pore pressure after insertion is in a range around 60 kPa in background sediment, and exceeds 80 kPa in the slide deposits. Cone resistance of the slope sediment ranges between 300 kPa and 500 kPa, corresponding to undrained shear strength of up to 40 kPa. The slid sediments (specifically the headwall material with <10 kPa strength) show velocity-weakening behaviour during ring shear experiments, indicating that those sediments are unlikely to show stable creep and instead may fail catastrophically.

KEYWORDS: CPT, LANDSLIDE, SHEAR STRENGTH, PORE PRESSURE

7.2.1 Introduction

Sediment stability at continental margins depends on given different soil mechanical conditions and a variety of trigger mechanisms (e.g. Hampton et al. 1996). This complexity demands a multi-disciplinary research approach, which has been achieved by several studies that combined geophysical, sedimentological and geotechnical methods (e.g. Storegga Landslide [Kvalstad et al. 2005]; Niger Delta [Sultan et al., 2007]). In these studies, the sediment physical properties were assigned a high priority, with shear strength and pore pressure playing a key-role in the assessment of sediment stability. Equally, there are several landslide occurrences north of Crete, an area that is regularly struck by neo-tectonic activity and earthquake tremors (Lykousis et al., 2002). During cruise P336 in April/May 2006 in the Cretan Sea, we studied landslide processes in two areas (here termed D and E). Bathymetric mapping and seismic profiling served to characterise the landslide-prone slopes. Subsequently, *in situ* CPT measurements were made

1 Research Centre Ocean Margins, Bremen University, Leobener Strasse, 28359 Bremen, Germany

2 Institute, ETH Zurich, Universitätstrasse 16, CHN, 8092 Zurich, Switzerland

3 Picker Engineering Program, Smith College, 51 College Lane, Northampton, MA 0106 ,USA

in undisturbed slope sediments as well as in the mass wasting deposits and were complemented by geotechnical measurements on adjacent sediment cores.

7.2.2 Geological background of the Cretan Sea (Eastern Mediterranean)

The Cretan Sea represents the northernmost portion of the forearc region in the Hellenic subduction zone (HSZ) between Africa and Eurasia, which is well recorded over the past ca. 35 million years (Le Pichon and Angelier, 1979). It is sandwiched between the Aegean backarc basin and island arc volcanoes (e.g. Santorini) in the north and the island of Crete, a prominent forearc-high, in the south (Fig. 1a). The island of Crete comprises a stack of nappes of variable lithologies (for details, see e.g. Fassoulas, 1999), parts of which got exhumed some 19 Ma ago and now are extending in both E-W-and N-S-direction. The main extensional phase of the Cretan Sea occurred between the Late Miocene and Pliocene however the Late Pleistocene experienced only minimal extension phenomena (Mascle and Martin, 1990). Tectonic movements still occur today, as indicated by recent seismicity and volcanic activity in the area (McKenzie, 1978).

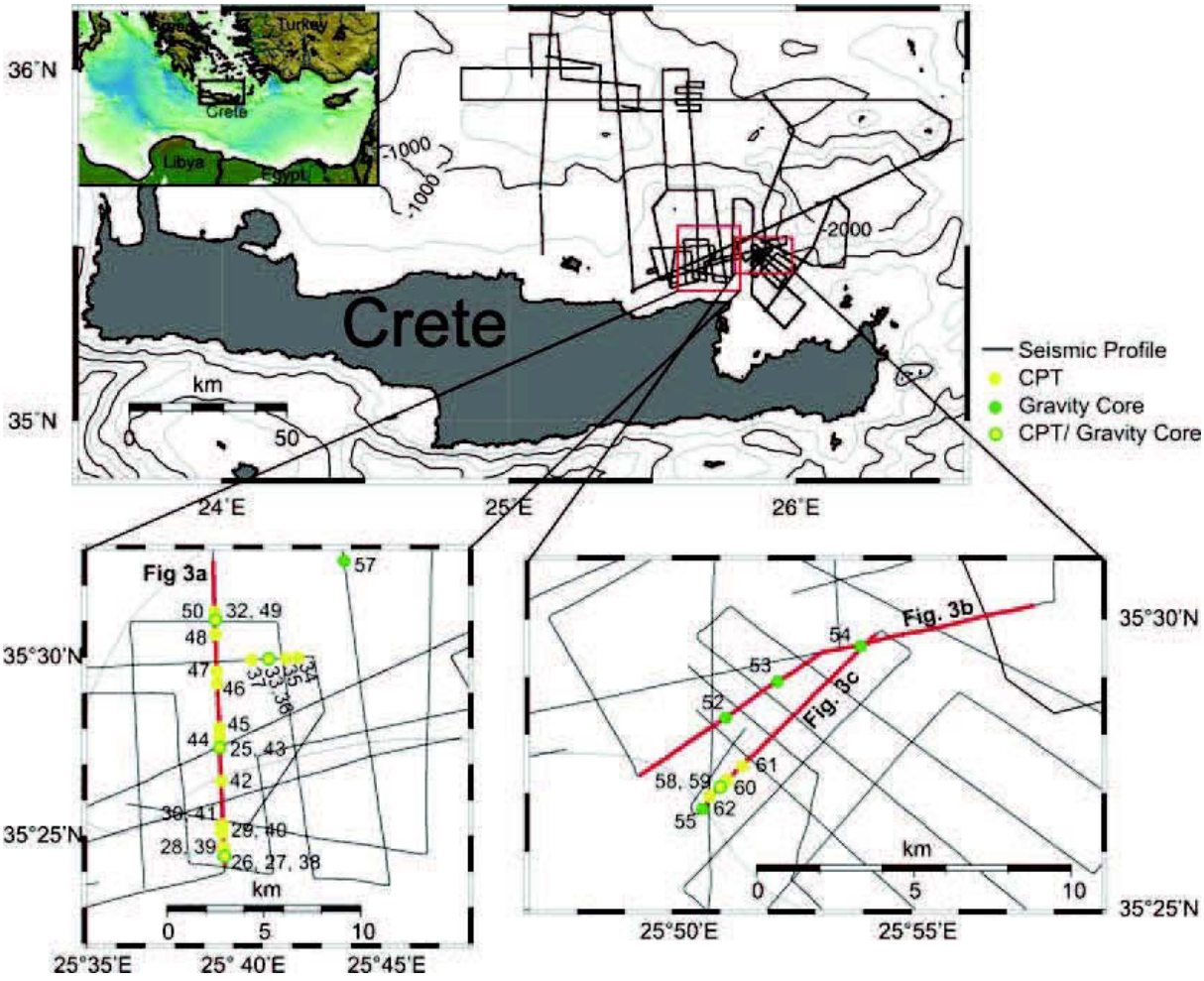

Fig. 1: Map of the complete study area in the Eastern Mediterranean off Crete, Greece (A). Mass wasting deposits at the Cretan Margin are identified in study area D (B) and study area E (C, D). Numbers and lines represent the position of seismic profiles, gravity core stations and CPT locations.

Landslides are one of the most immanent hazards in the Cretan Sea, being triggered by both the

tectonic movements of the Cretan block in the south (e.g. Chronis et al., 2000a, b) and the flank collapse of volcanic islands in the north (e.g. Dominey-Howes et al., 2000). Although the inherent mechanisms and factors governing slope stability and submarine landslides are comprehensively studied, their temporal and spatial variability are poorly understood.

Geomorphologically, the Cretan Basin is an elongated depression, trending E–W; it is bounded to the north by the Cyclades Plateau, a relatively shallow (500 m) complex of islands, and has water depths no larger than 1000 m (with localized, ca. 2500 m deep subbasins; see Kopf et al., 2006). Sediment accumulation processes at the southern margin of the Cretan Basin represent pro-delta deposition in the inner middle shelf, settling from bottom nepheloid layers in the shelf and upper slope, calcareous sediment formation due to settling from suspension, and re-deposition from suspension due to gravity processes and bottom currents (Chronis et al., 2000b). Hemipelagic sediments of the entire Cretan Sea are characterised by four different lithologies, regarded from top to bottom (Giresse et al., 2003):

(i) yellowish brown mud with bioturbation structures

(ii) grey mud mottled and moderate bioturbated with

(iii) brownish or olive black mud with >2% Corg, which represents sapropel S1 (96006400 yrs. BP)

(iv) yellowish, grey clay-rich mud. Sedimentation rates in the Cretan trough are estimated to be 4.3-15 cm/ka (Giresse et al., 2003).

7.2.3. Methodology

Cruise P336 with the RV *Poseidon* focused on slope instability and sedimentation at the northern Cretan Margin (Fig. 1a). A variety of geophysical, sedimentological, and geotechnical methods were applied, of which only a few are relevant for this paper. A detailed report of this cruise is given in Kopf et al. (2006).

7.2.3.1 Geophysical characterisation

Continuous seafloor mapping was routinely carried out with the multibeam echosounder ELAC SEABEAM 1050 in order to identify landslide scars. Seismic data were collected using a 3.5 kHz system and a high-resolution multi-channel system. The multi-channel seismic system consists of a Mini-Generator-Injector Airgun (frequency range 100-500Hz) and a 100-m-long 16 channel streamer. The presented seismic profiles (Fig. 1) are brute stacks generated by summing up the first three channels. The data were filtered with a wide bandpass (55/110-600/800 Hz). The combination of 3.5 kHz and seismic data were the basis for selecting coring and CPT-stations.

7.2.3.2 in situ Measurements

In situ measurements of sediment physical properties were carried out with two free-fall CPT devices. Their design and mode of deployment is described in the first part of this manuscript (see Stegmann and Kopf, this issue).

7.2.3.3 Sediment cores and physical properties

Sediment cores were taken with a 1.6 ton gravity corer. Cores were split and described on board including visual determination of lithological composition, colour and grain size classification. The mineralogy noted was based on a smear slide analysis. Shore-based work included logging of the archive half of each gravity core using a GEOTEK multi-sensor core logger (MSCL) at RCOM Bremen. Measured parameters included P-wave velocity, gamma ray attenuation (bulk density), and magnetic susceptibility. In addition, preliminary sediment shear strength cu was measured on board with a fall cone penetrometer. Based on its defined weight (80.51g) and geometry (30° cone), cu was derived from the penetration depth following Hansbo (1957). The rate-dependent shear behaviour of the disturbed and undisturbed sediments (see Fig. 2 for position of the samples) was measured using a Bromhead ring shear device. The specimen was placed into an annular chamber and loaded incrementally to normal stresses between 0.4 and 16 MPa. For each load increment, the sample was sheared at different rates (0.0005 mm/s, 0.001 mm/s, 0.01 mm/s and 0.1 mm/s). The friction coefficient, defined as the ratio of peak shear stress to normal stress, describes the strength of the material, whereas residual shear strength variations at different shear velocities (so called [*a*-*b*] parameter) define the frictional stability of the sediment (Scholz, 1998).

7.2.4. Results

7.2.4.1 Landslide targets

Based on the multibeam bathymetry and seismic data, two regions with characteristic mass wasting features were identified from their seafloor roughness and internal chaotic signatures (Fig. 2). Northeast of the island of Crete, area D shows a huge, roughly ~ 9 km long and 3-4 km wide lobe of displaced slope sediment consisting of two distinct slide units, with a relatively smooth surface (Fig. 2a). Some of the failed material seems to have slid as intact blocks while other portions appear to have been amalgamated. A headwall cannot be identified, but at the head of the slide body, the upper 20 m of sediments are missing and seem to be incorporated into the slide. Intact structures inside of the generally chaotic seismic facies of the slides suggest that the internal structure has not been totally destroyed and that the slide has not travelled very far. Further east, in area E, a smaller slope failure event was identified based on its steep head scarp (Figs. 2b, c). Undisturbed, well-stratified sediments upslope are cut at the headwall, which has a height of ~50 m at this location. Directly adjacent to the headwall, a relatively thin (< 50 m) chaotic unit overlies well-stratified sediments. Approximately 4 km down-slope of the headwall the chaotic unit thickens to roughly 100 m, which most likely represents the main depositional area of the slide. However, as this unit does not appear as a continuous feature, an estimation of the depositional area is difficult. It could be possible that the bulk part of the slide material is transported much further down-slope and was deposited in the deep basin. In the two slides identified in areas D and E, a total of 11 gravity cores with lengths of 1-4.6 m were recovered (Figs. 2-3; Kopf et al., 2006). The sediment is generally comprised of four different lithologies: Yellowish brown bioturbated mud (Unit 1) is underlain by mottled and moderately bioturbated grey mud (Unit 2), sometimes containing a volcanic layer of the Thera eruption (3370 B.P.). Below that, greyish-brownish to olive grey mud with Corg >2% and no bioturbation has been identified as sapropel S1 (Unit 3).). It is underlain by yellowish grey clayey mud, which is often slightly bioturbated (Unit 4). Surprisingly, there is no significant

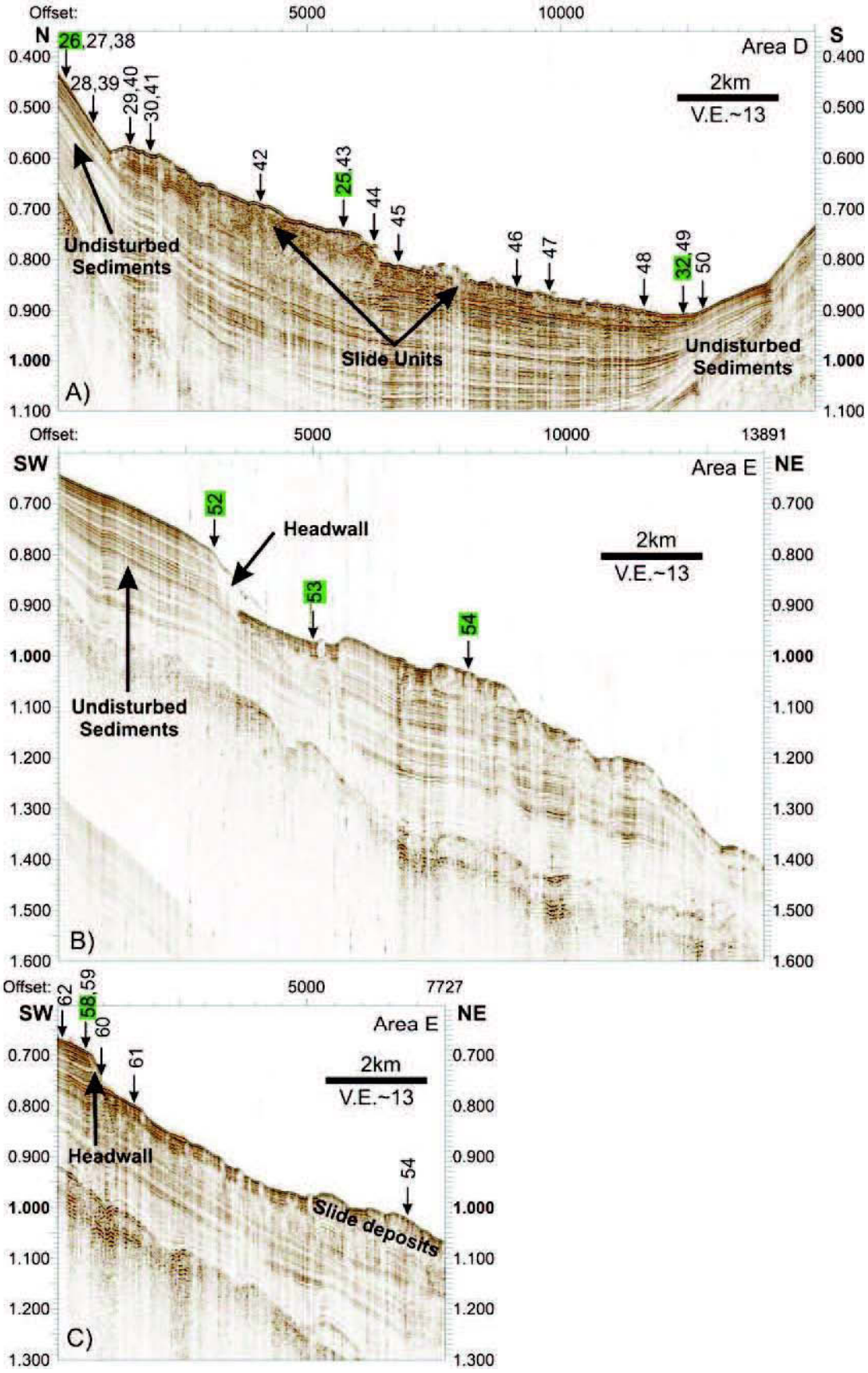

Fig. 2: Airgun profile of mass wasting events at the Cretan Margin in area D (A) and area E (B, C) with the positions of the CPT and gravity cores (green marked signature).

difference between cores taken in the undisturbed slope and in the wasted mass below. In fact, all cores from the large slide complex D as well as area E show the four lithological units (Fig. 3). The only exception to this fact is core 52, where both Unit 2 and S1 are traceable only as remnants of mm-thicknesses (Fig. 3b). It appears from visual inspection that Unit 3 (S1) and parts (or all) of Unit 2 are missing. We will revisit this aspect when looking at the MSCL data (see below). Other than that, there are only minor differences between areas D and E regarding the thickness (and hence sedimentation rate) of the units. In area D, the landslide cores show condensed successions of Units 1 and 2 when compared to the undisturbed reference site. In contrast, area E shows no systematic relationship, with both the hangingwall and slid mass deposits showing both normal and condensed successions.

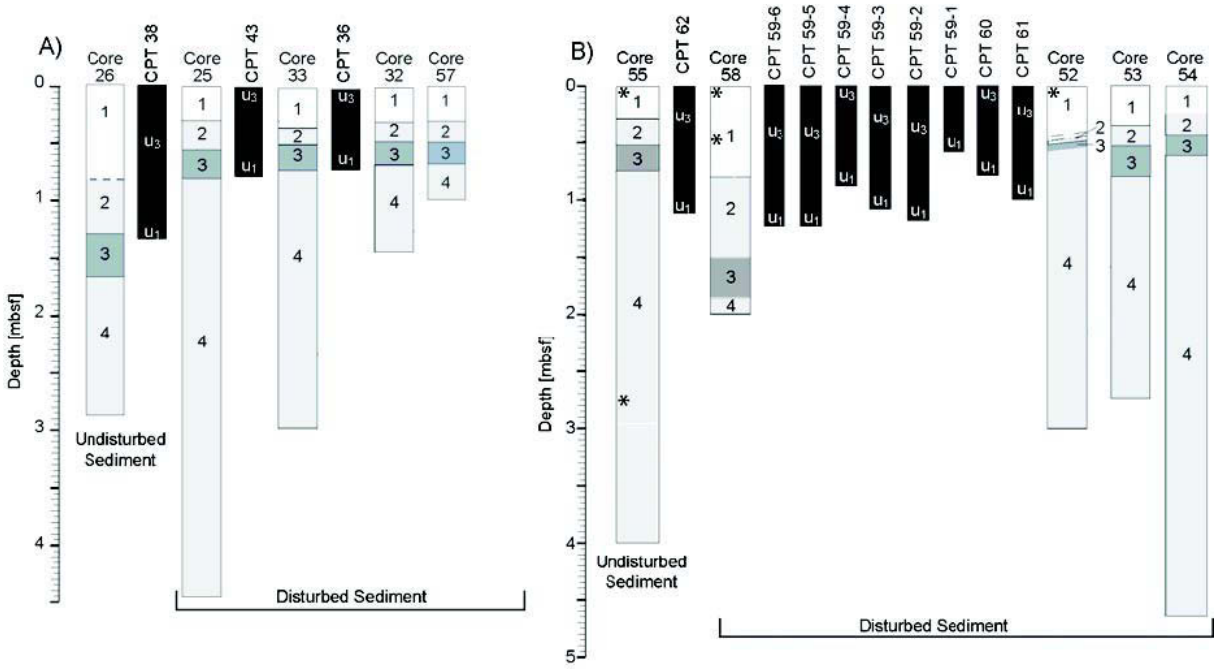

*Fig. 3: Lithology of cored sediments (see description in the text) and penetration depth of FF-CPT deployments in landslide sediments in areas D (A) and E (B). The position of specimens, which have been tested in the ring shear device (see description in the text and Fig. 5), are marked by *.*

7.2.4.2 *in situ* Physical properties

During the cruise, 26 FF-CPT deployments were carried out in areas D and E (Figs. 2-3). Unfortunately, the CPT cone failed during some of the deployments so that the strength parameters (qc, fs) could not be measured in each location. Consequently, we focus mainly on the differential pore pressure data in regions D and E. Initial penetration velocity of the complete CPT data set (derived from acceleration) ranged between 1.1 m/s and 1.8 m/s, which was mostly limited by winch speed (max. 2 m/s) and external conditions (waves, swell). Given the stiff nature of the sediments off Crete, total penetration depth was rather low. It appears as if the S1 layer, which has a higher strength than the surrounding sediments, is limiting the maximum penetration depth since it slows down the lance's momentum dramatically. In area D, penetration depth varied between 0.65 and 1.35 m (Fig. 3a), with the highest values in undisturbed sediments upslope of the scar, and between 0.6 and 1.25 m in area E (Fig. 3b). In nearly all measurements

the tilt of the penetrated lance did not exceed ±9°. *In situ* measured cone resistance is limited to undisturbed and failed sediments of area D because of problems with the CPT probe at the tip of the lance. However, based on the results collected, we can show that the undisturbed section shows higher strength than the remobilised portion. This is reflected by maximum qc plotting around 400-500 kPa upslope and 300-380 kPa on the landslide body. These findings correspond to the working hypothesis that the remobilised sediment has higher water content and lower strength, which is indicated further by the MSCL data. These attest to lower p-wave velocities and bulk densities in the upper portion of cores in the landslide body (stations 25, 33, 32, 57), but higher p-wave velocities in Unit 4 in the lower part. Here, the undisturbed material ranges between 1575-1590 m/s while the landslide cores range from 1510 to 1560 m/s, possibly related to fluids trapped during remobilisation. Measured pore pressure response generally shows an insertion peak followed by a sudden drop. At the time, the lance is still penetrating the sediment (Stegmann and Kopf, this issue, red portion in their Fig. 3). Pore pressure then rises again to a second maximum, which in turn is followed by an exponential decay (Stegmann and Kopf, this issue, black portion in their Fig. 3). Unfortunately, several of our measurements exceeded the upper limit of the differential pore pressure sensor immediately after the impact of the probe (again, maybe as a result of high excess fluid pressures in Unit 4; see previous paragraph). For all landslide measurements of u1, maximum excess pore pressure values after insertion ranged between 24 kPa to more than 82 kPa (this latter value being the upper range of the sensor). Pore pressure signals in area D show maximum insertion pore pressure (u1) between 40 and 60 kPa for the sapropel unit of area D. The sediment in area E is found less dense and with higher porosities compared to area D. Accordingly, T50 values range between 1.9 and 4.2 mins. in the sapropel unit (60-80% porosity) compared to T50=6 mins. in the muddy sediment (40-60% porosity). The u3 pore pressure signal was measured in only 76 % (area D) and 33% (area E) of the measurements, because penetration depth did not exceed 80 cm (see instrument design, Stegmann and Kopf, this issue). When recorded, the u3 signal often resembles that in u1 position (see Stegmann and Kopf, this issue, Fig. 3d). The insertion pressure values are higher in area D, varying between 27 kPa (station 40) and 52 kPa (station 39), than in area E with a range between 9.5 kPa (station 62) and 28.6 kPa (station 594).

7.2.4.3 Lab-based physical properties

Data from the MSCL do not allow a clear distinction between cores taken in the undisturbed slope cover (reference core) and that in the landslide material. In general, area D cores show low p-wave velocities (1500-1550 m/s) and smaller bulk densities of approximately 1.85 g/cm^3 than area E. Values increase gradually down section in the reference core (core 26) (ca. 1600 m/s, ca. 2 g/cm^3), but decrease in each of the landslide cores in Unit 4. Lab-determined physical properties such as undrained shear strength cu (determined with the fall cone penetrometer) mirror this trend. In the upper portion (i.e. unit 1-3) cu increases with depth from 10 to 20 kPa. In the deeper section (2-2.9 m) of the reference core, higher cu (40 ±8 kPa) coincides with a significant jump to lower porosity (av. 40 %). Failed material of the Cretan Margin (stations 25, 32, 33, 57) can be different to very similar to the intact sediments located above the scarp. In contrast, the farthest removed deposits reveal a process of homogenisation as a result of displacement, expressed with a relatively high porosity of 60 % and a density in a range around 1.8 g/cm^3. cu is more or less constant, which seems indicative of prograde consolidation history. Although the scarp structure of the area E landslide is very recognisable in

seismic data, landslide features are not very obvious to identify in the very homogeneous sediments with an average density of 1.8 g/cm^3. Upslope (station 55) and down-slope (station 54) materials are characterised by a linear increase of cu from 20 to 40 kPa. Immediately near the scarp (station 52) and within the channel-like failure structure (stations 53, 58) a less pronounced linear trend of cu is evinced.

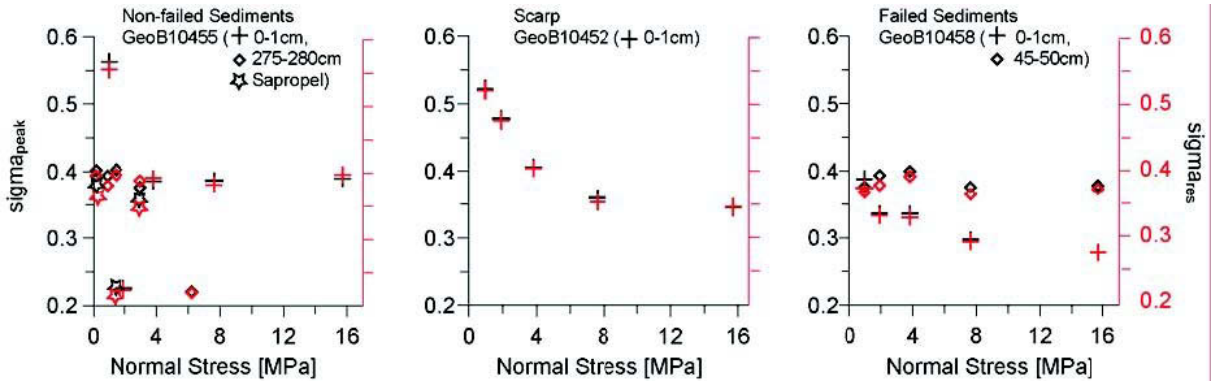

Fig. 4: Frictional behaviour of undisturbed and disturbed superficial (crosses) and sediments from depth (lozenges) of the head scarp region in area E. The coefficient of friction is plotted vs. normal stress due to incremental loading during ring shear tests with a shear velocity of 0.01 mm/s. Black colours signify the coefficient of peak strength μpeak while red colours show the coefficient of residual strength μ_{res}.

Ring shear data have only been collected in area E to characterise small-scale lateral variations across the headwall of the slide (Fig. 2b-c, 3b). The undisturbed sediments (station 55) indicate no significant difference between superficial (Unit 1) and deeper portion (Unit 4; 2.75-2.8 m) with an average μpeak of 0.4 (Fig. 4a). Unit 3 (sapropel S1) shows a μpeak range of 0.24-0.4, possibly reflecting a breakdown of the cohesive organic aggregates and fabric alignment. In contrast, μ peak of the surface sediment from the headwall and landslide (stations 52, 58) are significantly lower, ranging around 0.35 (52; Fig. 4b) and 0.28 (58; Fig. 4c). Even the deeper portion of the landslide core 58 shows μ peak ca. 0.36-0.4, which is slightly below that of the undisturbed core (Fig. 4a). This suggests to us that indeed some material is missing in the upper part of core 58 (see discussion below).

7.2.5. Discussion

Looking into the sedimentary and geotechnical results in more detail, we first revisit the seismic data. Despite the evidence for landslide features in area D with rough surface and internal features in the seismic images (Fig. 3), the gravity core description alone cannot unambiguously distinguish between the undisturbed vs. slid sediment. Based on sedimentological information, it can be speculated that:

(i) the lower part of the succession corresponds to amalgamated mud of the landslide body that would have occurred relatively shortly before the onset of sapropel deposition ~10 ka B.P., or that

(ii) the sedimentary succession represents primary sedimentary deposits and therefore, the landslide is either older and was not reached with coring, or all cores were recovered from an internally coherent slide, or out runner blocks. In case of the latter, the landslide can also be younger than S1 and the Thepra volcanic deposit (3370 B.P.).

When further consulting the results from the MSCL and *in situ* measurements, we observe some variations that identify the landslide material. These include lower cone resistance in the remobilised section of landslide D, lower p-wave velocity in the deeper portion of cores from area D, and low frictional strength from ring shear tests at the head scarp materials and shallow landslide deposits in area E (cores 52 and 58; Fig. 4b, c). If we assume that these interpretations of the superficial measurements are correct, then the landslide should be relatively young. This is supported by the seismic reflection data where, despite lack of mscale resolution, no seafloor-parallel, post-landslide reflections are found (Fig. 2). In study area E, the ~50 m high scarp is clearly visible in seismic reflection data (Fig. 2b, c). Apart from the low intrinsic friction (Fig. 4), mass wasting near the head scarp is confirmed by abundant clasts and carbonate concretions in core 58 immediately above sapropel S1 (see Kopf et al. [2006] for details). Also, sedimentation rates in that interval are roughly twice as high as in the other cores. However, given the overall lithostratigraphic similarities with S1 and other markers present, no final conclusion can be drawn on the timing and mechanism of scarp formation. Since we were unable to perform long-term pore pressure dissipation experiments, we cannot safely propose the physical trigger mechanism of the two landslides. Neotectonic activity and regional seismicity make earthquake tremor a likely candidate. Earthquake magnitudes have been reported to be as high as M7.4 (e.g. in 1956; see Perissoratis and Papadopoulos, 1999), causing significant subsidence and sediment remobilisation. Excess pore pressures exceed 82 kPa, however, an unquantifiable portion of that number relates to the impact of the CPT instrument and is found to decrease rapidly (i.e. T50 values of several minutes only). In any case, pore pressures are believed to be lightly supra-hydrostatic because of the moderately high sedimentation rates. Hence, significant extra pore pressure from (pre-)seismic stress release is needed to cause landslide initiation. Sliding, however, is facilitated by friction coefficients of μpeak ~0.3, or lower, as measured with the ring shear apparatus. Also, unstable sliding is likely given that these materials show velocity weakening behaviour when sheared at different rates, so that catastrophic mass wasting may occur.

Acknowledgements

We thank Master Michael Schneider and his crew for the friendly and efficient operations during cruise P336 with RV *Poseidon*. The manuscript benefited from constructive reviews and suggestions by Katrin Huhn and Nabil Sultan. Funding for this work was received by DFG through RCOM Bremen (project C8). This is RCOM publication #505.

References

Chronis, G., Lykousis, V., Georgopoulos, D., Poulos, M., Zervakis, V., Stavrakakis, S., 2000a. Suspended particulate matter and nepheloid layers in the southern margin of the Cretan Sea (NE Mediterranean): seasonal distribution and dynamics. Progress in Oceanography, 46, p.163–185.

Chronis, G., Lykousis, V., Anagnostou, C., Karageorgis, A., Stavrakakis, S., Poulos, S., 2000b. Sedimentological processes in the southern margin of the Cretan Sea (NE Mediterranean). Progress in Oceanography, 46, p.143-162.

Dominey-Howes, D., Cundy, A., Croudace, I., 2000. High energy marine flood deposits on Astypalaea Island, Greece: possible evidence for the AD 1956 southern Aegean tsunami. Mar. Geol., 163, p.303-315.

Fassoulas, C., 1999. The structural evolution of central Crete: insight into the tectonic evolution of south Aegean (Greece). Geodynamics, 27, p.23-43.

Giresse, P., Buscail, R., Charriere, B., 2003. Late Holocene multisource material input into the Aegean Sea: depositional and post-depositional processes. Oceanologica Acta, 26, p.675-673.

Hampton, M.A., Lee, H.J., Locat, J., 1996. Submarine Landslides. Reviews of Geophysics, 34/1, p.35-59.

Hansbo, S., 1957. A new approach to the determination of the shear strength of clay by the fall-cone test. Geotechnical Institute Proceedings, 14, p.50.

Kopf, A., Alves, T., Heesemann, B., Kaul., N.E., Kock, I., Krastel, S., Reichelt, M., Schäfer, R., Stegmann, S., Strasser, M., Thölen, M., 2006. Report and preliminary results of POSEIDON cruise P336: CRESTS -Cretan Sea Tectonics and Sedimentation. Berichte FB Geowiss., Univ. Bremen, No. 253: 140pp.

Kvalstad, T.J., Farrokh, N., Kaynia, A.M., Mokkelbost, K.H., Bryn, P., 2005. Soil conditions and slope stability in the Ormen Lange area. Marine and Petroleum Geology, 22, p.299-310.

Le Pichon, X., Angelier, J., 1979. The Hellenic Arc and Trench system: a key to the neotectonic evolution of the Eastern Mediterranean area. Technophysics, 6, p.1–42.

Lykousis, V., Roussakis, G., Alexandri, M., Pavlakis, P., Papoulia, I., 2002. Sliding and regional slope stability in active margins: North Aegean Trough (Mediterranean). Mar. Geol., 186, p.281-298.

Mascle, J., Martin, L., 1990. Shallow structure and recent evolution of the Aegean Sea: a synthesis based on continuous reflection profiles. Mar. Geol., 94, p.271–299.

McKenzie, D. P., 1978. Active tectonics of the Alpine–Himalayan belt: the Aegean Sea and surrounding regions. Geophysical Journal of the Royal Astrological Society, 55, p.217–254.

Perissoratis, C., Papadopoulos, G., 1999. Sediment instability and slumping in the southern Aegean Sea and the case history of the 1956 tsunami. Marine Geology, 161, p.287-305.

Scholz, C.H., 1998. Earthquakes and friction laws. Nature, 391, p.37-42.

Sultan, N., Voisset, M., Maresset, B., Marsset, T., Cauquil, E., Colliat, J.-L., 2007. Potential role of compressional structures in generating submarine slope failures in the Niger Delta. Mar. Geol., 237/3-4, p.169-190.

Stegmann, S., Kopf, A., 2007. Marine Deep-Water Free-Fall Cpt Measurements For Landslide Characterisation Off Crete, Greece (Eastern Mediterranean Sea) Part 1: A New 4000M Cone Penetrometer. In: Lykousis, V., Sakellariou, D., Locat, J. (Eds.) Advances in Natural and Technological Hazards Research, 1, Volume 27, Submarine Mass Movements and Their Consequences 3, Springer, pp. 171-177.

8. Conclusion and Outlook

The threat of submarine landslides to the growing offshore infrastructure indicates the societal need for the investigation of submarine mass wasting processes. Several studies show that most of the submarine continental slopes are stable and require external triggers or sediment destabilizing preconditioning factors (e.g. Hampton et al., 1996; Locat and Lee, 2002; Hühnerbach et al., 2004; Masson et al.; 2006, Lee et al., 2007). The distribution of submarine landslides may be controlled by the interaction of morphology, sediment composition (including preconditioning factors as e.g. lowered sediment strength) and external triggers. Figure 9 summarizes all the above mentioned aspects and shows the main consequences of submarine mass wasting processes, their hazardous impact on e.g. offshore installations, coast-near cities and harbours, and the required trigger mechanisms.

Within the presented thesis geotechnical properties of slid sediments were investigated to constrain the mechanics and the temporal evolution of three different submarine landslides sites. With the results a statement about the interaction of trigger mechanisms and generation of submarine landslides can be made. A combination of at least two/three trigger mechanisms in interaction with preconditioning factors is required for destabilizing the investigated slope sediments. According to the already existing literature, which deals with landslide mechanisms (e.g. Hampton et al., 1996; Sultan et al., 2004; Masson et al., 2006; Lee et al., 2007; Nadim, 2009; Masson et al., 2010; Thomas et al., 2010), the following results and conclusion can be taken from the present thesis.

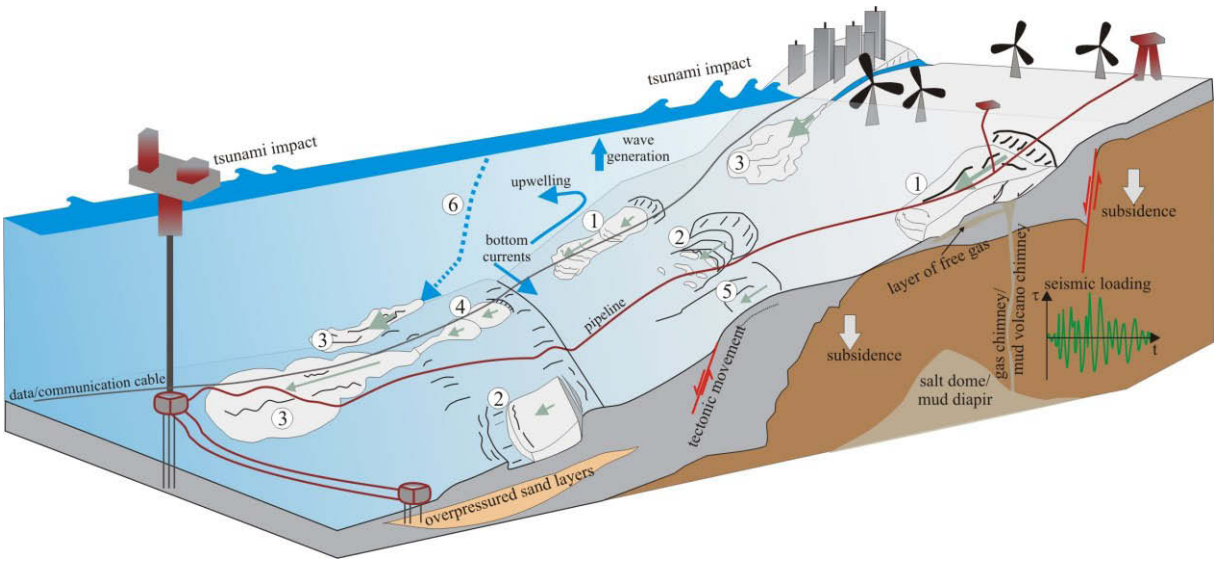

Fig. 9 Scetch of the consequences of submarine mass movement processes (1: rotaional slide, 2: translational slide, 3: turbidity current, 4: debris flow, 5: creep, 6: hyperpycnal flow) with their risk to people, submarine cables and pipleines and other offshore installations governed by several factors, e.g. tectonic movements, excess pore pressure as result of free gas, overpressured sedimentss, seismic loading, high sedimentation rates (after Nadim, 2009; Thomas et al., 2010; Norwegian Geological Institute, 2011).

- *Passive continental margins with low slope angles may allow the accumulation of thick sediment packages. Stronger trigger mechanisms are required to destabilize these sediments.*

  → At the Mauritania continental margin several mass wasting processes were observed, but most of them are generated in submarine canyon systems. The investigated Mauritania Landslide Complex is a huge slide with a total volume of ~600 km³ and an affected area of ~30.000 km². The slope angle is low with 1 to 3° (Jacobi, 1976; Wynn et al., 2000; Henrich et al., 2010). With sedimentological and geotechnical data at least two different mass wasting events could be distinguished occurred during 10.5 ka BP and 24.21 ka BP (Section 4).

  → The most likely main trigger mechanisms are the rapid sedimentation during glacial-interglacial dynamic changes in combination with the presence of a "weak layer". For the slid sediments of the Mauritania Landslide Complex the correlation of the friction values and the sediment composition shows that a higher content of quartz grains has sediment strengthening effect but no effect in the absolute shear strength (Section 4). The rapid sedimentation leads to excess pore pressure build-up and preserves consequently an underconsolidated state with low sediment strength (Section 4). Alternatively, migration of free gas, which might be generated during periods of sea-level fall/lowstand with low hydrostatic pressure (Section 4), can also produce high excess pore pressure (Nisbet and Piper, 1998). Several studies show indications for overpressured gas in the sediments of the Mauritania Landslide Complex (Krastel et al., 2006; Antobreh and Krastel, 2007). In essence the sediment composition, the related physical properties and friction characteristics as well as the consolidation history may provide pre-conditioning factors for sediment failure.

  → Strain analysis (after Fry, 1979) is a powerful tool to estimate the deformation of the sediments. The present thesis used this tool to understand the internal mechanics of slide evolution. The remobilzed sediments show high deformation intensities, while the undisturbed hemipelagic sediments just reflect deformation effects during burial. The evolution of the Mauritania Landslide Complex is controlled by at least two different slide events. One of these events was vigorous enough to rework sediment from an underlying unit in form of disintegrated clasts. These clasts show strong overconsolidation, intense deformation but low rotation. Hence the clasts are interpreted as unaffected by sliding, and therefore the high deformation values reflect initial pre-slide conditions (Section 4).

- *Along active continental margins the most important trigger mechanism for slope failure is probably earthquake loading.*

  → At the lower Ligurian Margin steep slope angles (~11°) could be observed with a high frequency of mass wasting processes. Without an external trigger the sediments should be stable. In the thesis, excess pore pressure was estimated from triaxial- and oedometer tests and had a stake in the total stress of 1-30%, depending on the sediment compostion. With these values, a slope stability analysis showed that already small

magnitudes earthquakes (M 0.77-~5) with peak ground acceleration (PGA) of 2-22 %g are required for sediment destabilization (Sections 5 and 6). The excess pore pressure generated by repeated cylic loading during earthquakes was not taken into account (Section 6). Through this process the sediment strength will be reduced and the worst case will be liquefaction of the sediments with extremely lowered shear strength (Lee et al., 2007; Masson et al., 2010). Therefore required magnitudes for sediment destabilization may be lower than the slope stability analysis offered.

→ Along canyon system undercutting may play along-term role in destabilization of slope sediments. One of the study areas of this thesis was located at a canyon at the lower slope of the Ligurian margin. The peak flow velocities of the Var Canyon were estimated to be high enough for erosion of the in-situ sediments and could also be a possible trigger mechanism (Section 6). Additionally, lateral fluid flow may play a role for sediment instabilities. For the upper Ligurian Margin lateral fluid flow is known, because the groundwater level near the coast is above sea level (Lee et al., 2007). However, evidences for fluid flow are missing for the lower slope (Sections 3 and 6).

→ Instead at the Cretan Sea Margin, where also steep slope angles could be observed, the recurrence time of mass wasting processes is low (Section 7). The explanation may be the development of high shear strength values of the thick sediment packages, which might be a result of repeated occurrences of earthquake with lower magnitudes. The cyclic loading is followed by pore pressure dissipation and may lead to sediment strengthening (Lee et al., 2007). Additionally, high carbonate content was observed in the Cretan Sea sediments, which might also lead to higher shear strength values. The case studies at the Cretan Sea show that high magnitude earthquakes are required for slope destabilization with peak ground acceleration of 37 %g - 64 %g. In-situ cone penetration tests showed that the pore pressures of the investiagted sediments were supro-hydrostatic because of high sedimentation rates in the research area. Pore pressure determination from seismic stress was missing, because long-term pore pressure experiments were not installed (Section 7, Stegmann and Kopf, 2007).

The investigation of submarine landslides should be further performed because of its hazardous impact of social and industrial community. The data of slope stability investigations may a good basis for risk assessment. However, for a better prediction of the stability of the slopes additional measurements such as in-situ piezometer tests are needed to determine the role of excess pore pressure on observed failure events and the development of excess pore pressure during seismic events. Furthermore, the investigations of submarine mass wasting sediments should include sedimentological analysis and dating of the sediments. Also measurements of geotechnical parameters across failure plane seem to be mandatory.

Acknowledgements

First and foremost, I owe my supervisor Prof. Dr. Achim Kopf for the possibility to write my doctoral thesis at the Marum. He initiated this research project with its interessting topic and has confessed to me with advice and constructive discussions aside. A special thank also to Prof. Dr. Tobias Mörz for his support over the last years and the second review of this work.

At this point, all employees of the two working groups Marine Geotechnics and Marine Engenieering Geology I would like to thank you for the fantastic time we had in Bremen. Special thanks go to my former roommates Annedore Seifert, Hendrik Hanff, Christian Zoellner, Nina Stark, Sylvia Stegmann and Andre Hüpers. Sincere thanks are given to Andre for taking care of my experiments at the week-ends or for the scientific and also off-topic discussions. Additionally, for several scientific discussions I would like to thank Michal Strasser, Tilman Schwenk and Daniel Hepp. I am much obliged to both Matthias Lange and Wolfgang Schunn for the technical support and the quick help after break-down of the ring shear device. Further, during my thesis work I attended several research cruises and I would like to thank along the way all my colleagues as well as the ship crew of the Meteor cruises M73/1 (2007), M74/2 (2007) and of the Poseidon cruise P386 (2009) for the great success, data sampling and discussions onboard. In addition, the scientific stuff and the crew of the Meteor cruises M58/1 (2003) and M65/2 (2005) and the Poseidon cruise P336 (2006) would be owed for collecting samples and preparing and allocation data, which I used also for my thesis.

All members of GLOMAR thanks are given, especially to Prof. Dr. Dierk Hebbeln and Dr. Uta Brathauer for the opportunity to join GLOMAR and the chance to benefit from educational advancement and scientific discussion with colleagues from different disciplines. My sincerest thanks go to Susanne Abeld, Solveig Bühring, Anna Fricke, Stephanie Kusch, Ose Leendertz, Diana Magens, Ute Merkel, Nina Stark, Franzsica Steinhoff, Simone Ziegenbalg and Prof. Dr. Ulrike Herzschuh (Alfred-Wegener Institute, Potsdam). We had a great time together… you know.

Last but not least, none of this would have been possible without the assistance and patience of my family and close friends, who always had an open ear for my relocations and problems. Without them this study, which ends with this work, would not have been possible.

Reference

Ambraseys, N. N., 2001. Far-field effects of eastern Mediterranean earthquakes in lower Egypt. Journal of Seismology 5, 263-268, doi:10.1023/A:1011476718680.

Anderson, H., Jackson, J., 1987. Active tectonica of the Adriatic Region. Geophysical Journal of the Royal Astronomical Society 91, 937-983.

Antobreh, A.A., Krastel, S., 2007. Mauritania Slide Complex: morphology, seismic characterisation and processes of formation. International Journal of Earth Sciences 96, 451-472.

Barley, B., 1999. Deepwater problems around the world. Leading Edge 18, 488-494.

Becker, D., Meier, T., Rische, M., Bohnhoff, M., Harjes, H-P., 2006. Spatio-temporal microseismicity clustering in the Cretan region. Tectonophysics 423, 3-16.

Béthoux, N., Ouillon, G., Nicolas, M., 1998. The instrumental seismicity of the western Alps: spatio-temporal patterns analysed with the wavelet transform. Geophysical Journal International 13, 177-194.

Béthoux, N., Tric, E., Chery, J., Beslier, M.O., 2008. Why is the Ligurian Basin (Mediterranean Sea) seismogenic? Thermomechanical modelling of a reactivated passive margin? Tectonics 27: TC5011, doi:10.1029/2007TC002232.

Bohnhoff, M., Rische, M., Meier, T., Becker, D., Stavrakakis, G., Harjes, H-P., 2006. Microseismic activity in the Hellenic Volcanic Arc, Greece, with emphasis on the seismotectonic setting of the Santorini-Amorgos zone. Tectonophysics 423, 17-33.

Booth, J.S, O'Leary, D.W., Popenoe, P., Danforth, W.W., 1993. U.S. Atlantic Continental Slope Landslides: Their Dirstribution, General Attributes, and Implications. In: Schwab, W.C., Lee, H.J., Twichell, D.C. (Eds.), Submarine Landslides: Selected Studies in the U.S. Exklusive Economic Zone. USGS Bulletin 2002, 14-22.

Bouma, A.H., 1962. Sedimentology of some Flysch Deposits: a Graphic Approach to facies Interpretation. Elsevier, Amsterdam, 168pp.

Brown, R.H., 1980. Triassic rocks of the Argana valley, Southern Morocco, and their regional structural implications. Bulletin American Association of Petroleum Geologists 64, 988-1003.

Bryn, P., Berg, K., Forsberg, C.F., Solheim, A., Kvalstad, T.J., 2005. Explaining the Storegga Slide. Marine and Petroleum Geology 22, 11-19.

Canals, M., Lastras, G., Urgeles, R., Casamor, J.L., Mienter, J., Cattaneo, A., De Batist, M., Haflidason, H., Imbo, Y., Laberg, J.S., Locat, J., Long, D., Longva, O., Masson, D.G., Sultan, N., Trincardi, F., Bryn, P., 2004. Slope failure dynamics and impacts from seafloor and shallow sub-seafloor geophysical data: case studies from the COSTA project. Marine Geology 213, 9-72.

Cassidy, M.J., Uzielli, M., Lacasse, S., 2008. Probability risk assessment of landslides: A case study at Finneidfjord. Canadian Geotechnical Journal 45, 1250-1267.

Chaumillon, E., Mascle, J., 1996. From foreland to forearc domains: Mew multichannel seismic reflection survey of the Mediterranean ridge accretionary complex (Eastern Mediterranean). Marine Geology 138, 237-259.

Chronis, G., Lykousis, V., Anagnostus, C., Karageorgis, A., Stavrakakis, S., Poulus, S., 2000. Sedimentological processes inthe southern margin of the Crete Sea (NE Mediterranean). Progress in Oceanography 46, 143-160.

Clauzon, G., 1978. The Messinian Var Canyon (Provence, Southern France) – Paleogrographic Implications. Marine Geology 27, 231-246.

Cochonat, P., Bourillet, J.F., Savoye, B., Dodd, L., 1993. Geotechnical characteristics and instability of submarine slope sediments, the Nice slope (N-W Mediterranean Sea). Marine Georesources & Geotechnology 11, 131-151.

Colman, J.G., Gordon, D.M., Lane, A.P., Forde, M.J., Fitzpatrick, J.J., 2005. Carbonate mounds off Mauritania, Northwest Africa: status of deep-water corals and implications for management of fishing and oil exploration activities. In: Freiwald, A., Roberts, J.M. (Eds.), Cold-water Corals and Ecosystems. Springer, Heidelberg, pp 417-441.

Contrucci, I., Nercessian, A., Béthoux, N., Mauffret, A., Pascal, G., 2001. A Ligurian (Western Mediterranean Sea) geophysical transect revisited. Geophysical Journal International 146, 74-97.

Corbett, D.R., McKee, B., Allison, M., 2006. Nature of decadal-scale sediment accumulation on the western shelf of the Mississippi River delta. Continental Shelf Research 26, 2125–2140.

Costanza, R., Farley, J., 2007. Ecological economics of coastal disasters: Introduction to the special issue. Ecological Economics 63, 249-253.

Coulomb, C.A., 1773. Sur une application des regles de maximis et minimis a quelques problems de statique, reltifs a l'architecture. Mémoires de Mathematique et de Physique, Royal Academy of Sciences 7, 343-387.

Courboulex, F., Duval, A. M., Deschamps, A., Lomax, A., Larroque, C., 2001. Les enseignements du peti séisme de Peille (Alpes-Maritimes, France). C. R. Acad. Sci. Paris, Sciences de la Terre et des planets - Earth and Planetary Sciences 333, 105–112.

Courboulex, F., Larroque, C., Deschamps, A., Kohrs-Sansorny, C., Gélis, C., Got, J.L., Charreau, J., Stéphan, J.F., Béthoux, N., Virieux, J., Brunel, D., Maron, C., Duval, A.M., Perez, J-L., Mondielli, P., 2007. Seismic hazard on the French Riviera: observations, interpretations and simulations. Geophysical Journal International 170, 387-400.

Dail, M.B., Corbett, D.R., Walsh, J.P., 2007. Assessing the importance of tropical cyclones on continental margin sedimentation in the Mississippi delta region. Continental Shelf Research 27, 1857-1874.

Dan, G., Sultan, N., Savoye, B., 2007. The 1979 Nice harbour catastrophe revisited: Trigger mechanism inferred from geotechnical measurements and numerical modelling. Marine Geology 245, 40-64.

Davison, I., 2005. Central Atlantic margin basins of North West Africa: Geology and hydrocarbon potential (Morocco to Guinea). Journal of African Earth Sciences 43, 254-274.

Dingle, R.V., 1977. The anatomy of a large submarine slump on a sheared continental margin (SE Africa). Journal of the Geological Society, London 4, 293-310.

Dugan, B., Germaine, J.T., 2008. Near-seafloor overpressure in the deepwater Mississippi Canyon, northern Gulf of Mexico. Geophysical Research Letters 35, L02304, doi: 10.1029/2007GL032275.

Fassoulas, C., 2001. The tectonic development of a Neogene basin at the leading edge of the active European margin: the Heraklion basin, Crete, Greece. Journal of Geodynamics 31, 49-70.

Fassoulas, C., Kilias, A., Mountrakis, D., 1994. Postnappe stacking extension and exhumation of high-pressure/low-temperature rocks in the island of Crete; Greece. Tectonics 13, 127-138.

Fry, N., 1979. Random point distributions and strain measurement in rocks. Tectonophysics 60, 89-105.

Ganas, A. Parsons, T., 2009. Three-dimensional model of Hellenic Arc deformation and origin of the Cretan uplift. Journal f Geophysical Research 114, B06404, doi: 10.1029/2008JB005599.

Gee, M.J.R., Uy, H.S., Warren, J., Morley, C.K., Lambiase, J.J., 2007. The Brunei slide: A giant submarine landslide on the North Wets Borneo Margin revealed by 3D seismic data. Marine Geology 246, 9-23.

Giresse, P., Buscail, R., Charrière, B., 2003. Late Holocene multisource material input into the Aegean Sea: depositional and post-depositional processes. Oceanologica Acta 26, 657-672.

Goldfinger, C., Kulm, LV.D., McNeill, L.C., Watts, P., 2000. Super-scale Failure of the Southern Oregon Cascadia Margin. Pure Applied Geophysics 157, 1189-1226.

Gueguen, E., Doglioni, C., Fernandez, M., 1998. On the post-25 Ma geodynamic evolution of the western Mediterranean. Tectonophysics 298, 259-269.

Gutmacher, C.E., Normark, W.R., 1993. Sur Submarine Landslide, a Deep-Water Sediment Slope Failure. In: Schwab, W.C., Lee, H.J., Twichell, D.C. (Eds.), Submarine Landslides: Selected Studies in the U.S. Exklusive Ecnomic Zone. USGS Bulletin 2002, 158-166.

Haflidason, H., Sejrup, H.P., Nygård, A., Mienert, J., Bryn, P., Lien, R., Forsberg, C.F., Berg, K., Masson, D., 2004. The Storegga Slide: Architecture, geometry and slide development. Marine Geology (COSTA Special Issue) 213, 201–234.

Hampton, M.A., Lee, H.J., Locat J., 1996. Submarine landslides. Reviews of Geophysics 3, 33-59.

Henrich, R., Hanebuth, T., Krastel, S., Neubert, N., Wynn, R. B., 2008. Architecture and sediment dynamics of the Mauritania Slide Complex. Marine and Petroleum Geology 25, 17-33.

Henrich, R., Cherubini, Y., Megger, H., 2010: Climate induced turbidite activity in a canyon system offshore the hyperarid Western Sahara (Mauritania): The Timiris Canyon. Marine Gelogy 275, 178-198.

Hsü, K.J., Montadert, L., Bernouilli, D., Bizon, G., Cita, M., Erickson, A., Fabricius, F., Garrison, R.E., Kido, R.B., Mellieres, F., Muller, C., Wright, R.C., 1978. Site 378: Cretan Basin. In: Hsü, K.J., Montadert, L., Bernouilli, D., Bizon, G., Cita, M., Erickson, A., Fabricius, F., Garrison, R.E., Kido, R.B., Mellieres, F., Muller, C., Wright, R.C., Kidd, R.B., Worstell, P. J. (Eds.), Initial Report of Deep-Sea Drilling Project 42, 1, U.S. Government Printing Office, pp. 321-357.

Hühnerbach, V., Masson, D.G., partners of the COSTA-Project, 2004. Landslides in the North Atlantic and its adjacent seas: an analysis of their morphology, setting and behaviour. Marine Geology 213, 343-362.

Jacobi, R.D. 1976. Sediment slides on the northwestern continental margin of Africa. Marine Geology 22, 157-173.

Klaucke, I., Cochonat, P., 1999. Analysis of past seafloor failures on the continental slope off Nice (SE France). Geo-Marine Letters 19: 245-253.

Kopf, A., Cruise Participants, 2006. Report and preliminary results of Poseidon cruise P336: CRESTS – Cretan Sea Tectonics and Sedimentation, Heraklion 28.04.-17.05.2006. Berichte Fachbereich Geowissenschaften, Universität Bremen 253, 140pp.

Kopf, A., Cruise Participants, 2008. Report and Preliminary Results of Meteor Cruise M 73/1: LIMA-LAMO (Ligurian Margin Landslide Measurements & Observatory), Cadiz, 22.07.2007 - Genoa, 11.08.2007. Berichte Fachbereich Geowissenschaften, Universität Bremen 264, 169pp.

Krastel, S., Wynn, R.B., Hanebuth, T., Henrich, R., Holz, Ch., Meggers, H., Kuhlmann, H., Georgiopolou, A., Schulz, H.D., 2006. Mapping of seabed morphology and shallow sediment structure of the Mauritania continental margin, Northwest Africa: some implications for geohazards potential. Norwegian Journal of Geology 86, 163-176.

Kvalstad, T.J., Andresen, L., Forsberg, C.F., Berg, K., Bryn, P., Wangen, M., 2005. The Storegga slide: evaluation of triggering sources and slide mechanics. Marine and Petroleum Geology 22, 245-256.

Laberg, J.S., Vorren, T.O., Mienert, J., Bryn, P., Lien, R., 2002. The Trænadjupet Slide: a large slope failure affecting the continental margin of Norway 4,000 years ago. Geo-Marine Letters 22, 19-24.

Larroque, C., Delouis, B., Godel, B., Nocquet, J-M., 2009. Active deformation at the southwestern Alps-Ligurian basin junction (France-Italy boundary): Evidence for recent change from compression to extension in the Argentera massif. Tectonophysics 467, 22-34.

Lastras, G., Canals, M., Hughes-Clarke, J.E., Moreno, A., De Batist, M., Masson, D.G. Cochonat, P., 2002. Seafloor imagery from the BIG'95 debris flow, western Mediterranean. Geology 30, 871-874.

Lee, H.J., 2009. Timing of occurrence of large submarine landslides on the Atlantic Ocean margin. Marine Geology 264, 53-64.

Lee, H.J., Locat, J., Desgagnes, P., Parsons, J.D., McAdoo, B.G., Orange, D.L., Puig, P., Wong, F.L., Dartnell, P., Boulanger, E., 2007. Submarine mass movements on continental margins. In: Nittrouer, C.A., Austin, J.A., Field, M.E., Kravitz,J.H., Syvitki, J.P.M., Wiberg, P.L. (Eds.), Continental Margin Sedimentation, Blackwell Publishing, pp. 213-274.

Locat, J., Lee, H.J., 2002. Submarine landslides: advances and challenges. Canadian Geotechnical Journal 39, 193-212.

Longva, O., Janbu, N., Blikra, L.H., Bøe, R., 2003. The 1996 Finneidfjord Slide; Seafloor Failure and Slide Dynamics. In: Locat, J., Mienert, J. (Eds.), Submarine Mass Movements and Their Consequences I , Kluwer Academic Publishers, pp. 531-538.

Lonsdale, P., 1982. Sediment drifts of the Northeast Atlantic and their relationship to the observed abyssal currents. Bulletin Institute Geologique Bassin Aquitaine, Bordeaux 31, 141-149.

Lykousis, V., Anagnostou, C., Pavlakis, P., Rousakis, G., Alexandri, M., 1995. Quaternary sedimentary history and neotectonic evolution of the eastern part of Central Aegean Sea, Greece. Marine Geology 128, 59-71.

Lykousis, V., Roussakis, G., Alexandri, M., Pavlakis, P., Papoulia, I., 2002. Sliding and regional slope stability in active margins: North Aegean Trough (Mediterranean). Marine Geology 186, 281-298.

Mackenzie, B., Hooper, J., Rushton, D., 2010. Spatial Analysis of Shallow Slope Instability Incorporating an Engineering geological Ground Model. In: Mosher, DC., Shipp, C., Moscardelli, L., Chaytor, J., Baxter, C., Lee, H., and Urgeles, R. (Eds.), Submarine Mass movements and their consequences IV. Advances in Natural and Technological Hazards Series, Springer, pp. 365-376.

Maltman, A., 1994. The Geological Deformation of Sediments. Chapman & Hall, University Press, Cambridge, 362pp.

Martinez, M.L., Intralawan, A., Vázquez, G., Pérez-Maqueo, O., Sutton, P., Landgrave, R., 2007. The coasts of our world: Ecological, Economic and Social Importance. Ecological Economics 63, 254-272.

Mascle, J., Martin, L., 1990. Shallow structure and recent evolution of the Aegean Sea: a synthesis based on continuous reflection profiles. Marine Geology 94, 271–299.

Maslin, M., Mikkelsen, N., Vilela, C., Haq, B., 1998. Sea-level –and gas-hydrate-controlled catastrophic sediment failures of the Amazon Fan. Geology 26, 1107-1110.

Masson, D.G., Canals, M., Alonso, B., Urgeles, R., Huhnerbach, V., 1998. The Canary Debris Flow: source area morphology and failure mechanisms. Sedimentology 45, 411-432.

Masson, D.G., Harbitz, C.B., Wynn, R.B., Pedersen, G., Løvholt, F., 2006. Submarine landslides: processes, triggers and hazard prediction. Philosophical Transaction of the Royal Society A 364, 2009-2039.

Masson, D.G., Wynn, R.B., Talling, P.J., 2010. Large Landslides on Passive Continental margins: Processes, Hypotheses and Outstanding Questions. In: Mosher, D.C., Shipp, C., Moscardelli, L., Chaytor, J., Baxter, C., Lee, H., Urgeles, R. (Eds.), Submarine Mass movements and their consequences IV. Advances in Natural and Technological Hazards Series 28, Springer, pp. 153-165.

McAdoo, B.,G., Pratson, L.F., Orange, D.L., 2000. Submarine landslides geo-morphology, US continental slope. Marine Geology 169, 103-136.

McAdoo, B.G., Capone, M.K., Minder, J., 2004. Seafloor geomorphology of convergent margins: Implications for Cascadia seismic hazard. Tectonics 23, TC6008, doi:10.1029/2003TC001570.

McClusky, S., Balassanian, S., Barka, A., Demir, C., Ergintav, S., Georgiev, I., Gurkan, O., Hamburger, M., Hurst, K., Kahle, H., Kastens, K., Kekelidze, G., King, R., Kotzev, V., Lenk, O., Mahmoud, S., Mishin, A., Nadariya, M., Ouzounis, A., Paradissis, D., Peter, Y., Prilepin, M., Reilinger, R., Sanli, I., Seeger, H., Tealeb, A., Toksöz, M.N., Veis, G., 2000. Global Positioning System constraints on plate kinematics and dynamics in the eastern Mediterranean and Caucasus. Journal of Geohysical Research 105, 5695-5719.

McKenzie, D., 1978. Active tectonic of the Alpine-Himalayan belt: the Aegean Sea and surrounding regions. Geophysical Journal of the Royal Astronomical Society 55, 217-254.

Meier, T., Rische, M., Endrun, B., Vafidis, A., Harjes, H-P., 2004. Seismicity of the Hellenic subduction zone in the area of western and central Crete observed by temporary local seismic networks, Tectonophysics 383, 149-169.

Meulenkamp, J.E., Wortel, M.J.R., Van Wamel. W.A., Spakman, W., Hoogerduyn Strating, E., 1988. On the Hellenic subduction zone and the geodynamic evolution of Crete since the late Middle Miocene. Tectonophysics 146, 203-215.

Middleton, G.V., Hampton, M.A., 1973. Sediment gravity flows: Mechanics of flow and deposition. In: Middleton, G.V., Bouma, A.H. (Eds), Turbidites and Deep-water Sedimentation. Pacific Section SEPM, Los Angeles, CA, pp.1-38.

Migeon, S., Savoye, B., Zanella, E., Mulder, T., Faugères, J.-C., Weber, O., 2001. Detailed seismic-reflection and sedimentary study of turbidite sediment waves on the Var Sedimentary Ridge 8SE France): significance for sediment transport and deposition and for the mechanisms of sediment-waves construction. Marine and Petroleum Geology 18, 179-208.

Migeon, S., Mulder, T. Savoye, B., Sage, F., 2006. The Var turbidite system (Ligurian Sea, northwestern Mediterranean) – morphology, sediment supply, construction of turbidite levee and sediment waves: implications for hydrocarbon reservoirs. Geo-Marine Letters 26, 361-371.

Milliman, J.D., Meade, R.H., 1983. World-wide delivery of river sediment to the oceans. Journal of Geology 91, 1-21.

Minisini, D., Trincardi, F., 2009. Frequent failure of the continental slope: The Gela Basin (Sicily Channel). Journal of Geophysical Research 114, F03014, doi: 10.1029/2008JF001037.

Moore, J.G., Clague, D.A., Holcom, R.T., Lipman, P.W., Normark, W.R., Torresan, M.E., 1989. Prodigious submarine landslides on the Hawaiian Ridge. Journal of Geophysical Research 94, 465-484.

Mosher, D.C., Moscardelli, L., Shipp, R.C., Chaytor, J.D.,Baxter, C.D.P., Lee, H.J., Urgeles, R., 2010. Submarine Mass movements and their consequences IV. Advances in Natural and Technological Hazards Series 28, Springer, pp. 1-8.

Mulchrone, K.F., 2002. Application of Delaunay triangulation to the nearest neighbour method of strain analysis. Journal of Structural Geology 25, 689-702.

Mulder, T., Alexander, J., 2001. The physical character of subaqueous sedimentary density flows and their deposits. Sedimentology 48, 269-299.

Mulder, T., Migeon, S., Savoye, B., Jouanneau, J.-M., 2001. Twentieth century floods recorded in the deep Mediterranean sediments. Geology 29, 1011-1014.

Nadim, F., 2006. Challenges to geo-scientists in risk assessment for submarine slides. Norwegian Journal of Geology 86, 351-362

Nardin, T.R., Hein, F.J., Gorsline, D.S., Edwards, B.D., 1979. A review of mass movement processes, sediment and acoustic characteristics, and contrasts in slope and base-of-slope systems versus canyon-fan-basin floor systems. In: Doyle, L.J., Pilkey, O. H. (Eds.), Geology of continental slopes. SEPM Special Publication 27, pp. 61-73.

Nemec, W., 1990. Aspects of sediment movement on steep delta slopes. In: Colella, A., Prior, D.B. (Eds.), Corse-grained Deltas. Special Publications of the International Association of Sedimentologists 10, 29-73.

Nisbet, E.G., Piper, D.J.W., 1998. Giant submarine landslides. Nature 392, 329-330.

Norwegian Geological Institute, 2011. International Centre for Geoharzads – Offshore Geoharzards in www. ngi.no/en/Geohazards/Research/Offeshore-Geohazards/html. [access: 21.02.2011]

Papazachos, C.B., Hatzidimitriou, P., Panagiotopoulos, D., Tsokas, G., 1995. Tomography of the crust and upper mantle in southeast Europe. Journal of Geophysical Research 100, 405–422.

Pichler, H., Friedrich, W., 1976. Radiocarbon-dates of Santorini Volcanics. Nature 262, 373-374.

Piper, D.J.W., Farre, J.A., Shor, A., 1985. Late Quaternary slumps and debris flows on the Scotian Slope. Geological Society of America Bulletins 96, 1508-1517.

Piper, D.J.W., Savoye, B., 1993. Processes of late Quaternary turbidity current flow and deposition on the Var deep-sea fan, north-west Mediterranean Sea. Sedimentology 40, 557-582.

Piper. D.J.W., Pirmez, C., Manley, P.L., Long, D., Flood, R.D., Normark, W.R., Showers, W., 1997. Mass-Transport Deposits Of The Amazon Fan. In: Flood, R.D., Piper, D. J. W., Klaus, A., Peterson, L.C. (Eds.), Proceedings of the Ocean Drilling Program, Scientific Results 155, pp. 109-146.

Piper, D.J.W., Cochonat, P., Morrison, M.L., 1999. The sequence of events around the epicentre of the 1929 Grand Banks earthquake: initiation of debris flows and turbidity current inferred from sidescan sonar. Sedimentology 46, 79-97.

Poag, C.W., Mountain, G.S., 1987. Late Cretaceous and Cenozoic evolution of the New Jersey continental slope and upper rise: an integration of borehole data with seismic reflection profiles. In: Poag, C.W., Watts, A.B. (Eds.), Initial Reports of the Deep Sea Drilling Project 95, U.S. Government Printing Office, pp.673-724.

Popenoe, P., Schmuck, E.A., Dillon, W.P., 1993. The Cape Fear Landslide: Slope Failure Associated with Salt Diapirism and Gas Hydrate Decomposition. In: Schwab, W.C., Lee, H.J., Twichell, D.C. (Eds.), Submarine Landslides: Selected Studies in the U.S. Exklusive Ecnomic Zone. USGS Bulletin 2002, 40-53.

Prior, D.B., Coleman, J.M., 1980. Sonograph Mosics of Submarine Slope Instabilities, Mississippi River Delta. Marine Geology 36, 227-239.

Rajendran, C.P., Ramanamurthy, M.V., Reddy, N.T., Rajendran, K., 2008. Hazard implications of the late arrival of the 1945 Makran tsunami. Current Science 95, 1739-1743.

Réhault, J-P., Béthoux, N., 1984. Earthquake Relocation In The Ligurian Sea (Western Mediterranean): Geological Interpretation. Marine Geology 55, 429-445.

Ring, U., Brachert, T., Fassoulas, C., 2001. Middle Miocene graben development in Crete and its possible relation to largescale detachment faults in the southern Aegean. Terra Nova 13, 297-304.

Rollet, N., Déverchère, J., Beslier, M-O., Guennoc, P., Réhault, J-P., Sosson, M., Truffert, C., 2002. Back arc extension, tectonic inheritance, and volcanism in the Ligurian Sea, Western Mediterranean. Tectonics 21, 1015, doi: 10.1029/2001TC900027.

Ryan, W.B.F., 2009. Decoding the Mediterranean salinity crisis. Sedimentology 56, 95-136.

Savoye, B., Piper, D.J.W., 1991. The Messinian event on the margin of the Mediterranean Sea in the Nice area, southern France. Marine Geology 97, 279-304.

Schwab, W.C., Danforth, W.W., Scanlon, K.M., 1993. Tectonic and Stratigraphic Control on a Giant Submarine Slope Failure: Puerto Rico Insular Slope. In: Schwab, W.C., Lee, H.J., Twichell, D.C. (Eds.), Submarine Landslides: Selected Studies in the U.S. Exklusive Ecnomic Zone. USGS Bulletin 2002, pp. 60-68.

Seibold, E., Hinz, K., 1974. Continental slope construction and destruction, West Africa. In: Burk, C.A., Drake, C.L. (Eds.), The geology of continental margins, Springer-Verlag, New York, pp. 179-196.

Shanmugam, G., 2000. 50 years of the turbidite paradigm (1950s – 1990s): deep-water processes and facies models - a critical perspective. Marine and Petroleum Geology 17, 285-342.

Shanmugam, G., 2009. Slides, Slumps, Debris Flows, and Turbidity Currents. In: Steele, J. H., Thorpe, S.A., Turekian, K.K. (Eds.), Ocean Currents, 2 Edition, Elsevier, pp. 418-467.

Sodoudi, F., 2005. Lithospheric structure of the Aegean obtained from P and S receiver functions. PhD-Thesis, FU Berlin, Germany, 166pp.

Stegmann, S., Kopf, A., 2007. Marine Deep-Water Free-Fall Cpt Measurements For Landslide Characterisation Off Crete, Greece (Eastern Mediterranean Sea) Part 1: A New 4000M Cone Penetrometer. In: Lykousis, V., Sakellariou, D., Locat, J. (Eds.), Advances in Natural and Technological Hazards Research, 1, Volume 27, Submarine Mass Movements and Their Consequences 3, Springer, pp. 171-177.

Stiros, S.C., 2001. The AD 365 Crete earthquake and possible seismic clustering during the fourth to sixth centuries AD in the eastern Mediterranean: A review of historical and archaeological data. Journal of Structural Geology 23, 545– 562.

Stow, D.A.V., Mayall, M., 2000. Deep-water sedimentary systems: New models for the 21st century. Marine and Petroleum Geology 17, 125-135.

Strozyk, F., 2009. Submarine landslides in active margin environments – Slope stability vs. neotectonic activity on the northeastern margin of Crete, eastern Mediterranean. PhD-Thesis, University of Bremen, Germany, 138pp.

Sultan, N., Cochonat, P., Canals, M., Cattaneo, A., Dennielou, B., Haflidason, H., Laberg, J.S., Long, D., Mienert, J., Trincardi, F., Urgeles, R., 2004. Triggering mechanisms of slope instability processes and sediment failures on continental margins: a geotechnical approach. Marine Geology 213, 291-321.

Tahchi E., Urgeles, R., Hübscher, C., Benkhelil, J., 2010. Mass Wasting at the Easternmost Cyprus Arc, Off Syria, Eastern Meditterranean. In: : Mosher, D.C., Shipp, C., Moscardelli, L., Chaytor, J., Baxter, C., Lee, H., Urgeles, R. (Eds.), Submarine Mass movements and their consequences IV. Advances in Natural and Technological Hazards Series 28, Springer, pp. 323-334.

Tappin, D.R., Watts, P., McMurtry, G.M., Lafoy, Y., Matsumoto, T., 2001. The Sissano, Papua New Guinea tsunami of July 1998 – offshore evidence on the source mechanism. Marine Geology 175, 1-13.

Tappin, D.R., Watts, P., Grilli, S.T., 2008. The Papua New Guinea tsunami of 17 July 1998: anatomy of a catastrophic event. Natural Hazards Earth System Sciences 8, 243-266.

Tari, G., Molnar, J., Ashton, P., 2003. Examples of salt tectonics from West Africa: a comparative approach. In: Arthur, T., Macgregor, D.S., Cameron, N.R. (Eds.), Petroleum Geology of Africa: New Themes and Developing Technologies. Geological Society, London, Special Publications 207, pp. 85-104.

Terzaghi, K., 1943. Theoretical Soil Mechanics. John Wiley & Sons, New York, 510pp.

Thomas, S., Hooper, J., Clare, M., 2010. Constraining Geohazards to the Past: Impact Assessment of Submarine Mass Movements on Seabed Developments. In: Mosher, DC., Shipp, C., Moscardelli, L., Chaytor, J., Baxter, C., Lee, H., Urgeles, R. (Eds.), Submarine Mass movements and their consequences IV. Advances in Natural and Technological Hazards Series, Springer, pp. 387-398.

Vanneste, M., Mienert, J., Bünz, S., 2006. The Hinlopen Slide: a giant, submarine slope failure on the northern Svalbard Margin, Arctic Ocean. Earth and Planetary Science Letters 245, 373–388

Winkelmann, D., Geissler, W., Schneider, J., Stein, R., 2008. Dynamics and timing of the Hinlopen/Yermak Megaslide north of Spitsbergen, Arctic Ocean. Marine Geology 250, 34-50.

Wissmann, G., 1982. Stratigraphy and Structural Features of the Continental Margin Basin of Senegal and Mauritania. In: von Rad, U., Hinz, K., Sarntheim, M., Seibold, E. (Eds.), Geology of the Northwest African Continental Margin, Springer, pp. 160-181.

Wynn, R.B., Masson, D.G., Stow, D.A.V., Weaver, P.P.E., 2000. The Northwest African slope apron: a modern analogue for deep-water systems with complex seafloor topography. Marine and Petroleum Geology 17, 253-265.

Wynn, R.B., Talling, P.J., Masson, D.G., Stevenson, C.J., Cronin, B.T., Le Bas, T.P., 2010. Investigating the Timing, Processes and Deposits of One of the World's Largest Submarine Gravity Flows: The 'Bed 5 Event' Off northwest Africa. In: Mosher, DC., Shipp, C., Moscardelli, L., Chaytor, J., Baxter, C., Lee, H., Urgeles, R. (Eds.), Submarine Mass movements and their consequences IV. Advances in Natural and Technological Hazards Series, Springer, pp. 463-474.

Zühlsdorff, C., Wien, K. Stuut, J.B.W., Henrich, R., 2007. Late Quaternary sedimentation within a submarine channel-levee system offshore Cap Timiris, Mauritania. Marine Geology 240, 217-134.

Appendix Part A

Makran Accretionary Prism – data report

In the framework of the thesis the PhD student participated in several research cruises (Section 1.2). One of them was the RV Meteor cruise M74/2 at the Makran Accretionary Prism in front off the Pakistan coast. For the Meteor Report 10-3 (Bohrmann et al., 2010) the PhD student made a contribution to the chapter of the Geotechnical measurements.

The following chapters give a short overview of the cruise objectives, a summary of the geotechnical measurements chapter of Bohrmann et al. (2010) and a discussion of the mechanical behaviour of the sediments and possible trigger mechanisms for the sediment instabilities at the research area at the Makran Accretionary Prism:

1. Introduction

The RV Meteor cruise M74/2 was part of the DFG and BMBF funded project “Nitrogen Cycle, Cold Seeps, Carbonate Platform Development in the Northwestern Indian Ocean” and also sited in the framework of the DFG funded RCOM project area “Fluid and Gas Seepage at Ocean margins”. The scientific goals of the cruise M74/2 were to investigate cold seeps and mapping of vent-related structures at the Markran Accretionary Prism (Fig. 10) with geophysical methods including deep-tow sidescan sonar (TOBI), sediment echosounder and high-resolution multi-channel seismic.A second objective was to understand the role of the Oxygen Minimum Zone on the Accretionary margin (Bohrmann et al., 2010). Besides the geophysical methods, water-, gravity- and multicurrency samples were taken to confirm the intuition of the cruise.

Additionally, a second cruise (M74/3; Bohrmann et al., 2008, 2010) was performed to identify active and recent fluid vents based on the results of M74/3.

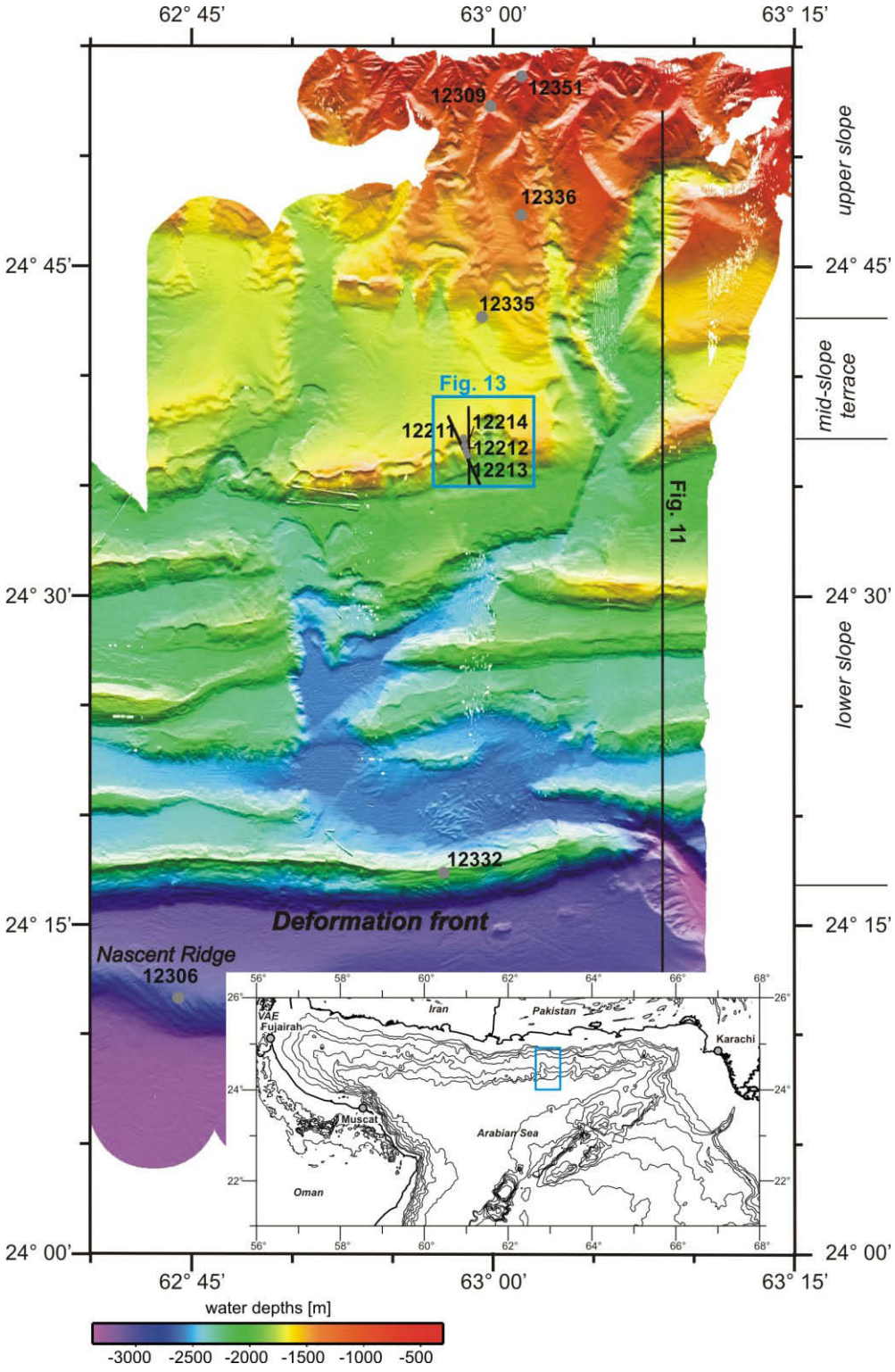

Fig. 10 Bathymetric map of the study area with dedicated core locations of cruise M74/2 and M74/3 in water depths ranging from 450 m to >3000 m (modified after Bohrmann et al., 2010). Small map: Map of the Arabian Sea with the study area indicated by the blue box.

The working area of both cruises is located at 24°-25° N and 62°40' - 63°15' E (Fig. 10) on the Accretionary Prism off the Makran subduction zone, where the Arabian plate is subducted beneath the Eurasian plate with an angle of <2°. The subduction process started at the Cretaceous and is still ongoing with a convergence rate of 4 cm/a (DeMets et al., 1990). At the deformation front a sediment pile of thickness > 7 km was created by terrigenous sediment input (0.5-0.93 m/ka) and limited the formation of a trench. In the study area of the Makran Accretionary Prism the oceanic plate reveals water depths >3000 m. The continental slope can be divided into three sections (Kukowski et al., 2001; Huhn, 2002):

i) the lower slope with slope angles of 2°-4° affiliated to the deformation front consisting of a numbers of imbricate thrust ridges with E-W orientated long parallel sequences and steep flanks. The first ridges rise ~ 1000 m above the oceanic plate, while the other ridges become shallower in elevation towards north. In front of the first ridge recent and still ongoing development of a new accretionary ridge (Nascent Ridge) can be observed (Fig. 11), where the ongoing main deformation will be marked.

ii) the transition to the upper slope is marked by the nearly flat mid-slope terrace (~1°). The western part in the study area is about 25 km wide.

iii) the upper slope with slope angles up to ~8° comprise a rough seafloor topography with several gullies, canyons and evidences of landslides. Figure 11 illustrates a seismic profile crossing the lower, middle and upper slope. Sediment ridges, canyons and subsidence basin structures could be observed as main elements. Within the research area, six sediment ridges were definable for dedicated studies of seepage and slope instabilities (Bohrmann et al., 2010).

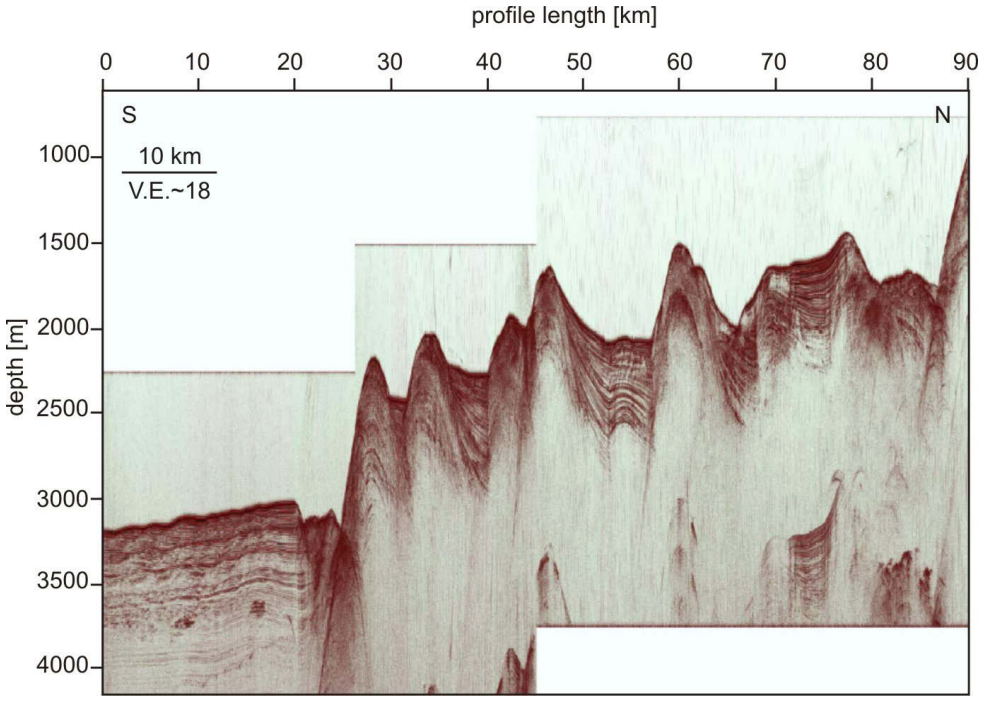

Fig. 11 Seismic profile crossing the upper, middle and lower slope with sedimentary ridges, canyons and subsidence basins (modified after Bohrmann et al., 2010).

The intention of the PhD student to participate to the cruise M74/2 was to recover some material from landslides. In the transition zone of the lower slope to the mid-slope terrace four cores were recovered from a slump location (Fig. 10). Along the transition zone several slumps and slides were recognized but the location were chosen after the availability of different potential trigger mechanisms such as gassy layers and a retrogressive development of a canyon. For comparison of the sediments from the transitional zone, dedicated geotechnical tests were performed on sediments of the upper and the lower slope from Meteor cruise M74/3 (Bohrmann et al., 2008; 2010).

2. Methods

Before start sediment coring TOBI, bathymetric, parasound and reflection seismic data were used to figure out slump locations. Along one of these slump structures 4 gravity cores with tube lengths of 6 m and 12 m and a weight of approximately 1.6 tons were used to obtain sediment cores. Each one gravity core was positioned in undisturbed sediment outside of the slump structure (GeoB12211), near the headwall (GeoB12214) and in the slump body (GeoB12212 and -12213; Tab. 4). After marking the orientation of cores on the liners, the tubes were cut on board into 1 m sections and split into two halves, one of which was stored as archive and the other used for sediment description, sampling, geotechnical tests, etc. Pore water from the undisturbed sediment was sampled after the geotechnical measurements by using the Rhizon technique (Seeberg-Elverfeldt et al., 2005) and a pore water squeeze.

Table 4 Station list of the gravity cores using in this study. The first four cores were taken from the slump structure inside the Makran Accretionary Prism at cruise M74/2. Cores from the upper and lower slope were taken during cruise M74/3 (Borhmann et al., 2008, 2010).

Station	Longitude	Latitude	water depth	recovery	comment
GeoB12211	24 37.245' N	62 58.52' E	1613 m	576 cm	undisturbed
GeoB12212	24 36.644' N	62 58.63' E	1758 m	562 cm	slump, upper part
GeoB12213	24 36.451’ N	62 58.71' E	1833 m	474 cm	slump, lower part
GeoB12214	24 36.899' N	62 58.57' E	1728 m	248 cm	headwall
GeoB12306	24 11.761’ N	62 44.31’ E	2861 m	380 cm	lower slope
GeoB12309	24 52.301’N	62 59.87’E	956 m	560 cm	upper slope
GeoB12332	24 17.482’ N	62 57.59’ E	2036 m	587 cm	lower slope
GeoB12335	24 43.10’ N	62 59.51’ E	1594 m	445 cm	upper slope
GeoB12336	24 47.777’ N	63 01.47’ E	1263 m	447 cm	upper slope
GeoB12351	24 53.65’ N	63 01.41’E	592 m	322 cm	upper slope

2.1 Sediment description

Split gravity cores were described from a largely sedimentological standpoint. Grain size, composition and colour of sediments were determined mainly visually using a simple hand-lens and HCl-testing. The size of grains was assessed based on Wenthworth’s (1922) classification. For each core, a composite core log sheet was compiled. It shows a graphical core log and gives

information on redeposition-/event layers and the assigned lithological units. The core log is combined with the undrained shear strength, S_u, and the sediment physical property values (see below). A wide variety of features, such as sediment lithologies, primary sedimentary structures and soft-sediment deformation is indicated by patterns and symbols in the graphic logs (Fig. 12). All core descriptions are provided in Chapter 6 (see below). The cores GeoB12332, -12335 and -12336 were not opened, so that a sediment description is absent.

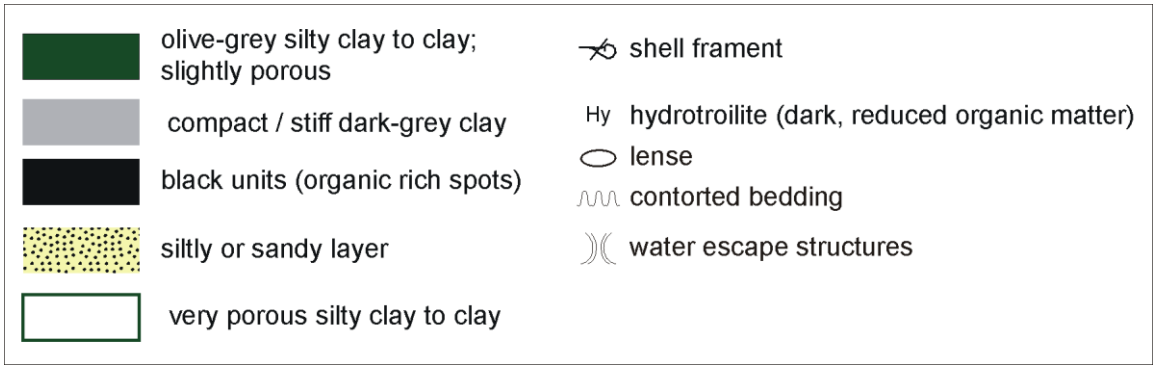

Fig. 12 Graphic log of the full set of patterns and symbols used on the barrel sheets. The symbols are schematic, but they are placed as close as possible to their proper stratigraphic position.

2.2 Physical Properties

Since a Multi-Sensor Core Logger (MSCL) was not available on board RV Meteor, the determination of the sediment physical properties (e.g. bulk density, p-wave velocity, porsosity, magnetic suszeptibility) was to be carried out on the undisturbed archive half of the cores after the cruise in Bremen. Also, during the cruise geotechnical measurements were restricted to falling cone penetration tests on the working half of the four gravity cores from the slump structure. For that, a Wykeham-Farrance cone penetrometer was used for a first-order estimate of the sediment's stiffness. The sample interval was every 5 cm. For the measurements the cone was brought to point on the core surface. A manual displacement transducer was used to measure the distance prior to and after release of the cone and so the penetration depth can be measured. Then the undrained shear strength, S_u, can be calculated from the variables mass (in this case 80.51 g) and tip angle of the falling cone (in this case 30°), gravity *g*, penetration depth *d* and the "cone factor" *k*. Wood (1985) calculated from fall cone test average values of cone factors (30° cone → $k = 0.85$). S_u can then be calculated using equation 2.1:

$$S_u = (k*m*g)/d^2 \quad (2.1).$$

2.3 Oedometer tests

To characterize the consolidation state of the headwall sediments (GeoB12214), oedometer tests were performed on different depths of the core at normal stresses up to 1500 kPa. The maximum stress, the sediments experienced previously (pre-consolidation pressure, σ_{pc}), was determined after Casagrande (1936). With the overconsolidation ratio (OCR), which is

defined as the ratio of the pre-consolidation stress, σ_{pc}, and the vertical effective stress, σ_{eff}, (equation 2.2) the recent consolidation state of the sediments could be estimated:

$$OCR = \sigma_{pc} / \sigma_{eff} \quad (2.2).$$

3. Slump of the transitional zone

3.1 Results

3.1.1 Sediment description

The area between 24°38'N / 62°58'E and 24°36'N / 62°59'E and water depths of 1500 - 2000 m was selected for gravity coring (Fig. 13). In this area a very steep slope appears in the bathymetric chart. We interpreted the structure from 24°36.89'N / 62°58.52'E to 24°36.89'N / 62°58.71'E as one slump scar (position of core GeoB12214 in Figs. 13 and 14).

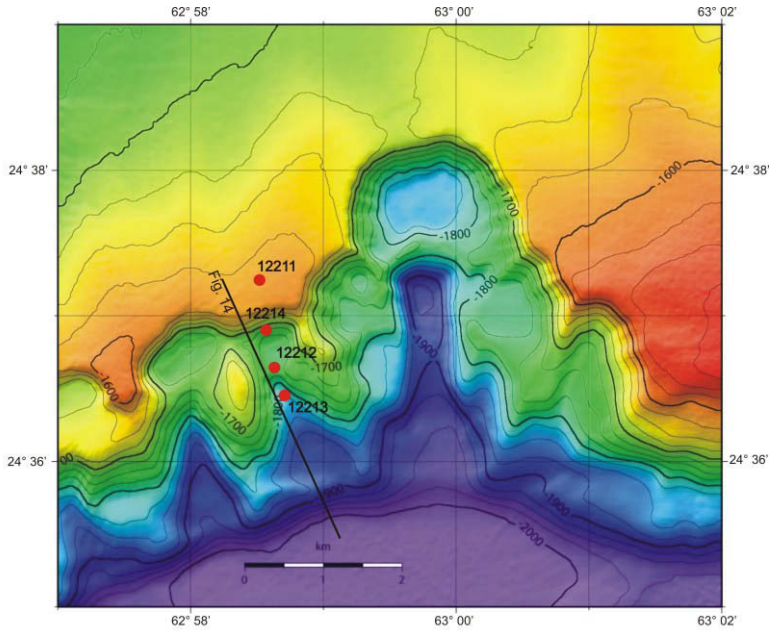

Fig. 13 Bathymetric map with conour lines of the researched slump body with core locations in water depths of 1500 to 2400 m.

The seismic profil crossing the head scar (Fig. 14), demonstrates the complexity of the study area at the transitional zone. The assumed slide body as imaged in Figure 14 is not very clear to identify due to side echoes and non implementation of the seismic profil. Also no glide plane is visible in the seismic data but the scarp of the headwall can be approximated with a height of 50-60 m.

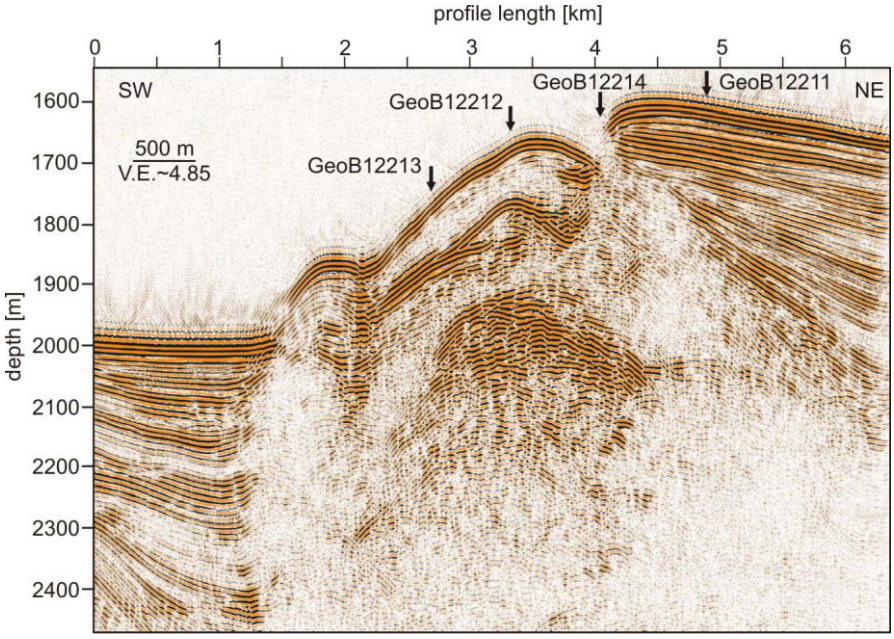

Fig. 14 Stacked seismic line GeoB07-345 (profil line Fig. 12) with core positions of the slump structure (Bohrmann et al., 2010).

The sediments, which were recovered, are dominated by lightly porous olive-grey silty-clay to clay. The facies is typically fine to medium grained and ranges from homogenous to mottled. There was a strong sulphured smell after opening all of the cores, indicating the absence of methane in the sediment, because methane and sulphur do not coexist in the same sediment depth (Whiticar, 1999). The two cores of the slump body (GeoB12212 and GeoB12213) look very similar. Between the silty-clay deposits, silty to sandy layers with clay lenses are found frequently. There are several minor redeposited intervals (1 cm thick sandy layers) that contain considerable amounts of shell fragments. The erratic clay lenses in the slump body cores hint to remobilization in a different way. In particular the sediment of the lower part of the slump body shows leakages filled with liquid (water and sediment). These observations indicate that the sediments were relocated and later deposited in a different way. In the cores of the upper part of the slump body and the headwall, organic-rich layers occur more frequently than in the lower

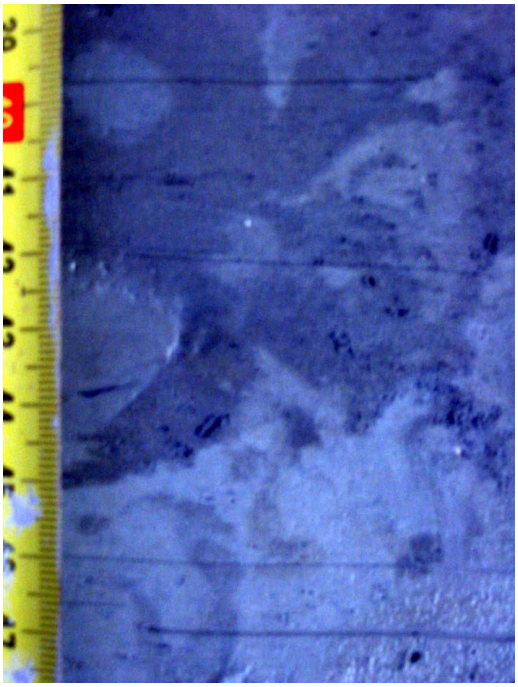

Fig. 15 Remobilization area of core GeoB12214 (97-104 cm) to show the features (Bohrmann et al., 2010).

part of the slump body. The only evidence for a real sediment remobilization along the head scarp is identified in core GeoB12214 (Fig. 14), which was recovered immediately below the scarp. Figure 15 shows a layer consisting of stiff, light-coloured clasts in a darker silty-clay matrix, and reversed

3.1.2 Geotechnical tests

The reference core (GeoB12211) comprises silty clay to clayey mud with several coarser layers and organic carbon rich spots. Bulk density increases slightly downward from ~1.8 g/cm^3 to 2 g/cm^3, while the magnetic suszeptibility is more ore less constant ~ 10x10^{-5} SI excepeted between 1.8-3 m core depth (increase up to 38x10^{-5} SI; Ch. 6). In this segment a higher input of magneitic minerals is assumed. Clay minerals such as montmorillionite have magnetic suszeptibility values of 28x10^{-5} SI, while quarz posess diagmagnitc properties with negative magnetic suszeptibility values of -1.59x10^{-} SI (Müller, 2004). S_u values with a linear increase from 5 kPa to 200 kPa show relatively high initial values for strong stiffness. Locations of 250 kPa correlate with the position of coarser layers (Ch. 6). Following Ladd et al. (1977) the S_u/σ_n-values were calculated with a S_u/σ_n-ratio of 0.2-0.5 for normally consolidated sediments. The sediments of the reference core are mostly normally consolidated with S_u/σ_n-values of 0.2-0.6, while layers with higher values were found (Fig. 16). This layers correlates with the appearance of sandy layers and shell fragments (Ch. 6).

The slump body could be separated in three different parts:

a) the upper part (GeoB12212) consists of silty clay to clayey mud with several coarser layers, clay lenses and organic carbon rich spots. Bulk density values behave equal as the values from the reference core with a slightly increase from ~1.75 g/cm³ to 2 g/cm³ with depths. Similar to the undisturbed sediments, the magnetic suszeptibility shows higher values of 35x10^{-5} SI for the sediemnts layers between 2.4 and 3 m. A higher content of paramagnetic minerals in the clay fraction can be the reason for this increase. The undrained shear strength S_u shows a slightly linear increase from 5 kPa to 100 kPa. Locations of 220 kPa to 420 kPa correlate with the position of coarser layers. Organic carbon-rich spots and isolated clay lenses are reflected in S_u with lower values all over the core (Ch. 6). Generally, the recovered sediments of GeoB12212 are normally consolidated with S_u/σ_n-values of 0.2-0.55 (Fig. 16).

b) the lower part of the slump body comprises also silty clay to clayey mud with several coarser layers, clay lenses and organic carbon rich spots. In contrast to the sediments of the upper slump body, the recovered sediments of GeoB12213 shows overconsolidation (Fig. 16) in areas of the cores with S_u/σ_n-values from 0.6 to 1.25 (1.15-1.5 m core depth) and from 1.1 to 1.5 (3.1-3.4 m core depth). This high values correlate with the appearance of eratic shell fragments. Furthermore, for the layers between 1.15-1.5 m porous layers of silty clay were observed. S_u-values show a slightly logarithmic increase from 5 kPa to 200 kPa. Below 260 cm core depth, the values decrease to 20 kPa and increase up to 200 kPa until 350 cm. In the last 70 cm the S_u-values are more or less stable around 30 kPa. The bulk density values reflect an equal trend as the S_u-values with an increase to 2.02 g/cm³ in the first 150 cm. Subjacent, the bulk density values are lowered but more or less constant ~1.95 g/cm³. Magnetic suszeptibilty is constant over the whole sediment core length with values of ~1x10^{-6} SI (Ch. 6).

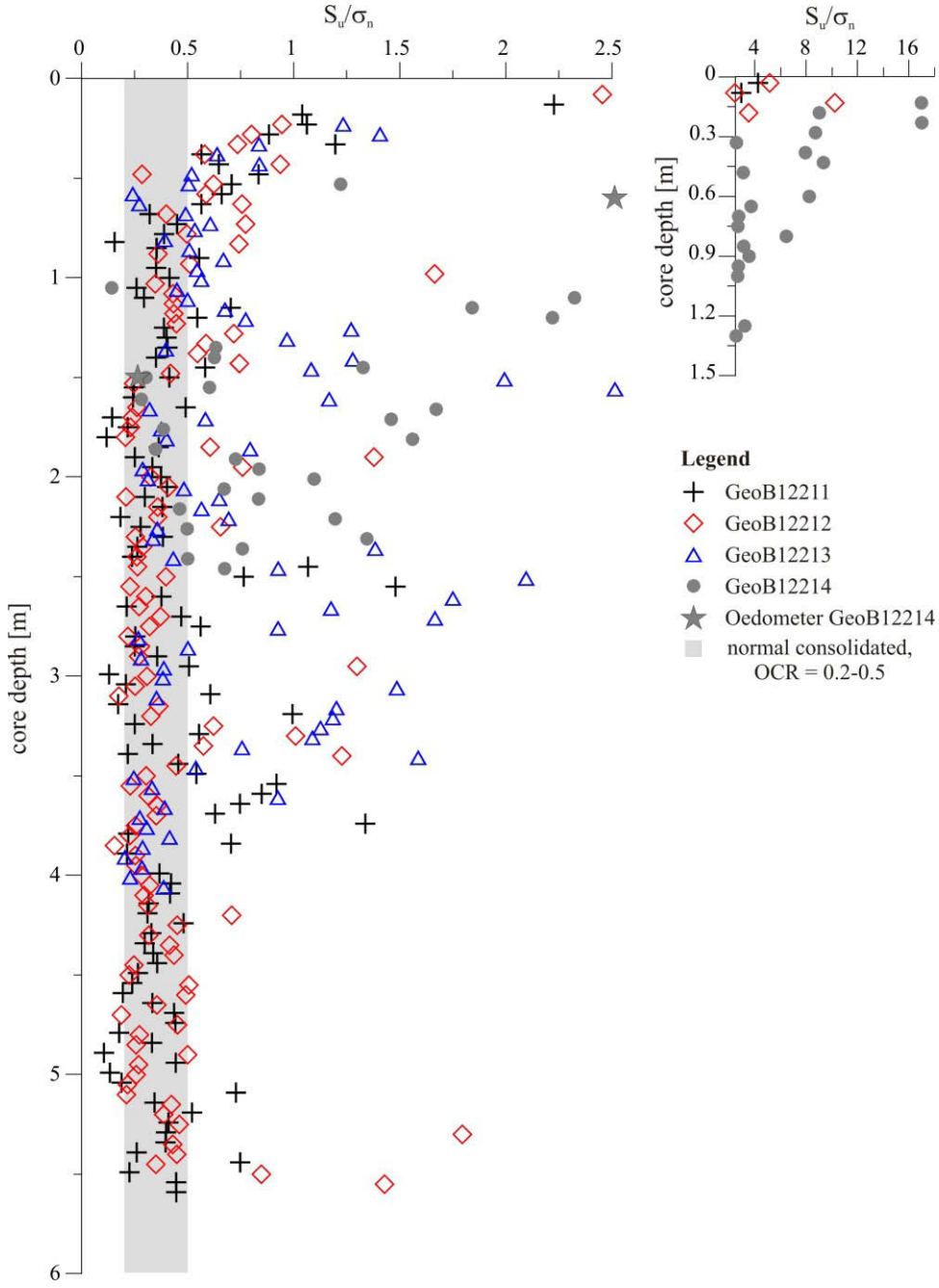

Fig. 16 S_u/σ_n-values as an indicator of the consolidation state of the sediments (after Ladd et al., 1977) from the slump location. S_u/σ_{pc} were estimated from oedometer tests for headwall sediemnts (GeoB12214). For calculation of σ_{pc} refer to Chapter 2.3.

c) sediments taken from the headwall area (GeoB12214) show a silty clay to clayey mud composition with several coarser layers, clay lenses and organic carbon rich spots. Similar to the sediments of the lower part of the slump region, the magnetic suszeptibilty is constant with values of ~$10x10^{-5}$ SI. Instead, the bulk density values are higher than its values determined in the slump body sediments. For the first 80 cm the bulk density values show a slightly increase from 1.92 g/cm³ to 1.98 g/cm³. Below that, two instinct jumps could be observed: i) in 80 cm to 2 g/cm³ and ii) in 170 cm to 2.1 g/cm³ followed by a slight decrease of the bulk density to 2.02 g/cm³

(Ch. 6). Instead, S_u-values show no visible trend. The values jump from 20 kPa to 350 kPa within the first 90 cm. Locations of 480 kPa correlate with the position of coarser layers. The sediments of the first 90 cm are stiffer than that from other cores. The S_u-values at 120 cm decrease from 180 kPa to 80 kPa. This decrease correlates with increasing clay content. Furthermore, S_u/σ_n-values show a strong overconsolidation (Fig. 16) but decreases from 16 to 0.5 from the top of the core down to ~200 cm. The remobilization area is reflected in the lowest S_u/σ_n-values (0.22-0.25) of the whole core. To characterize the consolidation history of the different sedimentological units (Ch. 3.1.1) oedometer tests were performed on samples from each unit (Tab. 5). Furthermore, after Cochonat et al. (1993) S_u/σ_{pc}-values were calculated to minimize the effect of "apparent" overconsolidation. The upper unit (0.60 m) shows a high overconsolidation value (OCR) with 3.28 and a high S_u/σ_{pc}-value of 2.51 that may reflect relocated sediments. Instead, the lower sediment unit is more or less normally consolidated with an OCR value of 1.14 a S_u/σ_{pc}-value of 0.27 (Fig. 16, Tab. 5).

Table 5 Results of the oedometer tests performed in sediments of the headwall core GeoB12214. For calculation of OverConsolidation Ration (OCR) see equation 2.2.

Sample	depth [m]	σ_{pc} [kPa]	σ_n [kPa]	OCR	S_u/σ_{pc}
GeoB12214	0.60	38.42	11.71	3.28	2.51
	1.50	34.11	29.74	1.14	0.27

3.2 Discussion

3.2.1 Mechanical behaviour of the sediments of the landslide at the transitional zone

For the superficial sediments in all sampled cores the Su/σ_n-values indicate overconsolidation (Figs. 16 and 17). This may a result of "apparent" overconsolidation (Sultan et al., 2000), which is often associated with physico-chemical processes (Ch. 3.1.1 and 3.2.1) and is typical for superficial sediments. In most of the sediment cores (GeoB12211, -12213, -12306, -12309 and -12351) the effect of the "apparent" consolidation decreases with depth and below 1 mbsf the sediments show normal consolidation (Su/σ_n=0.2-0.5). Instead, the recovered failed deposits of the lower part of the slump body (GeoB12213) are slightly or strong overconsolidated (Su/σ_n=0.6-2) with high S_u-values up to 200 kPa in 1.6 mbsf and 250 kPa in 2.5 mbsf. Also, bulk density values increase up to 2.02 g/cm³ in 1.5 mbsf (Ch. 6). These stiff sediments with high bulk density values may be a result from removal of overlying sediments by mass wasting.

Further upslope, at the headwall location GeoB12214, a sharp contact between two sedimentological units (dark green clay in oblique contact with light grey clay) was observed in 0.9 mbsf, which can be characterized by a distinct excursion in S_u- and bulk density values (Ch. 6). The overhead dark green sediments are strongly overconsolidated (OCR=3.28), while the underlying light grey sediment unit is normal to slightly overconsolidated (OCR=1.14). For the overconsolidated sediments we could estimate a missing sediment sequence of ~2.7 m for the upper part of the headwall material. Furthermore, we observed dark green clay lenses in the

underlying light grey clay, which may give indications of sediment remobilization. These observations may be explained by the hypothesis that during remobilization a block of older sediments unroofed recent hemipelagic sediments.. Another explaination may be that by a skewed penetration of the steel barrel (Ch. 2) into the sediments the sediment sequences can be reversed.

4.2 Potential trigger mechanisms

From active margins of the Mediterranean Sea it is known that high sedimentation rates on steep slopes may cause frequent sediment failures (Klaucke and Cochonat, 1999). For our study area, high sedimentation rates up to 1.2 m/ka (von Rad et al., 1999; Müller, 2004) were published. The slope angle varies from 6-8° in the transitional zone from the upper slope to the mid-slope terrace (Figs. 10 and 14). With an active uplift of 1.5 m/ka (Müller, 2004) the mid-slope terrace and upper slope rises and the slope angle will increase. This may result in oversteepening of the slope and lead with the high sediment input to sediment failures along the transitional zone. A second mechanism, which may cause oversteepening of the slope is undercutting by canyons. The bathymteric map (Fig. 10) shows a canyon system close to the study area. Kukowski et al. (2001) released that the canyons at the study area were formed by submarine turbidity currents and that the great depths of the canyons were also a result of the tectonic uplift. In several studies flow velocities of turbidity currents were published. Piper et al. (1999) estimated for the Grand Bank debris flow and turbidity current a flow velocity of ~28 m/s. An earthquake at the SW coast of Taiwan should have generated turbidity currents with flow velocities of 20 m/s for the steep slope and of ~4 m/s for the shallow slope (Hsu et al., 2008). In order to erode clay sediments critical medium erosion velocities of 0.5-8 m/s are required (Sundberg, 1956), depending on the consolidation state of the sediments and on the slope angle. Therefore it can be suggested that turbidity currents in the canyon may be strong enough to erode sediment from the canyon flanks. However, this assumption is uncertain, because Kukowski et al. (2001) pointed out that recent no erosion can be observed in the upper course of the canyon. But there are still evidences for some older erosional events in the canyon (Kukowski et al., 2001; Bourget et al., 2011).

Furthermore, some preconditioning factors may also be sufficient for sediment instabilities. Along the transitional zone of the lower slope and the mid-slope terrace (Fig. 10) several indications of methane gas/fluid seepage were observed by Bohrmann et al. (2008; 2010). The recovered sediments comprise mostly clay sediments (Ch. 3.1.1), which may act as a suppressor for gas or fluid migration and can led to excess pore pressure (Kayen and Lee, 1991). If the gas migration is not widespread, excess pore pressure may propagate and weak layers may evolve into sliding surfaces. Our geotechnical measurements did not comprehend the determination of the friction behaviour of the sediments. Hence, the presence of weak layers can not be excluded as a potential trigger mechanism for the landslide.

4. Reference sites at the lower and upper slope

The locations of the cores recovered at the lower and the upper slope can be taken from Figure 10 and Table 4. In general the sediment cores were recovered for analyses of gas hydrates (Bohrmann et al., 2008). The sediment description is limited to the cores GeoB12306, -12309 and -12351, because the other cores are not splitted already. The sediments from the upper slope (GeoB12309- and 12351) consist of finely laminated clay with organic-rich and terrigeneous dominated lamina. The different lamination may preserve different climate and sediment

transport conditions (for more details regard to Bohrmann et al., 2008). The facies of the sediment cores recovered at the Nascent Ridge (GeoB12306, Fig.10) is dominated by homogenous, slightly mottled clays with a low content of biogenic components. After opening the core a strong sulphured smell indicates the absence of methane and gas-hydrate bearing sediments.

Because the sediments and their geotechnical properties may be affected by their location, the results of the geotechnical tests and the determination of sediment physical properties are arranged in groups after the location of the sediments:

a) from 590-950 m water depth (GeoB12309 and -12351): the sediments consists of silty clay to clayey mud with several organic spots. The bulk density values increase from 1.62 g/cm³ to ~1.8 g/cm³ (in 3 m core depth). For core GeoB12309 a progressive increase can be oberserved up to 1.97 g/cm³ in 5.5 m core depth. The sediments of core GeoB12309 are more or less overconsolidated with S_u/σ_{pc}-values of 0.25-7. Instead, the sediments from GeoB12351 just show overconsolidation for the upper 100 cm of the sediments (Fig. 17). The magnetic suszeptibility as an indicator of changes in paleoclimate or environmental conditions (Müller, 2004, and references therein) provides information for a higher content of ferromagnitc particles in the sediments. This was observed for core GeoB12351 in the sediment layers from 1.8-2.6 m (~$15x10^{-5}$ SI), which can be correlated with higher bulk density values (Ch. 6). Instead in core GeoB12309 lowered magnetic suszeptibility (~$1x10^{-5}$ SI) was observed between 0.7 m and 1.6 m, which can be an indication for a higher content of quarz minerals (diagmagnitc properties with negative magnetic suszeptibility values).

b) from 1250-2000 m water depth (GeoB12332, -12335 and - 12336): all three cores were not opend during the cruise or for labortory measurements so that a correlation of the sediment physical properties and the sediment description can not be done. Undrained shear strength values were also not be taken. Bohrmann et al. (2008) recovered the cores from background stations, so that that the sediment may represent hemipelagic sedimentation. The bulk density values show for all cores a slight linear increase from 1.6 g/cm³ to ~1.82 g/cm³. Magnetic suszeptibility is more or less constant with values of ~15-$18x10^{-5}$ SI, except the sediemnts of core GeoB12335 between 3-3.35 m and of core GeoB12332 between 0.4-0.8 m core depths. In both sediments segments an increase of magnetic suszeptibility values to $30x10^{-5}$ SI was obsereved and can be an indication for a higher content of ferromagnitc particles such as illite or montmorillonite (Müller, 2004). Unlike core GeoB12351 from the lower water depth, an incease of the magnetic suszeptibility can not be correlated with higher bulk density values (Ch. 6).

c) 2850 m water depth (GeoB12306): the sediments consist of homogenoeus slightly mottled greenish clay. Due to the presence of biogenic components the sediments show some slight sandy intervals (Bohrmann et al., 2008). Bulk density increases slightly downward from ~1.45 g/cm^3 to 1.78 g/cm^3, while the magnetic suszeptibility is more ore less constant ~ $10x10^{-5}$ SI (Ch. 6). The undrained shear strength, S_u, shows a slightly linear increase from the surface to 3 m core depth (5 kPa to 50 kPa). Below 3 m core depth, heighten S_u-values of 140 kPa can be correlated with the position of coarser layers and a higher content of shell fragments. The core was recovered at the Nascant Ridge but shows in gerneal the same consolidation state as

the sediments from the upper slope (GeoB12309). For the upper 2 m of the core S_u/σ_n-values reflect an overconsolidation state with decreasing values from 11 to 0.6. Below 2 m the sediments are generally normally consolidated with S_u/σ_n-values from 0.2-0.5 (Fig. 17).

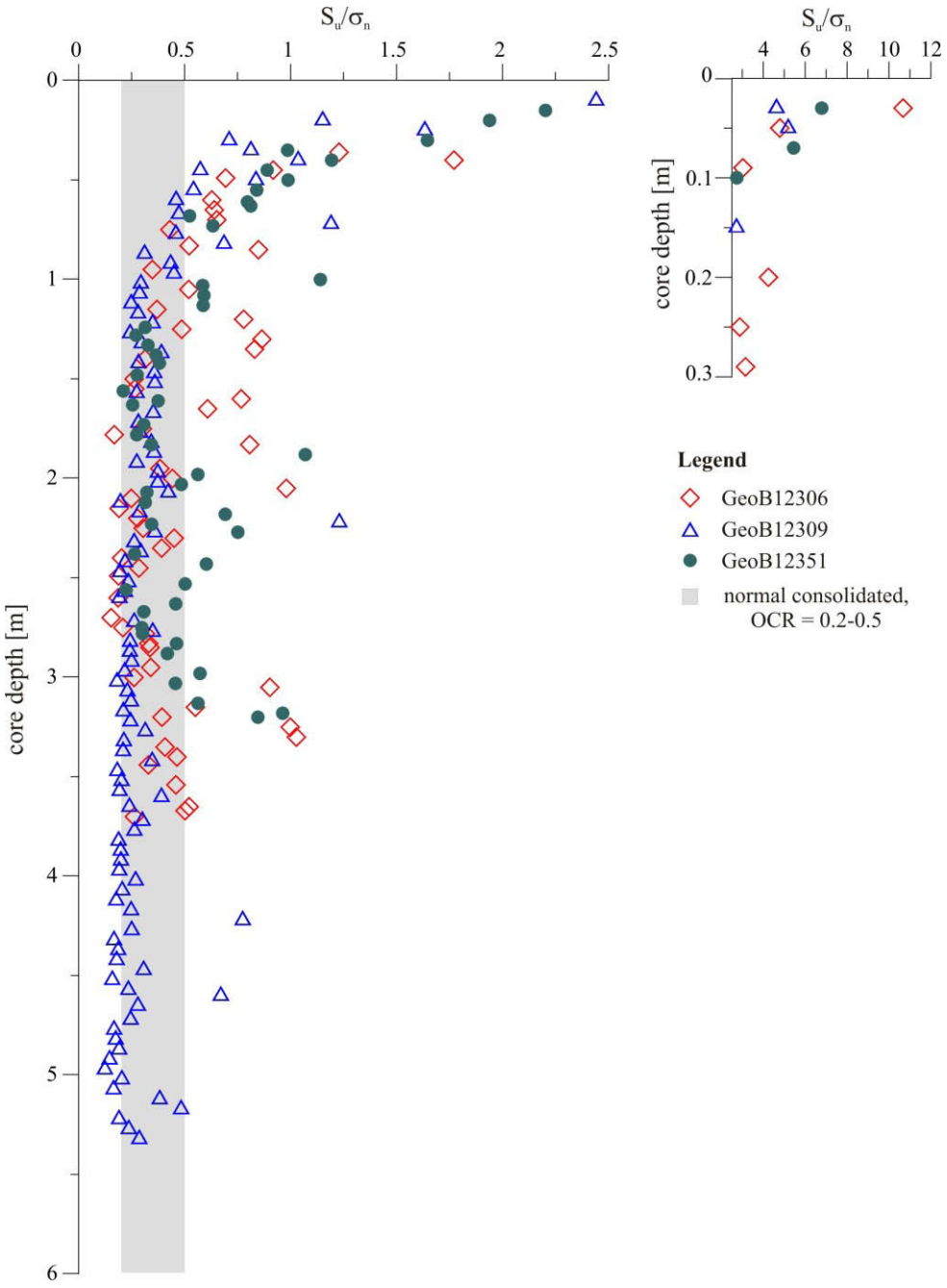

Fig. 17 S_u/σ_n-values as an indicator of the consolidation state of the sediments (after Ladd et al., 1977) from the referecne sites. For position of the cores refer to Fig. 1.

5. References

Bohrmann, G. and cruise participants, 2008. Report and preliminary Results of R/V Meteor Cruise M74/3, Fujairah – Male, 30 October – 28 November, 2007. Cold Seep Of The Makran Subduction Zone (Continental Margin of Pakistan). Berichte, Fachbereich Geowissenschaften, University of Bremen, 266, 161 p.

Bohrmann, G., Lahajnar, N., Gaye, B., Spiess, V., Betzler, C., 2010. Meteor Berichte 10-3, Nitrogen Cycle, Cold Seeps, Carbonate Platform Development in the Northwestern Indian Ocean, Cruise No. 74, August 31 – December 22, 2007, Heraklion (Greece) – Port Louis (Mauritius). Leitstelle Meteor/Merian, Hamburg, Germany, 214 pp.

Bourget, J., Zaragosi, S., Ellouz-Zimmermann, N., Mouchot, N., Garlan, T., Schneider, J.L., Lanfumey, V., Lallemant, S., 2011. Turbidite system architecture and sedimentary processes along topographically complex slopes: the Makran convergent margin. Sedimentology 58, 376-406.

Casagrande, A. 1936. The Determination of the Pre-consolidation Load and its Practical Significance. Proceedings of the 1st International Conference on Soil Mechanics and Foundation Engineering 3, 60-64.

Cochonat, P., Bourillet, J.F., Savoye, B., 1993. Geotechnical Characteristics and Instability of Submarine Slope Sediments, the Nice Slope (N-W Mediterranean Sea). Marine Georesources and Geotechnology 11, 131-151.

DeMets, C., Gordon, R.G., Argus, D.F., Stein, S., 1990. Current plate motions. Geophysical Journal International 101, 425-478.

Huhn, K., 2002. Analyse der Mechanik des makran Akkretionskeils mit Hilfe der Finiten und Diskreten Elemente Methode sowie analoger Sandexperimente.Dissertation, Scientific Technical Report STR02/02, GeoForschungsZentrum Potsdam, Germany, 160pp.

Hsu, S.K., Kuo, J., Lo, Ch.L., Tsai, Ch. H., Doo, W.B., Ku, Ch. Y., Sibuet, J.C., 2008. Turbidity Currents, Submarine Landslides and the 2006 Pingtung Earthquake off SWTaiwan. Terrestrial, Atmospheric and Oceanic Sciences 19, 767-772.

Kayen, R. E., Lee, H.J., 1991. Pleistocene slope instability of gas hydrate-laden sediment on the Beaufort Sea margin. Marine Georesources and Geotechnology 10, 125-141.

Klaucke, I., Cochonat, P., 1999. Analysis of past seafloor failures on the continental slope off Nice (SE France). Geo-Marine Letters 19, 245-253.

Kukowski, N., Schillhorn, T., Huhn, K., v. Rad, U., Husen, S., Flueh, E.R., 2001. Morphotectonics and mechanics of the central Makran accretionary wedge off Pakistan. Marine Geology 173, 1-19.

Müller, M., 2004. Rekonstruktion von Paläosäkularvariationen des Erdmagnetfeldes an holozänen marinen Sedimenten aus der Region des Makran Akkretionskeils. PhD-Thesis, University of Bremen, Germany, 151pp.

Piper, D.J.W., Cochonat, P., Morrison, M.L., 1999. The sequence of events around the epicentre of the 1929 Grand Banks earthquake: initiation of debris flows and turbidity current inferred from sidescan sonar. Sedimentology 46, 79-97.

Seeberg-Elverfeldt, J., Schlüter, M., Feseker, T., Kölling, M., 2005. Rhizon sampling of pore waters near the sediment/water interface of aquatic systems. Limnology and Oceanography 3, 361-371.

Sundberg, A., 1956. The River Klarälven: a study of fluid processes. Geografiska annaler 38, 127-316.

Von Rad, U., Schaaf, M., Michels, K.H., Schulz, H., Berger, W.H., Sirocko, F., 1999. A 5000-yr Record of Climate Change in Varved Sediments from Oxygen Minimum Zone off Pakistan, Northeastern Arabian Sea. Quaternary Research 51**,** 39-53.

Wentworth, C.K., 1922. A scale of grade and class terms for clastic sediments. Journal of Geology 30, 377-392.

Whiticar, M.J., 1996. Isotope tracking of microbial methane formation and oxidation. Mitteilungen der Internationalen Vereinigung für theoretische und angewandte Limnologie 25, 39-54.

Wood, D.M., 1982. Cone penetrometer and liquid limit. Géotechnique 32, 152-157.

6. Core log: Core descriptions, sediment physical properties and undrained shear strength

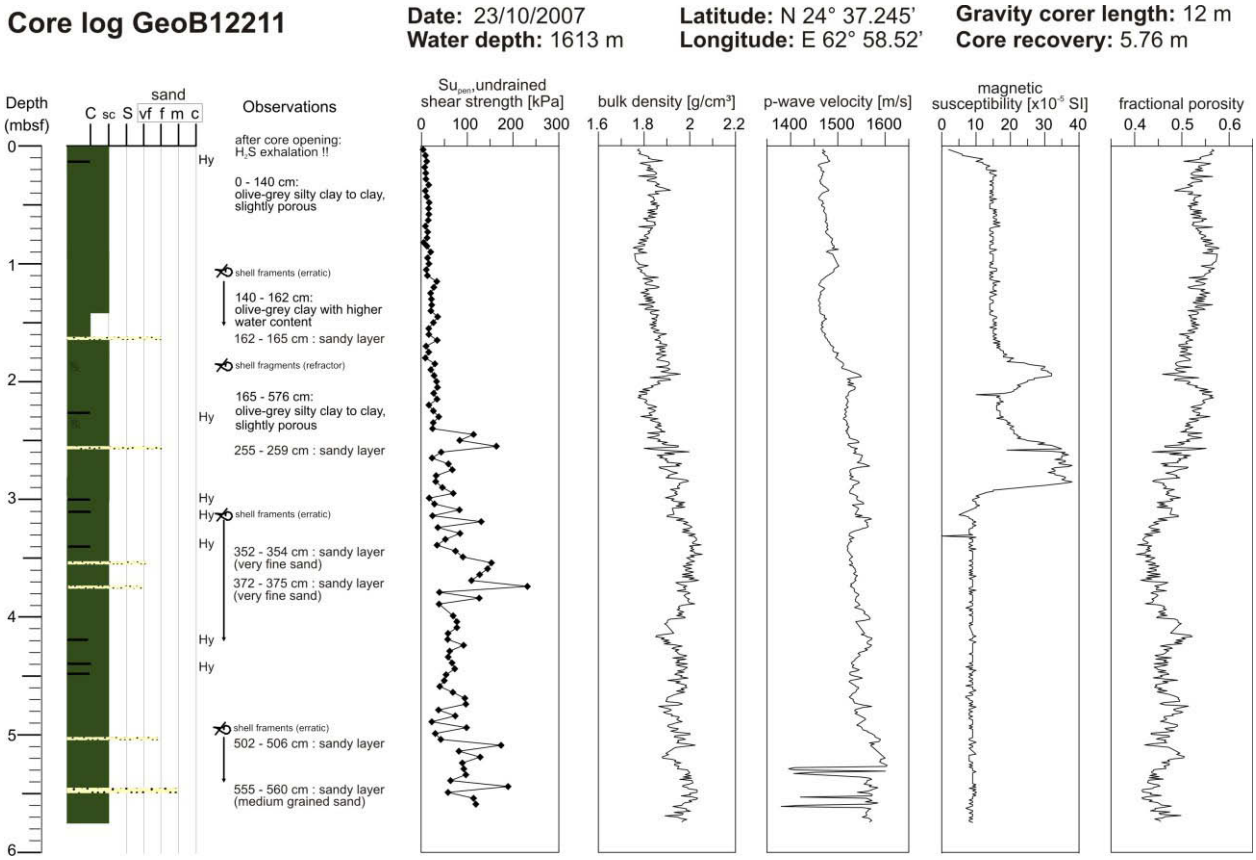

Core log GeoB12212

Date: 23/10/2007 **Latitude:** N 24° 36.644' **Gravity corer length:** 12 m
Water depth: 1758 m **Longitude:** E 62° 58.632' **Core recovery:** 5.62 m

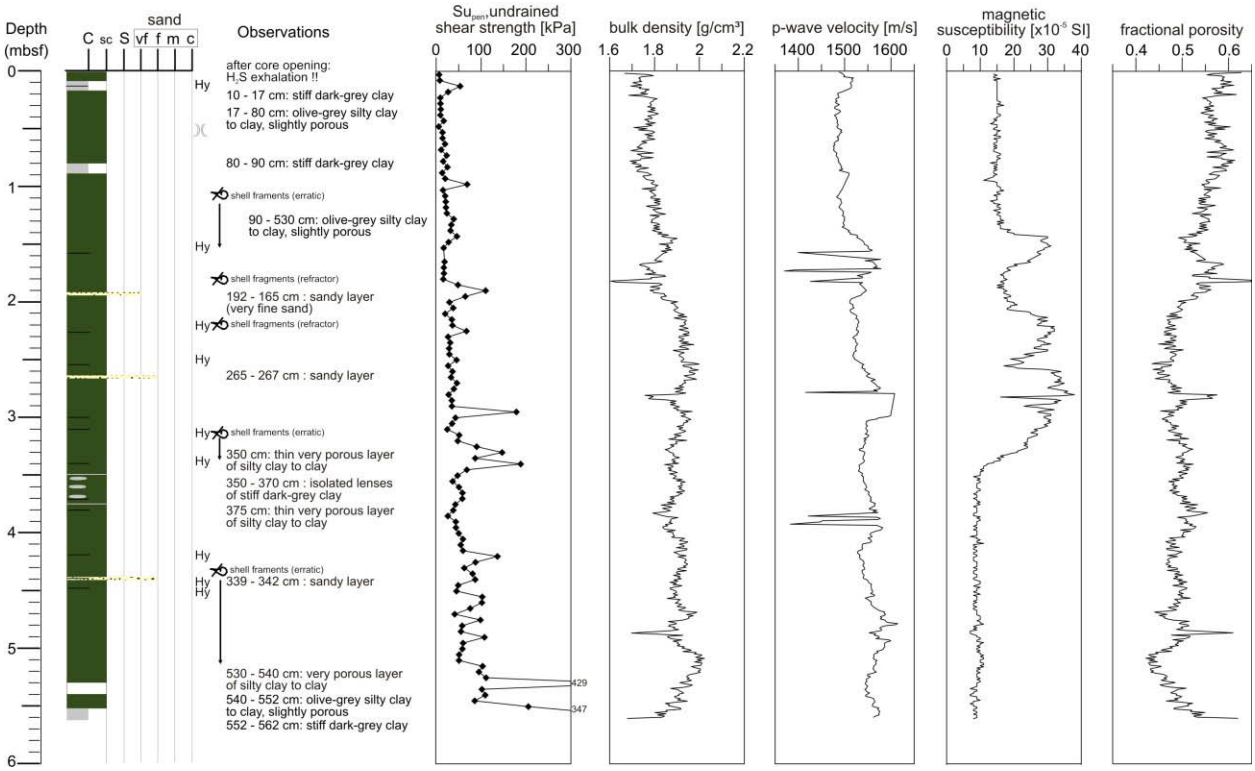

Core log GeoB12213

Date: 23/10/2007 **Latitude:** N 24° 36.451' **Gravity corer length:** 12 m
Water depth: 1833 m **Longitude:** E 62° 58.710' **Core recovery:** 4.24 m

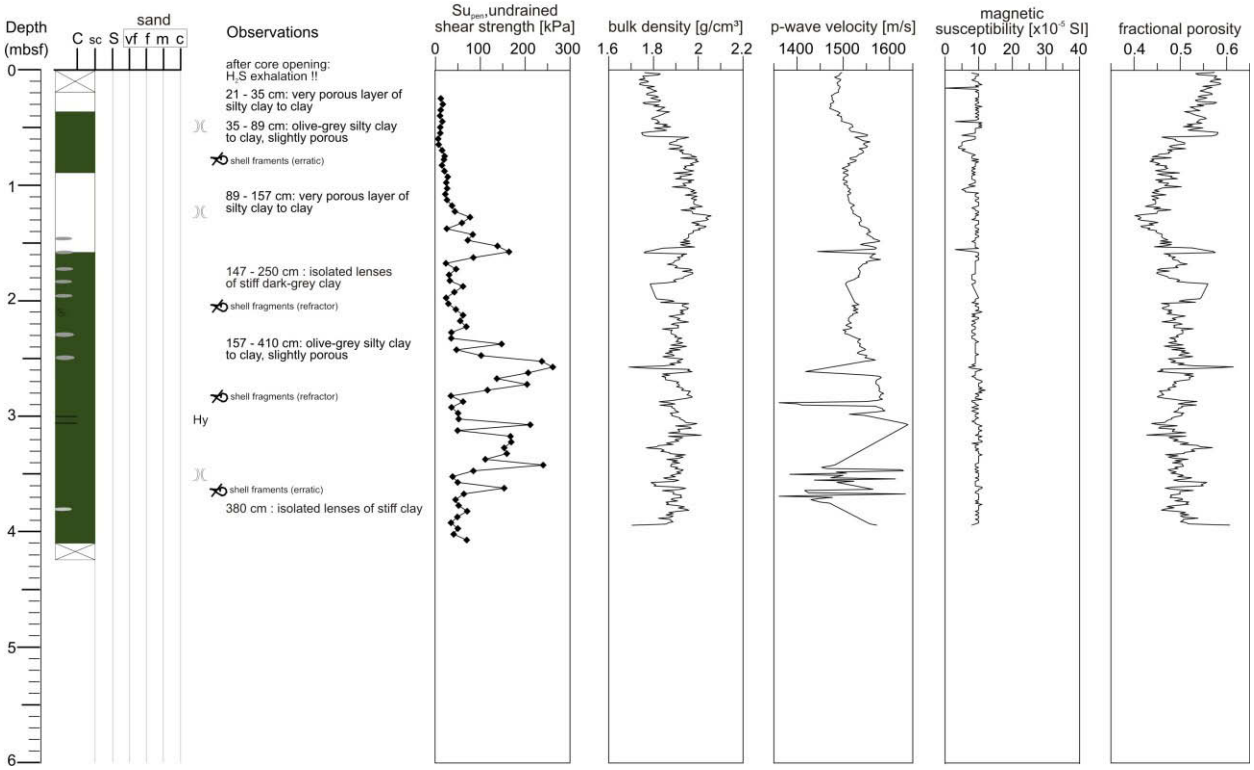

Core log GeoB12214

Date: 23/10/2007
Water depth: 1728 m
Latitude: N 24° 36.899'
Longitude: E 62° 58.57'
Gravity corer length: 6 m
Core recovery: 2.48 m

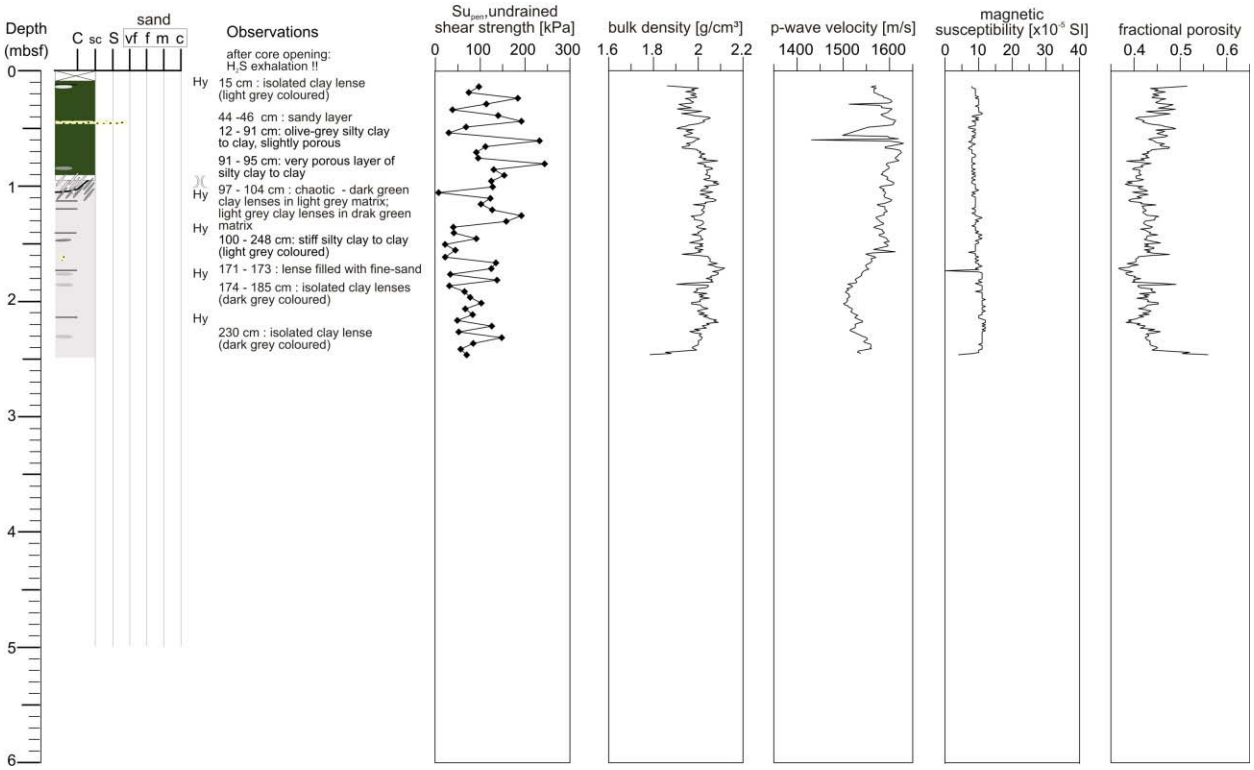

Core log GeoB12306

Date: 03/11/2007
Water depth: 2861 m
Latitude: N 24° 11.761'
Longitude: E 62° 44.311'
Gravity corer length: 6 m
Core recovery: 3.8 m

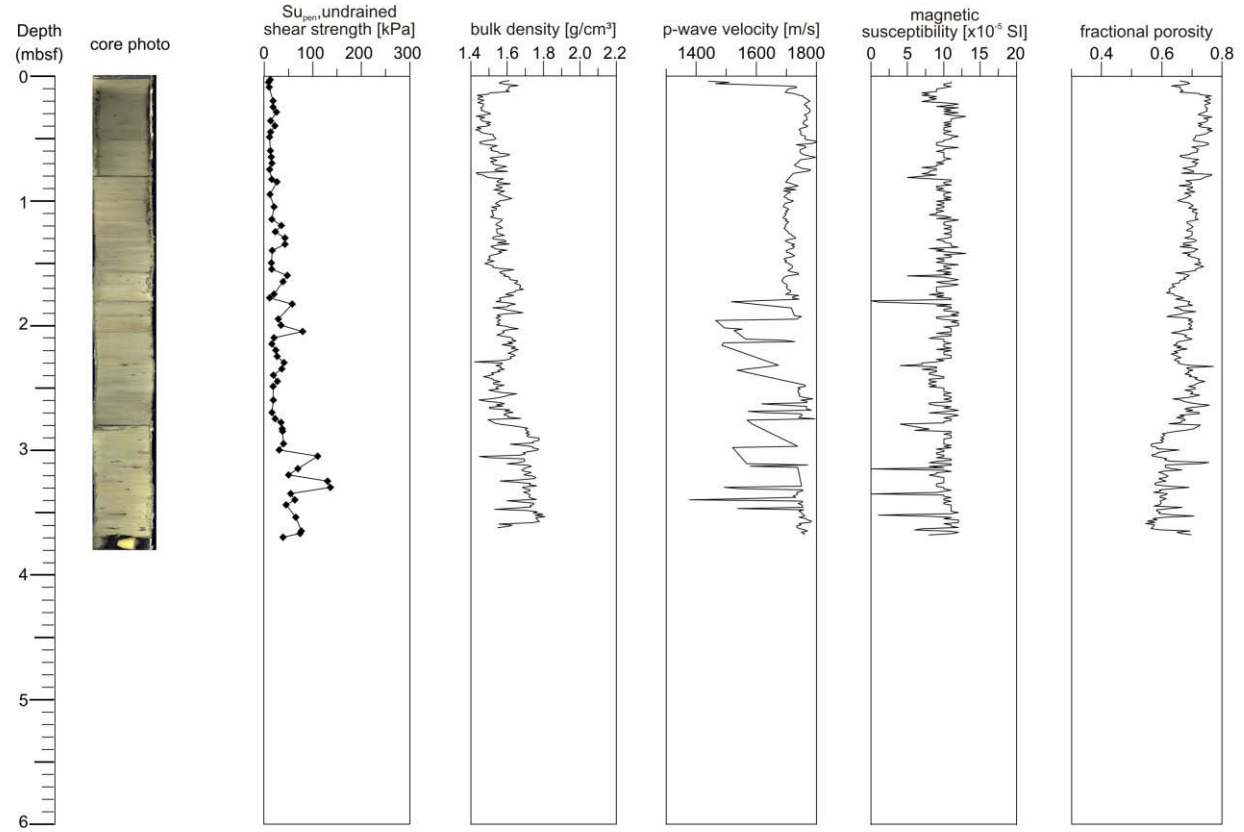

Core log GeoB12309

Date: 08/11/2007
Water depth: 956 m
Latitude: N 24° 52.301'
Longitude: E 62° 59.872'
Gravity corer length: 6 m
Core recovery: 5.60 m

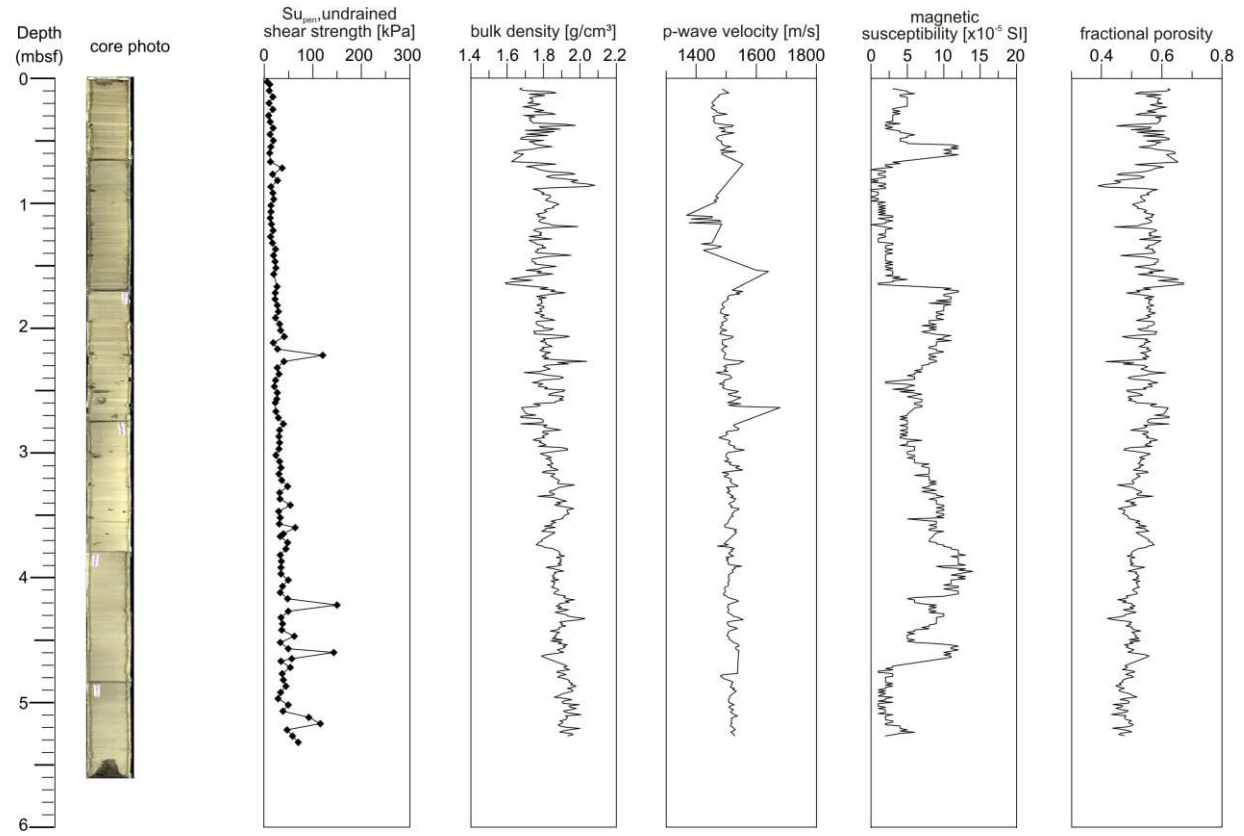

Core log GeoB12332

Date: 14/11/2007
Water depth: 2036 m
Latitude: N 24° 17.482'
Longitude: E 62° 57.586'
Gravity corer length: 6 m
Core recovery: 4.87 m

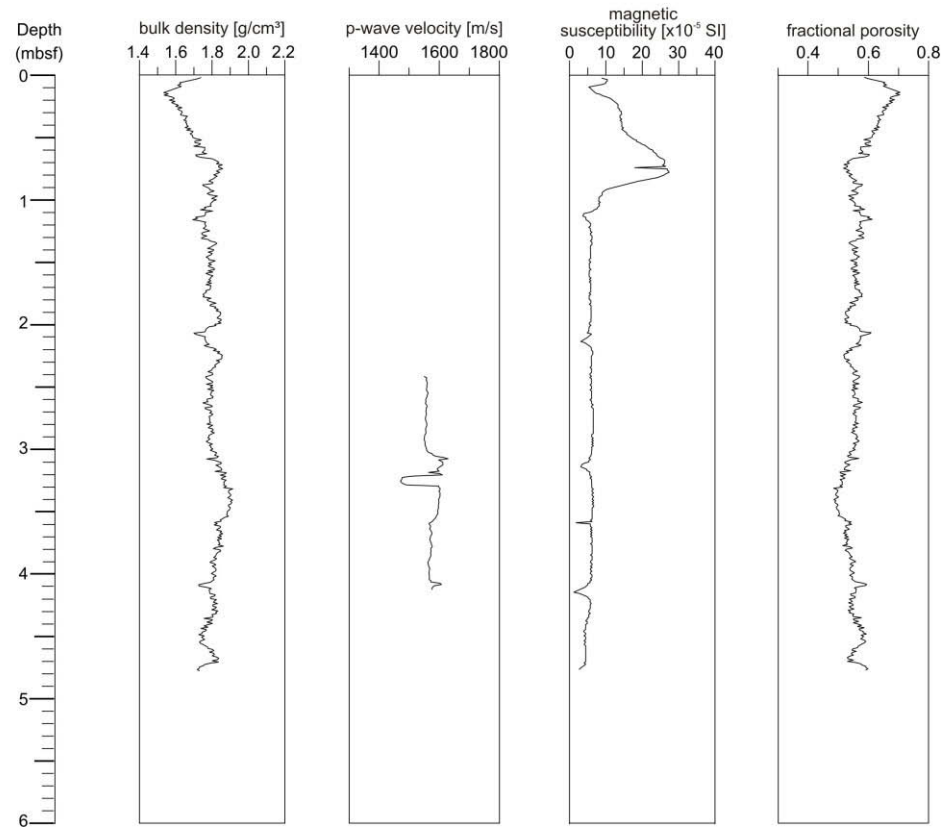

Core log GeoB12335

Date: 15/11/2007
Water depth: 1594 m
Latitude: N 24° 43.100'
Longitude: E 62° 59.511'
Gravity corer length: 6 m
Core recovery: 4.45 m

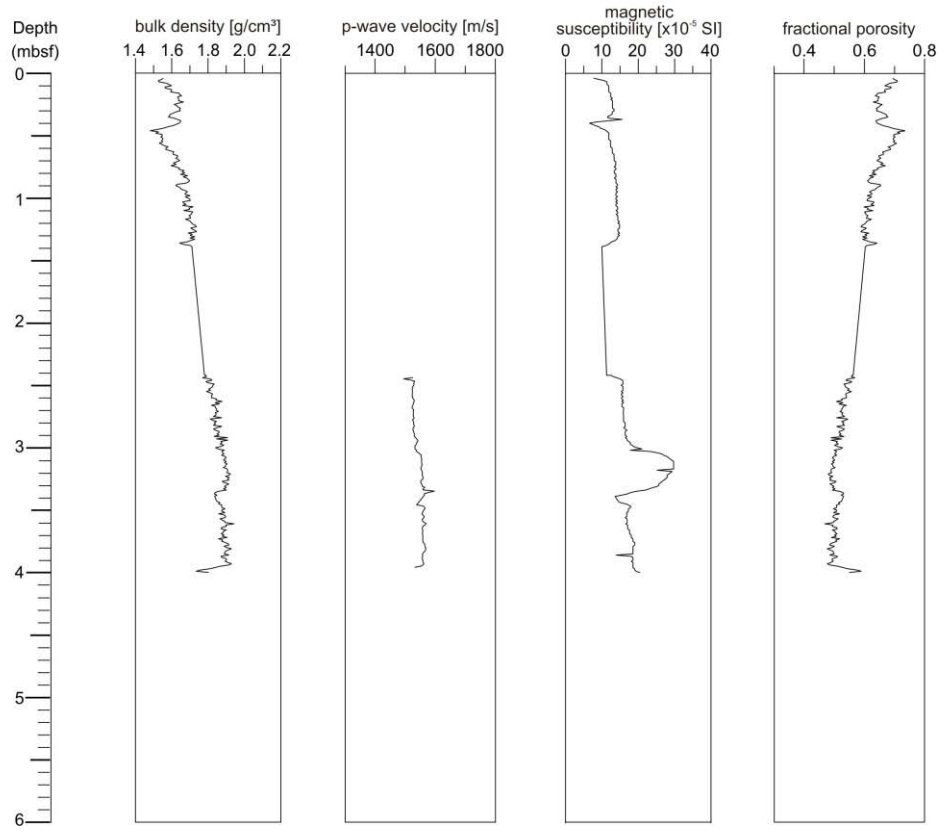

Core log GeoB12336

Date: 15/11/2007
Water depth: 1263 m
Latitude: N 24° 47.777'
Longitude: E 63° 01.471'
Gravity corer length: 6 m
Core recovery: 4.47 m

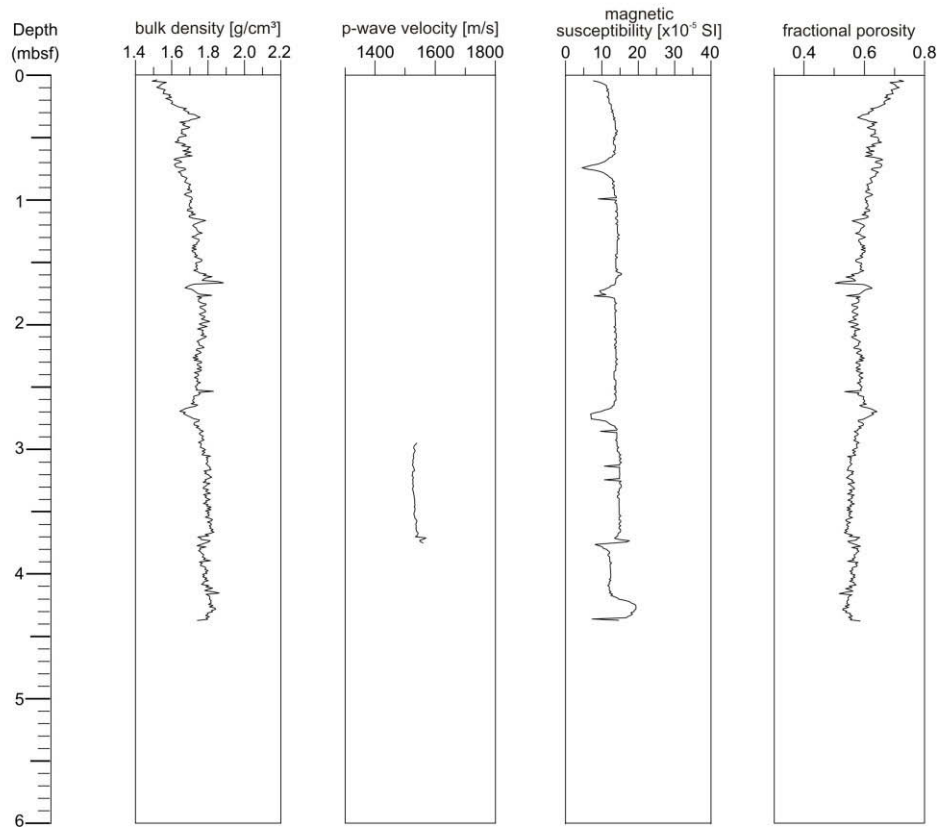

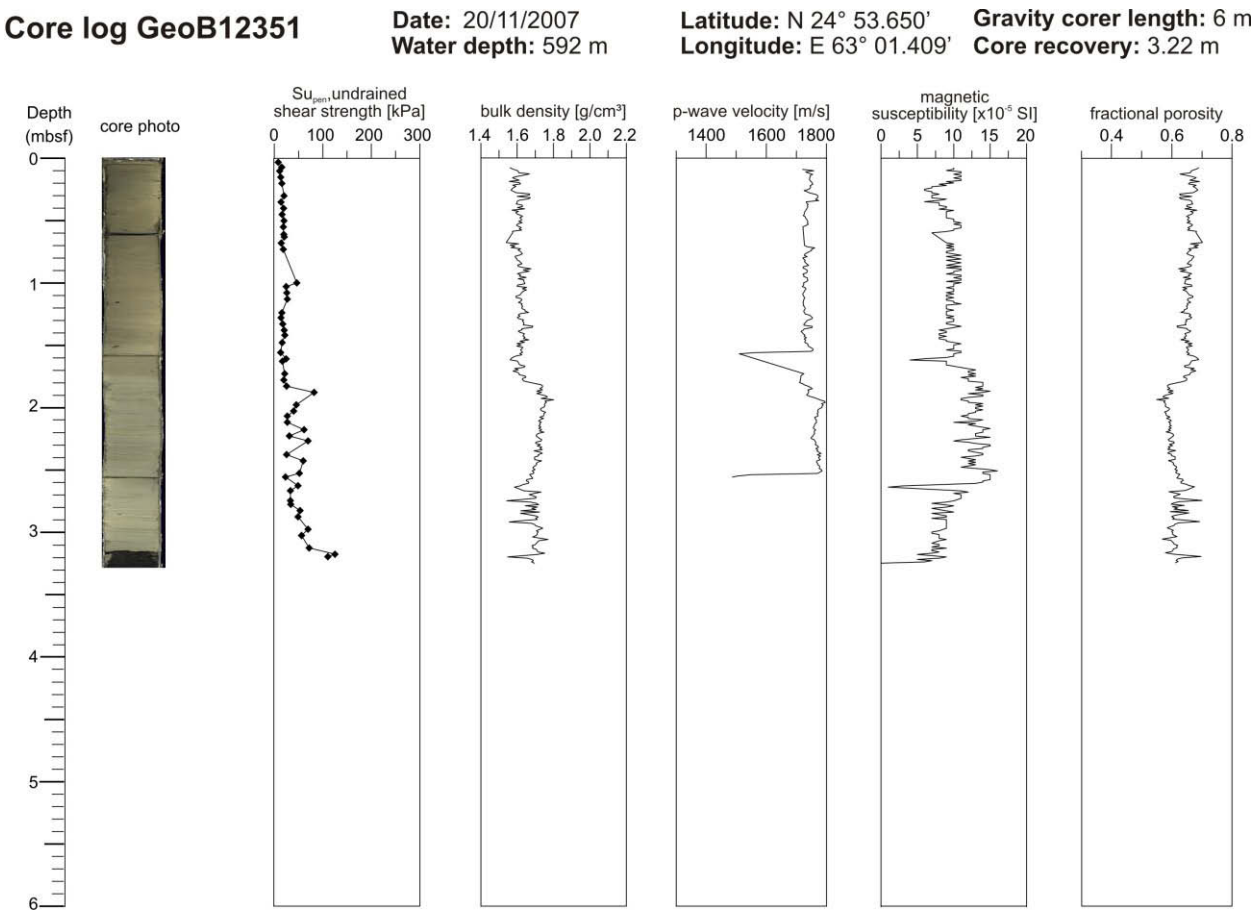
Core log GeoB12351
Date: 20/11/2007
Water depth: 592 m
Latitude: N 24° 53.650'
Longitude: E 63° 01.409'
Gravity corer length: 6 m
Core recovery: 3.22 m
Depth (mbsf)
core photo
Su pen, undrained shear strength [kPa]
0 100 200 300
bulk density [g/cm³]
1.4 1.6 1.8 2.0 2.2
p-wave velocity [m/s]
1400 1600 1800
magnetic susceptibility [x10⁻⁵ SI]
0 5 10 15 20
fractional porosity
0.4 0.6 0.8
0 1 2 3 4 5 6

Appendix Part B

Contributions to conferences

In the framework of the thesis, the PhD candidate participated in national and international conferences. The presented contributions (posters or talks) are listed below:

Förster, A., Stegmann, S., Meyer, M., Strozyk, F., Krastel, S., Kopf, A., 2007. Geotechnical investigations to characterise landslide-prone slope sediments in the Cretan Sea (Northern Crete). International Conference and 97th Annual Meeting of the Geologische Vereinigung eV., October 01.-05.,2007, Bremen, Germany.

S. Stegmann, S. Krastel, M. Irving, **A. Förster** & A.J. Kopf, 2007. Marine Free-fall CPT measurement for landslide characterisation off Crete, Greece (Eastern Mediterranean Sea). 3rd Symposium of Submarine Mass Movements and their Consequences, October 01.-03.,2007, Santorini, Greece.

Förster, A., Strasser, M., Strozyk, F., Spagnoli, G., Stegmann, S., Kopf, A., 2008. Characterization of landslide-prone slope sediments in the Cretan sea (eastern Mediterranean). 33rd International Geological Congress, August 06.-14.,2008, Oslo, Norway.

Annika Förster, Volkhard Spieß, Achim J. Kopf, Bernard Dennielou, 2009. Mass wasting dynamics at the deeper slope of the Ligurian Margin (Southern France). 4th Symposium of Submarine Mass Movements and their Consequences, November 08.-11.,2009, Austin, USA.

F. Strozyk, M. Strasser, S. Krastel, **A. Förster**, A.J. Kopf, K. Huhn, 2009. Landslide repetition in active margin environments – observations from the Hellenic forearc, eastern Mediterranean. 4th Symposium of Submarine Mass Movements and their Consequences, November 08.-11.,2009, Austin, USA.

Geotechnical investigations to characterise landslide-prone slope sediments in the Cretan Sea (Northern Crete)

Förster, A.[1], Stegmann, S.[1], Meyer, M.[1], Strozyk, F.[1], Krastel, S.[1], Kopf, A.[1]

International Conference and 97th Annual Meeting of the Geologische Vereinigung eV., October 01.-05., 2007, Bremen, Germany.

Submarine slides have been mapped on continental margin throughout the world. Numerous slide events are described south of Crete. In opposite to this, our study focus at the Cretan Sea, a fore arc basin between the Hellenic trench and the volcanic arc north of Crete. During the CRESTS (Cretan Sea Tectonics and Sedimentology) expedition P336 with the German research vessel *Poseidon* in April/May 2006 in the Cretan Sea landslide processes were studied in the neotectonically active submarine slope of northern Crete, Greece. We here present preliminary results from in situ and laboratory geotechnical experiments on submarine slope sediments off northern Crete.

Based on multibeam swathmapping and seismic reflection data, *in situ* CPT measurements and sampling/laboratory methods are used to characterise landslide and mass wasting deposits. The main objective is to characterise the physical behaviour and frictional stability of the sediments in order to relate the results to potential trigger mechanisms.

Four sediment cores from different parts of the landslide in the northeastern slope off Crete were taken near its headwall, along its flow path and outside of the landslide. At these cores, sediment physical properties (P-wave, density, water content, magnetic susceptibility and frictional porosity), grain size distribution, shear strength, frictional stability and consolidation behaviour were measured. On the core scale, landslide features are not very obvious to identify in the very homogeneous sediments with an average density of 1.8 g/cm^3. The undisturbed, upper slope sediments are characterised by a linear increase of c_u from 20 to 40 kPa. Immediately near the scarp and within the flow path of the slide, a less pronounced linear trend of c_u is evinced. Ring shear data provide information about small-scale mechanical lateral variations across the headwall of the slide. The undisturbed sediment indicates no significant difference in shear strength between superficial and deeper portion. In contrast, the data of the surface sediments from the headwall and landslide are significantly weaker. In the deeper portion of the landslide, which represents the upper flow path, the coefficient of friction μ_{peak} is slightly below that of the undisturbed core. The frictional response to an imposed increase or decrease in sliding velocities given by the [a-b]-value, which lies predominant below zero, exhibiting velocity weakening and potentially unstable behaviour and may fail catastrophically. In consideration of the ring shear data consolidation tests in sediment samples were made. All these data suggests us that indeed some material is missing in the upper part of the cores.

[1] Research Centre Ocean Margins, Bremen University, Leobener Strasse, 28359 Bremen, Germany

Marine Free-fall CPT measurements for landslide characterisation off Crete, Greece (Eastern Mediterranean Sea)

S. Stegmann[1], S. Krastel[1], M. Irving[2], A. Förster[1] & A.J. Kopf[1]

3rd Symposium of Submarine Mass Movements and their Consequences, October 01.-03., 2007, Santorini, Greece.

Pore pressure and sedimentary strength are controlling parameters for slope stability. Therefore two different free-fall CPT lances were designed for the *in situ* measurement of strength (cone resistance, sleeve friction) and pore pressure. In addition, deceleration and tilt are monitored for vertical profiling of the penetrated sediment column. Both CPT systems rely on an industry 15 cm^2 piezocone with the sensors at the cone and a pressure housing containing a microprocessor at the top. The lightweight (40-100 kg), shallow water (200 m depth) lance works completely autonomous and can be deployed from any platform, even without a winch. Length and weight of this system can be varied according to the sediment stiffness and hence allows variable penetration depth (up to 6.5 m). The sturdier, deeper water (3200 m depth) system uses both power and telemetry for data transmission from the research vessel. Initial use of the CPT systems attests their efficiency and reliability in the measurement of sediment physical properties.

Both devices were deployed in the marine expedition POS 336 (Cretan Margin), where the aim was to study landslide processes, turbidites, and other consequences of slope instability in the Cretan Sea north of the island. CPT tests were embedded in a multi-methodological approach, using multibeam swathmapping, seismic reflection systems (3.5 kHz and 16-channel MCS), heat flow, and gravity coring. Several large landslide complexes at the NE Cretan Margin as well as a small, but steep landslide scarp structure further east were identified on seismic reflection profile. Both penetrometer devices were deployed in undisturbed slope sediments, along the slide scar and in the main body of the slid formations. The maximum penetration depth of the probes was 1.55 m. After insertion of the CPT, the lance remained stuck in the sediment for 5-15 minutes to monitor pore pressure dissipation after the impact and to define T_{50} (the time required for a 50% decay of the maximum pore pressure, which may be used as a first-order indicator for permeability). Insertion pore pressure range around 60 kPa in background sediment and more than 80 kPa in the slid deposits. In the slide complex, T_{50} between 5 and 6 minutes indicates less permeable sediments in the upper intact slope, whereas a gradient down slope is observed where more permeable, possibly amalgamated landslide material with T_{50} between 0.2 and 3 minutes is found. Cone resistance ranges between 200 and 500 kPa, suggesting relatively soft sediments upslope of this slide. Vane shear tests confirmed undrained strengths of up to 40 kPa for the undisturbed sediments and lower than 30 kPa for the headwall deposits. Frictional characterisation of these sediments attests velocity weakening behaviour during ring shear experiments, indicating that those sediments are unlikely to show stable creep and instead may fail catastrophically.

[1] Research Centre Ocean Margins, University of Bremen, Leobener Strasse,28359 Bremen,Germany
[2] Picker Engineering Program, Smith College, 51 College Lane, Northampton, MA 0106 ,USA

Characterization of landslide-prone slope sediments in the Cretan sea (eastern Mediterranean)

Förster, A.[1], Strasser, M.[1], Strozyk, F.[1], Spagnoli, G.[1], Stegmann, S.[1], Kopf, A.[1]

33rd International Geological Congress, August 06.-14. ,2008, Oslo, Norway

Submarine slides have been mapped along continental margin throughout the world. Numerous slide events are described south of Crete. In opposite to this, our study focus at the Cretan Sea, a fore arc basin between the Hellenic trench and the volcanic arc north of Crete. We here present results from in situ and laboratory geotechnical experiments from the CRESTS (Cretan Sea Tectonics and Sedimentology) expedition P336, where landslide processes were studied in the neotectonically active submarine slope area. The main objective of this study is to characterise the physical behaviour and frictional stability of the sediments in order to relate the results to potential trigger mechanisms such as tectonic oversteepening, excess pore fluid pressure, weak clay horizons, or earthquake tremor.

Bathymetric and seismic reflection data show two distinctive slide complexes at the northern Cretan Margin with different geometries, thicknesses and internal deformations patterns. The continental slope differs in steepness from 8° (western Slide) to 1° (eastern Slide). The western complex, extended over 260 km_, represents multiple slide events with clear headwalls. In contrast, the eastern complex extends over approximately 60 km_ and seems to be slid down as a more or less intact block. Bathymetric data suggest genesis of new headwalls in the slid sediments further downslope.

Based on the geophysical observations, in situ CPT measurements and sampling for laboratory experiments were carried out. We here present the shipboard results which included core description, index properties, grain size analysis and various types of shear experiments. All gravity cores show similar lithostratigraphic successions characterised by yellowish brown sandy to silty mud, light olive grey sandy to silty mud and olive black sapropels. Density values in the undisturbed sediments increase in both complexes more or less linearly downward. It is noticeable that the densities of the eastern complex are lower than those of the western complex. Also, densities near the scarp and the failed sediments of the eastern complex are similar to the undisturbed slope sediments. However, the farthest travelled deposits at the western slide complex show lower densities as the undisturbed deposits, suggesting homogenisation as a result of displacement. The undisturbed sediments are characterised by a linear downward increase in undrained shear strength in both slide complexes. Along the flow path of the slides, however, strength remains more or less constant.

Ongoing research aims to shed light on slope instability triggers including static ring shear tests, oedometer tests and dynamic triaxial shear tests to simulate high strains, seismic tremor and rate-dependent strength.

[1] Research Centre Ocean Margins, Bremen University, Leobener Strasse, 28359 Bremen,Germany

Mass wasting dynamics at the deeper slope of the Ligurian Margin (Southern France)

Annika Förster[1], Volkhard Spieß[1], Achim J. Kopf[1], Bernard Dennielou[2]

4th Symposium of Submarine Mass Movements and their Consequences, November 08.-11., 2009, Austin, USA.

Landslide events are common in the tectonically complex, seismically active Mediterranean Sea, most prominently along the Ligurian Margin (Southern France). The main objective of this study were mass wasting processes in the Var Canyon and adjacent slopes. Bathymetric and seismic reflection data reveal two extensive slide complexes at the steep canyon slope (~ 11°) in about 1500-2000 m water depth. The western complex is affected by several scars and talus adjacent to the Var Canyon while the one further east of the canyon system shows one scar and an associated SSE-trending pathway. In situ CPT measurements and sampling for laboratory experiments were carried out along N-S transects across the headwalls of both slides. The majority of the gravity cores show similar lithostratigraphic successions characterised by homogenous fine-grained hemipelagic silty clay with some coarser sections.

The undisturbed sediments upslope of the western complex show sharp, tilted (20-45°) contacts in sedimentary layering related to listric gliding of the sediment above the steep, 40 m-high headwall. Along the landslide body, sediments are characterised by increasing density and undrained shear strength values (Su) along the N-S transect. The cores near the headwall contain displaced and reworked sediments consisting of stiff clasts and rounded pebbles and silty-clay or sandy intervals. In contrast, the most distal deposits show very low density, suggesting homogenisation as a result of long runout distance.

At the eastern slide complex, the headwall is not very pronounced and hence has not caused displacement and tilt of the hangingwall. Like in the west, the cores near the headwall contain displaced and reworked sediments and are characterised by higher density and Su values. Evidence for collapse structures is observed further downslope along the trace of the landslide, where lower sediment density and strength indicates amalgamation of seawater and surface sediment.

[1] MARUM- Center for Marine Environmental Sciences, University of Bremen, Leobener Straße, PO box 330440, 28334 Bremen, Germany
[2] IFREMER – French Research Institute for Exploitation of the Sea, Département des Géosciences Marines, PO box 70, 29280 Plouzané Cédex France

Landslide repetition in active margin environments – observations from the Hellenic forearc, eastern Mediterranean

F. Strozyk[1], M. Strasser[1], S. Krastel[2], A. Förster[1], A.J.Kopf[1] & K. Huhn[1]

4th Symposium of Submarine Mass Movements and their Consequences, November 08.-11.,2009, Austin, USA.

In this study we aim on the identification of factors and processes that can lead to a less frequent occurrence of landslide events along active margin slopes despite the general expectation of a more diffuse, extensive mass-movement pattern from the high neotectonic activity in such settings. The Hellenic subduction zone, eastern Mediterranean, represents an example where modern evidence for slope failure in active margin environments is scarce and only present as scattered landslide deposits of 0.5-2.5 km³ volumes e.g. along the northern margin of Crete. But taking the Kamilonisi Basin as one of the deepest parts of the Cretan Sea forearc basin into account, we found evidence for much larger landslide deposits of 30-50 km³ volumes at recurrence intervals of approximately 250 ka. Given neotectonic movements and local seismicity in the area, we rate this slope failure recurrence to be low. In order to improve our understanding on the relationship between such landslide recurrence rates and the required trigger, we focus on the mechanical strength of the slope sediment as well as slope geometry limiting slope instability scenarios. Seismic profiles and geotechnical measures from cores of midsize landslides in mid-slope positions are used to get control on sediment mechanics from one-dimensional, infinite slope models for static conditions as well as for the case of critical ground acceleration.

As a result, the measured high shear strength values require respective high peak ground accelerations (PGA) of >29%g, most likely up to 42%g for major events. Based on earthquake hazard catalog data for the entire Aegean region, such PGAs can be expected at frequencies similar to those estimated for major landslides. Therefore, we infer that only infrequent, nearby, high-magnitude earthquakes generate stresses sufficient for major failure of the cohesive, consolidated Cretan slope sediment. Further, slope architecture of at least 5° slide plane inclination combined with sediment truncation from faults prepare additional requirements for failure development, whereas all lower-inclined slope portions is still stable. The over-critical, lower slope is devoid of both intact sediment and landslide deposits and indicates consequent export of once released landslides or reactivated MTDs into the deeper basin. As our results are consistent with data and observations from other active margin slopes (e.g. western North America), this study implies that taper adjustment and dynamic compaction may favour larger resistance to regional seismicity and other potential triggers.

As an outlook, the multi-disciplinary research cruise SACRE (Slide activity along the northern Cretan margin) back to the study site will continue this CRESTS project (Cretan Sea Tectonics and Sedimentation) in June 2010. A deep core drill rig (MeBo) developed by the MARUM will be used to recover cores of up to 70 m depth from the undisturbed slope, headwalls and landslide bodies down to slide planes. This will hopefully provide more details on the slide plane material as well as its mechanical behaviour in terms of Cretan slope destabilization scenarios.

[1] MARUM, Centre for Marine Environmental Sciences - Cluster of Excellence: The Ocean in the Earth System, University of Bremen, P.O. Box 33 04 40, D-28359 Bremen, Germany
[2] IFM-GEOMAR, Leibniz Institute of Marine Sciences, Cluster of Excellence: The Future Ocean, Christian-Albrecht-University Kiel, D-24148 Kiel, Germany

Erklärung

Hiermit versichere ich, dass ich

1. die Arbeit ohne unerlaubte fremde Hilfe angefertigt habe.

2. keine anderen als die von mir angegebenen Quellen und Hilfsmittel verwendet habe.

3. die den benutzten Werken wörtlich oder inhaltlich entnommenen Stellen als solche kenntlich gemacht habe.

Bremen, den 07.11.2011

(Annika Förster)